Enhancement of gemcitabine and paclitaxel uptake and retention in metastatic cancer cells: A novel targeted combination delivery approach to eliminate breast cancer in blood and lymph

Jesse Yu

A dissertation

submitted in partial fulfillment of the

requirements for the degree of

Doctor of Philosophy

University of Washington

2020

Reading Committee:

Rodney JY Ho, Chair

Danny D Shen

Nina Isoherranen

Program Authorized to Offer Degree:

Pharmaceutics

University of Washington

Abstract

Enhancement of gemcitabine and paclitaxel uptake and retention in metastatic cancer cells:

A novel targeted combination delivery approach to eliminate breast cancer in blood and lymph

Jesse Yu

Chair of the Supervisory Committee:
Dr. Rodney JY Ho
Department of Pharmaceutics

The best current breast cancer treatments are limited by a lifelong concern for tumor recurrence. The inability of therapies to eliminate residual cancer cells after surgery leads to disease progression and metastasis. Gemcitabine (G) and paclitaxel (T) is an effective combination chemotherapy for metastatic breast cancer. However, the inability to synchronize GT in plasma and cancer cells by IV infusion limits its therapeutic potential. Off-target toxicity from diverging distribution of GT is also harmful to patients. If GT can be localized preferentially and retained together in cancer cells, the treatment impact will be enhanced with lower toxicity. Due to disparate physicochemical properties of GT, these drugs are challenging to formulate together for co-delivery to cancer cells. To overcome this gap, this dissertation describes the discovery of a novel technology that brings together water soluble G and insoluble T to form a novel GT drug combination nanoparticle (GT DcNP). This enabling technology allows GT to form a multi-drug-motif (MDM) structure in the presence of lipid excipients. When suspended in aqueous buffer, it produces an injectable GT DcNP dosage form. After IV injection, GT DcNPs (compared to free drug controls) increase the plasma exposure of G by 61-

fold and T by 4-fold. GT DcNPs are able to target GT to breast cancer cells with a 5-fold higher lung-to-plasma ratio of G in tumor bearing lungs compared to healthy lung tissue. The maintenance of the originally dosed ratio of G-to-T in tumor burdened tissue, suggests that the DcNPs are stable and able to synchronize delivery into cancer cells. A single intravenous dose of GT in DcNP can completely eliminate invading breast cancer cells with a therapeutic index of 15.8. In mammary tumors, subcutaneous dosing of GT DcNPs causes cancer regression and recovery of the mammary tissue. These data show that the coordinated delivery of GT by DcNPs overcome the limitations of current free drug infusions and achieves greater anti-tumor effects. The MDM structure in DcNPs enables the transformation of short acting combination therapies to long acting injectables and can extend to other cancers, infections or chronic diseases that target the blood or lymph.

TABLE OF CONTENTS

LIST OF FIGURES

LIST OF TABLES

ACKNOWLEDGEMENTS

I would like to first acknowledge my mentor, Rodney Ho, for his guidance and support throughout my graduate school experience. His passion for science and dedication to the scientific process is exemplary and has been instrumental in my growth and development as a pharmaceutical scientist. The training I have received in the Ho laboratory encompasses a broad scope of science that I am truly grateful for having experienced.

To Drs. Danny Shen, Nina Isoherranen and Bill Atkins, I would like to thank you all for your time, guidance and thoughtful discussions as members of my doctoral supervisory committee. My conversations with Danny have always been incredibly helpful and insightful and I thank him for his time and mentorship. I have really enjoyed getting to know Nina as both a faculty member and member of my committee and I'd like to thank her for her consistent support and advocacy for the graduate students at UW. I would like to thank Bill for setting up the pharmacological sciences training grant, and giving me the opportunity to interact with him and other graduate students in the medicinal chemistry and pharmacology programs.

To the members of the Ho lab, I am grateful for your friendship, support and encouragement over the years. Working with the team has been a unique experience that I'll always be thankful for. I would also like to recognize the staff and faculty of the pharmaceutics department. The pharmaceutics department has always felt like one big family to me and has fostered an incredibly positive and supportive research and learning environment.

Finally, I would like to thank my family and friends who motivated and supported me over the years. This has been an incredible journey that would not have been possible without everyone.

Introduction

Chapter 1. CURRENT BARRIERS TO SUPPRESSING BREAST CANCER METASTASIS: COMBINATION AND NANOPARTICLE DRUG DELIVERY SYSTEMS FOR TARGETED COMBINATION THERAPY

1.1 BACKGROUND AND SIGNIFICANCE

In the United states, approximately 1 in 8 women develop breast cancer over the course of their lives. There are many treatments for breast cancer including surgery, radiation therapy and drug therapies. Unfortunately, even with these multiple treatment options, ~30% of patients proceed to the metastatic stage. In most cases, patients with breast cancer will undergo surgery to remove the primary tumor but residual cancer cells remain. Tumor recurrence from these foci likely reflects an inability of subsequent interventions (like radiation or targeted therapy) to eliminate residual cells in the mammary or lymphatic tissue, which results in distant metastasis. Drug therapies that were used to treat the initial tumor, such as hormone receptor therapy or kinase inhibitor therapy, can become ineffective after recurrence due to drug resistance. Once disease progresses to metastatic breast cancer (MBC), chemotherapy remains as the last viable treatment option. Chemotherapy regimens used in the treatment of MBC effectively kill cancer cells but also exhibit dose-limiting toxicities from off-target exposure of healthy tissues. Additionally, chemotherapy is given in combination to maximize pharmacologic effects, but the cumulative toxicity of multiple drugs is difficult for patients to bear.

Combination regimens used in MBC are based on either an anthracycline (doxorubicin, epirubicin or daunorubicin) or taxane (paclitaxel, docetaxel) combined with other cytotoxic drugs.

Each class of chemotherapy has their own specific toxicity profile. For example, anthracycline therapy damages cardiac tissue by irreversibly binding to cardiolipin. Anthracycline cardiotoxicity is lifetime dose-limiting and is a major issue in late stage disease where patients have already been exposed to numerous cycles of anthracycline therapy. Taxane based regimens cause bone marrow toxicity, which is dose-limiting, but myelosuppresion is generally reversible and can be managed clinically. Anthracycline and taxane based therapies have comparable effects on cancer inhibition but the more manageable toxicity profile of taxane based therapies has resulted in their increased usage in late stage disease. Regardless of the regimen, the key to combination chemotherapy is to balance the effective killing of cancer cells with the off-target toxicity to healthy organs.

Gemcitabine (antimetabolite, logP = -1.4) and paclitaxel (tubulin inhibitor, logP = 3) are used as a taxane-based combination chemotherapy regimen (GT, G=gemcitabine, T= Taxol=Paclitaxel) to improve outcomes of MBC. These two drugs, which are often given sequentially in different formulations by the intravenous route, have very different physicochemical properties. These physicochemical differences are responsible for their varying disposition, clearance and plasma time course *in vivo*. If both drugs can simultaneously accumulate and persist in the same cancer cells following drug combination therapy, then antitumor effects could be maximized. In addition, the overall dose requirement could also be lowered to minimize drug exposure to healthy organs. Unfortunately, the diverging clearance and disposition of GT, soon after their IV administration makes this scenario unlikely. Simultaneous, sustained IV infusion of both drugs may synchronize plasma levels of gemcitabine and paclitaxel, but injection site reactions and incompatible dosage forms of the two drugs make this approach impractical. Due to these factors, maintaining the concentrations of both drugs in tumors after sequential infusion without causing off-target, dose-limiting toxicities is nearly impossible. To maintain drug

levels at therapeutic concentrations in plasma and target cancer cells, a high dose regimen is typically employed in MBC treatment guidelines to compensate for the varying disposition and elimination of GT. As a result of high drug exposure to healthy organs, dose-limiting toxicities of chemotherapy are a major barrier in the management of metastatic disease and highlight a significant limitation in the treatment of MBC. There are many potent and effective drugs that can be used in combination to treat MBC, but the lack of a consistent cure is due to off-target toxicity and inadequate exposure of combined drugs in target cancer cells. If chemotherapy were able to be delivered to target cancer cells together and remain in those cells long enough for antitumor effect, then off-target toxicity could be minimized and breast cancer treatment could be consistently curative.

Currently, many drug delivery systems are being explored to overcome dose limiting toxicities and improve target drug localization in breast cancer cells and tissues. In theory, drug delivery systems can be engineered with unique properties including size, shape and surface chemistry which help determine their *in vivo* disposition. By optimizing these characteristics, drug delivery systems can improve the *in vivo* behavior of cytotoxic drugs by increasing retention in target cancer cells and reducing off-target toxicity. Unfortunately, the optimal drug delivery system to enable targeted delivery to cancer cells has yet to be developed, partly due to the lack of a systems approach (Ho et al., 2015). In the context of MBC, a systems approach can be broadly defined as understanding how specific particles distribute dynamically in the body and how they are cleared, relative to tumor accumulation and drug stability within the drug delivery systems. In addition, unforeseen toxicity of nanoparticulate compositions need to be considered. Certain drug delivery systems have distinct toxicities related to off-target distribution. Specific excipients used in nanoparticle compositions are also associated with adverse events. Either of these scenarios

would preclude the clinical development of highly promising drug delivery strategies. As an example, liposomes are a nanoparticle system that are well established in the literature, but unmodified liposomes greater than 100 nm in diameter are extensively taken up into the liver (Hu, van Rooijen, & Liu, 1996). The sequestration of liposomes in the liver prevents drug access to target cancer cells and limits drug effect. Similarly, polymeric nanoparticles smaller than 10 nm (such as cyclodextrin, polyamidoamine (PAMAM) dendrimers, etc) are known to undergo renal filtration with a fraction of particles accumulating in renal tissues. The accumulation of particles in the kidney leads to toxicological concerns from both the free drug and polymeric particle. The high clearance and elimination by the renal route may also prevent polymeric particles from accessing cancer cells and limit the effectiveness of these carriers. Currently, a stable, established drug delivery system capable of carrying multiple, chemically diverse chemotherapeutic drugs is not broadly available. Thus, a novel approach is required to enable the targeted delivery of chemically diverse chemotherapy combinations. The ideal system would facilitate the delivery of multiple drugs to cancer cells for an extended time course to achieve full antitumor efficacy.

The goal of my dissertation research is to develop a stable, combination nanoparticle composed of gemcitabine and paclitaxel with the appropriate *in vivo* pharmacokinetic characteristics to enable targeted delivery and overcome the current limitations in the field. In previous work, the Ho laboratory has developed an injectable drug combination nanoparticle (DcNPs) composed of hydrophilic and hydrophobic HIV drugs. To develop a stable GT combination nanoparticle, I first developed an understanding of how controlled solvent removal can stabilize chemically diverse HIV drugs in lipid excipients. By applying the knowledge gained from antiviral particles, a new combination nanoparticle composed of hydrophilic gemcitabine and hydrophobic paclitaxel was formulated. Novel GT DcNPs were then characterized *in vitro* and *in*

vivo to assess the stability and suitability for use as a treatment for breast cancer. Experimental studies and pharmacokinetic modeling demonstrated robust stability of GT DcNPs in the systemic circulation with limited accumulation in healthy organs. *In vivo* models of breast cancer metastasis were then developed to assess the activity of GT DcNPs in eliminating target cancer cells. The targeted delivery of two chemically diverse drugs together to cancer cells profoundly improves the antitumor efficacy of GT combination therapy and can be used to eliminate cancer cells that migrate through both the blood and lymph. The tools and approaches outlined in this thesis lay the groundwork for future development of targeted, combination nanoparticles for hard to treat cancers (including metastatic breast cancer) such as pancreatic duct adenocarcinoma or colon cancer.

The purpose of this introductory chapter is to (1) briefly describe the pathophysiology of breast cancer and pathogenesis of metastasis to understand the physiological factors that can affect the efficacy of MBC treatment. The chapter will then (2) outline the current pharmacologic approaches to treating metastatic breast cancer and the pharmacologic basis for combination treatment. After establishing the pharmacologic rational for various agents used in breast cancer treatment, the next section will review (3) the factors that allow breast cancer cells to survive pharmacological treatment. This chapter will then (4) provide experimental evidence of pharmaceutical approaches that attempt to overcome mechanisms of breast cancer cell survival, and (5) introduce a novel approach to improving cancer cell uptake and retention of clinically effective drugs. The central hypothesis of this thesis will then be presented, which will be addressed by the specific aims in subsequent chapters.

1.2 PATHOPHYSIOLOGY OF BREAST CANCER

In the simplest terms, breast cancer can be defined as the uncontrolled growth of cells in the breast. There are two main types of tissue in the breast: the milk duct and the breast lobules.

The tissue that breast cancer originates from determines the clinical progression and behavior of disease. Cancer originating from the milk duct, classified as ductal carcinoma, account for 40-75% of all diagnosed breast cancers (Bombonati & Sgroi, 2011). The defining characteristics of ductal carcinomas are mutations of ERBB2, EGFR and P53 proteins and metastasis to the lungs, pleura and CNS (Arpino, Bardou, Clark, & Elledge, 2004; Harris et al., 1984). By comparison, cancer originating from the breast lobules, classified as lobular carcinoma, are less prevalent, accounting for ~10-15% of diagnosed breast cancers (Bombonati & Sgroi, 2011). Lobular carcinomas are more likely to overexpress hormone receptors such as the estrogen receptor (ER) or progesterone receptor (PR) and metastasize to the peritoneum, ovary and gastrointestinal system (Arpino et al., 2004; Harris et al., 1984). Although ductal and lobular carcinomas have different expression patterns for specific oncoproteins, treatment algorithms are not based on the tissue of origin but the molecular classification of breast cancer.

There is a strong association between the classification of breast cancer by molecular targets and survival/clinical prognosis. The two major molecular targets and classifications in breast cancer therapy are the estrogen/progesterone hormone receptors (ER/PR) and the erythroblastic oncogene B2 (ERBB2) receptor, which is also referred to as human epidermal growth factor receptor 2 (HER2). Breast cancers (regardless of tissue origin) are categorized as either ER/PR+ or ERBB2+ based on their expression of these receptors. Breast cancers that do not express any of the three major receptors (ER, PR or ERBB2) are known as triple negative breast cancer (TNBC), and the molecular pathogenesis of TNBC is least understood. In addition to these 3 major classifications, patients that carry mutations in breast cancer type 1 or type 2 susceptibility protein (BRCA1/BRCA2) are predisposed to breast cancer development and strongly associated with TNBCs. In general, ER/PR+ breast cancer has the best prognosis (70% of all cases), followed

by ERBB2+ cancers (~15-20% of all cases), and TNBC (~10%) which has the worst clinical prognosis and survival rates (Waks & Winer, 2019). The clinical outlook of different types of breast cancer is likely related to the available therapeutic agents. In the case of ER/PR+ breast cancer, drugs have been developed to specifically target these receptors such as selective estrogen receptor modulators or aromatase inhibitors. For ERBB2+ breast cancer, targeted agents such as monoclonal antibodies or kinase inhibitors can be used. Since TNBC does not express any clearly defined molecular targets, it is treated with broadly cytotoxic chemotherapy. Although chemotherapy is the primary treatment in TNBC, it is also used in ERBB2+ and ER/PR+ cancers. The individual agents used in each class will be discussed in later sections.

1.2.1 *Role of lymphatic tissue in breast cancer metastasis*

Currently the biggest issue in breast cancer treatment is not the primary tumor itself, but tumor recurrence and distant metastasis. When breast cancer is first detected, there are many options available for treatment including surgery, radiation therapy, hormone therapy, targeted therapy and chemotherapy. Surgical interventions consist of removing the primary tumor and in some cases, the draining lymphatic architecture adjacent to the tumor. Radiation therapy is performed by using high-energy waves or particles to irradiate the area where the primary tumor was removed (also known as the tumor bed) to eliminate residual cancer cells. Drug therapy is then administered based on the molecular characteristics of the primary tumor to further inhibit residual cancer growth. These multi-modal treatments are excellent at extending survival but are not consistently curative and disease progression (in the form of metastasis) is still prevalent. Once metastasis occurs, treatment goals shift towards palliative care and treatment options are limited (typically due to the emergence of drug resistance). As primary breast cancer tumors grow, cancer cells invade into the systemic circulation and the draining lymphatic system (Nathanson et al.,

2018; M. Rahman & Mohammed, 2015). Cancer cells detected in the sentinel lymph nodes adjacent to breast cancer tumors are a negative prognostic factor for clinical disease. Recently, studies have shown that the lymphatics are also an important part of metastatic pathogenesis in breast cancer. Two reports from independent laboratories provided time and spatial insight into the metastatic spread of breast cancer cells from primary sites (nodes and mammary gland) into blood and subsequent deposition in the lungs (Brown et al., 2018; Pereira et al., 2018). These two studies used 4T1 metastatic mouse tumors as models to show that removal of a primary tumor or inoculation of a small number of cancer cells in lymph node cortex invariably leads to metastatic nodule formation in the lungs. Regardless of where the cells are initially introduced (primary tumor followed by resection or directly into the lymph), cancer cells preferentially penetrate into the blood. The cited studies show that residual cancer cells will proliferate in the lymph and migrate into the blood. From there, the cells can transit to the lungs and colonize the pulmonary tissue as cancer nodules (Brown et al., 2018). These time-course and spatial 4T1 tumor spread data highlight the blood and lymph as important compartments for growing cancer cells. If the lymph is a tissue that cancer cells can grow in after removal of the primary tumor, then those cells have the opportunity to penetrate back into the blood and produce distant metastasis. Given the importance of blood and lymph in breast cancer metastasis, adequate concentrations of antitumor agents need to be maintained in both tissues to eliminate residual cells and prevent distant metastasis. The plasma (or blood) concentration time course of drugs used to treat breast cancer are well-characterized, but less is known about lymphatic drug concentrations over time. If there is poor penetration of chemotherapeutic agents into the lymph, this may explain persistent tumor recurrence and disease progression in breast cancer.

1.2.2 *In vivo models used to study breast cancer growth*

As researchers have developed a greater appreciation for the complexity of breast cancer pathophysiology, many preclinical models have been developed to mimic human breast cancer. Most of these models have been established in mice and are broadly categorized as (1) genetically engineered mouse models (GEMM), (2) cell-derived xenografts (CDX), (3) patient derived xenografts (PDX), and (4) syngeneic mouse models (Gould, Junttila, & de Sauvage, 2015). As the name implies, GEMMs are mice that have been genetically modified to over express tumor inducing genes or under express tumor suppressing genes. This leads to the spontaneous formation of tumors that feature a native tumor microenvironment, native vascular and stromal cells and an intact immune system, but these tumors lack heterogeneity as they are all driven by single point mutations. CDX models are immortalized human cancer cells that are transplanted into immune deficient mice. These models are well-characterized in the literature and can be used to study various human tumor types in mice but lack the intact immune component of breast cancer growth. PDX models are cancer cells directly harvested from a human patient and transplanted into an immunocompromised mouse. PDX models contain higher degrees of genetic heterogeneity compared to CDX models and may be more representative of human tumors but again lack the immune component observed in clinical breast cancer growth. Syngeneic mouse models are murine cancer cells that are transplanted into healthy mice. This model allows for controlled tumors to grow in their native environments in the presence of an intact immune system but are entirely murine (both tumor and stroma). Model selection is based on the hypothesis that is being tested; Table 1.1 summarizes the general strengths and weaknesses of each model.

After selecting the appropriate cell line and mouse background (immunocompetent versus immunocompromised), the next consideration for mouse models is the method of transplantation

(Rashid & Takabe, 2015). Ectopic transplantations are highly reproducible and consist of cells that are subcutaneously injected into the flank. Ectopic tumors can be precisely measured and tracked over time but typically display slower growth rates and are present in an unnatural stromal environment. Orthotopic transplantation is an alternative method where cancer cells are transplanted into their tissue of origin, typically the mammary fat pad for breast cancer. Orthotopic tumors grow in their native tissue and are often used to study spontaneous metastasis to distant organs. Finally, hematogenous models of breast cancer directly introduce cancer cells into the systemic circulation of mice by intravenous injection to study blood-based metastasis. Hematogenous models reproducibly form cancer nodule in the lungs and can recapitulate the transit of cancer cells through the systemic circulation. Intravenous administration of other types of cancer cells can also result in cancer nodule formation in the lungs due to the small size of the pulmonary capillary beds. However, hematogenous models are particularly useful for breast cancer due to the high prevalence of lung metastasis observed in the clinic. In general, 21 to 32% of the secondary tumors observed in metastatic breast cancer patients form in the lungs (Shibuya, 2011). Thus, hematogenous models are well-suited to study breast cancer.

With growing recognition that the lymphatics are involved with breast cancer metastasis, many mouse models for breast cancer metastasis are also used to investigate lymphangiogenesis, or the growth of new lymph vessels. Cancer cells have been shown to secrete vascular endothelial growth factors (VEGF), which promote the development of new blood (VEGF-A) and lymph (VEGF-C/VEGF-D) vessels inside of primary tumors (Padera et al., 2002). The development of new lymph vessels is considered a crucial step for cancer cell entry into the lymph. Surprisingly, studies have shown that while intra-tumoral lymphatic vasculature can be collapsed and non-functional, peritumoral lymph vessels are sufficient to allow for metastasis to occur (Y. He et al.,

2005). This observation is likely due to the dilation effect of VEGF-C/VEGF-D on collecting lymphatic vessels surrounding the sentinel lymph node (or primary draining lymph node from the tumor), which facilitates cell entry into the lymph (Thakkar & Mehta, 2011).

Mouse models of breast cancer metastasis are an invaluable tool to study the growth and metastasis of breast cancer. These models help elucidate the underlying physiological changes caused by cancer. In doing so, these models further highlight the importance of the lymphatic system. For example, the rapid association of lymphatic vessels with cancerous tumors may provide a novel route for the delivery of pharmacologic agents. Chemotherapy used to treat breast cancer is associated with significant off-target, systemic toxicity. If chemotherapy can target the lymph, it may reduce the systemic, off-target toxicity and still achieve cytotoxic effect in cancer cells. This dissertation will investigate the advantages of delivering two drugs, gemcitabine and paclitaxel, as a combination nanoparticle to breast cancer cells. It will also demonstrate the advantages of lymphatic-targeted drug delivery. However, in order to appreciate how combined delivery and lymphatic targeting may benefit gemcitabine and paclitaxel efficacy, it is important to understand the role of these two drugs in the overall treatment of breast cancer. Thus, the following section will provide a broad description of the current treatment approaches for breast cancer.

1.3 PRINCIPLES OF TREATMENT IN BREAST CANCER

For breast cancers diagnosed in a localized region (~90% of all cases), the main goal of treatment is to surgically remove the primary tumor. During surgical resection, assessment of local tissue with the aid of biopsies can reveal if cancer cells have migrated to the draining lymph nodes; the results guide future treatment plans. Local therapy to address cancer cells in regional lymph nodes can consist of surgical removal of the infiltrated lymph nodes or radiation therapy. Systemic

therapy is then used to eliminate any residual cells. Breast cancer subtype further guide the follow-up therapy to prevent metastatic recurrence. The following section will review the individual pharmacologic rationale behind specific drug classes used in each subtype of breast cancer and their role in overall treatment success.

1.3.1 *Pharmacologic basis for the treatment of ER/PR+ breast cancer*

Estrogen receptors (ER) are nuclear steroid receptors that act as ligand activated transcription factors. ERs exist as two isoforms: ERα and ERβ and both receptors play important roles in regular breast development. Activation of ERα occurs through binding of its endogenous substrate, estradiol, and the recruitment of coactivators to the gene promoters for transcription of genes associated with cell proliferation, inhibition of cell death, and new blood vessel formation (Kariagina, Aupperlee, & Haslam, 2008). This mechanism is a natural process in breast development and dysregulation of this pathway causes developmental aberrations and carcinogenesis. As a result, the overexpression (or over activation) of ERα results in uncontrolled cell proliferation and leads to the development of breast cancer. Since this pathway is endogenous to all breast cell development, dysregulation of this pathway accounts for the majority of breast cancers (70%). The progesterone receptor is also a nuclear steroid receptor that reflects ERα signaling (Daniel, Hagan, & Lange, 2011; Frasor et al., 2004). Interestingly, ERβ may act as a tumor suppressor gene and oppose the effects of ERα but the role of ERβ in breast cancer development is still unclear (Osborne, Wakeling, & Nicholson, 2004). Early lobular breast cancer has been shown to express both ERα and ERβ receptors, but ERβ receptors are lost in late stage lobular cancer (Nicholson et al., 1995). This may suggest that targeting the ERβ signaling pathway has a limited role in early stage disease. Nevertheless, there is still uncertainty behind ERβ

targeting and no ERβ agonists are used in the treatment of breast cancer. For that reason, this section will focus on ERα targeted drugs.

There are a number of pharmacologic agents that target the ERα signaling pathways to prevent breast cancer proliferation; they fall into 2 major categories: drugs that competitively inhibit the ERα or drugs that deplete the endogenous levels of estrogen. Selective estrogen receptor modulators (SERMs) are a group of molecules that can have both agonistic and antagonistic activity at the ERα in different tissues. In breast cancer cells, tamoxifen and raloxifene (two commonly used SERMs) compete with estradiol for binding to the ER (Simpson & Davis, 2001). This competitive inhibition of ERα signaling reduces cancer cell proliferation and prevents disease progression. Fulvestrant, a selective estrogen down regulator (SERD), also binds to the ERα similar to tamoxifen and raloxifene but has a significantly greater binding affinity for ERα (~40-fold greater than tamoxifen) (Pistelli, Mora, Ballatore, & Berardi, 2018). The fulvestrant-ERα complex is unstable and results in ERα degradation, a mechanism not observed with SERMs (Pistelli et al., 2018; M. Tan & Yu, 2007).

Aromatase inhibitors (AIs) target the ERα signaling pathway by interfering with the body's ability to produce estrogen from circulating androgens. After menopause, estrogen produced by the ovaries decreases and local levels of estrogen are generated by the aromatase enzyme present in various tissue such as the breast. In proliferative breast cancer, aromatase activity can be increased, and local levels of estrogen near the primary tumor can be increased (Harari & Yarden, 2000). By interfering with the formation of estrogen, AIs deplete the endogenous ligands necessary for the ERα signaling pathway and inhibit cancer cell growth. Some examples of aromatase inhibitors used in breast cancer include: letrozole and anastrozole (reversible inhibitors) and exemestane (irreversible inhibitor). As a point of clarification,

aromatase inhibitors are only effective at reducing levels of estrogen in women with post-menopausal ovaries. In pre-menopausal women, AIs can be used in women undergoing ovarian oblation or oophorectomy to reduce ovarian function but will not be effective in women with estrogen forming ovaries (Fuentes, Scaltriti, Baselga, & Verma, 2011). In general, approximately 2/3 of women diagnosed with breast cancer are above post-menopausal age and most patients are eligible for AI therapy.

An important distinction in hormone receptor targeted therapy is the availability of oral dosage forms. Tablets and capsules are convenient for patients, but medication adherence is crucial to maximally suppress the ERα signaling pathway and prevent cancer growth. Even with perfect medication adherence, oral drug dosing is subject to fluctuations in GI physiology that can affect dissolution or absorption. Additionally, orally administered medications undergo first-pass metabolism and P glycoprotein-mediated drug efflux in the gut and liver. These factors lower the systemic drug bioavailability after oral dosing and, in turn, the fraction of drug that can enter effect sites, such as the breast. In breast cancer patients, surgical resection of the primary tumor and radiation therapy also disrupt the local vasculature of the breast. Thus, it is possible that fluctuations in the systemic drug concentrations of orally administered SERMs and AIs can result in momentary instances of autocrine signaling of estrogen in the breast and contribute to cancer cell survival.

1.3.2 *Pharmacologic basis for the treatment of ERBB2+ breast cancer*

ERBB2, also known as HER2, is a membrane bound tyrosine kinase that is overexpressed in several cancers including breast cancer. Overexpression of ERBB2 promotes homo- or hetero-dimerization with other ERBB (1 through 4) receptors and dimerization with other receptors in activating cell proliferation pathways (Agus et al., 2002). There are a few key factors that make

the ERBB2 pathway particularly oncogenic: (1) ERBB2 has a relatively slow rate of endocytosis and can remain overexpressed on a cell surface for an extended period. (2) ERBB2 heterodimers have been shown to undergo recycling instead of degradation, and (3) activation of ERBB2 heterodimers persists due to the slow release of ligands from the complex (Franklin et al., 2004). These factors allow ERBB2 to stay present and active on the breast cancer cell surface but also makes these proteins attractive pharmacologic targets for the treatment of breast cancer.

Different therapeutic modalities are used to target ERBB2 including monoclonal antibodies, small molecule tyrosine kinase inhibitors, and antibody drug conjugates. The monoclonal antibodies, trastuzumab and pertuzumab bind to different extracellular domains of ERBB2 to mediate their effect. Trastuzumab binds to domain IV of ERBB2 that is not involved in heterodimerization (Sliwkowski et al., 1999). Pertuzumab, on the other hand, binds to domain II (a region associated with dimerization), and may sterically hinder heterodimerization of ERBB receptors. The net effect of either pertuzumab or trastuzumab binding to ERBB results in antibody dependent cell-mediated cytotoxicity and inhibition of tumor growth (J. Baselga et al., 2012; Scaltriti et al., 2009; Tolaney, 2014). The different binding domains of trastuzumab and pertuzumab allows both agents to be used in combination in achieving synergistic clinical effects (Collins et al., 2017; Widdison et al., 2006).

Targeting of ERBB2 to treat breast cancer is not only achieved through monoclonal antibodies, but also through small molecule kinase inhibitors such as lapatinib and neratinib. Both neratinib and lapatinib bind to the intracellular regions of ERBB receptors and prevent autophosphorylation and downstream effects. The main difference between the two drugs are their mechanism of inhibition and affinity for different members of the ERBB family. Lapatinib is a potent reversible inhibitor of ERBB1 (EGFR) and ERBB2 (HER2) and binding ERBB2 results in

decreased signaling in the P13K and MAPK pathways, pushing the cell towards apoptosis. Neratinib is an irreversible inhibitor of ERBB1 and ERBB2 but also ERBB4 and mediates the same inhibition of the P13K and MAPK signaling. Interestingly, lapatinib has been shown to stabilize HER2 expression on the cell surface and may synergize with trastuzumab therapy (Barok, Joensuu, & Isola, 2014), while neratinib decreases HER2 cell surface expression without the need for additional monoclonal therapy (Nakada, Sugihara, Jikoh, Abe, & Agatsuma, 2019).

The final modality used to target ERBB2 is the antibody-drug conjugates where the monoclonal antibody, trastuzumab, is used as a delivery vehicle for highly toxic agents such as emtansine and deruxtecan. Emtansine is a maytansine derivative that acts as a potent tubulin inhibitor. Early studies of maytansine showed that the compound was too toxic for use as chemotherapy in its free form. To mitigate those toxicities, future derivatives were conjugated to monoclonal antibodies to target cancer cells only (L. Chen et al., 2016). Emtansine is conjugated to trastuzumab through a non-cleavable thioether linker, which prevents the release of emtansine in the systemic circulation. After trastuzumab binds to ERBB2 and receptor mediated endocytosis occurs, proteolytic degradation of trastuzumab releases emtansine and causes cell death (van der Wall, Beijnen, & Rodenhuis, 1995). In a similar fashion, deruxtecan is a novel camptothecin analog that inhibits topoisomerase 1 and is chemically conjugated to trastuzumab with an enzymatically cleavable peptide linker. The release of trastuzumab deruxtecan also occurs through receptor mediated endocytosis. However, trastuzumab deruxtecan carries 8 deruxtecan molecules for every antibody, compared to trastuzumab emtansine which has a 3.5 to 1 drug to antibody ratio. This high loading capacity is thought to enable a bystander effect where cancer cells adjacent to the ERBB2+ cell will also experience cytotoxicity (Clemons et al., 1997; Weiss et al., 1990).

1.3.3 *Pharmacologic basis for the treatment of triple negative breast cancer*

TNBC does not express druggable, well-defined molecular targets; consequently, drugs targeted towards specific receptors such as ER, PR or ERBB2 are not effective. Chemotherapy inhibits actively replicating cells and has been generally proven to be effective in TNBC. Chemotherapy is often given in sequential, defined drug combinations which are a key treatment option for patients presenting with TNBC. By targeting various points in cancer cell replication, combination chemotherapy can maximize pharmacologic effect and prevent drug resistance. These combination regimens are typically composed of either anthracyclines or taxanes in combination with other cytotoxic drugs. As an example, anthracyclines (doxorubicin, epirubicin, daunorubicin) are used in combination with alkylating agents (cyclophosphamide, ifosfamide) and taxanes (paclitaxel, docetaxel) as a preferred regimen for post-surgical TNBC. Anthracyclines target topoisomerase II to cause cell cycle arrest in the G1 phase, alkylating agents damage DNA to cause cell death, and taxanes bind to microtubules to cause cell cycle arrest in the M phase. Alternative regimens can include the use of antimetabolites such as gemcitabine and capecitabine which act by blocking DNA replication. By targeting different points in cancer cell replication, the likelihood of cancer cell death is high, however, the cumulative toxicity to healthy tissue limits the effectiveness of these agents.

Extended use of anthracyclines results in heart failure due to the irreversible binding of anthracyclines to cardiolipin. This cardiotoxicity is lifetime dose-limiting and restricts the use of anthracyclines in late stage disease. Alkylating agents also have a number of dose-limiting toxicities including GI, hematopoietic, gonadal and pulmonary toxicities but these are more clinically manageable than the cardiotoxicity of anthracyclines (Feher et al., 2005). Taxanes are associated with neurotoxicity, hypersensitivity reactions and myelosuppression which can be dose-

limiting but can also be managed clinically (Velasco & Bruna, 2015). Antimetabolites generally have the safest toxicity profile compared to other agents, but they have limited efficacy in monotherapy (Blackstein et al., 2002). All of these therapeutic agents are highly potent and have the ability to eliminate cancer cells. Unfortunately, these drugs broadly distribute into healthy tissue. Many of the adverse events listed above are the result of higher drug burden in off-target tissues compared to cancer cells. If these agents could be directed towards cancer cells exclusively, breast cancer treatment could be improved but this is not achievable with the current clinical infusion protocols.

1.4 CURRENT GAPS IN PHARMACOLOGIC TREATMENT OF BREAST CANCER: BIOLOGICAL MECHANISMS FOR DISEASE PROGRESSION

The previous section outlines the various pharmacologic approaches used to target different subtypes of breast cancer. Despite all these available therapies, drug resistance and disease progression continue to persist as a major issue in breast cancer. Distant recurrent breast cancer is widely regarded as incurable and occurs in ~30% of all patients, despite the high overall 5-year survival rate of breast cancer (~90%). This suggests that pharmacologic treatment in breast cancer is effective at suppressing cancer cells, but current treatments cannot eliminate them entirely. This gap in breast cancer treatment could be due to a number of factors including acquired drug resistance, poor drug exposure in tissues or cells of interest, or off-target toxicity associated with treatment. The following section will identify biological mechanisms within subtypes of breast cancer cells that leads to disease progression and use of drug combinations to overcome those mechanisms.

1.4.1 *Biological mechanisms for disease progression in ER/PR+ cancer*

As the understanding of ER action has evolved over the years, the complexity of ER signaling has shed light on mechanisms of drug resistance. Breast cancer treated with anti-estrogen therapy can proliferate through alternate growth pathways or retain activity through the ER pathway in the presence of anti-estrogen therapy. For example, ER+ breast cancers that overexpress epidermal growth factor receptors (ERBB family) can undergo loss of ER expression and proliferate through the ERBB pathway, causing the tumor to become hormone independent and hormone therapy ineffective (McDonnell & Wardell, 2010; Osborne et al., 2003; C. L. Smith, Nawaz, & O'Malley, 1997). Alternatively, increased levels of specific coactivator proteins like AIB1 can shift the effect of the tamoxifen-ER complex from antagonism to agonism, leading to drug resistance (Hall & McDonnell, 2005; Johnston, Martin, Head, Smith, & Dowsett, 2005). This effect is due to the large role transcriptional co-regulators have on ER gene expression (Bunone, Briand, Miksicek, & Picard, 1996). The activation of the ER pathway is dependent on the recruitment of coregulator proteins and differences in protein levels (such as AIB1) in the cell cytoplasm or nucleus can change the effects of ligand binding to ER. The shift from antagonism to agonism effects of tamoxifen as a function of co-regulator protein expression is likely what causes the tissue specific effects observed in tamoxifen therapy (IE: breast vs ovary) (Preusser et al., 2018). The ability of cancer cells to utilize other growth pathways and the sensitivity of the ER pathway to other co-regulatory proteins are driving factors behind both intrinsic and acquired drug resistance.

To overcome these mechanisms, combination therapy is often used. For example, the combination of the aromatase inhibitor, letrozole, with the selective estrogen receptor down regulator, fulvestrant, utilizes two independent mechanisms to target hormone responsive cancer

cells (Pan et al., 2017). Letrozole reduces the endogenous levels of estradiol required to bind to the ER complex and cause cell proliferation. Fulvestrant binds to the ER and reduces the absolute levels of the receptor. By using both drugs, the substrate and the receptor are inhibited, and cell proliferation through the ER pathway does not occur. Although this approach is effective, it does not prevent the activation of alternative growth pathways and drug resistance still emerges (Pernas & Tolaney, 2019). Currently, the most effective combination therapy is letrozole with palbociclib, a CDK4/6 inhibitor. The CDK4/6 proteins are highly conserved in ER/PR+ breast cancers and are downstream from growth hormone signaling (José Baselga et al., 2016). Depletion of endogenous estradiol through letrozole and inhibition of CDK4/6, prevents signaling through the ER pathway and promotes cell death. Unfortunately, even with the best available options, cancer recurrence and progression remain a life-long issue (Lu, Zi, Zhao, Mascarenhas, & Pollak, 2001).

1.4.2 *Biological mechanisms for disease progression in ERBB2+ cancer*

Targeting ERBB2 has made significant improvements in progression free and overall survival in ERBB2+ breast cancer patients. However, most patients will still have disease progression and metastasis to the brain (Blackwell et al., 2012). Disease progression in ERBB2+ cancer cells is mediated through mechanisms similar to ER/PR+ resistance mechanisms. ERBB signaling can be activated downstream from the point of inhibition or an alternative growth pathway can be present. Specifically, the P13K pathways can be activated by the loss of PTEN expression, a signaling event downstream from ERBB2 dimerization (Canonici et al., 2013). The incomplete blockade of ERBB2 and compensatory mechanisms by receptors in the ERBB family (such as ERBB3) can also lead to resistance (Blackwell et al., 2012). The activation of other signaling receptor tyrosine kinases such as IGF-1 has also been associated with ERBB2+ drug resistance (Breslin, Lowry, & O'Driscoll, 2017).

To overcome these mechanisms, several combination approaches are used. One approach has been to use both trastuzumab and pertuzumab in combination to maximize ERBB2 blockade at the cell surface. In doing so, trastuzumab directly blocks the ERBB2 receptor while pertuzumab prevents heterodimerization with any compensatory family receptors such as ERBB3 (Widdison et al., 2006). Alternatively, trastuzumab and lapatinib have been used to concomitantly inhibit ERBB2 on the cell membrane (trastuzumab) and intracellularly (lapatinib) (Dhillon, 2014). There is some evidence to suggest that the irreversible binding of neratinib to ERBB2 can overcome trastuzumab resistance, however, resistance to neratanib will also develop (Breslin et al., 2017). It is important to note that ERBB2 targeted therapies are given in conjunction with conventional chemotherapy to pre-emptively counter the rapid emergence of drug resistance. Thus, antibody-drug conjugates with trastuzumab loaded with either emtansine or deruxtecan is in essence a combination approach where the chemotherapy and monoclonal antibody are administered as a single entity. Both trastuzumab emtansine and trastuzumab deruxtecan are only used in patients that have previously received ERBB2 targeted therapies with conventional chemotherapy.

1.4.3 *Biological mechanisms for disease progression in TNBC cancer*

Due to the various pharmacologic agents used in TNBC (IE: alkylating agents, topoisomerase inhibitors, tubulin inhibitors and antimetabolites), the mechanisms of resistance are diverse. In general, the major cellular mechanisms that lead to drug resistance and disease progression are based on increased drug inactivation and increased drug efflux. In addition to the cellular mechanisms that can lead to drug resistance, off-target toxicity in patients undergoing chemotherapy can lead to disease progression as patients can no longer bear the burden of additional treatment.

Many of the drugs used in TNBC require metabolic activation in order to perform their pharmacologic function. For example, the nucleoside analogue gemcitabine is sequentially phosphorylated to gemcitabine-triphosphate (gem-TP) before being integrated into DNA and causing chain termination. The enzyme responsible for the first phosphorylation event of gemcitabine is deoxycytidine kinase (dCK) and dCK activity is generally accepted as the limiting factor in gemcitabine therapy. dCK has been shown to saturate when plasma levels of gemcitabine are around 15-20 μM and dCK activity is strongly correlated to gemcitabine sensitivity (R. Grunewald, Abbruzzese, Tarassoff, & Plunkett, 1991; Peters et al., 2007). Interestingly, the competing inactivation of gemcitabine is also strongly correlated with gemcitabine effect. Most of gemcitabine clearance is driven by metabolic inactivation to dFdU by cytidine deaminase (CDA). This clearance pathway accounts for 90% of the fraction metabolized for gemcitabine, with the remaining clearance occurring through renal filtration. In comparison to the activation pathway of dCK, the metabolic inactivation of gemcitabine appears to saturate at much higher concentrations. In one pharmacokinetic study, linear plasma pharmacokinetics of gemcitabine was observed at doses up to 4000 mg/m^2; however, activated gem-TP levels peaked at 960 mg/m^2 and higher dosing did not increase measured gem-TP levels (R. Grunewald et al., 1991; Ralf Grunewald et al., 1990). Thus, any mutations that shift the relationship between gemcitabine activation and inactivation (i.e., dCK downregulation or CDA overexpression) can lead to drug resistance. Alternatively, reduced CDA expression is also associated with increased toxicity (Mercier et al., 2007).

Another mechanism for TNBC drug resistance is the active efflux of chemotherapy from breast cancer cells. This phenomenon is mediated by ATP-Binding Cassette (ABC) transporters specifically P-glycoprotein (P-gp) and breast cancer resistance protein (BCRP). There are other

ABC transporters that cause multi-drug resistance, such as multi-drug resistance associated protein 1 (MRP1) and lung resistance protein (LRP), but their expression has limited relevance in breast cancer. P-gp is an extensively studied ATP-dependent efflux pump that transport several drugs used to treat breast cancer including doxorubicin, paclitaxel, and vinblastine (B. Tan, Piwnica-Worms, & Ratner, 2000). In healthy tissue, P-gp is expressed in the GI, kidneys, liver and blood brain barrier and plays an important role in governing the oral absorption of xenobiotics (B. Tan et al., 2000). More importantly, P-gp is expressed in ~40% of breast cancers and is shown to be inducible by radiation therapy (Ng, Lam, Ng, Kwong, & Sham, 1998). An increase in P-gp expression is associated with drug resistance and suggests that P-gp efflux can prevent chemotherapeutic agents from binding to their intracellular targets. BCRP is another transporter protein that acts in a similar manner to P-gp to cause drug resistance. BCRP can be upregulated in breast cancer cells and can efflux topoisomerase I inhibitors, methotrexate and anthracyclines under certain conditions (Austin Doyle & Ross, 2003).

In contrast to ER/PR or ERBB2 targeted agents, disease progression after chemotherapy is typically due to reduced drug exposure and residence time at the intracellular target leading to reduced effect. Off-target toxicity and systemic adverse events also limit the achievable concentration of drugs in cancer cells. As such, combination chemotherapy is utilized with the rationale that cancer cells are unlikely to have multiple resistance mechanisms to overcome two different drugs targets. By using combination therapy, lower individual drug dosing can be administered to achieve a greater effect (although the total dose is still high). For example, in the case of gemcitabine and paclitaxel combination therapy, upregulation of P-gp can enable increased efflux of paclitaxel and likely cause drug resistance in monotherapy. However, it would be less likely for a cancer cell to have both increased efflux of paclitaxel (upregulated P-gp) and

increased metabolism of gemcitabine (upregulated CDA) in the same cell. Based on this rationale, combination chemotherapy would likely overcome drug resistance. Unfortunately, drugs used in chemotherapy display varying disposition, clearance mechanisms and plasma concentration time courses. Thus, the synchronization of combination drugs in target breast cancer cells after intravenous administration is unlikely. Additionally, with the use of combination chemotherapy compounds the toxicological burden placed on the body and adverse events may limit the effective doses that patients can receive.

1.4.4 *Summary of biological factors leading to disease progression*

Across the various subtypes of cancer, drug resistance, off-target toxicity and disease progression continue to be a major issue. In all forms of breast cancer, combination therapy has a role in addressing drug resistance, but cancer cells are incredibly adept at altering signaling pathways and developing intracellular mechanisms to prevent drugs from reaching their targets. Cancer cells can also develop resistance mechanisms to counteract the antitumor effects of drugs. For example, DNA repair processes can be upregulated in cancer cells to overcome the cytotoxic effect of DNA alkylating agents. Physiological factors can also play a role in causing drug resistance by limiting drug exposure in sites of effect. For example, breast cancer cells invade through the lymphatic and circulatory systems. Drug exposure in the systemic circulation is well established, but there may be limited penetration of drugs into the lymph where cancer cells can grow. Off-target toxicity further limits the total dose that can be safely administered intravenously to patients and reduces the maximum achievable concentrations of drug in target tissues where cancer cells may reside. Under these conditions, the therapeutic levels required to kill cancer cells may not be achieved in tissues like the lymph, allowing persistent cancer cells to grow.

Considering the various pharmacologic targets in breast cancer and the resistance mechanisms that occur from treatment, there is a clear distinction between targeted (ER/PR, ERBB2) and untargeted (chemotherapy) drug resistance. The pharmacology of targeted agents can change as cancer cells shift from one signaling pathway to another. When resistance to ER/PR or ERBB2 targeted agents occur, the drug can still engage their target receptors, but the cell proliferates through another pathway. In contrast, the pharmacology of chemotherapy is relatively stable over time and drug binding to target proteins will generally retain cytotoxic effect. Disease progression from chemotherapy is more due to resistance mechanisms preventing drugs from reaching their intracellular targets or from the patient suffering too many adverse events. In principle, we can overcome those limitations by specifically delivering combination chemotherapy to target cancer cells instead of healthy tissue. This approach can be demonstrated in a mouse model that recapitulates the clinical treatment of breast cancer to improve the translation of the concept and potentially overcome the current gap in MBC treatment.

1.5 STRATEGIES TO OVERCOME DRUG INSUFFICIENCIES AND IMPROVE CANCER CELL DRUG EXPOSURE

The intent of targeted drug delivery systems is to concentrate drugs in tissues and cells of interest while sparing healthy organs from unnecessary exposure. If designed with appropriate fit-for-purpose intent, targeted drug delivery systems can overcome drug insufficiencies. For a targeted drug delivery system to transport drugs from an injection site to specific cancer tissues and produce pharmacologic action, a number of criteria must be considered and achieved. The carriers should be engineered to have precise characteristics such as size, shape, surface charge and composition to produce specific effects such as defined distribution, exposure and clearance profile *in vivo*. Due to these additional characteristic requirements and demands, the formulation

of drug delivery systems is more complex than conventional dosage forms and requires more process control. Despite these challenges, some drug delivery systems have been developed and proven as useful strategies to overcome drug insufficiency with acceptable safety profiles. The purpose of the following section will be to summarize the current pharmaceutical approaches for drug targeting of chemotherapy based on drug delivery systems to treat breast cancer. The challenges and benefits associated with each drug delivery system will be discussed before providing the rationale for the need to develop a novel drug delivery system that is targeted and capable of simultaneously delivering multiple chemotherapeutic agents to tissues and cells at higher concentrations and longer duration.

1.5.1 *Approaches to enable drug delivery to breast cancer cells*

Modification of drug disposition and clearance through pharmaceutical carriers is an important strategy in delivering therapeutic agents to breast cancer cells versus healthy cells. Pharmaceutical carriers are typically nano- to micron- sized particles that can circulate in the systemic circulation and distribute into cancer tissue from leaky vasculature formed around tumors (a phenomena known as the enhanced permeation and retention effect or EPR) (Golombek et al., 2018). Examples of these carriers include liposomes, polymeric nanoparticles, dendrimers and antibody drug conjugates. In general, the rationale for associating drugs to particles is that particle-bound drug will have prolonged residence in the systemic circulation with a limited free fraction of drug. The reduced free fraction of drug from particle binding thus results in less off-target toxicity. As particle-bound drug continues to circulate in blood, accumulation in tumors can be achieved through different approaches such as active targeting or EPR.

1.5.1.1 Liposomes

Liposomes are spherical vesicles composed of phospholipids with a bilayer structure similar to cell membranes. Due to their aqueous core and lipid shell, liposomes have been used to incorporate both hydrophilic and hydrophobic drugs. In drug delivery, liposomes are the most studied and clinically successful nanoparticle system. For example, the pegylated liposome, Doxil, encapsulates the anthracycline doxorubicin to target various types of solid tumors. The major limitation in anthracycline therapy is the irreversible cardiotoxicity caused by binding to cardiolipin in the heart. Although the lifetime dose limitation for liposomal doxorubicin is the same as conventional doxorubicin, there is evidence to suggest that encapsulation reduces the cardiotoxicity by limiting the exposure of free doxorubicin to cardiac tissue (O'Brien et al., 2004). In addition, liposomal doxorubicin has been shown to localize in Kaposi's Sarcoma lesions 10-fold greater than conventional doxorubicin (Northfelt et al., 1996). By enabling a higher concentration of doxorubicin in the sarcoma lesions at the same dose as conventional doxorubicin, Doxil may have a greater pharmacologic effect against those cells and overcome drug resistance.

Liposomes are one of the most well-studied drug carrier systems and have demonstrated application in the clinic. However, there are also limitations to this drug delivery system. Depending on the lipid composition, liposomes can be associated with extensive hepatic and splenic uptake. For example, large (378 nm) and small (113 nm) liposomes were intravenously administered to mice and after 4 hours, 93% of large liposomes and 67% of small liposomes were recovered in the liver and spleen (Hu et al., 1996). Pegylated liposomes can reduce the splenic and hepatic uptake of liposomes for a single dose, but accelerated blood clearance is observed after multiple dosing (Ishida et al., 2005). Many studies have incorporated active targeting ligands to the surface of liposomes, but this approach has yet to be tested in the clinic. The hepatic/splenic

uptake of liposomes remains as a major barrier to liposomal targeted chemotherapy delivery and further study is required to optimize these drug delivery systems.

1.5.1.2 Polymeric Nanoparticles

Another drug carrier used to enable cancer targeting is polymeric nanoparticles made of amphiphilic copolymers. When placed in aqueous solution, polymers can self-assemble to form a hydrophobic core to stabilize water insoluble drugs. Polymeric nanoparticles can be calibrated based on the length of the monomers and polymer residues can be used as anchor points for covalent conjugation to improve stability. For example, CT-2103 is a polymer-drug nanoparticle that conjugates hydrophobic paclitaxel to water soluble, poly-L-glutamic acid polymers. Poly-L-glutamic acid is biodegradable and is broken down to glutamic acid. Chemical conjugation of paclitaxel occurs at the 2'-hydroxyl position, which is necessary for tubulin inhibition, and assures that conjugated paclitaxel will not have effect (Singer et al., 2005). Preclinical studies show that polymer-bound paclitaxel produces a 5-fold greater tumor AUC compared to conventional paclitaxel (Chun Li et al., 2000). Additionally, polymer-bound paclitaxel significantly increases aqueous solubility of the paclitaxel dosage form. Conventional paclitaxel is solubilized in a Cremophor EL/Ethanol co-solvent that is associated with significant hypersensitivity reactions (Gelderblom, Verweij, Nooter, & Sparreboom, 2001). By circumventing the need for these excipients, polymer-bound paclitaxel also reduces the toxicity of paclitaxel treatment and allows a higher dose to be administered. By administering a higher dose of drug, drug resistant cells can be eliminated without causing undue burden to the rest of the body. In addition to CT-2103, many other polymeric nanoparticles have advanced into clinical studies and show great promise.

Many polymeric nanoparticles have advanced to clinical studies but face similar biological barriers as liposomes. For example, a mass balance study of CT-2103 administered IV produced

an 8-fold greater paclitaxel AUC in the liver compared to the primary tumor in mice (C. Li et al., 2000). In addition to hepatic and splenic uptake, very small polymeric particles (<10 nm) can be passively filtered through the glomerulus which may present an additional barrier to tumor targeting. Surprisingly, a recent study demonstrated that even large polymeric particles (~400 nm) composed of PLGA-PEG could accumulate in the kidneys through active endocytosis by peritubular endothelial cells (R. M. Williams et al., 2015). This effect was not related to the surface charge of the particle and highlights the importance of understanding the biodistribution of drug carriers to enable tumor targeting. If renal accumulation were to occur, it could pose a potential toxicological effect from both the free drug and the polymeric particle.

1.5.1.3 Dendrimers

Dendrimers are macromolecules that are synthesized by sequential chemical reactions to form "generations" (referred as G0, G1, G2) of branches originating from a central core. Each sequential addition of a generation produces a radiating, well-defined, spherical morphology branching from the central core. Dendrimer size can be precisely controlled, and the surface properties of dendrimers are easily functionalized to produce highly monodisperse particles. The precision with which dendrimers can be modified allows novel approaches to targeting such as covalent attachment of monoclonal antibodies (Marcinkowska et al., 2018). Dendrimer synthesis is generally achieved through either a diverging method or converging method (Abbasi et al., 2014). The diverging method begins with a central core to which sequential arms are added in a step-wise fashion. The converging method pre-assembles the exterior arms of the dendrimer and covalently attaches them to the core as a final step. The flexibility through which dendrimers can be synthesized has led to the development of diverse structures such as block dendrimers, heterobifunctional dendrimers, and core-functionalized dendrimers (Sowinska & Urbanczyk-

Lipkowska, 2014). Although there is great potential for dendrimers, the ideal linkers, size and *in vivo* characteristics of dendrimer drug conjugates are still being identified in preclinical species and there has been limited clinical translation for this drug carrier (Kojima, 2015; Longmire, Ogawa, Choyke, & Kobayashi, 2011; Luo et al., 2012). Early biodistribution studies have shown that dendrimers can distribute into the kidney, liver and spleen. Kidney accumulation of dendrimers is thought to occur through electrostatic interactions between the cationic exterior of dendrimers and the negative charge of the glomerular basement membrane (Mager et al., 2012; Okuda, Kawakami, Akimoto, et al., 2006; Okuda, Kawakami, Maeie, et al., 2006). Pegylation of dendrimers can minimize this interaction and reduce renal accumulation (Okuda, Kawakami, Maeie, et al., 2006). Dendrimers are also known to distribute into pancreas to the same extent as the liver and spleen, which may represent a toxicological risk. Dendrimers enter cells through endocytic pathways and some data suggest that excess endocytosis of dendrimers may lead to hepatic toxicity (Duncan & Izzo, 2005; Roberts, Bhalgat, & Zera, 1996). Dendrimers are a relatively new drug delivery system and the specific physical properties that affect biodistribution and clearance of these macromolecules are still being defined. Once these properties are optimized, dendrimers may be a relevant strategy for drug delivery but the current biodistribution profile (accumulation in kidney, liver, spleen and pancreas) and off-target toxicity risk limits their application in clinical treatment.

1.5.1.4 Anti-body Drug Conjugates

Although previously addressed in the ERBB2+ targeted therapy section, anti-body conjugates (ADC) also constitute a form of targeted drug delivery. By covalently linking cytotoxic drugs to antibodies, ADCs reduce distribution to healthy tissue and selectively target cancer cells. After binding to target receptors and undergoing receptor mediated endocytosis, drug can be

released intracellularly for effect. Recently, clinical success with monoclonal ADCs for the treatment of various cancers (such as Kadcyla for ERBB2+ breast cancer and Adcetris for CD30+ lymphomas) has demonstrated the value of this approach in targeted drug delivery. This clinical success was achieved through significant effort and optimization. For example, the earliest generations of ADCs had limitations such as immunogenicity and relatively low *in vivo* stability. Gemtuzumab ozogamicin (GO) is an ADC designed to deliver highly toxic calicheamicin to CD33+ leukemia cells. Although effective and capable of achieving complete remission in 15-20% of patients with relapsed disease, GO is associated with major toxicities including myelosuppression and hepatoxicity (Giles, 2002). These toxicities are likely related to the (relatively) unstable linker between calicheamicin and gemtuzumab, with almost 50% of the drug released after 48 hours in mice (Doronina et al., 2003; Ho & Chien, 2014). As ADC technology has matured, the trend has shifted towards utilizing more stable linkers that can carry more potent payloads (such as those used in Kadcyla) (Bargh, Isidro-Llobet, Parker, & Spring, 2019). A focus on several key factors such as target selectivity, the drug-antibody linker, product homogeneity and finding the right patient population has resulted in clinical success and approval of multiple ADCs for the treatment of cancer.

ADCs can overcome the limitations of broadly toxic chemotherapy by using specific monoclonal antibodies targeted to receptors on cancer cells to preferentially deliver potent, cytotoxic drugs. In breast cancer, the well-defined signaling pathways such as ERBB2 present a validated molecular target for ADCs (as used in Kadcyla). Unfortunately, the most aggressive form of breast cancer, TNBC, does not have clear molecular targets. The pathogenesis of TNBC is least understood and while certain biomarkers have been identified (PD-L1, BRCA, PARP), there is not a single receptor that is unilaterally overexpressed in this breast cancer subtype. Thus, the

development of ADCs in TNBC could benefit from the identification of ubiquitous molecular targets in TNBC that have not yet been discovered.

1.5.1.5 Limited synchronization of combination drugs from single drug carriers

The targeted drug delivery approaches mentioned above highlight the potential to improve chemotherapy in breast cancer treatment. By associating with nanoparticles, cytotoxic drugs can overcome toxicity limitations, solubility limitations and may even partially avoid MDR efflux by undergoing receptor mediated endocytosis (Chun Li et al., 2000). However, most pharmaceutical drug carriers in clinical studies are single-drug delivery systems and face significant biological barriers before reaching target tumors. If a single drug delivery system avoided sequestration in healthy organs and accumulated in tumors, it may improve the efficacy (or decrease toxicity) of that drug but combination therapy would require a separate infusion. Unfortunately, sequential infusions will likely limit the synchronicity of multiple drugs in target cells. An ideal pharmaceutical carrier would target and deliver a clinically relevant combination of chemotherapeutic drugs to target cells to maximize cytotoxic effect. Given this limitation, there is an active interest in developing combination nanoparticles that can deliver multiple active drugs with a single pharmaceutical carrier.

1.5.2 *Combination nanoparticles in the treatment of cancer*

Currently, there is one clinically approved combination nanoparticle used for the treatment of acute myeloid leukemia. Vyxeos expands on the liposomal approach and encapsulates cytarabine and daunorubicin to allow both to circulate in plasma at a fixed ratio for an extended period of time. The liposomal properties of Vyxeos enables a targeted effect of both drugs towards important tissues associated with AML (bone marrow, spleen). This improved distribution into the bone marrow and spleen produces a greater effect than the conventional cytarabine/daunorubicin

regimen (Mayer et al., 2014). Although effective against liquid tumors, Vyxeos has not been tested in solid tumors such as breast cancer. Based on tissue distribution of the liposome, the combination liposomal approach demonstrated by Vyxeos may not be as effective in targeting solid tumors. For AML, bone marrow accumulation of Vyxeos is beneficial because the bone marrow is the site of effect. However, the site of effect in breast cancer is the solid tumor or individual cancer foci present in the breast or lymph. In this scenario, extensive accumulation in the bone marrow can be a risk for myelosuppression with no therapeutic advantage. Extensive distribution into the spleen would also limit the fraction of dose available for targeting to the solid tumor. Furthermore, the manufacturing process required to make Vyxeos is complex and specifically optimized for daunorubicin and cytarabine (Tardi et al., 2009). This manufacturing process may not directly apply to other drug combination regimens, especially considering the chemically diverse drugs used in breast cancer. The ability to stabilize and associate hydrophilic and hydrophobic drugs in a single particle remains elusive. Despite these challenges, the clinical development of Vyxeos clearly highlights the potential for combination nanoparticles to address the current limitations in cancer treatment by co-delivering chemotherapy to tissues of interest.

The combination nanoparticle approach has also gained attention in the treatment of solid cancers (such as breast cancer), but not all combination regimens are appropriate in the treatment of late stage metastatic breast cancer. As mentioned earlier, anthracyclines suffer from life-time dose limiting cardiotoxicity and even encapsulation in liposomes (as seen with Doxil) does not completely eliminate that toxicity. Consequently, taxane-based regimens like gemcitabine and paclitaxel have a greater role in late stage disease because they do not have any lifetime dose-limitations like anthracyclines. Based on the pharmacokinetic properties of gemcitabine and paclitaxel, this combination regimen will likely benefit from a combination nanoparticle approach.

Gemcitabine is a potent antimetabolite that undergoes rapid metabolism by cytidine deaminase, an enzyme expressed ubiquitously in healthy tissue. Rapid metabolism may limit the amount of active gemcitabine that can reach cancer cells before inactivation. Paclitaxel is a potent taxane but is a substrate for P-gp efflux, which may reduce the intracellular concentration of paclitaxel in cancer cells. Following a standard clinical infusion protocol, the time interval during which both drugs are present above their minimum inhibitory concentration in plasma is estimated to only be around 2 hours (Rowinsky, Jiroutek, Bonomi, Johnson, & Baker, 1999; L. R. Wang, Liu, Huang, & Xu, 2007). Thus, the time interval where GT is synchronized in cancer cells will potentially be even smaller than that of plasma. By binding both drugs to a targeted drug combination nanoparticle, GT can have greater synchronized exposure in cancer cells. With both drugs available intracellularly, the individual pharmacologic effects of gemcitabine (DNA chain termination) and paclitaxel (tubulin inhibitor) can be potentiated and the likelihood of cancer cells escaping cell death will decrease. If GT nanoparticles can distribute into tissues of interest (such as the lymph and blood) while avoiding healthy tissue, then this approach could also reduce off-target toxicity observed with the free drug. A schematic representation of this concept is presented in Figure 1.1.

The coordinated delivery of GT as a single drug combination nanoparticle to eliminate metastatic cancer cells is a compelling project to pursue. However, the co-formulation of water soluble (gemcitabine, LogP= -1.4) and water insoluble (paclitaxel, LogP=3) drugs together is challenging. To our knowledge, there are only a few published reports that have achieved the co-formulation of GT for breast cancer (Aryal, Hu, & Zhang, 2010; Dong et al., 2018; Lei et al., 2019; Meng et al., 2015; Noh et al., 2015; J. Zhang et al., 2018). In those studies, GT are chemically conjugated to polymers, encapsulated in monophosphate form or self-assembled to achieve drug loading. Each study notes an improved effect of GT combination nanoparticles versus free GT in

models of cancer and highlights the potential for GT co-delivery. Unfortunately, many of the processes used to synthesize these particles would be difficult to translate into a clinical product. For example, lipid-calcium-phosphate particles were used to co-formulate gemcitabine and paclitaxel in a 16-step process. These particles were very effective at inhibiting tumor growth, but the complex synthesis process and extensive use of organic solvents/surfactants (cyclohexane, THF, IGEPAL Co-520) would limit the large-scale manufacturing of this product. Thus, a new strategy is needed to make drug combination nanoparticles that can be easily scaled for clinical development.

1.6 A NOVEL APPROACH TO COMBINATION NANOPARTICLES: TARGETING CHEMOTHERAPY TO BREAST CANCER CELLS IN THE BLOOD AND LYMPH

The Ho laboratory has recently developed a novel method to stabilize hydrophobic and hydrophilic drugs together in lipid nanoparticles. Chemically distinct drugs and lipid excipients are combined to form drug combination nanoparticles (DcNPs). Controlled solvent removal is used to trap drugs with lipid excipients in the powder form, which can then be suspended in aqueous buffer to yield uniform particles after size reduction. This concept was initially proven with hydrophilic and hydrophobic HIV drugs stabilized in lipid excipients and tested subcutaneously in non-human primates (NHPs). In early iterations, DcNPs were thought to be structurally similar to liposomal products; however, DcNPs exhibited unique *in vivo* characteristics that are not typically associated with standard liposomes. DcNPs were able to target the lymphatic tissue of NHPs and produce long-acting plasma circulation after subcutaneous injection (Freeling, Koehn, Shu, Sun, & Ho, 2015; Koehn et al., 2018; Kraft et al., 2017; McConnachie et al., 2018; Perazzolo et al., 2018). Additionally, DcNP technology appears to be compatible with a wide range of constituent drugs, including tenofovir (logP = -1.6), lopinavir (logP = 4.7), atazanavir (logP =

4.5) and ritonavir (logP = 5.2). As the development and optimization of DcNPs continued, it became evident that the particles are very different from other lipid based formulations (such as liposomes). Structural analysis revealed that DcNPs have a discoid morphology with no evidence of membrane bilayers. The unique structure of DcNPs likely facilitates the binding of chemically distinct compounds together and enables stable, long acting circulation *in vivo*. DcNP manufacturing is also relatively simple and easy to scale, which has enabled sizable studies in NHPs. These results highlight the potential for novel DcNP technology to extend beyond what has been accomplished with current delivery approaches.

If DcNP technology can stabilize chemically distinct G & T in a single nanoparticle for use as an injectable dosage form, it may be able to overcome the current limitations in developing combination drug delivery systems for the treatment of breast cancer metastasis. GT DcNPs can synchronize both drugs in target cancer cells and maintain their concentrations above therapeutic levels for an extended period of time. The higher potency of both drugs (GT) in target cancer cells could translate into a lower overall dose needed and expand the useful therapeutic dose range without causing off target toxicity. If cancer cells have migrated into the lymphatic system, the *in vivo* stability and size of GT DcNPs can enable lymphatic targeting. By distributing and accumulating in the sentinel lymph nodes, GT DcNPs could eliminate those cancer cells in the lymph. Alternatively, long acting plasma circulation of GT DcNPs could eliminate cells in the blood. By combining gemcitabine and paclitaxel together as an optimized and stable DcNP and delivering them preferentially to cancer cells that reside in the lymph or blood capillaries, this technology could make an outstanding impact on breast cancer treatment and potentially eliminate cancer on its core of metastatic spread. Based on this compelling rationale, the overarching hypothesis of this thesis is as follow.

1.7 HYPOTHESIS AND AIMS

The overall hypothesis of this thesis research is that the coordinated and enhanced delivery of gemcitabine and paclitaxel together as a single combination particle to breast cancer cells will reduce cancer cell growth and prevent disease progression. The following aims are designed to test this hypothesis:

Aim 1: Design, develop, characterize and select stable, GT drug combination nanoparticles that are suitable for *in vivo* studies

Aim 2: Develop and evaluate an *in vivo* model of late stage breast cancer metastasis in the lungs, and evaluate the effect of DcNP on GT combination therapy

Aim 3: Develop and evaluate an *in vivo* model of early stage breast cancer metastasis in the regional lymph and evaluate the effect of DcNPs on GT drug combination therapy

The following dissertation chapters will begin with developing a physical understanding of how controlled solvent removal can stabilize chemically diverse HIV drugs with lipid excipients in powder form (Chapter 2). The insight gained from the development of anti-HIV DcNP powders will be applied towards the development of novel anti-cancer DcNP powder composed of gemcitabine and paclitaxel (Chapter 3). The subsequent chapter will describe the characteristics of novel GT DcNPs such as size, shape and association efficiency and pharmacokinetic studies will be used to understand the effect of DcNPs on GT tissue distribution and tumor targeting (Chapter 4). The next chapter will detail the development of an *in vivo* model of late stage breast cancer metastasis to the lungs and demonstrate the effect GT DcNPs have after IV administration (Chapter 5). Finally, subcutaneously administered GT DcNPs will demonstrate a lymphatic based targeting effect against early developing tumors to capture early stage metastasis (Chapter 6).

The current treatment options in breast cancer can meaningfully increase time of survival but disease remission and progression to metastasis is a constant concern. In women treated with targeted agents, breast cancer has been shown to recur on average after 17 years of disease-free status (Dent et al., 2007). In contrast, TNBC patients that are treated with chemotherapy alone have a higher risk of recurrence within 1-4 years; after 8 years of disease-free status, disease remission is no longer expected (Dent et al., 2007; Liedtke et al., 2008). The potency and ability for chemotherapy to eliminate cancer cells is supported by decades of clinical and experimental results. However, the role of chemotherapy as a cure for cancer is limited by toxicity. The adverse events associated with chemotherapy can reduce patient quality of life and lead to sub-optimal dosing, which may explain some of the higher early recurrence rates in TNBC patients. The purpose of this dissertation is to target GT at advancing breast cancer cells and eliminate those cells to prevent disease progression. To do so, a novel combination nanoparticle will be developed and tested in preclinical models. If we can achieve the targeting of GT to cancer cells and observe a corresponding increase in pharmacologic effect, this dissertation research will represent a major step towards improving chemotherapy in breast cancer and can be adapted for other solid tumors as well.

Table 1.1. Murine Models of Breast Cancer

Model	Model Origin	Strengths	Weaknesses
Genetically engineered mouse model (GEMMs)	• Genetic modification to promote spontaneous tumor development in mice	• Tumor growth in native tissue with stroma, vascular and immune components • Natural formation of tumor microenvironment • Potential to model all aspects of the metastatic cascade (initial tumor growth to distant metastasis) • Spontaneous metastasis likely	• Tumors driven by single mutations may overestimate the effect of agents targeting that mutation • Maintenance of colony is labor intensive and genetic drift a concern • Spontaneous tumors are less predictable and may complicate monitoring in early stages • Internal tumors are even more challenging to monitor
Cell-derived Xenograft (CDX)	• Established immortalized human cancer cell lines transplanted into immunocompromised mice	• Very well-characterized cell lines originating from various human tumor types • Consistent and reproducible initial tumor burden • Well-studied for primary tumors	• Immunocompromised host • Limited application for metastasis due to the lack of an immune component • Mouse stroma but human cancer cells • Homogeneous tumors with limited heterogeneity that would be observed in clinical tumors
Patient Derived Xenograft (PDX)	• Human cancer cells harvested from patients and transplanted into immunocompromised mice	• Highly diverse and heterogeneous tumors • Vascular and stromal components (from patient tumor) can be included in the xenograft • Primarily cell line that may directly reflect patient tumor response to a certain therapy • Well-studied for primary tumors	• Immunocompromised host • Limited application for metastasis due to the lack of an immune component • Mouse stroma but human cancer cells • Clinical tumors are not broadly accessible to all researchers
Syngeneic	• Established immortalized mouse cancer cell lines transplanted into immunocompetent mice	• Spontaneous metastasis likely • Tumor growth in the presence of an intact immune system • Consistent and reproducible initial tumor burden • Can be transplanted in native tissue for original stromal, vascular and immune components	• Limited number of established cell lines that can be used for syngeneic models • Rapid growth rate can lead to metastasis but may limit longer studies • Potential for immunogenicity and spontaneous remission

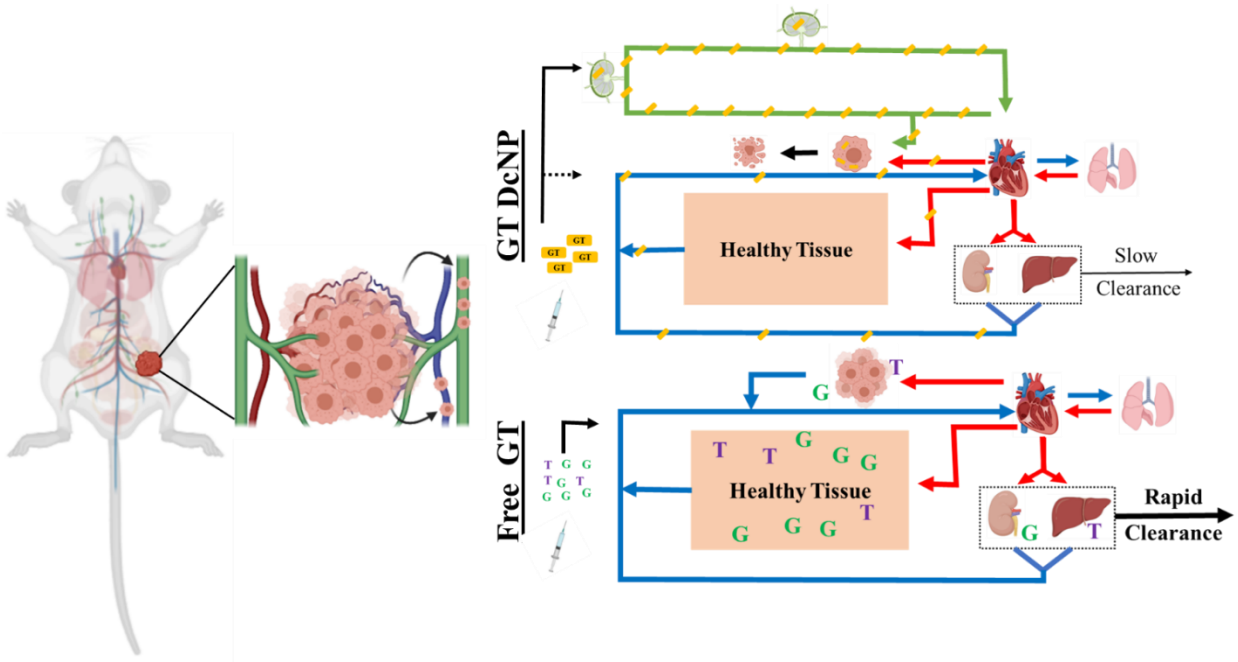

Figure 1.1. Schematic representation of how Gemcitabine (G)-Paclitaxel (T)-drug combination nanoparticles (DcNP) enhance tumor tissue and cell selectivity and likely mechanisms that lead to enhanced exposure and extension of effective drug concentrations in metastatic breast cancer cells

Breast cancer metastasis can occur through either the blood or the lymphatic system. Free drug (bottom panel) is rapidly taken into the systemic circulation and provides broad exposure of GT to cancer cells and healthy tissues. However, the differing distribution and clearance mechanisms for GT limit the intracellular coordination of both drugs. Off-target exposure to healthy tissue and rapid clearance also limit the effect of GT. By stabilizing GT in a single targeted drug combination nanoparticle (top panel), GT can be specifically taken up by target cancer cells to exert cytotoxic effect. Depending on the route of administration, GT DcNPs are taken up into the lymphatic system (top, green) and specifically delivered and retained in tumors. GT DcNPs are very stable in the systemic circulation and can maintain long acting plasma concentrations. Taken together, GT DcNPs can eliminate cancer cells in both the lymph and the blood to improve breast cancer therapy.

Chapter 2. CONTROLLED SOLVENT REMOVAL FROM ANTIVIRAL DRUGS AND EXCIPIENTS IN SOLUTION ENABLES THE FORMATION OF NOVEL COMBINATION MULTI-DRUG-MOTIFS IN PHARMACEUTICAL POWDERS COMPOSED OF LOPINAVIR, RITONAVIR AND TENOFOVIR

A version of this chapter was published in:

Yu J et al. Controlled Solvent Removal from Antiviral Drugs and Excipients in Solution Enables the Formation of Novel Combination Multi-Drug-Motifs in Pharmaceutical Powders Composed of Lopinavir, Ritonavir and Tenofovir. J Pharm Sci. 2020 Nov;109(11):3480-3489

2.1 ABSTRACT

Diverging physicochemical properties of HIV drug combinations are challenging to formulate as a single dosage form. We have found that 2-to-4 hydrophilic and hydrophobic HIV drugs in combination can be stabilized with lipid excipients under a controlled solvent removal process to form a novel pharmaceutical powder distinct from typical amorphous material. This discovery has enabled production of a drug combination nanoparticle (DcNP) powder composed of 3 HIV drugs—water-insoluble lopinavir (LogP = 4.7) and ritonavir (LogP = 5.6) and water-soluble tenofovir (LogP= -1.6). DcNP powder, exhibiting multiple drug motifs (MDM), is made by dissolving all constituents in ethanolic solution, followed by controlled solvent removal. The DcNP powder intersperses chemically diverse drug molecules with lipid excipients to form repeating MDM units. The proposed MDM structure is consistent with data collected with X-ray diffraction, differential calorimetry, and time-of-flight secondary ion mass spectrometry. The successful assembly of chemically diverse drugs in MDM structure is likely due to a novel process of making drug combination powders. The method described here has been successfully extended to formulating other clinically prescribed antiviral drug combinations, and thus may serve as a platform technology for developing drug combination nanoparticles for treating a wide range of chronic diseases such as HIV or cancer.

2.2 INTRODUCTION

The availability of well-characterized viral protein structures, coupled with success in developing drugs targeted to viral proteins, has significantly improved outcomes in HIV treatments. Chronic oral administration of HIV drug combinations sustains viral suppression and prevents people with HIV from progressing to AIDS. These patients take multiple drug combinations to reduce drug resistance, which occurs in long-term disease (Autran et al., 1997; Maartens, Celum, & Lewin, 2014). Multidrug regimens are effective, but are associated with significant pill burden. Patient adherence is necessary to sustain drug levels and mitigate the risk of harboring viruses resistant to oral regimens. A typical dosing regimen can require oral dosing between one and three times a day with multiple tablets, presenting a large burden to patients (Nachega et al., 2014). To improve patient quality of life, decrease multiple-pill fatigue, and risk of missed doses, oral fixed dose combinations (FDCs) have emerged as a "one-pill, once a day" option to treat people with HIV (Maitland et al., 2008; Nachega et al., 2014). This one-pill a day strategy is enabled by the development of advanced manufacturing approaches such as multi-layer tableting, multi-particulate systems, and monolithic systems that allow chemically diverse drugs to be stabilized together in a single oral dosage form (Desai, Wang, Wen, Li, & Timmins, 2013; Kelleher et al., 2018). The challenges in producing physically stable drug combination dosage forms as a single unit are well recognized and presently require complex, multilayer blending and compression strategies. However, if one can produce multiple chemically diverse HIV drugs as a physically stable and homogenous drug combination powder, then these challenges could be mitigated. Achieving such a product may also simplify the process for producing both oral solid dosage forms and drug-combinations in suspension.

In addition to the “one pill a day” strategy to make solid oral dosage forms for HIV drug combinations, long acting injectable dosage forms of antiretrovirals are an alternative means to treat patients with HIV. Long acting injectables can provide more consistent plasma drug levels over a longer period than daily dosing. Consistent drug levels over time can then, in turn, provide more predictable degrees of sustained viral suppression and improve patient adherence to chronic HIV treatment. The ability to deliver an effective, single injectable dose that potentially replaces 30 pills or more is appealing to patients and clinicians (Simoni et al., 2020). However, parenteral injectable products pose additional physical challenges such as aggregation, chemical degradation, and precipitation that may limit their development. To improve the physical stability of long acting parenteral injections, polymeric excipients such as poloxamer 338, polysorbate 20, or polyethylene glycol are used to stabilize drugs in suspension for use as long acting injectables (Trezza, Ford, Spreen, Pan, & Piscitelli, 2015; Williams, Crauwels, & Basstanie, 2015). These current polymers are designed to formulate single drug injectables. They are not suitable for the stabilization of multiple combination drugs with diverse physicochemical properties (e.g. compounds that are water soluble and insoluble) in a single parenteral injection. In addition to biopolymers, lipid excipients have been used—typically as liposomes or lipid-membrane vesicles—to formulate nanosuspensions with various physicochemical properties. Thus, certain lipid molecules may serve as excipients for developing multi-drug injectables (M. L. Chen, 2008; Muller, Radtke, & Wissing, 2002a, 2002b). Due to their ability to form various membrane-like structures in water, lipid excipients are typically used to encapsulate APIs within enclosed membrane layers (lipid vesicles or liposomes), or to bind and stabilize APIs within the membrane layers. These properties have allowed lipid excipients to be used extensively for developing parenteral administrations (Constantinides, Chaubal, & Shorr, 2008). Traditional lipid-based delivery systems (such as

liposomes) incorporate hydrophobic drugs within the acyl chains of the bilayer-membrane or encapsulate hydrophilic drugs within the aqueous core of membrane bilayers. However, liposomal drug manufacturing processes are complex and often face challenges in manufacturing scalability, the need to remove unincorporated (free) drug, and physical instability as a suspension in storage. Ideally, a method to stabilize hydrophobic and hydrophilic HIV drugs together as a single unit, without the need for encapsulation, can aid the development of long acting injectables in suspension.

Recently, our laboratory has reported a process by which drugs with disparate physicochemical properties can be stabilized with lipid excipients in powder form (Freeling et al., 2015; McConnachie et al., 2018; Perazzolo et al., 2018). In early studies, various lipid-based excipients were tested to incorporate antiviral drugs, beginning with single drug particles and expanding to 3 and 4 drug combination nanoparticles. These drug combination nanoparticles (DcNPs) are suitable for injectable dosage forms and demonstrate long acting effect. One anti-HIV DcNP composed of water-soluble tenofovir (TFV, LogP = -1.6) and water-insoluble lopinavir (LPV, LogP = 4.7) and ritonavir (RTV, LogP = 5.2) was reported to be stabilized by the lipid excipients: 1,2-distearoyl-sn-glycero-3-phosphocholine (DSPC) and 1,2-distearoyl-sn-glycero-3-phosphoethanolamine-N-[amino(polyethylene glycol)-2000] (DSPE-mPEG$_{2000}$). In this composition, DSPC is intended to stabilize hydrophobic drugs (such as LPV and RTV) through interactions within the acyl chains. While DSPE-mPEG$_{2000}$ is intended to stabilize hydrophilic drugs (such as TFV) through hydrophilic interactions within the polyethylene polymer. The ratio of the 3 drugs was selected based on the clinically relevant ratios used in oral dosage forms after consideration of their respective pharmacokinetic profiles and therapeutic target drug levels. Total drug-to-lipid ratios (and the ratio of the two lipid excipients) were iteratively tested and described

in previous reports (Duan, Freeling, Koehn, Shu, & Ho, 2014; Freeling, Koehn, Shu, Sun, & Ho, 2014; Kinman et al., 2003). Early studies optimized the composition and process for DcNP formation to yield consistent nano-particle size and association efficiencies for each drug listed. The resulting formulation is suitable for development as an injectable formulation in suspension and was used in multiple pharmacokinetic studies to produce reproducible long acting, *in vivo* results. When the 3 drugs—TFV, LPV and RTV in DcNP suspension—were tested in non-human primates (NHPs), only DcNPs and not free drug dosage forms exhibited long-acting pharmacokinetics in both plasma and lymphoid cells (Duan et al., 2014; Freeling et al., 2014, 2015; Kinman et al., 2003; Kraft et al., 2017). Due to its reproducibility and *in vivo* stability, free drug removal—commonly required for alternative liposome encapsulated dosage forms—is not needed in this novel DcNP suspension. The reported results, along with analysis by a validated, mechanism-based pharmacokinetic model, indicate that a majority of hydrophilic TFV and hydrophobic LPV and RTV are stabilized together in a DcNP form throughout the 2-week PK study.

In our initial studies, we employed rotary evaporation of drugs and excipients in solution as a controlled solvent removal process to form drug combination powder at a smaller scale. However, rotary evaporation used to produce DcNP powder had limited process control, inconsistent *in vitro* results and was not readily scalable for clinical evaluation of DcNP product (long acting suspension). With the need to improve process control and monitoring of powder characteristics, a spray drying method was developed. The improved process control is an essential step in forming stable, consistent drug combination powder for use as a suspension to provide long acting, targeted pharmacokinetics in larger scale NHP studies.

Thus, the objective of this study is to define the role of controlled solvent removal in producing drug-combination particles in powder form and to characterize the resultant DcNP powder properties and distinctive molecular properties, which may relate to the stable suspension intended for long-acting pharmacokinetics. After complete solubilization of 3 chemically diverse drugs and 2 lipid excipients together, controlled solvent removal by spray drying is a critical step in locking these constituents together. We found that controlled solvent removal of drugs and lipids in a single solution led to the formation of homogenous repeats of drug-lipid excipients in a unified matrix structure (which we have termed multi-drug motifs or MDM). This unique structure (and the technology used to achieve that structure) may enable the development of combination powders with chemically diverse drugs to treat a wide range of chronic diseases.

2.3 MATERIALS AND METHODS

2.3.1 *Materials*

GMP quality lopinavir (LPV), ritonavir (RTV) and tenofovir (TFV)—referred to as active pharmaceutical ingredients or APIs— were a gift from Mylan pharmaceuticals (Morgantown, West Virginia). Dolutegravir (DTG), rilpivirine (RPV) and lamivudine (3TC) were purchased from Carbosynth (Berkshire, United Kingdom). GMP grade 1,2-distearoyl-sn-glycero-3-phosphocholine (DSPC) and 1,2-distearoyl-sn-glycero-3-phosphoethanolamine-N-[amino(polyethylene glycol)-2000] (DSPE-PEG_{2000}) were purchased from Cordon Pharma (Liestal, Switzerland). Anhydrous ethanol was purchased from Decon Pharmaceuticals (King of Prussia, PA). All other reagents were analytical grade or higher.

2.3.2 *Preparation of Antiviral Drug Combination Nanoparticles in Powder and in Suspension*

To produce drug combinations stabilized with lipid excipients in powder form, two lipophilic APIs, LPV and RTV were first dissolved together with two lipid excipients, DSPC and DSPE-PEG_{2000} at 60°C in ethanol. To maintain an appropriate ionization state, hydrophilic TFV was dissolved in 200 mM $NaHCO_3$ buffer (pH~7.4) before being added drop wise into the two lipophilic APIs and two lipid excipients in ethanolic solution, and allowed to mix at 60°C. The bicarbonate buffer keeps TFV in solution and allows for complete mixing with the ethanolic solution containing LPV/RTV and lipid excipients. The final $NaHCO_3$ buffer to ethanol volume ratio is 3:97. Solvent removal from the 3 drugs and lipid excipients in ethanol/buffer solution was achieved with either rotary evaporation (New Castle, Delaware) or an electronically controlled ProCepT 4-M8TriX spray dryer (Zelzate, Belgium) to produce a DcNP powder product containing the 3 drugs and 2 lipids.

To make DcNP powder by rotary evaporation, a typical batch includes 10 grams of total lipid and drug dissolved in 200 mL of ethanol/buffer (5% w/v solid). Rotary evaporation is performed at a constant temperature of 60°C with vacuum pressure increasing from 300 mmHg to 760 mmHg over 1 hour. Under these conditions, rotary evaporation can produce approximately 10 grams of material (to make ~50 mL of suspension) with 100% recovery.

To make DcNP powder by spray drying, a typical batch includes up to 200 grams of total lipid and drug dissolved in 2 liters of ethanol/buffer (10% w/v solid). Spray drying is performed at a constant temperature of 70°C with the feedstock solution introduced via peristaltic pump at a rate of 300 RPM. The spray drying parameters were as follows: inlet air speed of 0.3 m^3/min, chamber pressure of 25 mbar, atomization air flow of 25 L/min, cyclone air flow of 0.1 m^3/min and a nozzle size of 0.6 mm. With these parameters, typically 65% of the mass in the original

feedstock solution is recovered; there is no change in the drug or lipid excipient ratios compared to that of the initial mixture in solution. This spray drying process has been used to generate as much as 200 grams of dried product (to make ~ 1 Liter of suspension). No residual ethanol is detectable in the dried product by GC-MS (with 3000 ppm equal to the lower limit of quantification). Dried product, referred to as DcNP powder, is stored under vacuum desiccation conditions at ambient room temperature and analyzed for physical characteristics as detailed below. The powder particle size was visually analyzed with transmission electron microscopy (TEM) and ranges from 1 to 5 microns in size.

The methods to prepare DcNPs as injectable suspensions have been described in detail in previous reports (Freeling et al., 2015). Briefly, to produce 1 L of DcNP in aqueous suspension, 220g of DcNP powder is added to sterile half-normal saline (0.45% NaCl solution) containing 20mM $NaHCO_3$ (pH= 7.4). This process provides a DcNP in suspension with a nominal drug concentration of 10.7 mg/mL LPV, 3.1 mg/mL RTV, 6.1 mg/mL TFV, and total lipid concentration of 180 mM (9:1 DSPC to DSPE-PEG_{2000} molar ratio) with an osmolarity of ~306 mOsm. After suspension, particle size reduction is achieved with homogenization to yield uniform particles with an average diameter of 52.4 ± 9.1 nm as measured by photon correlation spectroscopy (NICOMP 380 ZLS, Particle Sizing Systems, Santa Barbara, CA) (Freeling et al., 2015).

2.3.3 *Powder X-ray Diffraction*

Powder X-ray Diffraction (PXRD) was used to characterize the matrix structure and crystallinity of DcNP powder. PXRD analysis is performed on a Bruker D8 Focus X-ray Diffractor (Madison, WI, USA) with Cu-Kα radiation. Operational voltage and amperage were set to 40.0 kV and 40.0 mA, respectively. Experimental parameters include a step size of 0.035°2θ in an

operating range of 5° to 50° 2θ. Powder (~100-200 mg) was pressed into a sample container to obtain a flat upper surface. The data collected were plotted as intensity (counts) vs angle (2θ). A minimum of 3 batches were used for each sample in this analysis.

2.3.4 *Differential Scanning Calorimetry*

Differential scanning calorimetry (DSC) was performed on the DcNP dry powder to characterize the thermal behavior of individual API, excipient, physically mixed combination of API and excipient, and the DcNP product. For this purpose, we used a TA DSC Q20 (New Castle, DE, USA). Baseline calibrations were performed every day prior to collecting DSC data by ramping 10°C/min up to 200°C under constant nitrogen (50 mL/min). The samples (1-4 mg each) were placed in a hermetically sealed aluminum pan and subjected to increasing temperature at 10°C/min from 25°C to 200°C. The change in heat flow delta-H (W/g) was collected and plotted against increasing temperature. A minimum of 3 batches were used for each sample in this analysis.

2.3.5 *Scanning Electron Microscopy (SEM)*

Dry DcNP powder composed of LPV, RTV, TFV and two lipid excipients-DSPC and DSPE-PEG_{2000} was visualized using a FEI Sirion XL30 Scanning Electron Microscope (SEM) (Hillsboro, Oregon). The powder samples were placed on a conductive and adhesive carbon backplate and placed under a nitrogen stream to remove non-adhered particles. These samples were then sputter coated with Au/Pd for 20 minutes prior to visualization for an estimated coat depth of 15 nanometers. The SEM was operated under a working distance of 4.7 to 5.1 mm and an accelerating voltage of 5 to 15 kV. The electron micrograph was collected digitally and analyzed

based on equivalent amplification for each variant. An individual batch of physically mixed of spray dried DcNP powder was used for this analysis.

2.3.6 *Time of Flight Secondary Ion Mass Spectrometry (ToF-SIMS)*

Time of Flight Secondary Ion Mass Spectrometry was performed to evaluate molecular distribution within DcNP powders. Distribution profiles for each component in the DcNP (LPV, RTV, TFV and two lipid excipients DSPC and DSPE-PEG_{2000}) were acquired simultaneously with a 25 keV $Bi3^+$ cluster ion source in the pulsed mode. Secondary ions of these components were captured with the IONTOF ToF-SIMS spectrometer (Münster, Germany) to determine the spatial arrangement of the constituents. Depth profiles were acquired in the non-interlaced mode using alternating analysis and sputter cycles. Data was acquired over a mass range of m/z = 0 to 850 using a primary ion current of 0.035 pA in delayed extraction mode over a 100-micron x 100-micron area centered within the sputter crater. Based on these parameters, an estimated depth of 100 nm to 200 nm was analyzed for the depth profile. The Secondary ions of a given polarity were extracted and detected using a reflectron time-of-flight mass analyzer. The primary ion dose for each spectrum was $2.3x10^{11}$ ion/cm^2. Sputtering was carried out using a gas cluster ion beam with 10 keV argon 1000 clusters rastered over a 500-micron x 500-micron area for 7 seconds at a current of 7nA giving a sputtering dose of $1.22x10^{14}$ ion/cm^2. Positive ion spectra were calibrated using the CH_3^+, $C_2H_3^+$, and $C_3H_5^+$ peaks. The negative ion spectra were calibrated using the CH^-, OH^-, and C_2H^- peaks. Calibration errors were kept below 20 ppm. Mass resolution (m/Δm) for a typical spectrum was 3400 for m/z = 27 (pos) and 3600 for m/z = 25 (neg). Data was assembled by overlaying sequential X-Y spectra along the Z-axis of the drug and lipid constituents over a 100 micron by 100-micron grid with each constituent represented by its own color. Further analysis was performed with ImageJ software to estimate the relative abundance of each species across the

x-axis of the acquired grid. An individual batch of physically mixed of spray dried DcNP powder was used for this analysis.

2.4 RESULTS

2.4.1 *Effects of Controlled Solvent Removal by Spray Drying on the Physical Structure of Antiviral Drug Combination Powder Products Based on X- Ray Diffraction Analysis*

We first determined the effects of spray drying as a process to remove solvent under controlled conditions from drugs and lipids mixed in ethanolic solution. To do so, we dissolved LPV, RTV and two lipid excipients—DSPC and DSPE-PEG_{2000}—in ethanol; followed by the addition of TFV in an $NaHCO_3$ buffer such that the final solution contains 3% aqueous buffer. The ethanol-based solvent in the drug-combination mixture was removed under controlled conditions by spray drying. The spray dried drug-combination powder containing 3 drugs and 2 lipids was analyzed with a powder x-ray diffraction (PXRD) instrument. In Figure 2.1, the individual constituents within the DcNP powder—LPV, RTV, TFV, DSPC or DSPE-PEG_{2000}—all exhibit crystalline signatures as seen by their distinct X-ray diffraction (peak) patterns. Analysis of each single drug or single excipient control (Figures 2.1, Panels A-C, E+F) shows various peaks at the respective 2θ angle positions where Bragg's law is fulfilled. In Figure 2.1 Panel H, the diffraction pattern of the physical mixture of drugs and excipients in the same molar ratio as the DcNP powder is similar to DSPC alone (Panel E) due to the high mass % of this excipient in the DcNP formulation. However, additional peaks attributable to the other constituents are apparent, particularly in lower angle regions (5° to 15° 2θ). In contrast to these unique and assignable X-ray diffraction patterns for each component within the DcNP powder, the DcNP powder itself (prepared under controlled solvent removal) did not contain any assignable signature of each constituent. Instead, the 5 components in the DcNP powder are assembled in such a way that they

produce two new and distinct diffraction peaks observed at 5.64°2θ and 21.47°2θ (Figure 2.1 Panel I).

To verify this result, a control composed of just the two lipid excipients (9:1 DSPC: DSPE-PEG_{2000}) without the APIs (LPV, RTV, and TFV) was subsequently produced under the identical spray drying process and analyzed with PXRD. By omitting drugs in this composition, this control is used to evaluate the effect of the controlled solvent removal process on lipid excipients. As shown in Figure 2.1, Panel G, compared to DcNP products, the excipient product produces two additional peaks at the 19.1°2θ and 23.1°2θ positions, in addition to the main peak observed at 21.47 °2θ for DcNP with all components (Panel I vs G). The additional peaks correspond to the peaks observed in the DSPE-PEG_{2000} control and may indicate a PEG crystalline structure within the powder product of two lipid excipients (Panel F). Another powder control containing 3 drugs only (LPV, RTV, and TFV) without lipid excipients exhibits a characteristic amorphous halo (Panel D). Collectively, the PXRD data suggests that (1) controlled solvent removal by spray drying produces a new unique structure, revealed in PXRD as one minor and one major peak at 5.64°2θ and 21.47°2θ. (2) None of the original 3 drug signatures are present indicating that there is no unchanged, crystalline API remaining. (3) The structural signature is not achieved with excipient alone undergoing an identical spray drying process, (4) drug alone undergoing complete amorphous transformation, or (5) by a physical admixture of an identical composition. Thus, the controlled solvent removal of this composition leads to a unique repetitive organization of DcNP powder, revealed by PXRD. This repetitive organization is referred to as multi-drug motif or MDM structure.

2.4.2 *Verification of DcNP Powder's Unique Organizational Structure with Differential Scanning Calorimetry*

We next investigated the thermal behavior of the DcNP powder. To do so, we employed differential scanning calorimetry as a complementary technique to characterize this unique structure among 3 drugs and 2 lipid excipients formed from controlled solvent removal. As shown in Figure 2.2, line G, the spray dried DcNP product exhibits a single endothermic transition apparent with an onset transition temperature of 70.28°C and a melting point peak at 74.29°C. This endotherm occurs at a position independent of individual drug and excipient controls (Figure 2.2), indicating that it is not the melting of the crystalline structure for each of the drugs or excipients in the DcNP composition. In agreement with the PXRD data, we do not see any evidence of PEG (from the DSPE-PEG_{2000} lipid excipient) melting which would be expected around 49°-52°C (Figure 2.2, line E). Interestingly, the DcNP thermogram also contains a broad exotherm beginning at temperatures >120°C and extending until the end of the heating ramp. A possible source of this exotherm is mass loss from heating the drug combination powder formulation, which was observed to be ~3.5% based on thermogravimetric analysis measurements at a ramp rate of 10°C/minute to 200°C. This weight change may be due to atmospheric water adsorbed to the powder through the spray drying process. It is possible that the exotherm may mask the presence of glass step transitions at higher temperatures. Nevertheless, the thermal characterization of spray dried DcNP powder shows that the individual endothermic transitions of the drugs and excipients are no longer observed in lower temperature ranges and a single endotherm for the spray dried powder occurs at a unique temperature. This suggests that novel nonbonding interactions are formed through the spray drying process and is likely related to the new MDM motif or structure in the DcNP powder product.

2.4.3 *Effects of Controlled Spray Dried Process on Distribution of LPV, RTV, TFV, DSPC and DSPE-PEG$_{2000}$ within DcNP Powder*

To further characterize the unique structural organization of drug and excipient molecules within DcNP, we analyzed the powder with a Time of Flight Secondary Ion Mass Spectrometry (ToF SIMS). ToF-SIMS is a surface analysis technique that provides information on the molecular distribution of each of the five components: LPV, RTV, TFV, DSPC, and DSPE-PEG$_{2000}$ assembled together within the DcNP powder product. We also used scanning electron microscopy (SEM) as a complementary technique to provide the overall morphology of the product compared to that of individual molecules in solid states. If the MDM motif is organized in a repeated pattern—as suggested by PXRD and consistent with thermal behavior noted in DSC (as described above)—each molecular component in the DcNP powder will be homogenously distributed throughout, and detectable as such, in the time-of flight ion scan under ToF-SIMS analysis. On the other hand, if each constituent in the mixture forms micro domains of each representative molecular species according to their respective physical characteristics and lowest energy state (instead of presenting well-distributed and repeated motifs of 5 distinct molecular species), this technique will identify the formation of such clusters within the DcNP powder.

As shown in Figure 2.3, the SEM overall morphological analysis reveals a well-distributed morphology for the DcNP powder prepared by the spray drying process (Figure 2.3, B). In contrast, the morphology of drugs and lipids prepared by admixing (Figure 2.3, A) retained a heterogeneous polymorphic drug and lipid crystalline morphology. The morphology of the spray dried material does not retain any of the physical characteristics of drugs and lipids prepared by admixture, but rather has a homogeneous, spherical shape (~1 to 5 μm). The spherical morphology and size are likely due to atomized droplets formed from the feedstock solution in the spray drying process.

Furthermore, ToF-SIMS depth profiles (Figure 2.4, A-C) of the spherical DcNP particles observed in SEM reveal that the three drugs (LPV, RTV and TFV) as well as the excipients (DSPC and DSPE-PEG_{2000}) are evenly distributed in the X-Y plane of the powder and continue to be well-distributed along the Z-axis through depth profile analysis (100 nm to 200 nm). These data suggest that there is no preferential accumulation of API or excipients within a single particle (at the surface or interior) and that each individual particle has a uniform composition and shape. The ToF-SIMS depth analysis provides enough resolution to distinguish individual drug crystals in the physical mixture (Figure 2.4, D-F), but no microdomains are observed with the spray dried powder in the X, Y or Z-axis. Taken together with the PXRD and DSC analyses, the molecular and spatial distribution of drugs and excipients revealed by ToF SIMS suggests that controlled solvent removal enables the formation of a stable, non-bonding interactions among drug and excipient molecules (MDM structure). These MDM structures cannot be attained through physical mixture but only when the solubilized drugs and lipids have undergone a controlled solvent removal process.

2.4.4 *Effect of drug substitutions on formation of multi-drug motif (MDM) using controlled solvent evaporation*

To understand whether the MDM structure observed for LPV, RTV, and TFV with lipid excipients is unique to those three APIs or could be substituted with other HIV drugs, we evaluated additional drug combinations targeted to HIV proteins. These drug combination powders employed the same lipid excipients with similar total drug-to-lipid ratios as the lead LPV, RTV, TFV formulation. The hydrophobic drugs, LPV and RTV, were replaced with an integrase strand inhibitor (dolutegravir, DTG, logP = 2.4), a non-nucleoside reverse transcriptase inhibitor (rilpivirine, RPV, logP = 4.5), or both. In some compositions, the hydrophilic nucleoside reverse

transcriptase inhibitor (TFV) was either replaced or added in combination with a drug from the same class (lamivudine, 3TC, logP = -0.9) (Table 2.1). Drug combinations were chosen based on the current WHO recommended list of anti-HIV drug combination therapies, which typically contains one-to-two hydrophilic nucleoside reverse transcriptase inhibitors plus a hydrophobic protease inhibitor, non-nucleoside reverse transcriptase inhibitor, or integrase strand inhibitor of HIV. The variants to the reference DcNP composition were analyzed with PXRD to assess the structural features of these new DcNP powders and are listed in Table 2.1. To our surprise, we found that with the listed diverse class of HIV drugs, the controlled solvent removal process for DcNP powder preparation produced the same MDM structure as that observed with LPV, RTV and TFV (Figure 2.1, panel I) by PXRD analysis (Table 2.1). These results highlight the broad range of hydrophobic and hydrophilic drugs that are amenable to produce MDMs by this method and process. Hence, other antiviral combinations could be suitable for this approach. Collectively, these data suggest that the controlled solvent removal of hydrophobic and hydrophilic APIs with lipid excipients in solution may enable the formation of a stable structure with repeating multi drug motifs (MDM) with multiple combinations of drugs.

2.5 DISCUSSION

Current HIV treatment requires 2-3 oral antiviral drugs in combination to achieve sustained viral suppression. A typical combination regimen is composed of hydrophilic nucleoside reverse transcriptase inhibitors (NRTIs) with hydrophobic integrase or protease inhibitors to achieve viral suppression in plasma. The varying physicochemical—water-soluble and water-insoluble—properties of these drugs can be challenging to formulate in either oral fixed dose combinations or in long acting injectables. We used a simple controlled solvent removal process to stabilize the physical interactions of chemically distinct drug combinations with lipid excipients in DcNP

powder form. The controlled solvent removal process forms multi-drug motifs (MDM) where drugs and lipids are locked together in repeating units. In this report, we have characterized the molecular organization of that motif in detail. The stabilization of 3 chemically diverse HIV drugs by 2 lipid excipients may address the challenges in co-formulating oral fixed dose combinations or long acting injectables and simplify their development processes.

The poor aqueous solubility of many drugs used in HIV such as protease inhibitors or integrase inhibitors is well described. This insolubility limits the rate and extent of HIV drug absorption in oral dosage forms. One approach to overcome the lower bioavailability of oral dosage forms is to use amorphous solid dispersions (ASDs), instead of crystalline drugs, to enhance drug solubility and bioavailability from oral dosing (Arca, Mosquera-Giraldo, Dahal, Taylor, & Edgar, 2017; P. Sharma & Garg, 2010; Vasconcelos, Sarmento, & Costa, 2007). ASDs are meta-stable amorphous API molecules dispersed in polymeric matrices, which can be easily identified as an amorphous halo in PXRD diffraction patterns (Arca et al., 2017; Trasi, Bhujbal, Zhou, & Taylor, 2019). The high energy state of amorphous materials increases solubility at the cost of physical stability; specifically, an increased chance of crystallization or phase separation during storage (Vasconcelos et al., 2007). The spontaneous devitrification of amorphous material is also a known phenomenon and can limit amorphous dosage forms (Vasconcelos et al., 2007). In our work, we have stabilized chemically diverse APIs in lipid excipients to form a drug combination nanoparticle (DcNP) powder. This DcNP powder does not appear to follow amorphous characteristics, instead presenting clear PXRD diffraction peaks in the powder (Figure 2.1, panel I). The two PXRD peaks of DcNP are not attributable to any of the individual drugs or lipid excipients shown in Figure 2.1 A-C, E and F. The solvent removal process generates a new ordering of drugs, lipids, and DSPE-linked PEG polymer (Figure 2.1 panel I). It is likely that this

new structure is due to the large overall faction of lipid molecules and their physical interactions in the DcNP powder composition and structure (Figure 2.1, H). However, the loss of PEG lipid (DSPE-PEG_{2000}) peaks in PXRD is observed when antiviral drugs are introduced to the lipid excipients through spray drying, suggesting specific PEG polymer-drug interactions within the DcNP powder. Further thermo-analysis of DcNP powder by DSC corroborates the PXRD data. For purely amorphous material, we would expect to observe a glass transition temperature as detailed in literature (Hou et al., 2019). Instead, when DcNP powder is analyzed with DSC, an endothermic event specific to DcNP powder is observed (Figure 2.2 Panel G). The endothermic event suggests that new nonbonding physical interactions exist between drug, lipid, and polymer in the DcNP powder that are not present in the physically mixed or excipient only controls (Figure 2.2 Panel H & F).

Like ASDs, nanocrystals are an alternative approach to improving the aqueous solubility of poorly aqueous drugs. Small particle size allows for more surface area contact with water and greater achievable concentrations in aqueous environments. This approach has been used to improve the bioavailability of drug products and is well established in the literature (Gao et al., 2012; Sverdlov Arzi & Sosnik, 2018). In a recent study, dual nanocrystals of simvastatin and ezetimibe were assembled together in mannitol microparticles to improve the solubility of both cholesterol-lowering drugs, enabling nano-sized combination formulations (Nandi, Kaur, & Bansal, 2020). While DcNP powder achieves a similar outcome (multiple drugs stabilized in powder), there are key distinctions to the DcNP process. Simvastatin (logP = 4.7) and ezetimibe (logP = 4.0) are both hydrophobic drugs that have similar aqueous insolubility. In contrast, TFV (logP = -1.6) and LPV (logP = 4.7) or RTV (logP = 5.6) have very different aqueous solubilities. The ability to incorporate chemically diverse compounds together as a single combination drug

powder is particularly important in HIV therapy, where multiple agents with divergent solubility are required in current fixed-dose combination to provide sustained viral suppression. If both hydrophilic and hydrophobic drugs are present in nanocrystal form, it is likely that the hydrophilic drug will rapidly dissolve and separate from the combination powder and lead to asynchronous drug bioavailability and overall exposure. In contrast, the consolidation of TFV, LPV and RTV in DcNP powder with lipid excipients may confer greater physical stability allowing the chemically diverse drugs to remain together *in vivo* (Duan et al., 2014; Kraft et al., 2017).

In addition to stabilizing LPV, RTV, and TFV together, we also discovered that the DcNP process can form a similar structure with other antiviral drug combinations that contains both hydrophilic and hydrophobic drugs. For the hydrophobic drugs (LPV, RTV, DTG, and RPV), the average logP was 4.3 with a range from 6 (RTV) to 2.4 (DTG). For hydrophilic drugs (TFV and 3TC), the average logP was -1.25 with a range of -1.6 to -0.9. When we consider the polar surface across hydrophobic and hydrophilic drugs, we do not observe a large difference (129.65 $Å^2$ vs 124.5 $Å^2$). However, when we consider the % of the molecule that the polar surface area encompasses, we observe a large difference between the hydrophobic and hydrophilic groups (28.6% vs 53.6%, respectively). It is possible that hydrophobic drugs have some portion of their structure exposed to hydrophilic regions (28.6%) while the remainder of the molecule is embedded in the acyl chains of DSPC and DSPE-$PEG_{2000.}$ For hydrophilic drugs, the opposite may be true, where the majority of the molecule is retained in the hydrophilic PEG regions of DSPE-$PEG_{2000,}$ but a fraction of the molecule can interact with the acyl chains. The hydrophobic drugs that were tested also encompass different drug classes and this observation is consistent across classes. When we compare non-nucleoside reverse transcriptase inhibitors (RPV) with integrase inhibitors (DTG), the % of molecular polar surface area is similar at 28.0% and 29.8%, respectively.

Regardless of the exact mechanism of interaction, multiple pharmacokinetic studies in non-human primates have shown that the MDM structure is a platform technology that can facilitate long acting pharmacokinetics with different drug combination nanoparticles (Freeling et al., 2014; McConnachie et al., 2018; Perazzolo et al., 2018).

While the molecular mechanisms leading to MDM formation in the powder remain elusive, it is possible that after initial dissolution of DSPC, DSPE-PEG_{2000}, LPV, RTV and TFV in 97:3 v/v ethanol/water, the 5 constituents of the DcNP interact freely in ethanolic solution. As ethanolic solvent is gradually removed under controlled conditions, the hydrophobic constituents LPV and RTV align with the hydrophobic fatty acyl chains of DSPC; while hydrophilic TFV aligns or gradually replaces bound water on the poly-ethylene-glycol (PEG) polymer of the DSPE-PEG_{2000}. With continued solvent removal, it is possible that the PEG moieties of DSPE-PEG_{2000} and hydrophilic TFV interact with higher affinity and replace bound water on PEG with TFV hydrogen bonding to repeating units of ethylene glycol. As residual bound water is removed, the substitution of hydrogen bonds occupied by water with TFV then stabilizes the overall DcNP powder. Since the controlled solvent removal process is enabled by a spray-dryer, the process of lipid drug interactions within each atomized droplet of drug and lipid excipients in solution produces uniform, repeating units of MDM collected as a spray-dried DcNP powder (Figures 2.3 and 2.4). While the elucidation of these and other mechanisms is of interest, it is beyond the scope of the current report. The interactions between drugs and lipid excipients detected by PXRD and DSC appear to be consistent with a repeating structure in the combination powder. This structure has been referred to as MDM and is graphically represented in Figure 2.5. The proposed model includes each of the 5 components in the DcNP, their respective molecular structures and corresponding molar ratios within the composition. The energy minimization function of

ChemDraw 3D was then used to allow the molecules to assume their lowest energy (and theoretically most stable) conformation.

In this study, spray drying was used to allow for larger batches of powder to be generated with greater consistency compared to previous methods of controlled solvent removal (rotary evaporation). However, spray drying has been shown to produce heterogeneous distribution of drugs and excipients in aerosolized particles (Bhujbal et al., 2018). For example, a recent study of naproxen and PVPVA spray dried together was characterized as an ASD by PXRD, but had heterogeneous surface distribution of drug and excipients as visualized by ToF-SIMS (Bhujbal et al., 2018). In contrast, the DcNP powder in our study revealed distinct diffraction peaks with PXRD (unlike the amorphous halo of ASDs) while ToF-SIMS analysis showed much greater homogeneity of not only one, but all three chemically distinct drugs. This homogeneity may prevent the phase separation of individual constituents in DcNP powder and convey greater physical stability compared to other amorphous products (Bhujbal et al., 2018). Evidence of this physical stability is observed by the storage of DcNP powder for up to 6 months at room temperature (vacuum desiccation) with no observed change in organizational structure as measured by PXRD. After 6 months of storage, DcNP powder does not exhibit changes in suspension behavior such as aggregation or precipitation. Although our data suggest specific interactions between drugs and lipid polymer regions, current techniques and instruments do not provide enough resolution to assign molecular binding domains within the lipid or PEG chains. To further gain mechanistic insights on MDM formation, additional tools and experimental techniques are required. For example, molecular dynamic (MD) simulations have been used to study the effect of pegylated lipid excipients on bilayer assembly in aqueous environments (Lee & Pastor, 2011). However, for our composition, simulating molecular interactions between 3 chemically diverse

drugs molecules, 1 lipid excipient, and 1 pegylated lipid excipient is computationally intensive and requires significant time allocation. Additionally, there is limited information on the molecular structures of drugs and lipid-polymer conjugates. We are in the process of investing in MD simulations, but progress on these studies is limited and have yet to provide clarity. Nevertheless, with additional advancements in knowledge and tools, MD simulation may be a useful tool to test further characterize of the proposed MDM structure.

A key distinction of MDM structures over conventional crystalline or amorphous drug combinations is the ability to stabilize multiple drugs together. Crystalline protease inhibitors, such as LPV, RTV, and darunavir have low aqueous solubility and are strong candidates for formulation as amorphous drugs to increase solubility. Recently, reports have shown that when amorphous protease inhibitors are dissolved in the same aqueous environment, the dissolution of one drug negatively affects the solubility of the other and vice versa (Nguyen & Van den Mooter, 2014; Trasi & Taylor, 2015). This observation is important because protease inhibitors are often included in oral fixed dose combination products and, as these multiple drug products dissolve in the stomach, each constituent needs to be able to reach acceptable luminal concentrations for absorption to occur. In contrast, DcNP powder can associate LPV, RTV, and hydrophilic TFV together and—after suspension in buffered saline—no solubility or precipitation issues are observed with hydrophobic LPV or RTV. After particle size reduction, the resultant injectable dosage does not appear to aggregate in suspension. Thus, it may be used as a single injectable dosage form with both hydrophilic TFV and with hydrophobic LPV/RTV together. After injection, this new MDM powder in suspension produces long acting *in vivo* (plasma drug concentration time-course) behavior in NHPs as previously reported. The suspended DcNP powder continues to be stable *in vivo* with all three drugs circulating together in plasma and taken up by cells. These

DcNPs in suspension were verified in NHPs to transform short-acting oral drug combinations of LPV, RTV, and TFV (terminal $t_{1/2,}$ 5.5, 3.5 and 17 hours) to a targeted, long-acting injectable dosage form ($t_{1/2,\ app}$ 477, 44 and 65 hours) with persistent *in vivo* stability for up to 4 weeks (Kearney, Flaherty, & Shah, 2004; Kraft, McConnachie, et al., 2018; Murphy et al., 2001; Perazzolo et al., 2020). The previous *in vivo* results and the structural results outlined in this report highlight the potential for this DcNP process to develop into a platform technology that can stabilize hydrophilic and hydrophobic drugs together in powder form. We envision that these novel drug combination powders, enabled through controlled solvent removal, can be suspended and homogenized to carry chemically diverse API together to target cells and tissues *in vivo*.

The presented controlled solvent removal method has the potential to generate novel drug combination powders based on therapeutic compounds with wide ranging and disparate physicochemical properties. However, there are also limitations to this approach. The techniques used to characterize drug combination powders (such as PXRD and DSC) provide evidence that novel interactions are formed through the controlled solvent removal process. Additional studies, such as FTIR or Raman spectroscopy, would further support and identify the specific nonbonding and molecular domain interactions to provide additional insights. Solid state NMR may also be a tool to describe the interactions between drugs and excipients at the molecular and atomic level. These mechanistic insights would be valuable in predicting other drugs that could be included into the DcNP structure and are in consideration for future studies. However, in our experience, the overall diffraction pattern of drug combination powders in the 2 peak orientation (Figure 2.1, panel I) has been sufficient in predicting long acting *in vivo* circulation after SC administration in NHPs. To support future studies with other antiviral or cancer drug combinations, elucidation of the DcNP design space such as drug to drug ratios, drug to lipid ratios, and lipid to lipid ratios will be pursued.

It would also be important to further define the drivers of success in the formation of stable MDM structures. Such studies, while of interest, are beyond the scope of this report and are under consideration for future investigation. Given the complexity of the DcNP system, a design of experiment analysis will be considered.

In summary, we have discovered that a number of 2 to 3 antiviral drug combinations with disparate physical properties (including LPV, RPV, DTG, RTV, TFV or 3TC) can be stabilized together with lipid excipients in a powder form through a controlled solvent removal process. Through physical, morphological, thermal, and X-ray diffraction analysis, we have found that stable DcNP powder exists as a novel MDM structure that is distinct from the crystal polymorphs of individual constituents and from amorphous powder products. DcNP powder itself displays significant molecular homogeneity as seen in ToF-SIMS, which may be related to the observed MDM structural stability. By using a simple spray drying process to unite chemically diverse drugs together as a stable combination powder, this discovery may enable the development of more effective combination APIs in suspension for treatment of wide-ranging chronic diseases such as HIV, cancer, and diabetes.

Table 2.2 Select drug combination nanoparticle powder (DcNP) compositions evaluated for the formation of multi-drug-motif structures[a].

DcNP (tested)	**Hydrophilic Drugs** (Log P<1)		**Hydrophobic Drugs** (Log P>2)		**Multi-Drug Motif (MDM) structure**
	Lamivudine	**Tenofovir**	**Lopinavir**	**Ritonavir**	
Reference	-	+	+	+	**Yes**[b]
Variant-1	+	+	+	+	Yes
Variant-2	-	+	-	-	Yes
Variant-3	-	-	+	+	Yes
Variant-4	-	-	+	-	No[c]
	Lamivudine	**Tenofovir**	**Dolutegravir**	**Rilpivirine**	
Variant-5	+	+	+	+	Yes
Variant-6	+	+	+	-	Yes

[a]*A partial list of drug combinations with respective antiretroviral APIs were tested using the controlled solvent removal method as described. The resulting DcNP powder products were evaluated with PXRD for formation of MDM repeating units in powder form.*
[b]*Yes, indicates formation of MDM structure as evaluated by PXRD diffraction signature for MDM similar to the lead or "Reference" composition as presented in Figure 2.1, panel I.*
[c]*No, indicates the PXRD diffraction pattern retains significant signature of API or excipient profile.*

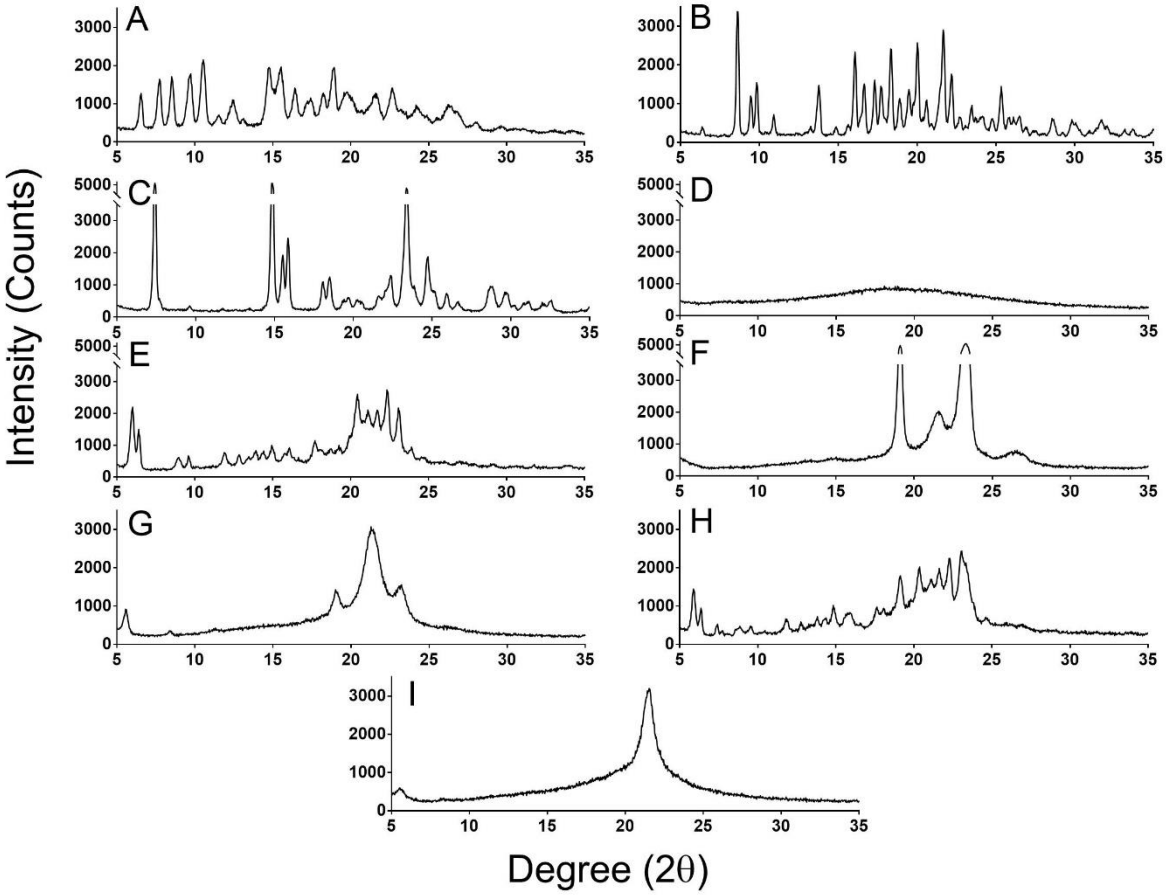

Figure 2.1. Effects of the controlled solvent removal process on the formation of a unique drug combination powder product containing 3 APIs—lopinavir (LPV), ritonavir (RTV) and tenofovir (TFV) and 2 lipid excipients—DSPC and DSPE-PEG_{2000}.

The indicated component or combination of APIs plus lipid excipient products was subjected to powder X-Ray Diffraction (PXRD) analysis (Panels A—I). The PXRD scans are presented as Degrees (in 2θ) vs Intensity (counts). Representative PXRD scans for (A) LPV, (B) RTV, (C) TFV, (D) amorphous mixture of LPV/RTV/TFV after controlled solvent removal without excipients, (E) DSPC, (F) DSPE-PEG_{2000}, (G) DSPC and DSPE-PEG_{2000} after controlled solvent removal without drugs are presented. (H) A physical mixture of drugs and excipients (LPV/RTV/TFV/DSPC/DSPEPEG_{2000}), and (I) all constituents after controlled solvent removal (LPV/RTV/TFV/DSPC/DSPE-PEG_{2000}) are presented.

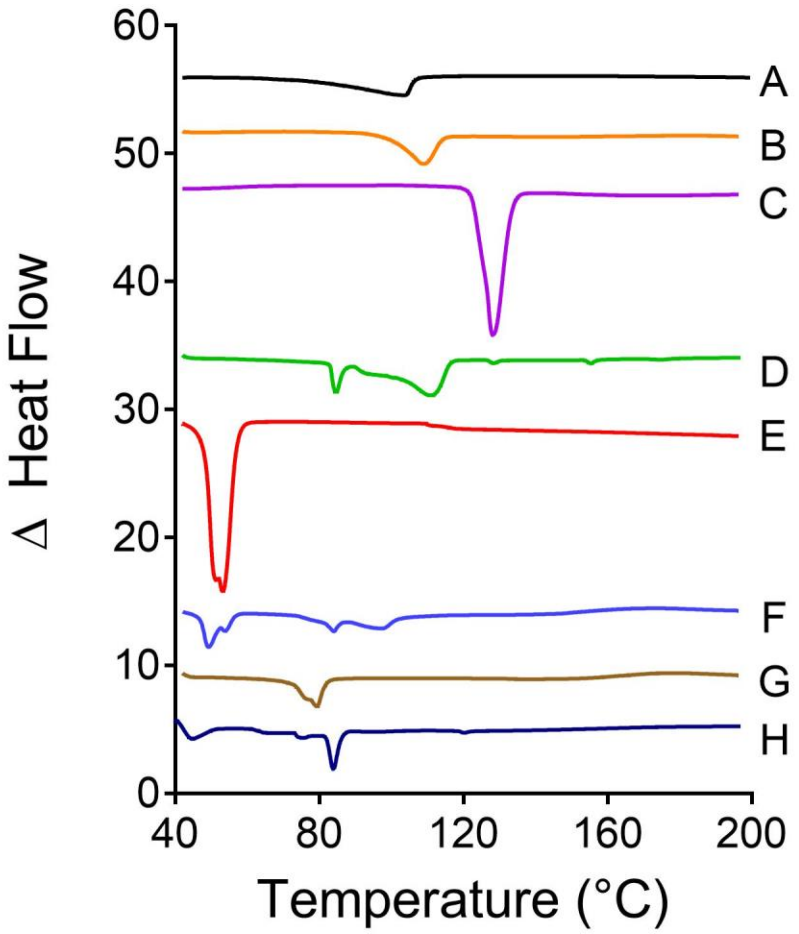

Figure 2.2. Analysis of test and control products of DcNP constituents by Differential Scanning Calorimetry (DSC).

The DSC thermograms of combination antiretroviral drugs and excipients are presented in lines A through H. Panel (A) TFV, (B) LPV, (C) RTV, (D) DSPC, and (E) DSPE-PEG_{2000}. The physical mixture of components A-E is presented in panel F. Panel (G) presents the spray dried LPV/RTV/TFV/DSPC/DSPE-PEG_{2000} (test powder) and Panel (H) presents the spray dried DSPC/DSPEPEG_{2000} (lipid excipients control).

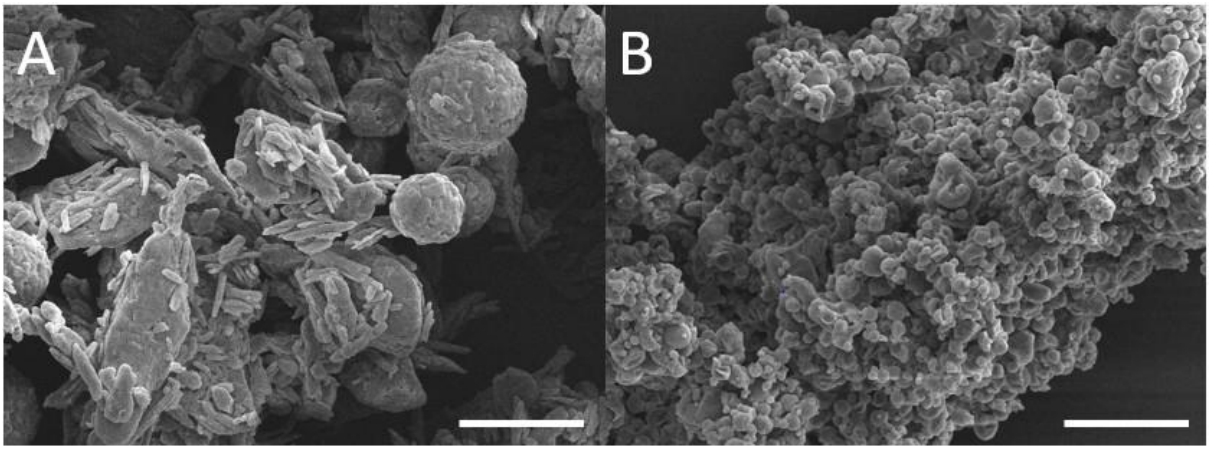

Figure 2.3. Scanning Electron Microscopy (SEM) analysis of the morphology exhibited by DcNP powder containing lopinavir, ritonavir, tenofovir, DSPC and DSPE-PEG_{2000}

Panel A presents the distinct morphology of DcNP prepared by (B) solvent removal process or (A) admixture process. Each bar indicates 10 μm.

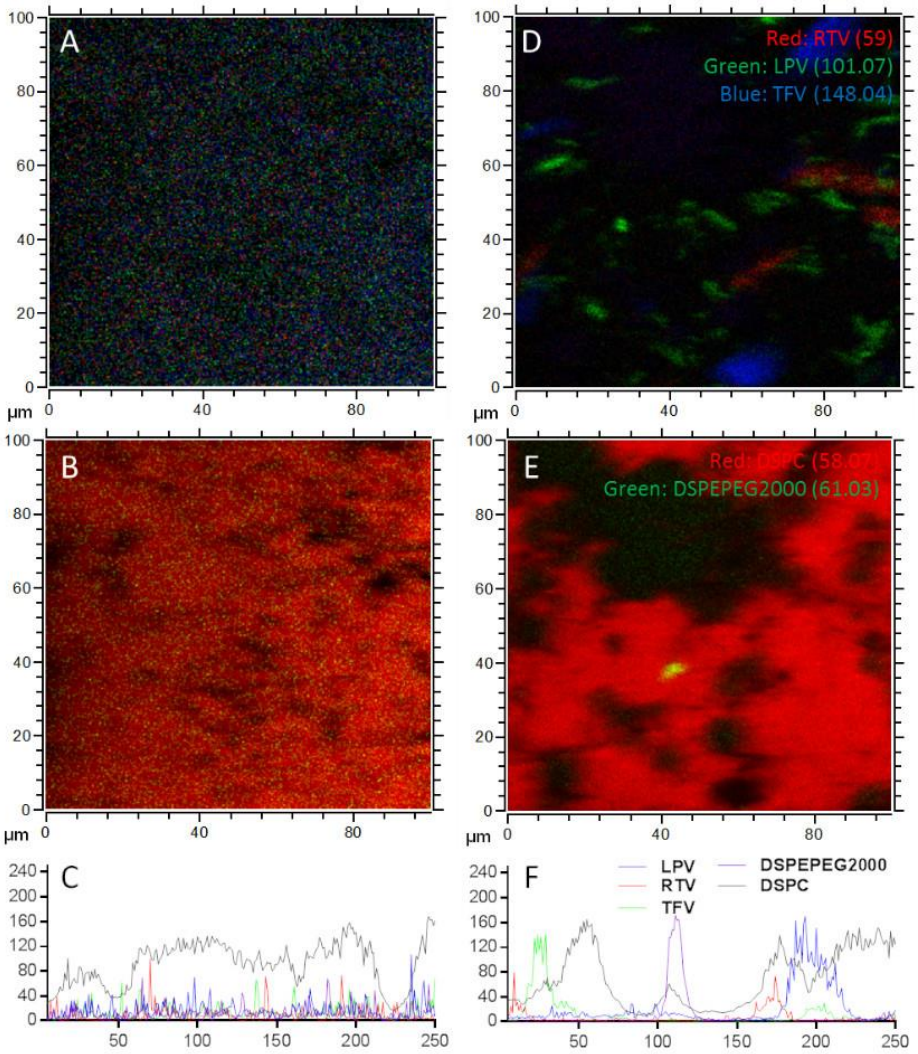

Figure 2.4. ToF-SIMs Analysis of lopinavir, ritonavir, tenofovir, DSPC and DSPE-PEG$_{2000}$ DcNPs prepared by controlled solvent removal (Panels A-C) and by admixture control (Panels D-F).

RTV (red, mass fragment of 59 AMU), LPV (green, mass fragment of 101.07 AMU) and TFV (blue, mass fragment of 148.04) are shown in panels A and D. DSPC (red, mass fragment of 58.02) and DSPE-PEG$_{2000}$ (green, mass fragment of 61.03) are shown in panels B and E. The figures generated are composites of the X, Y, and Z axis, with sequential Z-planes overlaid to present a depth profile of 100 to 200 nm. The X and Y axis in panels A, B, D and E are a µm scale grid that corresponds to the plane of powder that was analyzed. Panels C and F are a pixel analysis using ImageJ software to show the relative abundance of pixels over the X-coordinate of each image. The X and Y axis in panels C and F represent pixel counts.

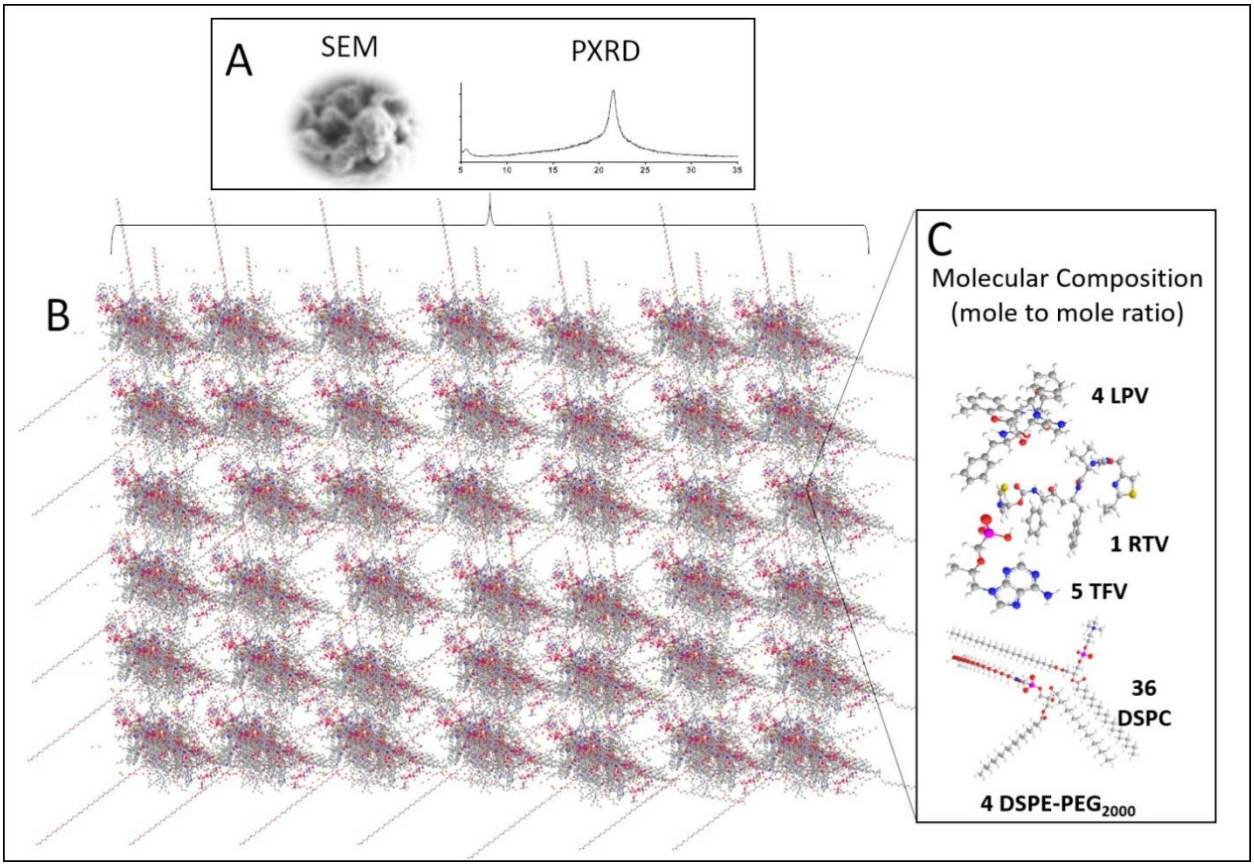

Figure 2.5. Schematic representation of multi-drug-domain or MDM repeating units of drugs and excipients in powder state.

Based on each of the 5 components in the DcNP, their respective molecular structures and corresponding molar ratios within the composition are shown. A proposed structure with MDM repeating units-representing electron dense and sparse regions- is generated using ChemDraw3D with a top-down field of view (Panel B). The repeating units of MDM are consistent with the PXRD (x-ray diffraction) analysis and scanning electron micrograph (SEM at 2000x magnification) presented in panel A. The mole (molecular) ratio of each type of compound within the repeating unit of MDM is presented in Panel C (i.e., LPV/RTV/TFV/DSPC/DSPE-PEG_{2000} at 4:1:5:36:4 mole ratio). Carbon, oxygen, nitrogen, hydrogen, phosphate and sulfur are shown in grey, red, blue, white, purple and yellow respectively. (Data not drawn to scale).

Chapter 3. DEVELOPMENT AND CHARACTERIZATION OF GEMCITABINE AND PACLITAXEL IN A DRUG COMBINATION NANOPARTICLE AS A CANCER THERAPEUTIC CANDIDATE

3.1 ABSTRACT

Gemcitabine and paclitaxel (GT) are a clinically relevant combination chemotherapy regimen used in the treatment of metastatic breast cancer. Although effective, GT combination therapy is limited by the diverging physicochemical and pharmacokinetic behavior of both drugs. In previous work, hydrophilic and hydrophobic drugs were stabilized together by lipid excipients through the formation of a multi-drug motif (MDM) structure enabled through controlled solvent removal. This study demonstrates that MDM structure can also be achieved with G, T and lipid excipients undergoing controlled solvent removal to enable the development of GT drug combination nanoparticles (DcNPs). Powder X-ray diffraction analysis confirms the structural assembly of GT in MDM form. Subsequent variations in drug to drug and total lipid to total drug ratios were pursued to optimize the composition. A 10:1 G-to-T drug ratio with a total lipid to total drug ratio of 0.6 was selected for further evaluation *in vivo*. The results from this study bridge the discovery of MDM structure in antiviral DcNPs and the application of the MDM approach in developing GT DcNPs as an optimized cancer therapeutic candidate.

3.2 INTRODUCTION

Breast cancer is the most common form of cancer in women and the second most common cause of cancer death for women in the United States (Siegel, Miller, & Jemal, 2020). Treatment for primary breast cancer consists of a combination of surgical, radiological and therapeutic interventions. The current measures used in breast cancer are effective at extending survival but are not consistently curative with almost 30% of patients advancing to metastatic disease. In regard to drug therapy, combination regimens are used to maximize antitumor effect by targeting different mechanisms in cancer cell proliferation. The combination therapy approach can also prevent drug resistance. For example, gemcitabine (G) and paclitaxel (T) are a taxane-based combination regimen used in the treatment of metastatic breast cancer (Albain et al., 2008). Gemcitabine promotes cell death by incorporating into DNA and causing chain termination; thus, inhibiting DNA synthesis and causing cell death (Mini, Nobili, Caciagli, Landini, & Mazzei, 2006). Paclitaxel promotes cell death by stabilizing tubulin and causing mitotic arrest (Jordan & Wilson, 2004). The combination of G & T increases the likelihood of eliminating cancer cells through different cancer inhibitory pathways and mechanisms. The GT combination has also been reported to have comparable clinical efficacy as other combination regimens (such as doxorubicin and cyclophosphamide) for metastatic breast cancer treatment with a manageable toxicity profile (Gudena, Montero, & Gluck, 2008). The combination of GT is typically administered as sequential infusions to avoid hypersensitivity reactions and other adverse events. However, G & T exhibit distinct pharmacokinetic properties such as clearance (G: 41-92 L/hr/m^2, T: 12.2-17.2 L/hr/m^2) and volume of distribution (G: 50-370 L/m^2, T: 227-688 L/m^2) that are affected by both dose and infusion time. Thus, the sequential infusion of these two drugs may limit the synchronization of GT concentrations in plasma or cancer cells and reduce their combination effect. In principle, if

both GT could be administered together as a single formulation or particle, then the combination effect can be enhanced, and breast cancer treatment may be improved.

From a physicochemical perspective, gemcitabine is hydrophilic (logP = -1.5) and can be reconstituted in normal saline up to 40 mg/ml for intravenous infusion. In contrast, paclitaxel is hydrophobic (logP = 3) with poor water solubility which requires CremophorEL and ethanol to form micellar solution for intravenous infusion. Due to the diverging physicochemical properties of GT, physical instability can occur when both drugs are present in the same formulation (such as precipitation due to limited water solubility). Currently, there is no established process to stably combine gemcitabine and paclitaxel together in a single formulation. In the previous chapter, we have described a novel method to stabilize hydrophilic and hydrophobic drugs together. Using a controlled solvent removal process, chemically diverse HIV drugs were stabilized by lipid excipients to form a novel multi-drug motif (MDM) structure. Subsequent suspension of the MDM powder in aqueous buffer resulted in the formation of drug combination nanoparticles (DcNPs) that exhibit long acting plasma circulation. The controlled solvent removal process was capable of achieving MDM structure with multiple different HIV drug combinations (Table 2.1) and may be adaptable to drug combination regimens for other disease conditions.

Therefore, the purpose of this chapter is to develop and characterize gemcitabine and paclitaxel drug combination nanoparticles (GT DcNPs) which could be used for treatment of breast cancer. We hypothesize that the controlled solvent removal process can be used to assemble GT in MDM structure and enable the formation of GT DcNPs after suspension in aqueous buffer. Given the exploratory nature of developing novel GT DcNP powder, rotary evaporation will be used initially (instead of spray drying) for controlled solvent removal. Since gemcitabine and paclitaxel are hazardous materials, spray drying would require a dedicated containment facility

that we do not have ready access to. Furthermore, we have shown that in smaller batches of antiviral DcNPs, rotary evaporation provides enough process control to form MDM structure. Thus, for these small scale studies, rotary evaporation will be used to generate GT DcNP powder. Subsequent analysis with powder x-ray diffraction will ensure the quality and consistency of the rotary evaporated powder. After suspension, the stabilized GT DcNPs can then be evaluated *in vivo* to determine whether the synchronized delivery of both drugs can improve anti-tumor effect. This brief chapter will act as a bridge between the discovery of MDM structure in antiviral DcNP powder presented in Chapter 2 and the evaluation of GT DcNPs *in vivo* presented in Chapter 4.

3.3 MATERIALS AND METHODS

3.3.1 *Materials*

Gemcitabine free base (>99%; 2',2'-Difluorodeoxycytidine; CAS 95058-81-4) and paclitaxel (>99.5%; CAS 33069-62-4) were purchased from LC Laboratories (Woburn, Massachusetts). 1,2-distearoyl-sn-glycero-3-phosphocholine (DSPC) and 1,2-distearoyl-sn-glycero-3-phosphoethanolamine-N- [amino (polyethylene glycol)-2000] (ammonium salt) (DSPE-PEG_{2000}) (GMP grade) were purchased from Cordon Pharma (Liestal, Switzerland). Anhydrous ethanol was purchased from Decon Pharmaceuticals (King of Prussia, PA). All other reagents used were of analytical grade or higher.

3.3.2 *Preparation and characterization of gemcitabine and paclitaxel (GT) drug combination particles*

The in-depth preparation and characterization of the final GT DcNP product is presented in Chapter 4, Materials and Methods, 4.3.2. Briefly, T and G were solubilized together in hot ethanol (60°C) with DSPC and $mPEG_{2000}$-DSPE in a round bottom flask. Each tested composition

of G,T, DSPC and mPEG$_{2000}$-DSPE is presented in Tables 3.1 and 3.2. In all compositions, the total concentration of solutes (drugs + excipients) in ethanol was 5% w/v. Solvent was removed by rotary evaporation followed by vacuum desiccation. Rotary evaporation was used for the preliminary assessment of GT DcNPs instead of spray drying to preserve resources. The dry film was removed from the round bottom flask and triturated to achieve a uniform dry powder. This dry powder was used for powder analysis.

To make GT DcNP in suspension, dry GT DcNP powder was rehydrated in 0.45% NaCl with 20 mM $NaHCO_3$ buffer at 70°C and a pH of 7.4 to achieve a nominal concentration of 100 mM total lipids. Particle size reduction was achieved through bath sonication (Avanti Polar Lipids, Inc. Alabaster, AL) (5 min on, 5 min off, 3 cycles). Particle size was determined by photon correlation spectroscopy using a NICOMP 380 ZLS (Particle Sizing Systems, Santa Barbara, CA). Drug association efficiency (AE%) was determined by dialyzing 100 µl of the DcNP suspension (6-8k MWCO) against 1000 x volume (100 mL, pH=7.4) of bicarbonate buffered saline for 4 hours at room temperature. AE% was calculated as the ratio of pre- over post-dialysis concentrations of G or T.

3.3.3 *Powder X-ray Diffraction*

Powder X-ray Diffraction (PXRD) was used to characterize the matrix structure and crystallinity of DcNP powder. PXRD analysis is performed on a Rigaku Benchtop XRD instrument (The Woodlands, TX, USA) with Cu-Kα radiation. Operational voltage and amperage were set to 40.0 kV and 40.0 mA, respectively. Experimental parameters include a step size of 0.035°2θ in an operating range of 5° to 50° 2θ. Powder (~100-200 mg) was pressed into a sample container to obtain a flat upper surface. The data collected were plotted as intensity (counts) vs angle (2θ).

3.4 RESULTS

3.4.1 *Development and characterization of gemcitabine and paclitaxel drug combination nanoparticles (GT DcNP) in powder MDM form*

To investigate whether MDM structure can be achieved with a combination chemotherapy regimen used in breast cancer, gemcitabine and paclitaxel were chosen to formulate as a DcNP. As a starting point, GT was evaluated in a fixed 10:1 G:T mass ratio based on the clinical dosing of GT combination regimens (Albain et al., 2008). GT combination powder was formulated with the same lipid excipients (DSPC and DSPE-PEG_{2000}) in a similar lipid to drug ratio using the rotary evaporation method for smaller scale studies described above (Materials and Methods 2.3.2). The resultant powder, and the pure drug powders were analyzed with powder x-ray diffraction. In Figure 3.1, gemcitabine free base (Panel A) and paclitaxel (Panel B) exhibit individual crystalline signatures as observed by their respective diffraction patterns. DSPC (Panel C) and DSPE-PEG_{2000} (Panel D) also exhibit their individual crystalline signatures. The physical mixture of gemcitabine, paclitaxel and lipid excipients (Panel E) results in an aggregate diffraction pattern of the crystalline composition. When the same composition undergoes controlled solvent removal, a transition towards the MDM is observed similar to that previously observed with antiviral DcNP powder.

In previous studies with antiviral DcNP powder, we have established this PXRD signature as a criterion for successful powder formation. When antiviral DcNP powder exhibits the PXRD signature presented in Figure 2.1, I, we have observed consistent association efficiency of drugs measured through membrane dialysis and extended plasma circulation when administered subcutaneously to non-human primates. Alternatively, when additional peaks are observed in the diffraction pattern (associated with the presence of crystalline material), association efficiency of drugs tend to be low and we do not proceed with *in vivo* studies. This criterion has been applied

for the various drug combinations presented in Table 2.1 and has been consistent across studies. These results taken together show that the controlled solvent removal process can assemble the chemotherapy combination of gemcitabine and paclitaxel together in a similar MDM structure as previously reported DcNP powders.

3.4.2 *Optimization of gemcitabine and paclitaxel drug combination nanoparticles (GT DcNP) in suspension*

We next evaluated the effect of different G to T mass ratios on the formation of MDM structure. The fixed dose ratio of gemcitabine and paclitaxel in DcNPs can impact the antitumor effect and toxicity profile of GT combination therapy. Thus, it is of interest to investigate the range of ratios that can be formulated in MDM form. The total lipid to paclitaxel ratio was held constant (as much as possible) due to the reported physical stability parameters of paclitaxel and lipid excipients (A. Sharma & Straubinger, 1994). Previous studies have shown that paclitaxel alone can rapidly precipitate from lipid bilayers when the molar % of drug exceeds 3% (A. Sharma & Straubinger, 1994). As a result, testing of different drug and lipid ratios was designed around that documented limitation. The mass ratio between gemcitabine and paclitaxel was changed to generate 7 variations of GT DcNP powder. The resultant powders were analyzed with PXRD to evaluate MDM formation. Figure 3.2 presents the diffraction patterns of GT DcNP powder with varying G to T mass ratios. In higher G:T mass ratios (20:1, 10:1 and 5:1), the PXRD signature is consistent with the MDM structure observed in antiviral DcNPs (Figure 2.1, Panel I). As the amount of gemcitabine in the composition decreases (2:1 and 1:1), small changes in structure are observed with new peaks appearing in the diffraction pattern. In the single drug control powders (10:0 and 0:1, G:T), gemcitabine with lipid excipients produces an MDM structure, while additional peaks are apparent in the paclitaxel with lipid control. These data indicate that the MDM

structure is fairly stable across a range of different G to T mass ratios. When the ratio of G to T is very low (or G is not present in the composition), additional peaks attributable to the distinct diffraction pattern of PEG is observed, suggesting that hydrophilic G is important to the overall stability of the MDM structure. We next evaluated the effect of different G to T mass ratios on the physical characteristics of GT DcNP powder suspended in aqueous buffer. The final product of GT in DcNP is intended to be an injectable formulation and consequently, the characterization of GT DcNPs as a suspension is important. As shown in Table 3.1, the AE% and particle size of GT DcNPs with different G to T mass ratios appear to be fairly similar. Greater variability is observed with G AE% but there is no clear trend in the data. No precipitation or aggregation was observed in any of the GT DcNP variants. Based on these results, the 10:1 G to T ratio was chosen for further investigation to reproduce the clinical dosing of GT combination regimens.

Using the 10:1 GT ratio, further optimization of GT DcNP was performed by testing different total lipid to total drug molar ratios. By evaluating different lipid to drug molar ratios, we can begin to determine the maximum and minimum number of lipid excipient molecules required to stabilize gemcitabine and paclitaxel. These new variants were formulated and characterized using the same approach described above. As shown in Table 3.2, MDM structure was achieved in every ratio except for the lowest ratio (0.1). When these variants are suspended in aqueous buffer (as described above), notable changes in suspension behavior were observed. In the variant with very low total lipid to total drug molar ratio (0.1), the resultant powder was prone to agglomeration during the trituration step (Materials and methods 3.3.2). When the low lipid variant was added to buffer, the agglomerated powder did not suspend and attempts to mechanically break up the agglomerate with a spatula was unsuccessful. The variants with higher total lipid to total drug molar ratios (1.3 and 1.9) were able to suspend successfully but gelled within 30 minutes of

suspension. These data show that there is likely a range of total lipid to total drug molar ratios between 0.1 and 1.3 that can achieve a successful liquid suspension of DcNPs. Future studies that utilize smaller steps between molar ratios may be able to more clearly define the range of lipid to drug ratios that are capable of achieving MDM structure. Taken together, these results show that the GT DcNP with a 10:1 G to T mass ratio and a 0.6 total lipid to total drug molar ratio is a suitable lead composition for further development and *in vivo* evaluation.

3.5 DISCUSSION

This study presents an extension of the controlled solvent removal process used to form long acting, HIV DcNPs into chemotherapy combinations. The chemotherapy combination of gemcitabine and paclitaxel were stabilized with lipid excipients through rotary evaporation by forming MDM structure across a number of compositional variants. The empirical screening of GT DcNP variants guided the selection of a lead composition for testing *in vivo*. Subsequently, GT DcNPs will be evaluated through *in vivo* pharmacokinetic studies. Based on the MDM structure of GT DcNPs, we expect that GT DcNPs will exhibit similar long acting plasma circulation. If GT DcNPs are stable *in vivo*, then they can be used to synchronize the delivery of gemcitabine and paclitaxel to cancer cells for improved anti-tumor effect and test the overarching hypothesis of this dissertation. The extension of DcNP technology into oncology may enable the development of novel, long acting injectables capable of delivering combination chemotherapy drugs together to target cancer cells with improved antitumor effect.

Table 3.1. Effect of G to T mass ratios on GT DcNP characteristics after suspension and particle size reduction*.

GT DcNP Composition (% in weight)				G:T ratio (w/w)	MDM	Association to DcNP (%)		Size (nm)
DSPC	DSPE-PEG_{2000}	G	T			G	T	
59.8	23.6	16.6	-	10 to 0	+	9%	-	50.2 ± 31.6
50.6	20.0	28.1	1.4	20 to 1	+	7%	>99%	50.0 ± 34.3
58.8	23.2	16.7	1.6	10 to 1	+	19%	>99%	54.8 ± 35.5
64.0	25.2	8.9	1.8	5 to 1	+	14%	>99%	57.8 ± 37.9
67.6	26.7	3.8	1.9	2 to 1	-	11%	>99%	44.5 ± 32.7
68.9	27.2	1.9	1.9	1 to 1	-	18%	>99%	55.9 ± 26.9
70.3	27.7	-	2.0	0 to 1	-	-	>99%	48.8 ± 34.1

*The gemcitabine and paclitaxel drug combination powders with varying G-to-T ratios presented in Figure 3.2 were suspended in aqueous buffer (0.45% NaCl (w/v) containing 20 mM $NaHCO_3$buffer) and sonicated for particle size reduction as described in the Materials and Methods. The suspended products with varying G-to-T ratios were analyzed by membrane dialysis under sink conditions (6-8 Da MWCO, 1000x volume for 4 hours). Association efficiencies of G and T are calculated as the ratio of pre- over post-dialysis concentrations of G and T and presented as a %. The particle size of suspended DcNPs with varying G-to-T ratios was determined by photon correlation spectroscopy and reported as a mean ± standard deviation based on z-average distribution. The specific weight composition of drugs and lipids in combination are presented in the table as a % of total mass.

Table 3.2. Effect of lipid to drug ratio on GT DcNP powder and suspension characteristics with a fixed 10:1 G to T mass ratio*

Total Lipid to Total Drug Ratio (mole/mole)	Composition by mole %				MDM	Notes
	DSPC	DSPE-PEG_{2000}	Gemcitabine	Paclitaxel		
0.1	5	1	91	3	-	Powder was glassy in appearance and prone to agglomeration. Suspension of powder in buffer was unsuccessful.
0.6	35	4	59	2	+	**Powder suspension was uniform, sonication was successful.**
1.3	51	6	42	1	+	Powder suspension thickened into a gel after 30 minutes. Sonication was unsuccessful.
1.9	59	7	33	1	+	Powder suspension thickened into a gel after 30 minutes. Sonication was unsuccessful.

*The 10:1 G-to-T ratio was kept constant and the ratio of total lipid to total drug was varied using a fixed 9:1 DSPC to DSPE-PEG_{2000} ratio. The listed compositions were dissolved in ethanol and rotary evaporated using the same controlled solvent removal process described. The dried product was then analyzed by PXRD to determine MDM formation. The dried product was also suspended in aqueous buffer as described, and observations on suspension are provided

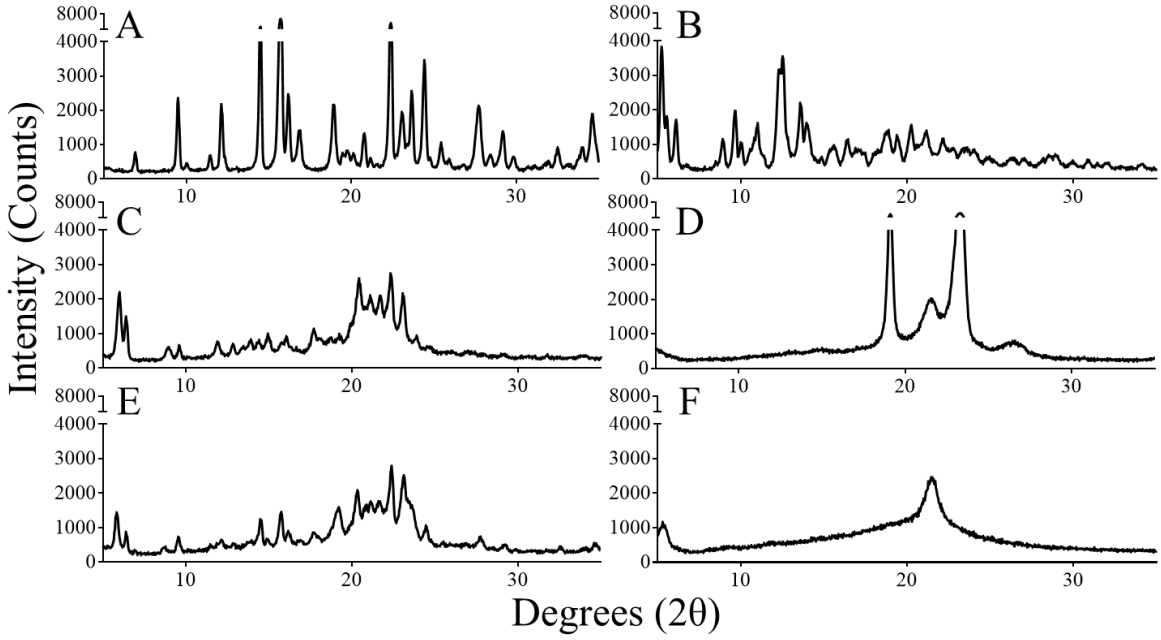

Figure 3.1 Formation of MDM structure in novel cancer drug combination powder product composed of gemcitabine and paclitaxel in the presence of lipid excipients DSPC and DSPE-$PEG_{2000,}$ after processing under the controlled solvent removal technology (as described in Chapter 2)

The current metastatic cancer drug combination composed of gemcitabine and paclitaxel were formulated with lipid excipients, DSPC and DSPE-PEG_{2000}, and rotary evaporated by the controlled solvent removal method described in Chapter 2 and detailed in the Materials and Method. The powder product was analyzed by powder X-Ray Diffraction (PXRD) analysis. The PXRD scans presented as Degrees (in 2θ) vs Intensity (counts) for the test and control powder products are as follows: (A) Gemcitabine or G, (B) Paclitaxel or T, (C) DSPC lipid excipient, (D) DSPE-PEG_{2000} lipid excipient, (E) A physical mixture of both GT drugs and lipid excipients (G/T/DSPC/DSPE-PEG_{2000}-control) and (F) all constituents after controlled solvent removal (G/T/DSPC/DSPE-PEG_{2000}-test) are presented. The sample composition of Panel (E) and (F) are identical and the mass ratio of G/T/DSPC/DSPE-PEG_{2000} is 16.7/1.6/58.8/23, respectively.

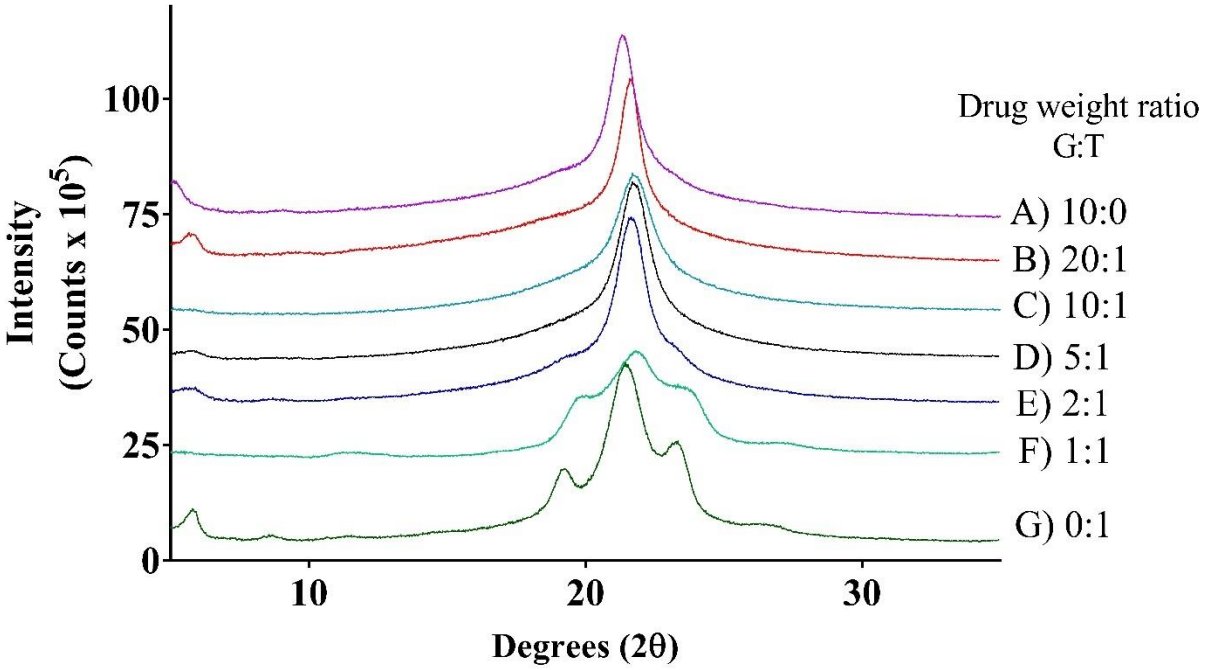

Figure 3.2 Effect of varying G to T ratios on formation of GT DcNP MDM structure.

The total drugs to lipid ratio (w/w) were kept constant while varying the weight ratio of Gemcitabine-to-Paclitaxel (G-to-T) in the compositions. The GT DcNP powder products were analyzed based on PXRD as described in Figure 3.1. The result of the PXRD pattern for the varying G-to-T mass ratios: (A) 10:0, (B)20:1, (C) 10:1, (D) 5:1, (E) 2:1, (F) 1:1 and (G) 0:1 are presented as intensity (counts) vs. degrees (2θ).

Chapter 4. NOVEL LONG-ACTING DRUG COMBINATION NANOPARTICLES COMPOSED OF GEMCITABINE AND PACLITAXEL ENHANCE LOCALIZATION OF BOTH DRUGS IN METASTATIC BREAST CANCER NODULES

A version of this chapter was published in:

Yu, J. et al. Novel Long-Acting Drug Combination Nanoparticles Composed of Gemcitabine and Paclitaxel Enhance Localization of Both Drugs in Metastatic Breast Cancer Nodules. Pharm Res 37, 197

4.1 ABSTRACT

Gemcitabine and paclitaxel is a combination drug regimen prescribed used to treat metastatic breast cancer. By utilizing two drugs with different mechanisms of action, this combination is meant to maximally suppress cancer cells while minimizing the development of drug resistance. This combination is used extensively in the clinic but dose-limiting toxicities and a lack of synchronized exposure of both drugs in plasma and cancer cells limits its effect. To enhance the coordinated exposure of both drugs in cancer cells, drug combination nanoparticles (DcNPs) composed of hydrophilic gemcitabine (G) and hydrophobic paclitaxel (T) were developed. GT DcNPs were evaluated based on particle size and drug association efficiency (AE%). An optimized GT DcNP composition (d=59.2 nm ±9.2 nm) was found to be suitable for IV formulation. The effect of DcNP on GT plasma time-course and tissue distribution was characterized in mice and a pharmacokinetic model was developed. Plasma exposure of G and T were enhanced 61-fold and 3.8-fold when given in DcNP form compared to the conventional formulation, respectively. Pharmacokinetic modeling and simulation showed that both G and T remain highly associated to DcNPs *in vivo* (G: 98%, T:75%). GT DcNPs have minimal distribution to healthy organs with selective distribution and retention in tumor burdened tissue. Mice tumor bearing lungs exhibited a 5-fold higher tissue-to-plasma ratio of gemcitabine in GT DcNPs compared to healthy lungs. Taken together, these data suggest that DcNPs can deliver hydrophilic G and hydrophobic T together to cancer nodules and produce long acting exposure, likely due to stable GT association to DcNPs *in vivo*.

4.2 INTRODUCTION

With improved diagnosis, novel targeted therapies and hormone-based therapies, the odds of 5-year survival in early-stage breast cancer patients is high at approximately 95% (Siegel et al., 2020). However, almost 30% of these patients progress to metastatic disease and subsequently, 5-year survival rates are low at 27% (R. Wang et al., 2019). Once they reach the metastatic stage and drug resistance emerges, early-stage hormone receptor targeted treatments are no longer effective. Thus, metastatic patients are often treated with highly potent but toxic (and dose-limiting) chemotherapy. Under those circumstances, drug combination regimens are prescribed as a combination of two or more chemotherapeutics to maximize cancer cell death and overcome drug resistance. These regimens are typically based on anthracyclines (i.e. doxorubicin, daunorubicin, epirubicin) or taxanes (i.e. paclitaxel, docetaxel) in combination with other agents. Neither taxanes nor anthracyclines are superior to one another, but metastatic patients will likely have a limited duration of treatment with anthracyclines due to the cumulative lifetime risk of cardiac toxicity (A. M. Rahman, Yusuf, & Ewer, 2007). This cumulative cardiotoxicity risk is inherent to anthracycline therapy. Once patients have reached their lifetime anthracycline dose, they can no longer be treated with doxorubicin, daunorubicin or epirubicin without the risk of heart failure. To overcome anthracycline dependent dose-limiting cardiotoxicity, taxane combinations with gemcitabine are used. Gemcitabine and paclitaxel (GT, Gemcitabine = G, Paclitaxel = T) is a combination regimen with a 41.4% response rate in breast cancer, similar to that of anthracycline combinations (Albain et al., 2008). However, GT is given as sequential infusions (T over 3 hours followed by G over 30 to 60 minutes) to minimize adverse events, which also reduces the time where both G and T circulate in plasma at pharmacologically relevant concentrations.

When G is given as a single agent, it requires intracellular phosphorylation to a tri-phosphate form to mediate cytotoxicity. In patients with leukemia, the concentration of G tri-phosphate in cancer cells is proportional to the plasma concentration of G up to 3 μg/mL (Ralf Grunewald et al., 1990). At higher plasma concentrations of G, the tri-phosphate levels no longer increase above 3 μg/mL; thus this target concentration is currently used for G in plasma (Luu et al., 2010). The target therapeutic plasma concentrations of T were determined by establishing the threshold concentrations for neutropenia (0.09 μg/mL) with the intent to maximize T dosing before adverse events occur (Gianni et al., 1995). Despite having target therapeutic plasma concentrations, there is only a 2-hour window in which G and T circulate above those concentrations under the current recommended dose and time sequences. This is because of the varying physicochemical and pharmacokinetic profile of GT. Longer or simultaneous infusions have been attempted in clinic, but poor patient tolerability and the physical incompatibility of GT limit these approaches (R. E. Smith et al., 1999). Given the physicochemical and clinical characteristics of GT, the pharmacologic effect of this regimen can be improved by synchronizing distribution and retention of both drugs in target tissues to maximize therapeutic benefit. This way, a lower overall dose may be needed to eliminate cancer cells and healthy tissues will be less exposed to drug, potentially reducing off-target toxicity. One approach to producing intracellular GT synchronization in target tissues is using a drug carrier that enables accumulation in the target tissues and cells, and in turn reduce the presence of free drugs in plasma. By reducing the fraction of free drug in plasma, systemic toxicity associated with high concentrations of cytotoxic drugs in off-target tissues is minimized (Ait-Oudhia, Mager, & Straubinger, 2014).

To achieve the synchronized delivery of GT to target cells, drug delivery systems can be used to carry multiple chemotherapeutic agents as a single particle. However, water soluble G

(logP= -1.4) and water insoluble T (logP=3) are difficult to co-formulate with existing formulation strategies. Drug delivery systems such as liposomes (100 nm to several microns in diameter) or small polymeric nanoparticles (<10 nm in diameter) may, in some cases, mitigate systemic toxicity by reducing the high concentration of free drugs that cause toxicity. However, targeting these particles to cancer cells is a challenge. Biological barriers such as the reticuloendothelial system can sequester liposomes (>200nm) into the liver and spleen for elimination. Thus, premature clearance prevents liposomal drugs from reaching target cells. Small polymeric nanoparticles or micelles (<10 nm) can undergo renal filtration and elimination by the kidney, leading to short plasma half-life and limited effect.

Recently, our team has developed a method to co-formulate hydrophobic and hydrophilic drugs together in a stable manner as a drug combination particle suitable for injectable dosage form. This novel drug-combination delivery platform uses a simple approach to combine chemically distinct (e.g., water soluble and insoluble) drugs and stabilize them with lipid excipients to generate a drug combination nanoparticle (DcNP) in suspension. DcNPs have been used to deliver a combination of 3 or more water soluble and insoluble anti-HIV drugs in non-human primates (NHP). After subcutaneous administration into NHPs, anti-HIV DcNPs were shown to produce long-acting drug concentrations in lymphocytes and lymph nodes as well as in plasma (Freeling et al., 2015; Koehn et al., 2018; Kraft, McConnachie, et al., 2018; Perazzolo et al., 2018). This DcNP platform has been successfully applied to a range of HIV antiviral drugs, including tenofovir (logP=-1.6), lopinavir (logP=4.7), atazanavir (logP=4.5) and ritonavir (logP=5.6) (Maartens et al., 2014; McConnachie et al., 2018). The long acting plasma circulation of anti-HIV DcNPs for up to 4 weeks suggests that these particles have specific characteristics that

allow them to overcome biological barriers such as sequestration in healthy (e.g. liver and kidney) organs or premature elimination.

Thus, the goal of this study is to determine whether water soluble G and water insoluble T can be stably assembled together in DcNP form and allow synchronization of both drugs in metastatic breast cancer burdened tissue. We have stabilized GT in DcNP form and transformed GT from a current short-acting combination therapy into a long-acting combination therapy in target tissues and cells. In addition, we have used pharmacokinetic modeling and simulations as a novel approach to distinguish DcNP associated and dissociated fractions of GT in plasma. By doing so, we can begin to understand how the fraction of drug association to DcNP *in vivo* impacts the overall pharmacokinetics and exposure of GT when formulated together in DcNP dosage form.

4.3 MATERIALS AND METHODS

4.3.1 *Materials*

Gemcitabine free base (>99%; 2',2'-Difluorodeoxycytidine; CAS 95058-81-4) and paclitaxel (>99.5%; CAS 33069-62-4) were purchased from LC Laboratories (Woburn, Massachusetts). 1,2-distearoyl-sn-glycero-3-phosphocholine (DSPC) and 1,2-distearoyl-sn-glycero-3-phosphoethanolamine-N- [amino (polyethylene glycol)-2000] (ammonium salt) (DSPE-PEG_{2000}) (GMP grade) were purchased from Cordon Pharma (Liestal, Switzerland). Anhydrous ethanol was purchased from Decon Pharmaceuticals (King of Prussia, PA). All other reagents used were of analytical grade or higher.

4.3.2 *Preparation and characterization of gemcitabine and paclitaxel (GT) drug combination particles*

T (0.7 mg/mL) and G (7 mg/mL) were solubilized together in hot ethanol (60°C) with DSPC (25 mg/mL) and $mPEG_{2000}$-DSPE (10 mg/mL) in a round bottom flask. The total concentration of solutes (drugs + excipients) in ethanol was 5% w/v. Solvent was removed by rotary evaporation followed by vacuum desiccation. The dry film was removed from the round bottom flask and triturated to achieve a uniform dry powder. Dry powder was rehydrated in 0.45% NaCl with 20 mM $NaHCO_3$ buffer at 70°C and a pH of 7.4 to achieve a nominal concentration of 100 mM total lipids. Particle size reduction was achieved through bath sonication (Avanti Polar Lipids, Inc. Alabaster, AL) (5 min on, 5 min off, 3 cycles). Particle size and zeta potential were determined by photon correlation spectroscopy using a NICOMP 380 ZLS (Particle Sizing Systems, Santa Barbara, CA). The pH of the DcNP suspension was measured using MQuant pH-indicator test strips (Supelco|Sigma Aldrich, St. Louis, MO). The osmolarity of GT DcNPs was measured using a Vapro osmometer (Wescor Inc, Logan, UT).

The morphology of GT DcNPs was investigated compared to a liposome control using transmission electron microscopy (TEM) with negative staining. Liposome controls were formed by dissolving egg L-α-phosphatidylcholine (EPC) (Avanti polar lipids, Inc. Alabaster, AL) in chloroform. Chloroform was removed via rotary evaporation and the dry lipid film was rehydrated in normal saline. The rehydrated lipid film was then extruded through 100 nm pores to yield a liposome suspension. Sample suspensions containing either GT DcNPs or liposomes were transferred onto a TEM grid (copper grid, 300-mesh, coated with carbon and Formvar film). Particles from the sample suspensions were allowed to settle onto the grid and excess suspension was removed by filter paper after 5 min. The grid was then stained with 4 μL 5% uranyl acetate. After one minute, excess staining solution was removed by filter paper and the grid was air-dried.

All images were acquired on a Tecnai G2 F20 electron microscope (FEI, Hillsboro, OR) operating at 200 kV.

Drug association efficiency (AE%) was determined by dialyzing 100 μl of the DcNP suspension (6-8k MWCO) against 1000 x volume (100 mL, pH=7.4) of bicarbonate buffered saline for 4 hours at room temperature. Drugs were extracted by acetonitrile and drug concentrations in pre and post- dialysis DcNP suspensions were measured with a Shimadzu HPLC-UV system (Kyoto, Japan). Chromatographic separation was achieved using a Kinetex C18 column (100 Å, 5 μm, 4.6 mm × 100 mm) (Phenomenex, Torrance, CA). The flow rate was set to 1.0 mL/min with a 10 μl sample injection volume. The mobile phase for separation consisted of pump A (Acetonitrile) and B (10 mM Ammonium Acetate in water). The gradient program used was as follows: pump B was set to 40%, and increased to 100% over 5 minutes. The wavelength for detection of gemcitabine and paclitaxel was 254 nm. AE% was calculated as the ratio of pre- over post-dialysis concentrations of G or T. Five independent batches were characterized to assess batch to batch reproducibility.

4.3.3 *Preparation and characterization of gemcitabine and paclitaxel (GT) combination in Cremophor El suspension (CrEL)*

To prepare an equivalent GT drug combination for use as a control formulation, T was first dissolved in ethanol (20 mg/mL). To make a stable suspension, the 20 mg/mL T was diluted with Cremophor EL [1:1, (v/v)] (Sigma-Aldrich, St. Louis, MO). The resultant T in suspension was further diluted 10-fold with PBS containing pre-dissolved G (hydrochloride salt, 12.65 mg/mL). The final concentrations of drug combination in suspension were 10 mg/ml G and 1 mg/ml T. The control drug combination in CrEL suspension was used in animal studies within the same day of preparation due to instability.

4.3.4 *Pharmacokinetic study of gemcitabine and paclitaxel (GT) in DcNPs compared to CrEL*

Animal studies were conducted in accordance with the University of Washington Institute of Animal Care and Use Committee (IACUC) approved protocol number 2372-06 and federal guidelines. Five- or six-week old female BALB/c mice were purchased from The Jackson Laboratory (Bar Harbor, Maine) and housed in an animal research facility for at least one week before use. Mice were approximately 8 to 9 weeks old for the pharmacokinetic studies. Mice were administered GT either as DcNP or CrEL suspensions intravenously by tail vein injection at 50/5 mg/kg (G/T) in a 100 µl bolus volume (G ~10 mg/mL, T ~1 mg/mL). Blood was collected through retro-orbital bleeding at 5, 60, 180, 360, 1440 (24 hour), and 2880 min (48 hour) for DcNP and at 5, 15, 60, 120, 180 and 360 min for the GT CrEL formulation. Each mouse represented a single biological replicate and 3 mice were used to estimate the mean plasma concentration time course of G and T at each time point. Necropsies were performed on each animal to harvest respective tissues for tissue distribution studies.

4.3.5 *Drug extraction from plasma and tissues*

Protein precipitation was used to extract G, 2′,2′-difluoro-deoxyuridine (dFdU), and T from plasma or tissue homogenates. Briefly, 50 µL of sample was transferred into 1.5 mL tubes with or without dilution by blank matrix to an appropriate concentration range. Samples were spiked with internal standards followed by the addition of 9 volumes of acetonitrile (450 µL). Samples were then vortexed for 6 minutes and centrifuged at 4°C for 15 minutes at 20,817 RCF. The supernatant was removed and dried under nitrogen at 40°C. The dried samples were reconstituted to 50 µL containing 20% methanol and 80% water.

4.3.6 *Quantification of gemcitabine, paclitaxel and dFdU by LC-MS/MS*

Drugs extracted from biological matrices such as plasma or tissue homogenates were quantified by a Shimadzu HPLC system coupled to a 3200 QTRAP mass spectrometer (Applied Biosystems, Grand Island, NY). The HPLC system consisted of two Shimadzu LC-20A pumps, a DGU-20A5 degasser, and a Shimadzu SIL-20AC HT autosampler. The mass spectrometer was equipped with an electrospray ionization (ESI) TurboIonSpray source. The system was operated with Analyst software, version 1.5.2 (ABSciex, Framingham, MA). Chromatographic separation of G and T was achieved using a Synergi column (100 × 2.0 mm; 4-µm particle size) (Phenomenex, Torrance, CA) with an inline C8 guard column (4.0 × 2.0 mm) also from Phenomenex. The flow rate was set to 0.5 mL/min with a 5 µl sample injection volume. The mobile phase for separation consisted of pump A (20 mM Ammonium Acetate in water) and B (Reagent Alcohol). The gradient program used was as follows: pump B was maintained at 20% for 1.0 minute, then increased to 97% at 2.0 minutes, held at 97% until 3.0 minutes, ramped to 3% by 4.0 minutes and held until 5.5 minutes. The needle was washed with isopropanol after each injection. Analytes were monitored using multiple-reaction monitoring (MRM) for positive ions. The following ion transitions were monitored: gemcitabine, m/z 264.066→112.000; dFdU, m/z 265.084→113.200; paclitaxel, m/z 854.266→286.200; a stable labeled isotope of gemcitabine ($C_8C^{13}H_{12}ClF_2N^{15}N_2O_4$) (m/z 267.067→115.100) was used as an internal standard for gemcitabine and dFdU; docetaxel (m/z 830.312→549.3) was used as an internal standard for paclitaxel.

4.3.7 *Estimating the maximum dissociated fraction of gemcitabine and paclitaxel in vivo when administered as a DcNP*

To estimate a maximum dissociated fraction ($f_{diss.\ max}$) of GT from DcNPs *in vivo*, we first utilized a non-compartmental approach based on the plasma AUCs of equi-molar injections of *DcNP* and *CrEL* formulations (Perazzolo et al., 2020):

$$f_{diss.\ max} = \frac{AUC_{0\ \to\infty, CrEL}}{AUC_{\ 0\to\infty, DcNP}} \tag{4.1}$$

In Eq. 4.1, we assume that systemic clearance of G or T administered as DcNPs only occurs after drug dissociates from the particles, and dissociated drug has the same clearance pathways as the free drug control (CrEL). This non compartmental approach also assumes that drug clearance occurs solely in the central compartment. For our two drugs of interest, T is mainly metabolized in the liver by CYP3A4 and CYP2C8 but G is metabolized by ubiquitous cytidine deaminase (CDA) (Veltkamp, Pluim, van Tellingen, Beijnen, & Schellens, 2008). To understand the impact of the ubiquitous metabolism of G on its pharmacokinetic profile, we used the plasma concentration of the primary metabolite of G, dFdU, as a biomarker for dissociated drug. For Eq. 4.2, we also assume that G conversion to dFdU exhibits linear kinetics. The equation below then provides an estimate of the fraction of the G dose metabolized to dFdU. If the calculated fraction metabolized ($f_{diss.G\to dFdU}$) from Eq. 4.2 equals the $f_{diss.\ max}$ from Eq. 4.1, we can surmise that once G is released from DcNPs at all locations in the body it exchanges readily with the circulating G and subsequently undergoes metabolism (i.e., metabolism of all dissociated drug occurs in the central compartment). However, if some or all of the drug released from DcNPs in peripheral tissue is immediately metabolized to dFdU without exchanging with G in circulation, we would then expect the $f_{diss.G\to dFdU}$ estimates from Eq. 4.2 to exceed the $f_{diss.\ max}$ from Eq. 4.1 (i.e, dissociated drug is metabolized in both the central and peripheral compartments).

$$\frac{G\ AUC_{\ 0\rightarrow\infty,CrEl}}{dFdU\ AUC_{\ 0\rightarrow\infty,CrEl}} = \frac{f_{diss.G\rightarrow dFdU}\cdot G\ AUC_{0\rightarrow\infty,DcNP}}{dFdU\ AUC_{\ 0\rightarrow\infty,DcNP}}$$

Which can then be simplified to:

$$f_{diss.G\rightarrow dFdU} = \frac{G\ AUC_{\ 0\rightarrow\infty,CrEl}}{dFdU\ AUC_{\ 0\rightarrow\infty,CrEl}} \cdot \frac{dFdU\ AUC_{\ 0\rightarrow\infty,\ DcNP}}{G\ AUC_{\ 0\rightarrow\infty,\ DcNP}} \quad (4.2)$$

G $AUC_{0\rightarrow\infty,\ CrEL}$ is the plasma AUC of G given in free drug form. G $AUC_{0\rightarrow\infty,\ DcNP}$ is the total AUCs of associated and dissociated G given in DcNP form. dFdU $AUC_{0\rightarrow\infty,\ CrEL}$ is the AUC of dFdU formed after administration of free G. dFdU $AUC_{0\rightarrow\infty,\ DcNP}$ is the AUC of dFdU after dosing G in DcNP, which reflects the amount of dissociated G released from DcNPs and available for metabolic conversion. $f_{diss.G\rightarrow dFdU}$ represents the fraction of DcNP-dose that is released as free drug and available for conversion to dFdU by CDA.

The assumptions underlying Eq. 4.2 are as follows: [1] Dissociated (free) G, but not associated G, is readily available for metabolism by CDA. [2] Dissociated G is rapidly and extensively metabolized to dFdU by CDA (Kiani et al., 2003; Shipley et al., 1992). [3] The free fraction of dissociated G in plasma and tissue is independent of drug concentration (i.e., protein binding does not change with G concentration). A detailed pharmacokinetic model for the associated and dissociated species will be presented next to simulate the *in vivo* association of both drugs.

4.3.8 *Mechanism Based Pharmacokinetic Modeling (MBPK) to estimate DcNP associated and dissociated fractions of GT*

To further evaluate the strong in vivo association of both G and T to DcNPs, we have utilized a mechanism-based pharmacokinetic model (MBPK) to simulate the plasma time course of the associated and dissociated drugs. A previously developed MBPK model for long-acting anti-HIV DcNP (Kraft, McConnachie, et al., 2018; Perazzolo et al., 2020) was adapted for the present

analysis of G and T pharmacokinetics following DcNP administration. This extended MBPK (or MBPK2) model was initially described and validated in non-human primates given subcutaneous and intravenous injections of DcNPs containing 3 anti-HIV drugs. The systemic portion of the MBPK2 model was slightly modified to fit the time course of total drug plasma concentrations (i.e. DcNP-associated plus dissociated drug species) after DcNP injection and that of plasma dissociated drug concentrations after CrEL suspension (Perazzolo et al., 2020).

Briefly, the model adopted here for GT is composed of two sub-models representing DcNP-associated drug and dissociated drug species. Each sub-model has a central compartment and a peripheral compartment. A visual representation of the model is presented in Fig. 4.1. The observed plasma concentration is the sum of DcNP-associated and dissociated species since they cannot be measured separately. The dissociated drug pharmacokinetic parameters, $k_{1,2}$, $k_{2,1}$ and $k_{0,1}$, were determined by fitting the dissociated drug sub-model to the observed plasma concentration-time data for G and T after injection of CrEL (free-drug) suspension. These parameters were then fixed and the linked sub-models were fit to the observed total concentrations for G and T obtained after injection of the DcNP-dose. The model reasonably assumed that the pharmacokinetics of drugs released from particles will be the same as that of the free-drug (CrEL) control. We assumed that G and T are released from the particle at independent rates ($k_{1,3}$) in the central compartment and only dissociated drugs are subject to clearance from the system ($k_{0,1}$). The model input was the dose, which was assumed to be 100% associated for T based on the high in vitro association (95%) and corroborated by Eq. 4.1 (>75%, See results). Although G *in vitro* association was 9%, we assumed that G was also 100% associated per the *in vivo* results from Eq. 4.1 (>98%, See results). In fact, when 9% G association (based on *in vitro* dialysis under sink conditions) was assigned to the DcNP-dose, the model fit did not converge due to gross

underprediction of the observed plasma G concentration-time data. The peripheral compartment features purely drug exchange between plasma and a group of slowly equilibrating tissues ($k_{4,3}$, $k_{3,4}$). In other words, the DcNP-associated drug is cleared only via its release from the particles in the central compartment. Thus, we expect Eq 4.1 will provide a reasonable boundary estimate for the dissociated fraction after DcNP-associated drug injection and should be close to the estimate from the modeling. The model predictions fit the observed total plasma drug concentration-time data well (R^2>0.9 for both G and T). MBPK modeling and parameter estimations were performed using SAAM II v2.3 (The Epsilon Group, Charlottesville, VA).

4.3.9 *Establishment of cancer nodules in lungs to assess GT DcNP targeting*

Female BALB/c mice were injected with 2×10^5 4T1 metastatic breast cancer cells that express luciferase as a marker (referred to as 4T1-luc cells and kindly provided by Dr. Stanley Riddell from the Fred Hutchinson Cancer Research Center) intravenously by tail vein on day 0. Stable expression of luciferase in these cells allows for bioluminescent monitoring of tumor growth and metastasis (Tao, Fang, Alroy, & Sahagian, 2008). Over a 14-day period, mouse behavior and health conditions were monitored daily and body weight measurements were taken every 2 days. On day 14, mice were administered 150 mg/kg D-luciferin through intraperitoneal injections 10 to 15 min before *in vivo* imaging to confirm establishment of tumor nodules in lungs. The bioluminescence imaging was acquired through a XENOGEN IVIS 200 imaging system (PerkinElmer, Waltham, MA). The bioluminescence imaging parameters for live mice were set as follows: field of view, 24; excitation filter, closed; emission filter, open; exposure time, 180 sec; binning factor, 4; f/stop, 2. Bioluminescence intensity from mice were integrated using Live Image software (PerkinElmer, Waltham, MA). Mice were then intravenously administered GT in DcNPs

at a dose of 50 mg/kg G and 5 mg/kg T or the same dose of drug in control suspension (CrEL) and sacrificed at fixed time points.

4.3.10 *Statistical Analysis*

Statistical analysis was performed using GraphPad Prism 7.04 (GraphPad Software Inc., San Diego, CA). Statistical comparisons were performed using 2-sided t-tests with Welch's correction for unequal variances. Significance probability α was set at 0.05. Pharmacokinetic parameters from non-compartmental analysis were calculated using the trapezoidal rule and relevant pharmacokinetic equations shown in Table 4.2.

4.4 RESULTS

4.4.1 *Preparation and characterization of injectable GT combination in drug combination nanoparticle form*

To determine whether two chemically distinct cancer drugs of interest (G, logP= -1.4 and T, logP= 3) can be formulated together in a single particle suitable for IV injection, we have evaluated several lipid excipient combinations that exhibit amphipathic properties. Hydrophobic T may interact with the acyl chains of phospholipids while the hydrophilic G may interact with the pegylated periphery of lipids when drugs and lipid excipients are assembled together. We found that two lipid excipients in the composition were able to stabilize GT in a DcNP suspension. In the treatment of metastatic breast cancer, G and T are infused in a weight by weight ratio of 14.3 to 1 (G-to-T) per cycle of chemotherapy. This clinical drug ratio was used as a starting point for DcNP optimization. A DcNP composition with 10:1 (w/w) G-to-T ratio containing two lipid excipients (DSPC, DSPE-PEG_{2000}, 9:1 m/m) produced a stable DcNP suspension with a total drug to total lipid ratio of 1:12 (w/w) for use as an IV injectable dosage form. With the intent to streamline

scale-up processes, the preparation procedure was designed to minimize processes such as removal of unbound drug. This process appears to be robust and reproducible with consistent AE% of drugs (see below). We have further evaluated product characteristics including degree of drug association (AE%) to DcNP in suspension under sink conditions and batch to batch variability in size, drug concentration and association efficiency. These data are presented in Table 4.1. The pH, zeta potential, osmolarity and morphology of GT DcNPs were also characterized.

A total of 5 batches were tested for formulation process and quality with respect to reproducibility. The mean particle size for all 5 batches was 59.2 ± 9.2 nm and suitable for IV dosing. The degree of drug association to DcNP was measured and expressed as AE% measured under sink conditions in buffered normal saline. For G, the average AE% for 5 batches was 9 ± 1; for T, the average AE% for 5 batches was 96 ± 2. The pH and osmolarity of GT DcNPs in suspension were consistent across batches and measured to be pH=8.0 and 355 milliosmoles, respectively. Both of these parameters fall within acceptable boundaries for IV injectable products. The average zeta potential of GT DcNPs was measured to be -16.4 mV. The morphology of GT DcNPs was investigated using transmission electron microscopy (TEM). GT DcNPs have a distinct, discoid-like shape (Fig. 4.2, A) with no apparent bilayer structure. In contrast, the conventional liposome controls (Fig. 4.2, B) are observed to have lipid vesicles with enclosed bilayer membranes.

Collectively, these data indicate that GT DcNPs are suitable for injectable dosage forms and can be prepared in a reproducible manner. The final composition for GT DcNPs had nominal concentrations of 16 mg/ml G and 1.6 mg/ml T. The GT DcNP injectable dosage form was subsequently diluted to 10 mg/mL and 1 mg/mL for use in pharmacokinetic studies in mice.

4.4.2 *Effect of DcNP formulation on gemcitabine and paclitaxel plasma time course and pharmacokinetics*

We next investigated the effects of DcNP formulation on G and T *in vivo*. Due to the limited solubility of T, we used a Cremophor EL (referred to as CrEL) suspension to stabilize the GT control dosage form for IV administration. Although this CrEL-based micellar formulation may not fully represent a free and soluble T control, it does represent the clinical dosage form of T (Taxol). Thus, we compared intravenously administered G and T (50/5 mg/kg G/T) to mice in either DcNP or control CrEL-solubilized form. The total drug concentrations of G and T were determined in plasma at indicated time points. These data are presented as a plasma concentration time course comparison in Fig. 4.3. Pharmacokinetic parameter estimates are presented in Table 4.2.

As shown in Fig. 4.3, the plasma drug concentration time course of G and T were substantially different when administered as DcNPs in comparison to CrEL control dosage form. Based on their respective *in vitro* AE% (9% for G and 95% for T under sink conditions), we would expect a greater difference in exposure for T than G. To the contrary, we found much greater enhancement in plasma concentrations of G than T when comparing DcNP to that of the CrEL control (Fig. 4.3 A and 4.3 B). For example, 3 hours after DcNP dosing, mean plasma G concentration was 470 times greater than at the same time point for mice treated with the control CrEL (41,065 ng/mL vs 87.28 ng/mL at 3 hours, $p<0.05$). For T, there was also a higher plasma drug concentration in mice treated with DcNP compared to the CrEL control; however, the formulation effect was more modest. At 3-hours, the plasma T concentration for DcNP was 3.3x greater than CrEL (642.9 ng/mL vs 193.6 ng/mL at 3-hour, $p<0.05$). By 24 hours, the plasma G and T concentrations in mice treated with the CrEL control formulation fell below the detection limit (LLOD). In contrast, for the test group treated with DcNP dosage form, persistent G

concentrations in plasma were detected for the entire 48-hour study in mice administered DcNPs (Fig. 4.3 A). No T concentrations were detected in plasma after 6 hours in mice likely due to its much lower dose (50 mg vs 5 mg/kg G to T ratio in DcNP formulation) (Fig. 4.3 B).

The plasma drug concentration time course was further analyzed using non-compartmental analysis. The pharmacokinetic parameters are presented in Table 4.2. The total exposure or area under the curve (AUC) of G plasma concentration-time curve is increased by 61-fold when administered as a GT DcNP compared to the control CrEL suspension (56218.6 vs 920.8 μg*min/mL). Since both DcNP and control groups received the same dose of G (50 mg/kg), the apparent clearance (represented by dose/AUC) for the DcNP cohort decreased reflective of the increase in exposure (1.1 vs. 65.2 mL/hour). No major change is observed in the concentration of G in plasma at time 0 (C0) after administration in DcNP or control suspension (181.4 versus 165.1 μg/mL). The apparent half-life ($t_{1/2}$ app) increased 8.6-fold when administered in DcNP form compared to the control suspension (13.7 vs 1.6 hours), reflecting a change in the long-acting plasma time-course that extended the apparent terminal slope of G. There was a limited reduction in volume of distribution at steady state for G in DcNP and free forms (12.1 mL vs 16.6 mL). Mean residence time for G, or the average time G molecules stay in the body, increases when given in DcNP form (11.3 vs. 0.25 hours). If we consider the relative change in exposure between G administered in DcNP form versus free form, it is unlikely that G is only 9% associated as indicated by *in vitro* dialysis under sink conditions. Alternatively, if we assume that systemic clearance of G administered in DcNP form can only occur after dissociation and the clearance mechanisms do not differ between free and DcNP form, then Eq. 4.1 can provide an *in vivo* estimate of the maximum dissociated fraction ($f_{diss.\ max}$) of G. This estimate is calculated to be 1.6% and suggests that G is mostly associated *in vivo*.

For T, the total exposure or AUC is increased by 3.8-fold when administered as a DcNP versus a CrEL control suspension. Both groups were administered the same dose of T (5 mg/kg) and apparent clearance decreased reflective of the increase in exposure (10.2 vs 38.3 mL/hour). Interestingly, the volume of distribution at steady state changed in concert with clearance when given in DcNP or control form (10 mL vs 35.6 mL) and to a greater degree than G. No major change is observed in the initial concentration of T in plasma when administered as either the CrEL suspension or DcNP. In contrast to G, no change is observed in the apparent half-life or mean residence time of T when given in DcNP or control suspension (2.0 vs 1.8 hours; 1.0 vs 1.0 hours, respectively) (Table 4.2). Using the same assumption stated above, the *in vivo* association of T can be estimated by Eq. 4.1. The $f_{diss.\ max}$ of T is calculated to be 26.6%.

The changes to the *in vivo* behavior of GT administered as a DcNP compared to their conventionally solubilized control suggests that DcNPs are reasonably stable *in vivo*. If DcNPs degraded rapidly in plasma after IV administration, we would expect drug to release from the particles and behave like the CrEL control suspension. Instead, we observe a remarkable enhancement in G concentrations in plasma for up to 48 hours and a lesser but notable enhancement with T. Collectively, these data suggest that large fractions of both G and T remain associated to DcNPs after IV administration. This effect is surprisingly more remarkable for water soluble G, which was initially predicted to readily dissociate in blood according to *in vitro* predictions in buffer.

4.4.3 *Effect of DcNP on gemcitabine metabolism to dFdU and estimation of dissociated drug*

To further investigate the discrepancy between low *in vitro* G association and the much higher than anticipated overall drug exposure in mice attributed to DcNP (Fig. 4.3 and Table 4.2), we next evaluated metabolic conversion of G to 2',2'-difluorodeoxyuridine (dFdU) in cells and

tissues. In this instance, we assume that when G is bound to DcNPs, it is not accessible to CDA, the primary metabolizing enzyme of G that is present in plasma and peripheral tissues. Due to the ubiquitous expression of the CDA enzyme and its ability to convert G to dFdU in peripheral tissues, dissociated drug that undergoes immediate metabolism in the periphery is not directly accounted for using Eq. 4.1 (which is based on plasma G levels). With these assumptions, we utilize this primary metabolite of G (dFdU) as a marker for the fraction of G that dissociates from DcNPs, which subsequently undergoes metabolism in all tissues (following free G to dFdU conversion kinetics) as per Eq. 4.2. In our studies with IV injections, we assume that G in the control CrEL formulation is 100% freely soluble and available to CDA for conversion to dFdU in the body. The elimination of dFdU from the body occurs primarily through the kidneys and we assume that all dFdU formed in the body (peripheral tissues) will readily return to the central compartment for renal elimination. Under these conditions, when G is stably associated with DcNPs in the body, G is not available for conversion to dFdU. When G dissociates from the particle in either the central or peripheral compartment, it is then free to interact with CDA and undergo metabolism to dFdU.

The results in Fig. 4.4 A show the time course of G and dFdU after IV administration of GT in the CrEL control dosage form. The plasma concentrations of the primary metabolite (dFdU) rose rapidly and reached concentrations equivalent to G within 15 minutes (11,836.7 ng/mL and 12,023.5 ng/mL, respectively) and in 3 hours the concentration of dFdU in plasma was 50x times higher than G (4,343.2 ng/mL vs 87.3 ng/mL). Over time, this gap became larger with the G to dFdU ratio falling to 0.01 in 6 hours. In contrast, when G was given as a GT DcNP dosage form the plasma concentration of dFdU did not reach the G levels throughout 48 hours of study (Fig. 4.4 B). At 3 hours, plasma dFdU is 3.4x lower than G. The variation in G/dFdU ratios over time

can be seen in Fig. 4.4 C with open circles representing the CrEL control and closed circles representing DcNPs. Based on these data (Fig. 4.4) and Eq. 4.2, the estimated fraction of dissociated G accessible for metabolism ($f_{diss.G \rightarrow dFdU}$) is calculated to be 8%. In other words, 92% of G in DcNP dosage form is not accessible for dFdU conversion after IV GT-DcNP administration. The higher dissociated fraction of G derived from dFdU analysis is higher than the 1.6% estimate provided by Eq. 4.1 and suggests that peripheral metabolism competes with the redistribution of dissociated drug back into systemic circulation. Nevertheless, both estimates collectively point to the majority of G (>92%) remaining associated to DcNPs *in vivo* and being likely inaccessible by CDA for metabolic conversion.

These data are consistent with our initial premise that GT DcNP particle are sufficiently stable *in vivo*, and that G association to DcNPs is high throughout the course of the pharmacokinetic study. Additionally, the plasma time course of G and dFdU show that dFdU kinetics are elimination rate limited when given in free form and changes to formation-rate limited (or release-rate limited) kinetics when administered in DcNP form. DcNPs enabling a shift to release-rate limited kinetics may essentially act as an extended infusion of G and may be beneficial for therapeutic effect (Veltkamp, Beijnen, & Schellens, 2008).

4.4.4 *Mechanism-based pharmacokinetic simulation of DcNP-associated and dissociated drug time-courses*

To further understand the effect of DcNP on the pharmacokinetic behavior of GT, we next employed a mechanism-based pharmacokinetic model (MBPK) to simulate the time course of DcNP-associated and dissociated drugs in plasma. The MBPK model adapted for GT-DcNPs is based on a validated MBPK model developed for long-acting HIV drug combination nanoparticles tested in non-human primates (Perazzolo et al., 2020). Experimentally, we can measure total drug

concentrations in plasma (i.e. DcNP-associated plus dissociated), but we cannot distinguish between DcNP-associated and dissociated drugs. Due to these limitations, direct comparisons of the pharmacokinetics of GT when administered in DcNP or CrEL control form are difficult to interpret. The MBPK model presented in Fig. 4.1 utilizes data from both DcNP and CrEL control formulation treated animals to estimate plasma concentrations of DcNP-associated and dissociated drug species over time and their respective time-averaged fractions *in vivo*. After intravenous administration as a DcNP, GT can theoretically exist in at least two species: DcNP-associated drug and dissociated drug. The latter can be reasonably assumed to distribute and be cleared as free G and T after administration of CrEL control formulation. By using the experimental data from the CrEL control group as an anchor for dissociated drug, the model simulates the contribution of DcNP association to the observed increase in plasma concentrations and is reported in Fig. 4.5.

4.4.4.1 *Analysis of MBPK Structure and Assumptions*

Individual distribution, metabolism and elimination of G and T are well characterized. G undergoes rapid and complete deamination to inactive metabolite (dFdU) by ubiquitous CDA. T is metabolized in the liver primarily by CYP3A4 and CYP2C8 with subsequent excretion of metabolites into the bile. In this model, the $k_{0,1}$ term represents the aggregate elimination processes of G and T through their independent described pathways. A peripheral compartment for both G and T was added and distribution was parameterized with the $k_{1,2}$ and $k_{2,1}$ terms (de Jonge, Huitema, Schellens, Rodenhuis, & Beijnen, 2005; Reid et al., 2004). With these considerations, we then added a parallel compartment to represent DcNP associated drug and assumed the following: [1] at the moment of injection, G and T are both completely associated to DcNPs, but are released at different rates; [2] apart from release, there is no other mechanism of clearance for drug bound to the DcNP; [3] when either G or T has been released from DcNPs their

pharmacokinetic behavior will be the same as that of the CrEL control and [4] the amount of drug released from particles in the peripheral compartment is negligible. With these assumptions in place, we set the $k_{1,3}$ term to link the two sub-models and represent the release mechanism of drug from DcNP into the central compartment. The DcNP associated species of G and T was then parameterized with the $k_{4,3}$ and $k_{3,4}$ to account for distribution. By fitting the additive sum of compartments 1 and 3 to the observed GT concentrations, we estimated the fraction of drug that is associated or dissociated in plasma and the relevant pharmacokinetic parameters.

4.4.4.2 *Model simulations and verification with experimental data*

For G, the estimated volume of central compartment decreased 4.6 times when administered as DcNP compared to administration in CrEL form (24 mL vs 5.2 mL) which likely reflects a reduced distribution of DcNP-G into tissues. For T, the estimated volume of distribution was slightly less than the physiological plasma volume of a mouse (~0.8 mL) in both DcNP and CrEL groups. It is likely that T association to DcNPs or CrEL micelles limits the distribution of T from the plasma. Thus, the volume parameter was fixed at 0.8 mL to retain physiological context. It is important to note that our dissociated T parameters were derived from an injection of the CrEL control and not completely soluble drug (due to solubility limitations) and the CrEL micelles may limit distribution of T from plasma. The estimated release parameter of G ($k_{1,3}$) was 9.5-fold lower than T (0.2 hour-1 vs 1.9 hour-1, Table 4.3) and corresponds to the relative 11.3-fold difference in mean residence times of G and T after DcNP administration (11.3 hours vs 1.0 hour, Table 4.2). Based on the parameters generated in this model (Table 4.3), a simulation was performed to predict the plasma concentration time course kinetics of dissociated and associated G and T (Fig. 4.5). The ratio of dissociated over total G AUCs as simulated by the model was 1.5%, which agrees with our maximum fraction dissociated in plasma estimate of 1.6% from Eq. 4.1. For T, the model

simulated ratio of dissociated over associated T AUCs is 24.7% and in close agreement with our boundary estimate using Eq. 4.1 (26.6%). It is interesting to note that the *in vivo* association of G is greater than T (~98% vs ~73%), but the opposite is true for *in vitro* association (9% versus 95%). There is likely an unknown *in vivo* mechanism that enables the substantial association of G to DcNPs, however further investigation is required. Despite these unknowns, the current results clearly show that DcNPs retain hydrophilic G and hydrophobic T together in plasma (up to 8 hours) and may enable the co-delivery of GT to target cancer cells.

4.4.5 *Effect of DcNP formulation on gemcitabine and paclitaxel tissue distribution*

We next determined the effect of DcNP on preferential GT tissue distribution in mice. Non-specific, off-target accumulation of drugs in healthy tissues can limit the therapeutic potential of GT DcNPs. In addition, accumulation of cytotoxic drug in healthy tissues can pose a safety concern. Therefore, we compared tissue-to-plasma drug concentration ratios at 3 hours after IV administration in mice dosed with GT in DcNP or the CrEL control dosage form. The 3-hour time point was selected to ensure that both drugs are detectable in both plasma and tissues for animals treated with DcNP or CrEL control. As shown in Fig. 4.6, DcNPs retain G in the plasma relative to CrEL control 3 hours post-injection in all tissues tested ($p < 0.05$, Student's T-Test). For T, lung and kidney tissue-to-plasma ratios were reduced in DcNP vs CrEL control; while liver and spleen ratios increased. These data indicate that G in DcNPs does not accumulate in off-target organs such as the liver and spleen and, instead, GT in DcNP are better retained in blood and plasma. The effect of DcNPs on T distribution is less dramatic but there does not appear to be a substantial trend towards healthy organ accumulation (Fig. 4.6). Taken together, these data suggest that G bound to DcNPs does not accumulate in any of the sampled tissues and likely provides drug associated to DcNP a greater opportunity to reach target tumor cells by remaining in the systemic

circulation. It is possible that T binding to serum protein, as well as stripping of T from DcNPs, may contribute to the differential tissue distribution of G and T in healthy mice. However, this difference, particularly the T increase in liver and spleen, is minimal. The large reduction of G in the four off-target tissues are significant compared to that of CrEL control formulation and may result in less off-target toxicity.

4.4.6 *Effect of DcNP formulation on gemcitabine and paclitaxel localization in healthy versus tumor bearing lung tissue*

To determine whether DcNPs enhance GT distribution into target tissues, namely cancer nodules, we next investigated the differential localization of GT in DcNP or CrEL form in healthy versus cancer nodule bearing mice. Since lungs are a common metastatic site for breast cancer disease progression, we utilized a model for metastasis that forms cancer nodules in the lungs. Cancer nodules were established in female BALB/c mice via intravenous inoculation of syngeneic breast cancer cells (4T1). This process has been shown to consistently produce detectable and multiple 4T1 cancer nodules in lungs within 14 days. Once nodules were established and confirmed with IVIS imaging, mice were administered with GT in either DcNP or conventionally solubilized form at equivalent doses (50/5 mg/kg, GT) and euthanized at pre-determined time intervals. We compared the effect of DcNP and CrEL dosage forms on GT distribution at two time points. To capture rapidly cleared free GT (CrEL) in the lungs and plasma, an early time point (1 hour) was chosen. After 1 hour, GT in both DcNP and CrEL are in their distribution phase after IV dosing. A later time point (24 hours) was chosen to capture GT distribution after distribution equilibrium is reached. Nodule-free and nodule-bearing lungs were harvested, and lung tissue drug concentrations were compared in these two groups.

As shown in Table 4.4, mice bearing 4T1 cancer nodules had a higher concentration of G ($p<0.01$) and T ($p<0.12$) in lung tissue 1 hour after CrEL administration compared to healthy tissue. Increases of lung concentration reflect increases of plasma concentration of G ($p=0.14$) and T ($p<0.01$). Comparison of lung-to-plasma ratios 1 hour after CrEL administration shows that G ($p=0.24$) and T ($p=0.4$) distribution are not significantly different between healthy and cancer nodule burdened animals. For cancer nodule burdened mice given DcNPs, no statistical significance was observed in lung, plasma, or lung-to-plasma ratios. At later time points (24 hour), free drug rapidly clears from the systemic circulation and only the DcNP group has detectable levels of drug in plasma and lung. The lung-to-plasma ratios of G in cancer nodule bearing mice at 24 hours are 5 times greater than in healthy with a p-value of 0.02. Although a lung-to-plasma ratio of T cannot be determined at 24 hours due to rapid plasma clearance, the concentration of T is 7x greater in cancer nodule bearing mice versus healthy mice ($p = 0.008$). These data are summarized in Table 4.4. The results from this experiment show that when administered to healthy mice, DcNPs can sustain drug levels in the lung (a major site of metastasis) for a longer time than the CrEL control formulation. When mice have cancer nodules present, G and T levels in the lung are increased relative to healthy mice. These increases in lung concentrations are disproportionately larger than the elevated concentrations in plasma, suggesting that the particles preferentially target cancer burdened tissue. Furthermore, when we compare the GT concentration ratios in lungs, an 8.8 to 1 ratio is observed, similar to the original drug ratio in formulation. This further supports the idea that particles may selectively deposit and retain in cancer burdened tissue.

4.5 DISCUSSION

A key challenge in the treatment of breast cancer is metastasis and poor tolerability of highly potent, chemotherapeutic drug combinations. Off-target drug distribution and asynchronous

concentrations of drug combinations in target tissues (tumors) likely contribute to the high dose requirements for metastatic control and dose-limiting toxicities. To coordinate the anticancer effects of two chemotherapeutic agents, we have successfully co-formulated chemically distinct gemcitabine (G) and paclitaxel (T) in a drug combination nanoparticle (DcNP). When intravenously given to mice laden with metastatic 4T1 breast cancer nodules in the lung, the GT DcNP demonstrated improved tissue selectivity and long-acting exposure of both drugs in metastatic cancer bearing tissues (Table 4.4).

Interestingly, the single nanoparticle composed of the unlikely partners—water soluble G and water insoluble T—not only demonstrated long acting tissue selectivity for breast cancer nodules in the lung, but also minimal distribution into healthy organs. The tissue-to-plasma ratios of GT DcNPs, which also produced long acting plasma circulation, did not significantly differ from the control GT administration in mice 3 hours after IV injection (Fig. 4.6). An unexpected finding is that both G and T remain well associated to DcNPs for the duration of the time course study, which may be related to target tissue localization and the long-acting pharmacokinetics of GT enabled by the DcNP platform. *In vitro* association efficiency suggests that paclitaxel has a greater affinity for DcNPs than does gemcitabine. However, when given in DcNP form, gemcitabine has a greater enhancement in plasma exposure than paclitaxel compared to their respective controls. Pharmacokinetic modeling and simulation was used as a novel tool to distinguish the *in vivo* associated and dissociated fractions of gemcitabine. This approach may be used to estimate the associated and dissociated fractions of drug over time for other nanoparticle drug delivery systems where isolation of *in vivo* associated and dissociated drug is experimentally challenging. Although this work focuses specifically on the use of combination G and T, DcNPs

represent a potential approach to the synchronized delivery of other combination regimens used in breast cancer treatment such as targeted therapy or hormone therapy.

Combination drug nanoparticles have been previously reported as potential therapies for cancer. However, it remains a challenge to co-formulate chemically dissimilar drugs such as G and T (water soluble and insoluble drugs). To our knowledge, there are only a few published reports that achieve the co-formulation of GT to target breast cancer and each study notes an improved effect of combination particles versus individual GT which highlights the potential for combination particles (Aryal et al., 2010; Dong et al., 2018; Lei et al., 2019; Meng et al., 2015; Noh et al., 2015; J. Zhang et al., 2018). Water soluble G and water insoluble T are brought together by approaches such as chemical conjugation of both drugs to polymers (Aryal et al., 2010; Noh et al., 2015) or encapsulation in calcium phosphate nanoparticles with a lipid bilayer coating (J. Zhang et al., 2018). However, chemical conjugation will produce a new chemical entity that requires a long journey of regulatory approval and filing as a new drug. Calcium phosphate precipitation requires multiple filtration steps to remove organic solvents such as THF or chloroform.

In contrast, the distinction of the DcNP process is that no chemical conjugation is required to produce substantial *in vivo* association of both gemcitabine and paclitaxel. The DcNP process does not require filtration of unassociated drug or co-solvents as described in other reports. Even with a limited AE% of 9% for gemcitabine, a 50-fold increase in gemcitabine plasma exposure is observed when compared to the CrEL control. Further analysis based on a combination of metabolite kinetics and MBPK modeling suggests that water soluble gemcitabine is highly associated with DcNP *in vivo*. Paclitaxel was found to be highly associated both *in vitro* and *in vivo*, although the lower dose (5 mg/kg) limits its duration in plasma. While the exact mechanism

leading to the stable association of water soluble gemcitabine to GT DcNPs is beyond the scope of this report, it is worth noting the resemblance with another similarly-manufactured DcNP formulation for HIV antivirals. Lopinavir, ritonavir and tenofovir association to DcNPs resulted in stable water insoluble drug association (lopinavir and ritonavir) both in-vitro and in-vivo in non-human primates (NHP). On the other hand, water soluble tenofovir exhibited low in-vitro association (10%), but high *in vivo* association in NHPs (97%) (Perazzolo et al., 2020). The stable circulation of GT well associated to DcNPs in plasma demonstrates the ability of one carrier to load two anticancer drugs while targeting cancer cells (Fig. 4.3).

Clinical studies have shown that prolonged infusion rates of G (10 mg/m^2/min) confer a survival advantage over standard 30-minute infusions (Tempero et al., 2003). Deoxycytidine kinase (dCK), which converts G to its active triphosphate form, has been shown to be rapidly saturated after G infusion (R. Grunewald et al., 1991). As a result, a large fraction of the total dose of G is lost to metabolism by CDA before activation by dCK. Increasing the infusion time of G can allow more drug to be converted to active form and produce a greater pharmacologic effect. As an example, Eckel et al. showed that 24 hour infusions of G can have similar pharmacologic effect as a 30 minute conventional infusion for advanced pancreatic adenocarcinoma at 1/10th the dose (100 mg/m^2 vs 1000 mg/m^2) (Eckel, Schmelz, Erdmann, Mayr, & Lersch, 2003).

In this study, we have found that a single dose of GT in DcNPs can increase the apparent plasma half-life of G from 1.6 hours to 13.72 hours in mice (Fig. 4.3). No infusion is necessary in this case with GT DcNP administration. Although total drug concentration in plasma does not directly reflect the free fraction of G available for phosphorylation, the persistent circulation of parent drug can increase the opportunity for drug to reach target cells for phosphorylation instead of inactivation as seen with other long-acting nucleoside analogs (McConnachie et al., 2018).

Thus, extending the plasma circulation of parent G may act similarly as a prolonged infusion and may produce a greater pharmacologic effect. Regarding T, clinical studies have not established a relationship between infusion rate and pharmacologic effect. Instead, conventional Taxol is infused over 3 hours to mitigate the toxicity of Cremophor EL, a solubilizing excipient. Minor and major hypersensitivity reactions have been linked to rapid infusion of Cremophor El. When this excipient is not present, such as in albumin bound paclitaxel formulations (Abraxane), infusions can be administered in as little as 30 minutes without prophylactic medications for hypersensitivity reactions (Gradishar, 2006). In our study, the use of biocompatible lipid excipients with proven human safety in other dosage formulations (Bulbake, Doppalapudi, Kommineni, & Khan, 2017) enables T to stay suspended in nanoparticle form. T in DcNP can be administered in a single dose (with G) without the need for Cremophor EL.

The pharmacokinetic profiles of nanoparticle delivery systems are often described using total drug concentrations instead of unbound drug concentrations. This is partly due to the complexity of separating bound and unbound fractions of drug from biological matrices (Skoczen, McNeil, & Stern, 2015). Total drug concentrations can provide an adequate description of particle circulation but may confound the prediction of pharmacologic effect. In this report, we offer novel approaches to estimate the fraction of drug that is associated to nanoparticles *in vivo*. GT association to DcNPs was first estimated by *in vitro* dialysis under sink conditions (G: 9%, T= 95%). However, this estimate did not correspond with our *in vivo* results and may be due to the lack of blood components in the dialysis experiment, which can affect drug dissociation.

In the biologic milieu and limited blood volume, our *in vivo* data indicates an association of G to DcNPs much greater than the 9% found *in vitro*. We reconcile these differences by using a non-compartmental approach to estimate the maximum time-averaged fraction of dissociated

drug that can be present *in vivo* (Eq. 4.1, $f_{diss.\ max}$). This approach was first utilized with anti-HIV DcNPs and we have further extended its application toward an estimate for the fraction of drug available for metabolism when administered as a DcNP (Eq. 4.2, $f_{diss.G \rightarrow dFdU}$). For G, the estimate for $f_{diss.G \rightarrow dFdU}$ was greater than $f_{diss.\ max}$ suggesting that metabolism for DcNP-G can occur in tissues that are not part of the central compartment (such as lean tissue). It is possible that DcNPs distribute into peripheral tissue where local dissociation and metabolism of G can occur. Since this loss of parent drug does not re-enter the systemic circulation, Eq. 4.1 may underpredict the dissociated fraction. Alternatively, Eq. 4.2 captures the transit of dFdU from peripheral tissue back into the central compartment and account for peripheral metabolism but both $f_{diss.\ max}$ and $f_{diss.G \rightarrow dFdU}$ indicate that G is highly associated to DcNPs. Regarding T association to DcNPs, the clearance pathway for dissociated T is in the liver, which resides in the central compartment. Under these conditions, $f_{diss.\ max}$ can provide an estimate of the dissociated fraction without needing to account for loss of parent drug in peripheral tissues; it shows that T is also highly associated to DcNPs *in vivo*. Taken together, both estimates show that G and T mostly circulate *in vivo* as associated forms.

As an extension to those non-compartmental estimates, we next adapted a mechanism-based pharmacokinetic model (MBPK) to derive a dynamic simulation of both G and T association to DcNPs in plasma (Kraft, McConnachie, et al., 2018). Results from this MBPK model showed that both hydrophilic G and hydrophobic T are well associated *in vivo* and correlate closely to our non-compartmental estimates. These early results demonstrate a novel application of pharmacokinetic modeling to understand the species of GT that circulate *in vivo*. In future studies, we plan to incorporate metabolite markers for both G and T to further expand the concept of accounting for peripheral clearance. Use of non-compartmental estimates and further expansion of

this MBPK model to include metabolite markers can provide a quantitative tool to characterize novel nanoparticle formulations in development.

Our next finding was that GT DcNPs do not appear to accumulate in healthy organs. Depending on the composition and size of nanoparticle formulations, the liver and spleen can sequester as much as 99% of other types of nanoparticles (Y. N. Zhang, Poon, Tavares, McGilvray, & Chan, 2016). This is mainly due to the fenestrations in liver and spleen microvasculature and direct interactions of traditional nanoparticles with endocytic cells. Although the removal of particulates constitutes an essential component of the immune system, the premature clearance of particles prior to their interaction with target cells poses a barrier to effective nanoparticle delivery. Lipid-based particles such as liposomes are often associated with liver and spleen uptake (Allen & Everest, 1983). For example, when large (378 nm) and small liposomes (113 nm) were intravenously administered in mice, 93% of large liposomes and 67% of small liposomes were recovered in the liver and spleen after 4 hours (Hu et al., 1996). The hepatic uptake of particles is also observed with non-lipid nanoparticle delivery systems. Yeo et al. intravenously administered albumin bound paclitaxel (Abraxane, 30 mg/kg) in mice and found that after 3 hours, liver concentrations of paclitaxel were 100-fold greater than plasma concentrations. In the same study, an F127 stabilized nanocrystal form of paclitaxel was intravenously injected (30 mg/kg) in mice and after 3 hours, liver concentrations were 50-fold greater than plasma (Park et al., 2018). Compared to these liposome and nanoparticle drug delivery systems, the GT in DcNP form have remarkably different biodistribution characteristics. The biodistribution properties of GT DcNPs may be related to the discoid-like morphology and absence of a membrane structure (as opposed to enclosed, spherical liposomes).

GT DcNPs are a combination particle that contains multiple active drugs to overcome drug resistance unlike single drug particles. Both water soluble G and water insoluble T are stabilized together by two lipid excipients, without the need for a membrane structure such as liposomes. Electron microscopic analysis of GT DcNP product reveals that they contain neither membrane structures nor spherical enclosures typically observed with liposomes. After IV injection, GT DcNPs do not appear to distribute into or accumulate in the liver or spleen. For G administered as DcNPs, the tissue-to-plasma ratios show that DcNPs significantly limit tissue distribution compared to the control formulation (<1/10th across all tissues) (Fig. 4.6 A). This effect on G disposition is particularly promising as hepatic distribution of free drug is associated with hepatic abnormalities and dysfunction (King & Perry, 2001). For T, there is no clear trend on tissue distribution of drug when administered as a DcNP compared to the conventionally solubilized form. T is known to interact readily with albumin, while G does not, and this drug specific property may affect T disposition (Paal, Muller, & Hegedus, 2001). Regardless of how T can dissociate from combination nanoparticles, the overall accumulation of both G and T in off-target organs is minimal compared to previous reports and may lead to improved safety.

In metastatic breast cancer, solid tumors and metastatic nodules induce major changes to their surrounding microenvironment. These changes can limit the effectiveness of nanoparticle delivery systems by reducing penetration into solid tumors (Jain, 2001). Various approaches have been investigated to overcome these limitations such as active targeting and tumor priming with limited clinical success (Jain, 2001). In our study, we found that intravenously administered DcNPs can produce greater concentrations in tumor burdened pulmonary tissue compared to healthy pulmonary tissue. This enhancement of drug accumulation in tumor-bearing lungs is likely due to increased distribution of DcNP from plasma to peripheral tumor fenestrations within tumor

foci. The small size (60-70 nm) and prolonged circulation (48 hours) in plasma of DcNPs may allow particles to penetrate the fenestrations of tumor foci, which typically range from 0.3 to 4.7 microns in size (Hashizume et al., 2000; Nagy, Chang, Dvorak, & Dvorak, 2009). Other nanoparticle systems such as liposomes or polymeric particles have been reported to leverage the leaky neovasculature around tumors to enhance drug permeation and retention (commonly referred to as the EPR effect). In these scenarios, new blood vessels formed to support rapid tumor growth are leaky due to poorly developed endothelial cells lining the vessels. This allow for the passive distribution, diffusion or penetration of nano-sized particles into solid tumors. In the current work, metastatic 4T1 cancer cells present as lung cancer nodules in already highly perfused capillary beds. Under these conditions, it is not clear whether neovasculature has formed or the role of the EPR effect on the observed tumor tissue targeting by GT DcNPs. Nevertheless, our data suggests the selective deposition of GT DcNPs in tumor burdened tissue. When we calculate the concentration ratios of G and T in tumor burdened lungs, we yield a ratio similar to the administered dose (8.8:1 versus 10:1, G/T). This suggests that intact DcNPs are depositing in tumor bearing lungs without having a large fraction of the dose sequestered in the reticuloendothelial system, reflected in the liver and spleen. The observation that untargeted DcNPs can have a tumor specific deposition in pulmonary tissue is a promising feature of DcNPs. In future studies, we will investigate the role of the EPR effect in the selective accumulation of GT DcNPs in cancer burdened tissue. While one could seek to improve the dispositional advantage of GT DcNPs with the use of active targeting ligands (such as those targeted to EGFR, integrin or other MBC markers), such studies are beyond the scope of this report but are under consideration for future studies.

We have recently evaluated the therapeutic effects of this GT DcNP composition on 4T1 breast cancer metastasis to lungs in mice (Mu et al., 2020). A single GT (20/2 mg/kg) dose in DcNP form nearly eliminated breast cancer colonization in the lungs, while this effect was not achievable by a CrEL drug combination at a 5-fold higher dose (i.e., 100/10 mg/kg GT). Dose-response curves of cancer nodule inhibition and systemic toxicity through body weight loss demonstrated a therapeutic index of about 15.8. These results may be related to the preferential distribution and long acting pharmacokinetic properties contributed by stable association of GT to DcNPs *in vivo*.

4.6 CONCLUSION

In summary, we have developed stable drug combination nanoparticles composed of water soluble gemcitabine and water insoluble paclitaxel. GT DcNP stabilization is enabled by lipid excipient composition and a novel but simple process that does not require complex free drug removal. By doing so, this highly potent combination of chemotherapy has been transformed from a short-acting regimen to a long-acting regimen. The development and application of a mechanism based pharmacokinetic model elucidates the time course of associated and dissociated fractions of GT *in vivo*. This model indicates that GT remains associated to DcNP *in vivo* and displays an enhanced distribution toward cancer burdened tissue over healthy tissue, which may improve the therapeutic effect of this combination. In a recent report, these novel GT DcNPs were evaluated as a treatment using a highly aggressive 4T1 model of breast cancer metastasis. The DcNP platform is able to incorporate multiple drugs and allow water soluble and insoluble chemotherapeutic agents to form a single nano-dosage form. Thus, it may be used for other cancer drug combinations, either in clinical use or in development, with higher potencies. In addition, it may be possible to incorporate targeting ligands in the DcNP to provide additional cancer cell selectivity and

preferential distribution of the chosen drug combinations. The long-acting and cancer tissue selective drug combination kinetics provided by this DcNP platform technology may lead to a meaningful impact on the development of targeted, combination treatment of metastatic breast cancer.

Table 4.1. Characterization and batch-to-batch variability of GT DcNPs.

Batch	**Size (nm)[a]**	**AE%[b]**		**[Drug Conc]** (mg/mL)	
		PTX	**GEM**	**PTX**	**GEM**
1	49.2 ± 35	95	7	1	13.9
2	59.9 ± 44	97	9	1.2	13.9
3	69.7 ± 47	97	10	1.3	15.3
4	68.7 ± 46	97	10	1.1	14.5
5	48.5 ± 30	92	8	0.7	14
Average	59.2	96	9	1.1	14.3
S.D	9.2	2	1	0.2	0.5

[a]*Mean particle diameter was determined by photon correlation spectroscopy and presented as the mean ± standard deviation*

[b]*Association efficiency of Gemcitabine (Gem) and paclitaxel (PTX) was determined by dialysis under sink conditions as described in Materials and Methods.*

Table 4.2. Effect of DcNP formulation on pharmacokinetic parameters of gemcitabine and paclitaxel administered together in GT DcNP or control suspension.

		Gemcitabine			Paclitaxel		
Parameter	**Units**	**Control**	**DcNP**	**Ratio**	**Control**	**DcNP**	**Ratio**
$AUC_{0 \text{ to } \infty}$ [a]	μg min/ml	920.8	56218.6	61.0	156.5	588.8	3.8
$T_{1/2,app}$ [b]	hr	1.6	13.7	8.6	1.8	2.0	1.1
C_0 [c]	μg/mL	165.1	181.4	1.1	17.7	13.9	0.8
Dose/AUC[d]	mL/hr	65.2	1.1	0.02	38.3	10.2	0.3
Vss[e]	mL	16.6	12.1	0.7	35.6	10.0	0.3
MRT[f]	hr	0.25	11.3	45.2	1.0	1.0	1.0

Sparse sampling was used to derive single pharmacokinetic estimates from the data shown in Fig. 4.1.

[a]*Non compartmental analysis was used to estimate area under the curve (AUC) from 0 to ∞ of gemcitabine and paclitaxel in DcNP and CrEL control.*

[b]*Apparent half-life was estimated from the slope of the last 3 time points collected in each condition.*

[c]*Concentration at time 0 was back extrapolated from the first time point in each condition.*

[d]*Dose/AUC is shown for the relative apparent clearances of gemcitabine and paclitaxel.*

[e]*V_{ss} was calculated using Dose*AUMC/AUC^2 extrapolated to infinity*

[f]*Mean residence time (MRT) was calculated by dividing the area under the moment curve (AUMC) by the AUC from 0 to infinity.*

Table 4.3. Model derived pharmacokinetic parameters for gemcitabine and paclitaxel when administered as a single IV dose in GT DcNP dosage form.

DcNP Dissociated Parameters	**Gemcitabine**	**Paclitaxel**
V (mL)	24 ± 12	0.8[a]
$k_{0,1}$ (1/hour)	3.9 ± 0.9	7.0 ± 2.0
$k_{1,2}$ (1/hour)	0.5 ± 0.2	0.6 ± 0.1
$k_{2,1}$ (1/hour)	0.2 ± 0.1	4.4 ± 1.0
DcNP Associated Parameters	**Gemcitabine**	**Paclitaxel**
V_{DcNP} (mL)	5.2 ± 0.6	0.8[a]
$k_{1,3}$ (1/hour)	0.2 ± 0.02	1.9 ± 0.1
$k_{3,4}$ (1/hour)	0.6 ± 0.1	0.7 ± 0.2
$k_{4,3}$ (1/hour)	1.8 ± 0.5	1.6 ± 0.5

[a]*Volume was fixed to plasma volume assuming a blood volume of ~2 mL for 8 to 9-week-old mice and a hematocrit of 40%*

Pharmacokinetic parameters were estimated using the SAAM II software (The Epsilon Group). The data are presented as the geometric mean ± the standard deviation of each parameter. Rate constants for mass transfer between compartments are presented in 1/hour. Volume of the estimates for the accessible (central) compartments of associated (V_{DcNP}) and dissociated (V) drug are presented in mL. Peripheral volumes (Figure 4.1, Compartments 4 and 2) were not parameterized in the model.

Table 4.4. Effect of 4T1 tumors on gemcitabine and paclitaxel localization in tumor-ladened lung tissues after dosing with GT DcNP or CrEL control formulation

	Gemcitabine			Paclitaxel		
	Healthy	**4T1**	**p-value**	**Healthy**	**4T1**	**p-value**
1 hour after control						
Lung (μg/g)	0.9 ± 0.4	6.0 ± 0.8	<0.01*	1.0 ± 0.3	1.7 ± 0.5	0.12
Plasma (μg/mL)	0.9 ± 0.2	2.8 ± 1.4	0.14	0.3 ± 0.05	0.7 ± 0.1	0.01*
Lung/Plasma Ratio	0.9 ± 0.3	2.2 ± 1.4	0.24	3.3 ± 1.2	2.5 ± 0.8	0.40
1 hour after DcNP						
Lung (μg/g)	7.5 ± 1.2	12.5 ± 4.9	0.21	0.6 ± 0.4	0.9 ± 0.5	0.46
Plasma (μg/mL)	52.2 ± 64	72.6 ± 60.0	0.71	1.4 ± 0.9	2.2 ± 1.1	0.39
Lung/Plasma Ratio	0.1 ± 0.2	0.2 ± 0.1	0.85	0.4 ± 0.01	0.4 ± 0.2	0.92
24 hours after DcNP						
Lung (μg/g)	0.3 ± 0.1	3.5 ± 1.0	0.01*	0.06 ± 0.01	0.4 ± 0.1	0.03*
Plasma (μg/mL)	12.7 ± 1.5	34.2 ± 0.6	<.01*	BDL	BDL	NA
Lung/Plasma Ratio	0.02±.01	0.10±.03	0.04*	NA	NA	NA

Data in the table are presented as the geometric mean of three animals ± standard deviation. No drug was detected with the CrEL control 24 hours after drug administration.

** denotes $p<0.05$.*

NA denotes a ratio not calculable

BDL denotes no detectable drug in the sample

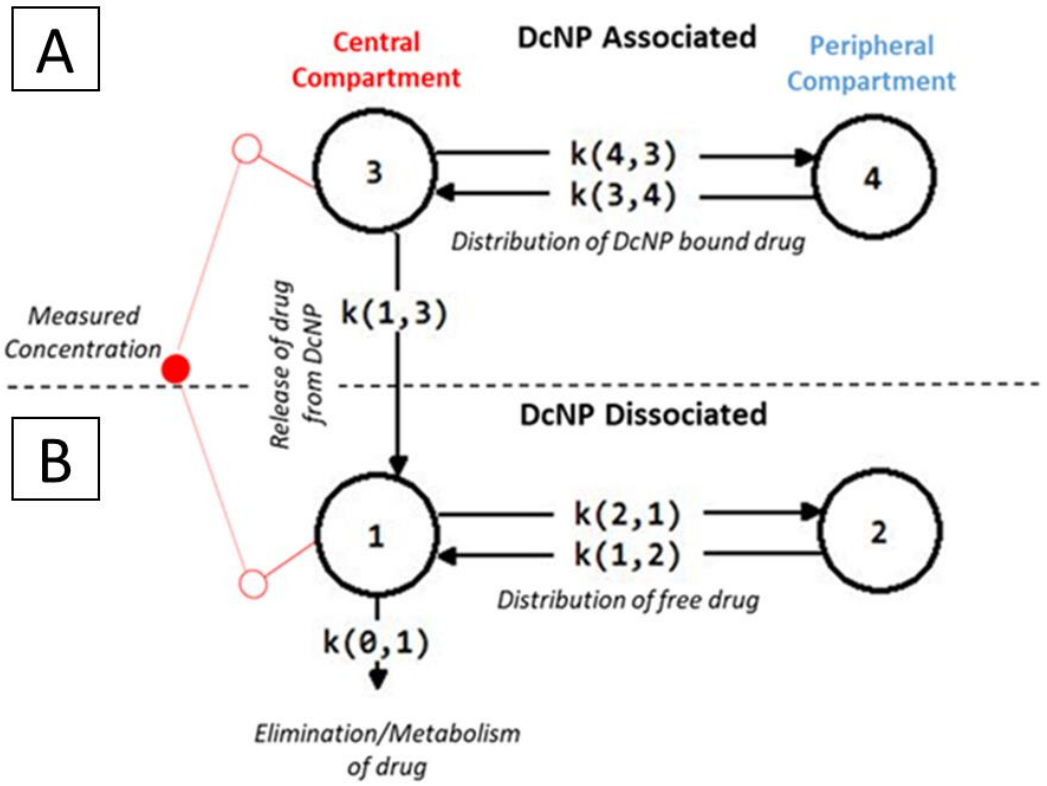

Figure 4.1. Schematic representation of a mechanism-based pharmacokinetic model for DcNP associated and dissociated gemcitabine and paclitaxel in plasma after IV dosing.

Mechanism-based pharmacokinetic (MBPK) model was developed to describe the association and dissociation of drug from DcNPs in plasma. The model features two parts: (A) the behavior of the fraction of gemcitabine or paclitaxel associated to DcNPs and their distribution to peripheral compartments. (B) The behavior of the fraction of DcNP dissociated gemcitabine or paclitaxel in plasma including distribution into peripheral compartments and clearance as dissociated drug. The DcNP associated and dissociated models are linked by the release parameter k1,3 in the central compartment. After dissociation through the release parameter, gemcitabine and paclitaxel are assumed to behave as they would in their free drug form as presented in the conventional CrEL dosage form control.

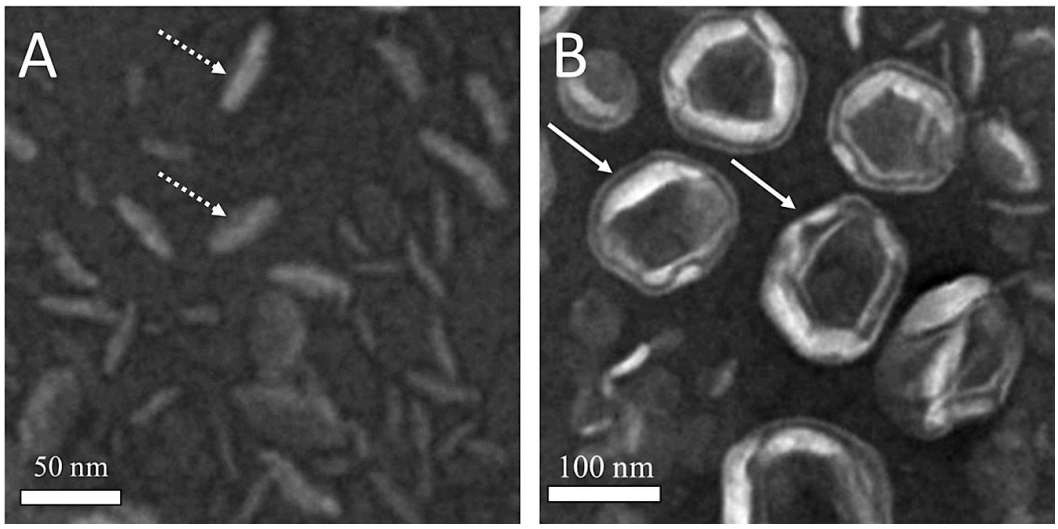

Figure 4.2. Structural morphology of GT DcNPs by electron microscopy

GT DcNPs was evaluated using negatively stained transmission election microscopy and compared against conventional liposomes. Electron microscopy of GT DcNPs (Panel A) exhibits a discoid morphology with no evidence of bilayer structure (dashed arrows). In comparison, conventional liposome controls (Panel B) exhibit typical spherical structures with visible bilayer membranes (solid arrows).

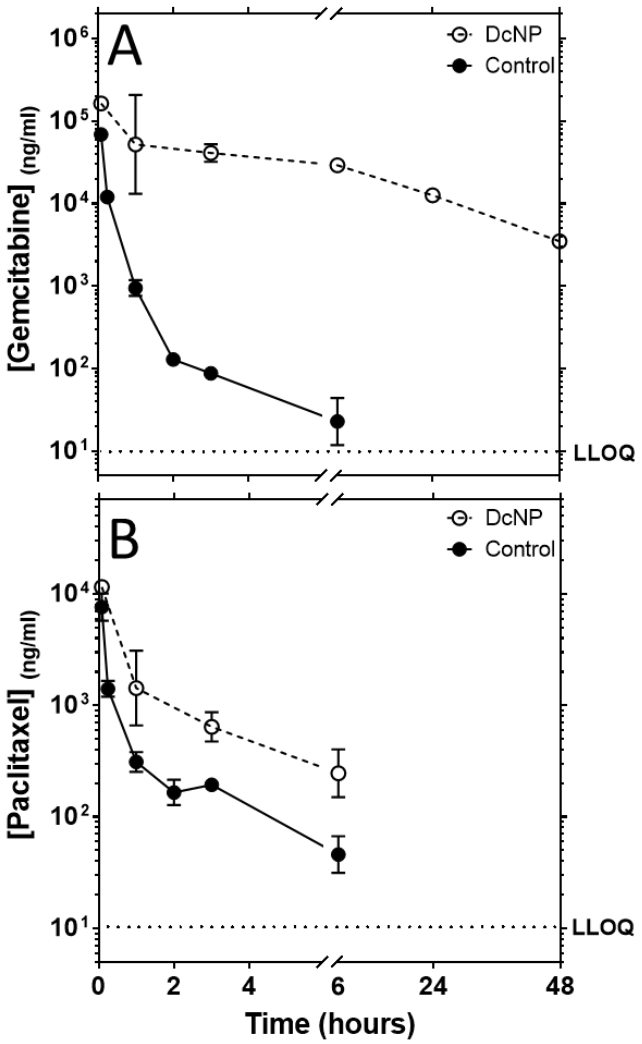

Figure 4.3. Association of GT to DcNPs increases the concentration of GT in plasma over time compared to CrEl control suspension.

Gemcitabine (50 mg/kg, Panel A) administered as a DcNP (Dashed, ○) substantially increases the plasma circulation levels in healthy BALB/c mice (n=3 per time point) measured at identical time points to the *CrEL* control (Cremophor El/saline suspension, solid line, ●). The plasma concentration of paclitaxel (5 mg/kg, Panel B) was also increased in plasma relative to the control suspension but a smaller effect is observed . Paclitaxel levels fall below the LLOQ of our LC-MS/MS assay after 6 hours. The LLOQ of gemcitabine or paclitaxel is represented as dotted lines for both panels.

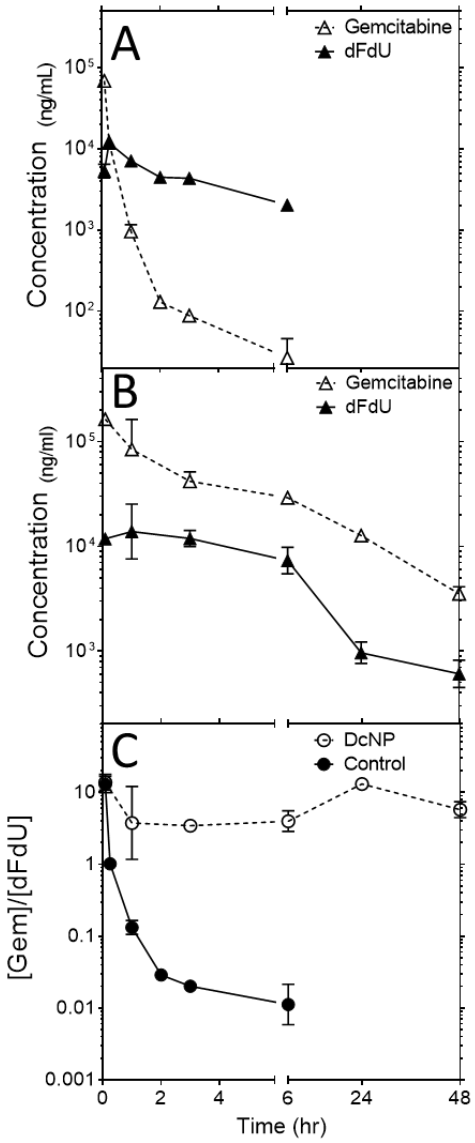

Figure 4.4. Effect of DcNP formulation on dFdU formation over time compared to CrEL

Panel A shows the plasma time course of gemcitabine (□) and its metabolite dFdU (▲) in control soluble gemcitabine (50 mg/kg; in *CrEL*) dosage form. Panel B represents the plasma time course of mice treated with gemcitabine in GT DcNP at equivalent doses to the soluble control; the symbols are the same as those represented in Panel A. The ratios of gemcitabine to dFdU over time for mice treated with gemcitabine are presented in Panel C comparing gemcitabine in a DcNP (○) or *CrEL* (●) control dosage form.

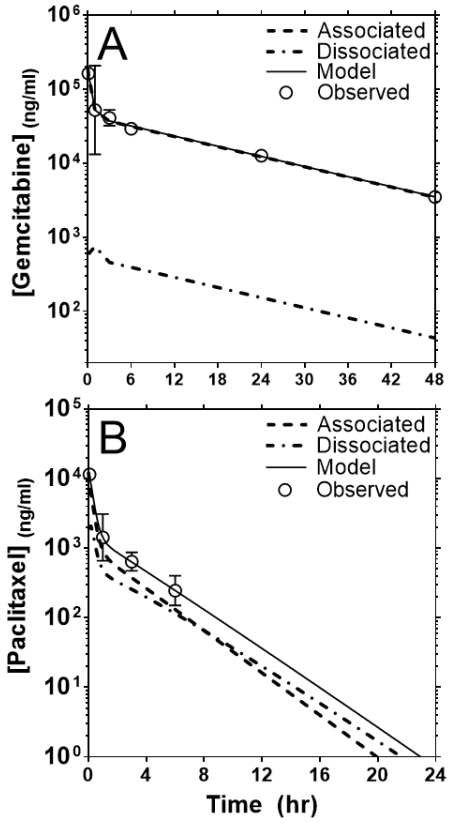

Figure 4.5. Confirmation of an MBPK model predicted concentration time curve for gemcitabine and paclitaxel with experimental data in mouse plasma after intravenous administration of GT DcNPs.

Panel A represents the gemcitabine plasma time course of associated and dissociated fractions of drug. The experimental data are presented in open circles (○) with an SD error bar. The MBPK model simulated values are plotted as a continuous solid line. The dotted lines represent the DcNP dissociated gemcitabine concentration over time, simulated by the model. Panel B presents the experimental data and simulated DcNP associated and dissociated fractions over time for paclitaxel. The symbol and line representations for Panel B are the same as for Panel A. It is interesting to note that the total simulated plasma concentrations and the DcNP associated species of gemcitabine overlap with most of the gemcitabine remaining DcNP associated throughout the study period.

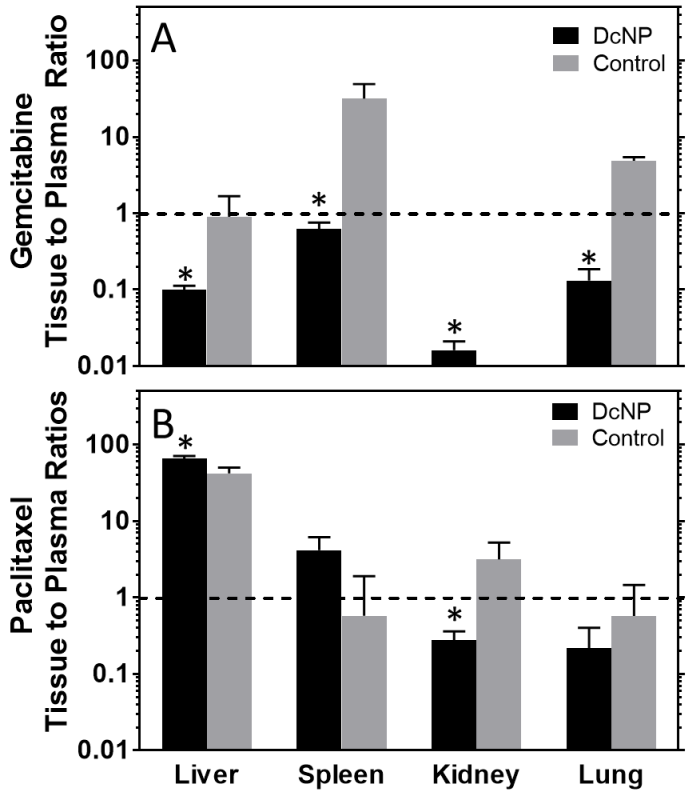

Figure 4.6. Effects of DcNP on gemcitabine and paclitaxel tissue distribution 3 hours after intravenous injection compared to the control suspension

Mice (n=3) were intravenously administered with GT DcNP or a control dosage form (CrEL suspension) at 50 mg/kg gemcitabine and 5 mg/kg paclitaxel. Gemcitabine and paclitaxel concentrations were measured in the listed tissues 3 hours after injection; the respective tissue to plasma ratios for each animal were analyzed and presented as a mean ± SD for each dosage form. Panel A represents gemcitabine and panel B represents paclitaxel tissue to plasma ratios. The black bars indicate GT DcNP while the gray bars indicate the CrEL control dosage form. *denotes $p < .05$

Chapter 5. NOVEL DRUG COMBINATION NANOPARTICLES EXHIBIT ENHANCED PLASMA EXPOSURE AND DOSE-RESPONSIVE EFFECTS ON ELIMINATING BREAST CANCER LUNG METASTASIS

A version of this chapter was published in:

Mu, Q. et al. Novel drug combination nanoparticles exhibit enhanced plasma exposure and dose-responsive effects on eliminating breast cancer lung metastasis. PLoS One 15, (2020).

5.1 ABSTRACT

Early diagnosis along with new drugs targeted to cancer receptors and immune checkpoints have improved breast cancer survival. However, complete remission remains elusive for metastatic breast cancer due to dose-limiting toxicities of heavily used, highly potent drug combinations such as gemcitabine and paclitaxel. Therefore, novel strategies that lower the effective dose and improve safety margins could enhance the effect of these drug combinations. To this end, we developed and evaluated a novel combination of gemcitabine and paclitaxel (GT). Leveraging a simple and scalable drug combination nanoparticle platform (DcNP), we successfully prepared an injectable GT combination in DcNP (GT DcNP). Compared to a Cremophor EL/ethanol assisted drug suspension in buffer (CrEL), GT DcNP exhibits about 61-fold and 8.6-fold increases in plasma drug exposure (area under the curve, AUC) and apparent half-life of gemcitabine respectively, and a 3.8-fold increase of AUC for paclitaxel. Using 4T1 as a syngeneic model for breast cancer metastasis, we found that a single GT (20/2 mg/kg) dose in DcNP nearly eliminated colonization in the lungs. This effect was not achievable by a CrEL drug combination at a 5-fold higher dose (i.e., 100/10 mg/kg GT). A dose-response study indicates that GT DcNP provided a therapeutic index of ~15.8. Collectively, these data suggest that GT DcNP could be effective against advancing metastatic breast cancer with a margin of safety. As the DcNP formulation is intentionally designed to be simple, scalable, and long-acting, it may be suitable for clinical development to find effective treatment against metastatic breast cancer.

5.2 INTRODUCTION

Breast cancer is a leading cause of death in women in the US and worldwide. Estimates suggest that in 2019 over 270,000 people will be newly diagnosed and that 42,000 people will die of the disease in the US alone (Siegel et al., 2020). The NIH, the Congressionally Directed Medical Research Program (CDMRP), and other foundations have made significant progress through ~ $1 billion in annual research investment. However, a cure for breast cancer remains elusive. Early diagnosis, resection of breast cancer tumors, and receptor targeted therapeutics (that inhibit human epidermal growth factor and hormone receptors) are effective at extending survival rates. However, many cancers still progress to the metastatic stage due to drug resistance and genetic mutation/evolution. Treatment options for these metastatic breast cancer patients are limited and outcomes are dismal. Even with current best agents—including drug-combinations and multiple cycle chemotherapy—metastatic breast cancer treatments provide about 27% five-year survival (Siegel et al., 2020). Patients at the metastatic stage exhibit cancer cells spread to highly perfused organs and local lymph nodes, detectable as colonies and nodules (Steeg, 2006). Physiological mechanisms and the time-course of cancer cells metastasizing into lymph nodes and tissues are not fully understood. This gap has prevented the development of treatment interventions, specifically those targeted to these sites early in the course of advancing cancer.

Two recent reports from separate laboratories have provided time-and-spatial insight into the metastatic spread of breast cancer cells from primary sites (lymph nodes and mammary gland) into blood (becoming apparent in the lungs as nodules) (Brown et al., 2018; Pereira et al., 2018). The two independent studies using 4T1 metastatic mouse tumors as models suggest that either removal of the primary tumor or introducing a small number of cells in the lymph node cortex (within the sinuses of the lymph node) would invariably lead to their appearance (through invasion

into blood) in the lungs as nodules or colonies of breast cancer cells. The studies suggest that cancer cells rapidly proliferate in blood and migrate into the lungs to form colonies detectable as nodules (Brown et al., 2018). The time-course and spatial 4T1 tumor spread data thus suggests that early systemic intervention with highly active chemotherapeutic or targeted agents responsive to metastatic cells could enhance response rate in metastatic breast cancer and delay the rate of disease progression.

According to NCCN (National Comprehensive Cancer Network) guidelines in the US, patients with newly diagnosed or recurrent breast cancer are treated with surgery if applicable prior to multiple cycles of adjuvant therapy. Metastatic breast cancer patients are often treated with intensive chemotherapeutic drug combinations targeted to topoisomerase or DNA synthesis plus microtubules, such as doxorubicin and paclitaxel, gemcitabine and paclitaxel (GT), capecitabine and docetaxel, or capecitabine and ixabepilone. These combination chemotherapies, while more effective than monotherapies, often exhibit dose-limiting toxicities. Intolerabilities ultimately prevent patients from completing their treatment cycles. For example, gemcitabine (1250 mg/m^2 IV day 1, day 8) and paclitaxel (175 mg/m^2 IV d1) combinations are reported to provide 41.4% response rate compared to paclitaxel alone (26.2%) (Albain et al., 2008). Median survival of this combination as a first-line treatment was 18.6 months versus 15.8 months on paclitaxel only. In another study in patients who failed neo-adjuvant anthracycline-based chemotherapy, the same dosing regimen produced a 50% objective response rate in the 12-month study (Xu, Shen, Jiang, Guan, & Zhang, 2010). However, significant side effects such as neutropenia, leukopenia, and poor tolerability were reported for these combination therapies. Collectively, if one can co-deliver an effective drug combination to advancing metastatic breast cancer cells, a lower overall dose would be needed to overcome dose-limiting toxicities.

In developing long-acting (LA) and combination anti-retroviral (drug) therapeutics or cART, our laboratory has discovered a simple, scalable technology that enables the incorporation of 2-3 HIV drugs that are water insoluble such as lopinavir, ritonavir, atazanavir, and efavirenz together with water soluble tenofovir and lamivudine (Koehn et al., 2018; Kraft et al., 2017; McConnachie et al., 2018; Perazzolo et al., 2018). This drug-combination nanoparticle (DcNP) technology has proven to be a platform that allows high loading of both hydrophobic and hydrophilic HIV drugs. With at least 4 different sets of cART tested in non-human primates, DcNP enhances lymphoid tissue and cell drug accumulation while exhibiting long-acting cellular exposure (Koehn et al., 2018; Kraft et al., 2017; McConnachie et al., 2018; Perazzolo et al., 2018). With this novel enabling technology, we have investigated whether gemcitabine (G, water soluble) and paclitaxel (T, water insoluble) can be assembled into a drug-combination particle able to enhance pharmacokinetics and also inhibit the growth of metastatic breast cancer. To this end, we leverage knowledge gained from recent studies using the advancing 4T1 cells in the lungs as a surrogate marker of disease progression (Brown et al., 2018; Pereira et al., 2018). Our results suggest that a single dose of DcNP formulated GT combination (20/2 mg/kg GT in DcNP) could reduce 4T1 to nearly non-detectable levels by day 14, while there was little to no effect on 4T1 with equivalent CrEL drug dosing.

5.3 Materials and Methods

5.3.1 *Reagents and cell line*

1,2-Distearoyl-sn-glycero-3-phosphocholine (DSPC) and N-(carbonylmethoxypolyethyleneglycol with MW=2000)-1,2-distearoyl-sn-glycero-3-phosphoethanolamine, sodium salt (DSPE-mPEG$_{2000}$) (GMP grade) were purchased from Corden Pharma (Liestal, Switzerland). Paclitaxel (>99.5%), gemcitabine free form (>99%), and

gemcitabine hydrochloride (>99%) were purchased from LC Laboratories (Woburn, MA). All other chemicals and reagents were analytical grade or higher. 4T1 cell line transfected and verified to express luciferase and green fluorescence protein (GFP) (referred to as 4T1-luc) was kindly provided by Stanley Riddell laboratory (Riddell et al., 2014), Fred Hutchinson Cancer Research Center.

5.3.2 *Formulation and characterization of GT DcNP*

DcNP composed of DSPC and DSPE-mPEG$_{2000}$ as lipid excipients, paclitaxel, and gemcitabine (90:10:2.5:80 molar ratio) were prepared aseptically as follows: Lipid excipients and drugs were solubilized together in ethanol at 60°C. Ethanol was removed by controlled solvent evaporation at 60°C, followed by vacuum desiccation to remove residual solvent. The dry film was rehydrated to 100 mM lipids in 0.45% NaCl with 20 mM $NaHCO_3$ buffer at 60°C for 2 h. Particle size was reduced at ~40°C using a bath sonicator (Avanti Polar Lipids, Inc. Alabaster, AL) (5 min on, 5 min off, 3 cycles). Previous results have shown that the vast majority of GT is associated to DcNPs; thus, filtration of free drug was not performed (Chapter 4.4.4). GT DcNP formulations were stored at room temperature for further use. Particle size was determined by a NICOMP 380 ZLS (Particle Sizing Systems, Santa Barbara, CA). Drug extraction with acetonitrile followed by HPLC were used to quantify drugs in the formulations. Drug association was measured by dialysis (6-8 kDa) of DcNP against 0.9% NaCl 20 mM $NaHCO_3$ buffer for 4 h and quantification by HPLC.

5.3.3 *Preparation of GT CrEL drug combination*

Paclitaxel was dissolved in ethanol (20 mg/mL) and diluted with an equal volume of Cremophor EL (Sigma-Aldrich, St. Louis, MO). The solution was then diluted 10x with a premade

PBS solution of gemcitabine (hydrochloride salt) (12.65 mg/mL). Final concentrations of drugs were 10/1 mg/mL GT. CrEL drug suspensions were used within the same day of preparation due to instability.

5.3.4 *Pharmacokinetic study*

All animal studies were conducted in accordance with University of Washington Institute of Animal Care and Use Committee (IACUC) approved protocols (protocol number 2372-06). The UW IACUC has specifically approved this study. Isoflurane was used for anesthesia during live animal imaging. 5-6 week-old female BALB/c mice were purchased from The Jackson Laboratory (Bar Harbor, Maine) and housed in an animal research facility for at least one week before use.

Mice were administered with either a CrEL drug combination or GT DcNP intravenously with doses of 50/5 mg/kg GT. Blood was collected through retro-orbital bleeding from groups of animals at 5, 15, 60, 120, 180 and 360 min for CrEL GT and 5, 60, 180, 360, 1440, 2880 min (48 h) for GT DcNP. Each group had three animals and each animal was bled once only. Retro-orbital blood collection in this study was a terminal procedure and animals were under anesthesia at the time of bleeding. After blood collection, mice were euthanized by CO2 overdose followed by cervical dislocation as the secondary method of euthanasia. Drugs in plasma were extracted and analyzed by LC-MS/MS as described below.

A protein precipitation method was used to extract drugs from plasma. 50 μL of sample were transferred into 1.5 mL tubes with or without dilution by blank matrix to an appropriate concentration range. Samples were spiked by internal standards (see below) followed by the addition of acetonitrile. Samples were then vortexed and centrifuged at 4°C for 15 minutes at 20,817 RCF. The supernatant was then removed and dried under nitrogen at 40°C. The dried samples were reconstituted in 20% methanol and 80% water in 50 μL.

Drugs were quantified by a Shimadzu HPLC system coupled to a 3200 QTRAP mass spectrometer (Applied Biosystems, Grand Island, NY). The HPLC system consisted of two Shimadzu LC-20A pumps, a DGU-20A5 degasser, and a Shimadzu SIL-20AC HT autosampler. The mass spectrometer was equipped with an electrospray ionization (ESI) TurboIonSpray source. The system was operated with Analyst software, version 1.5.2 (ABSciex, Framingham, MA). Chromatographic separation of drugs was achieved using a Synergi column (100 × 2.0 mm; 4-µm particle size) with an inline C8 guard column (4.0 × 2.0 mm) (Phenomenex, Torrance, CA). Chromatographic conditions are stated in Chapter 4.3.6. Briefly, the mobile phase for separation consisted of pump A (20 mM Ammonium Acetate in water) and B (Reagent Alcohol). Pump B was maintained at 20% for 1.0 minute, then increased to 97% at 2.0 minutes, held at 97% until 3.0 minutes, ramped to 3% by 4.0 minutes and held until 5.5 minutes. Analytes were monitored using multiple-reaction monitoring for positive ions. The following ion transitions were monitored: gemcitabine, m/z 264.066→112.000; paclitaxel, m/z 854.266→286.200; a stable labeled isotope ($C_8C^{13}H_{12}ClF_2N^{15}N_2O_4$) (m/z 267.067→115.100) was used as an internal standard for gemcitabine; docetaxel (m/z 830.312→549.3) was used as an internal standard for paclitaxel.

5.3.5 *4T1 cell inoculation*

Six-week-old, female BALB/c mice were used in this study. 4T1 cells were transfected with luciferase and green fluorescence protein (GFP) (4T1-luc); thus, 4T1 growth could be monitored based on that bioluminescence (Tao et al., 2008). 4T1-luc (0.5, 1 or 2 × 10^5 cells) suspended in a 100 µL ice-cold HBSS suspension was intravenously inoculated through mouse tail veins. Mice were monitored for a two-week period. Bioluminescence of 4T1-luc from living mice was examined by a XENOGEN IVIS 200 imaging system (PerkinElmer, Inc. Waltham, MA). Mice received 150 mg/kg D-luciferin through intraperitoneal injections 10~15 min before

imaging. The bioluminescence imaging parameters for living mice were set as follows: field of view, 12; excitation filter, closed; emission filter, open; exposure time, 120 sec; binning factor, 4; f/stop, 2. Total 4T1-luc bioluminescence emission from living mice was integrated using Live Image software (PerkinElmer, Waltham, MA).

5.3.6 *Effects of CrEL drug combinations and DcNP on metastatic breast cancer colony formation in the lung*

Six-week-old, female BALB/c mice were inoculated with 2×10^5 4T1-luc cells IV in 100 µL HBSS on day 0. Three hours later, mice were given a single administration of saline, a CrEL drug combination, or GT DcNP through IV injections (n = 8-15). The GT doses were 50/5 mg/kg for CrEL and DcNP formulations. On day 14, mice were euthanized immediately after live imaging and lungs were collected and placed in 12-well plates to quantify luminescence images. The images were acquired by a Xenogen IVIS-200. The bioluminescence imaging parameters for living mice were set as follows: field of view, 24; excitation filter, closed; emission filter, open; exposure time, 180 sec; binning factor, 4; f/stop, 2. *Ex-vivo* imaging parameters for lungs were set as follows: field of view, 10; excitation filter, closed; emission filter, open; exposure time, 30 sec; binning factor, 4; f/stop, 2. Bioluminescence intensity from living mice and lungs was integrated using Live Image software. Mouse lung tissue was fixed in formalin and stored in 70% EtOH before being embedded in paraffin blocks. GFP staining of thin sections (5 µm) was carried out by UW histology and imaging core.

5.3.7 *Dose dependence of GT DcNP on 4T1 metastases*

Six-week-old, female BALB/c mice were inoculated with 2×10^5 4T1-luc cells in 100 µL HBSS through IV injections on day 0. Three hours later, mice received a single administration of

saline or a different dosage of GT DcNP through IV injections (n = 8-15). The dosages for DcNP were 0.125/0.0125, 1.25/0.125, 5/0.5, 10/1, and 20/2 mg/kg GT, respectively. Mouse behavior and overall health conditions were observed on a daily basis and body weight was measured every 2 days. On day 14, bioluminescence from living mice was examined with the IVIS imaging system as described above. Lung metastasis was detected by isolating lungs and imaging with IVIS as described above. After euthanasia, all organs were collected and visually examined for apparent toxicity.

5.3.8 *Statistical Analysis*

Data were presented as the arithmetic mean ± standard error of the mean (SEM). The number of mice in all groups ranges from 8 to 15. Students' t-tests were performed for comparison between two treatment groups, one-way ANOVA was used to determine statistical significance between saline treated mice in replicate studies and two-way ANOVA was used to determine statistical significance for multiple treatment groups across studies. A P-value of <0.05 was considered statistically significant. Statistical analyses were performed using GraphPad Prism (Version 7.0).

5.4 RESULTS

5.4.1 *Development and characterization of gemcitabine and paclitaxel together in an injectable DcNP formulation*

We first determined whether water soluble gemcitabine (LogP = -1.5) and water insoluble paclitaxel (LogP = 3) could be integrated into a drug combination particle in suspension presented as an injectable dosage form. We tested the GT combination by employing a composition of lipid excipients previously reported to stabilize 3-to-4 HIV drugs with disparate hydrophobicity in

DcNP form (Kraft et al., 2017). We found that at a fixed G:T 32:1 (m/m; equals to 10:1 w/w) and lipid excipients–DSPC, DSPE-mPEG$_{2000}$ (9:1 m/m), a stable and scalable DcNP with approximately 60 nm diameter can be made. We have tested at least 4 batches of DcNP preparation and verified that this process is reproducible, that DcNP products are stable, and that they can be scaled-up for the *in vivo* studies described. As the resulting GT DcNP product is less than 200 nm in diameter and stable in suspension (to at least 3 months and amenable for sterilization by 0.2 μm filtration), it is suitable for IV administration. Since the current clinical dose for GT is approximately 10:1 (w/w) (gemcitabine 1000~1250 mg/m^2, paclitaxel 80~175 mg/m^2), we used the DcNP with a similar drug ratio for the studies in mice described below.

5.4.2 *Enhanced plasma gemcitabine and paclitaxel exposure when presented in DcNP dosage form*

We subsequently determined the effect of co-formulating GT in an injectable DcNP on plasma GT concentration time course. Compared to a CrEL drug combination counterpart, GT DcNP formulation greatly improve the total plasma drug exposure of GT at an equivalent dose. After a 50/5 (GT) mg/kg IV dose, gemcitabine in DcNP exhibits about 61-fold higher exposure (AUC) and 8.6-fold longer apparent half-life than an equivalent CrEL drug combination dosage in mice (Table 5.1). The dramatic increase in gemcitabine AUC per dose reflects both a small (~10%) increase in Cmax and an ~8.7-fold increase in apparent half-life. Paclitaxel given as GT DcNP at a 10-fold lower dose than gemcitabine (5 mg/kg) exhibited a ~21% increase in Cmax but a similar half-life (1.97 vs 1.81 h). Due to the longer persistence of paclitaxel in DcNP, the overall AUC enhancement is about 3.8 fold (Table 5.1). Collectively, these data indicate that a co-formulation of GT in DcNP can provide longer acting and higher GT exposure in mice compared to CrEL drug dosages.

5.4.3 *Characterization of 4T1-luc in BALB/c mice as a syngeneic metastatic tumor establishment and nodule growth model for intervention studies.*

To determine whether enhanced GT exposure can translate into improvements in inhibition of metastatic tumor establishment and growth, we first evaluated if 4T1 inoculated intravenously into BALB/c mice could model hematogenous metastasis. 4T1 introduced into the blood have recently been shown to establish and grow in the lungs as nodules, and at a much faster rate than in the lymph nodes and the sinuses within the lymph nodes (Brown et al., 2018). In addition, the 4T1 (labeled with luciferase for live tracking) are able to invade blood capillaries in the nodes and spread to lungs, which are detectable as 4T1 nodules (Pereira et al., 2018). Therefore, we first performed a titration study to find a dose of 4T1 cells that produces tumor nodules in the lungs while not overburdening the mice with tumors. To do so, we employed a 4T1 cell line carrying luciferase marker (4T1-luc) (Tao et al., 2008). The transfection of luciferase did not affect cell proliferation or migration (Brown et al., 2018). After verifying luciferase expression by the 4T1-luc, these breast cancer cells were inoculated into the tail veins of BALB/c female mice. We studied a dose range between 50 to 200 x 10^3 4T1-luc cells in the inoculum per mouse. Bioluminescence (of 4T1-luc), body weight, and general behavior were monitored over two weeks. We found that bioluminescence signals increased exponentially from days 10 to 13 (from 0.5 to 3.5 x 10^5 photo counts). Furthermore, the body weight of mice gradually declined (~10% from day 10 to day 13) at a higher inoculum dose in mice corresponding to the exponential increase in the lung bioluminescence intensity. We found, with 200 x 10^3 cells, that about 20~30 tumor nodules and 2.0~3.0 x 10^5 photon count of bioluminescence could be detected in the mouse lungs—showing that colonies establish and grow over time in these tissues with acceptable weight and overall health for interventional studies. Thus, 200 x 10^3 4T1-luc cells in the inoculum was used for the following studies.

It is well known that animal studies are highly variable due to individual differences, batch variances, etc. To verify the reproducibility of this model, we repeated our study five times with a total of 21 mice and compared lung bioluminescence intensities using a 200 x 10^3 cell inoculation number. Results indicate that the model is highly reproducible and reliable with 100% tumor uptake and no significant difference between the mean bioluminescence ($p=0.0681$ by one-way ANOVA). The rapid and aggressive 4T1 tumor growth at this dose has limited our ability to keep untreated mice for up to 14 days. The effectiveness studies in following sections were determined using a 200 x 10^3 4T1 cell inoculation with saline treated controls run in parallel for each set of experiments or replication.

5.4.4 *Effects of DcNP on gemcitabine and paclitaxel combinations for inhibiting 4T1 syngeneic mouse metastasis*

To determine the effects of enhanced GT exposure when presented in DcNP dosage form, we first used 50/5 mg/kg (GT) based on the current clinical (surface area converted to weight based) dose. Mice were first inoculated with 4T1 cells and given a single IV dose of GT either in CrEL or DcNP form. We intentionally chose identical GT doses (50/5 mg/kg) for the two formulations to evaluate DcNP effect on this treatment model (and without using dose compensations to match plasma drug exposures between the two formulations). The short interval between cell inoculation and GT administration (3 hour) was also purposefully designed, as the goals of this study were to examine the clearance of advancing cancer cells in blood and eliminating formation of lung metastasis nodules. Tumor nodule formation was monitored over 14 days. As shown in Fig 5.1 (A and B), at day 14 mice treated with GT DcNP formulation completely inhibited 4T1 colonies in the lungs, while the CrEL dosage form only inhibited 60~70%. The bioluminescence intensity data are verified with lung nodule counts and ex-vivo 4T1-luc-

luminescence verification of the excised lungs (Fig 5.1 C). However, we noticed a trend toward weight loss around day 4-6 in mice treated with 50/5 GT mg/kg or higher dose. These quantitative data indicate that a single dose of GT co-formulated in DcNP could completely inhibit the establishment and growth of 4T1 metastatic cancer in the lungs at a significantly higher rate than that provided by CrEL drug combinations in this syngeneic mouse model.

To further characterize lung metastasis and treatments at the microscopic level, lung sections were examined with GFP immunohistochemistry given GFP is expressed by 4T1-luc, and the microstructures were evaluated in comparison to controls (Fig 5.1 D). First, we observed that the metastatic nodules in lungs often occur near blood vessels, indicating that 4T1-luc cells deposit in lungs following invasion into narrow vasculature. Second, we evaluated the lung tissues of 4T1 inoculated mice treated with placebo or drug combinations. As shown in Fig 5.1 D (second rows of graphs), the cross-sections of lungs treated with CrEL dosage form and placebo exhibited a larger number of 4T1 cells positive for GFP while those from a GT DcNP single dose treatment did not. These data are consistent with bioluminescence measures *in vivo* and *ex vivo* of lung analysis where we found a high single IV dose GT DcNP treatment completely prevented the occurrence of 4T1 cancer nodules in the lungs.

5.4.5 *Dose-dependent tumor inhibitory and gross toxicity (weight loss) effect of GT combination in DcNP to estimate therapeutic index*

To confirm the initial results of the GT fixed-ratio combination in DcNP on 4T1 nodules in the lungs and establish preliminary dose-dependent effects, we performed a dose-finding study. Within the range of a single IV dose of DcNP carrying 0.125 to 50 mg/kg gemcitabine and 10/1 w/w paclitaxel (0.0125 to 5 mg/kg), we followed the growth (based on 4T1-luc bioluminescence intensity) of tumor nodules as therapeutic outcome measures. No clinical behavioral or

hematological effects were notable for animals in all treatment groups for the 14-day study. However, a reproducible measure is the weight loss detected within 4-6 days after dosing (Fig. 5.3). Thus, we used this measure as a gross toxicity, likely similar to that observed with general GI toxicity associated in humans treated with gemcitabine (Beane et al., 2015; Loehrer et al., 2011). As shown in Fig 5.2 A, dose-dependent measures of tumor nodule count and tumor intensity were noted, and the graded response trend of these two measures was similar. At 20 mg/kg gemcitabine plus 2 mg/kg paclitaxel in DcNP, these two measures exhibit a 90-95% inhibition of 4T1-luc tumor burden, indicating a smaller dose requirement for cancer clearance compared to initial data presented in Fig 5.1. The same level of clearance was not achievable for the CrEL drug combination, even with 5-fold higher doses (i.e., 80-90% inhibition at 100/10 mg/kg GT). The 50% effective doses (ED50s) for GT in DcNP fixed dose combinations were determined to be 1.655/0.1655 and 2.958/0.2958 mg/kg based on luminescence intensity and nodule count respectively (Fig 5.2 B). Based on the 20% weight loss (a maximum number allowable for experimental study) as a gross toxicology measure, the dose-dependent weight loss profile exhibited a much higher dose range and did not occur until 30/3 GT mg/kg dose. The dose-response curve for weight loss, referred to as a toxic dose (TD) is steeper and well-separated from the GT DcNP dose range that inhibited 4T1-luc tumor. The 50% toxic or TD50 was determined to be 36.48/3.648 mg/kg GT. Using the mid-point of effective dose and toxic (weight-loss) doses, and the average therapeutic index — the ratio of toxic-to-effective dose is estimated to be about 15.8 mg/kg for GT DcNP. Taken together, dose-ranging studies indicate that the effective dose range is lower and well-separated from the toxicity range for GT combination by about 16 fold when given in DcNP dosage form. These data also confirmed that a single IV dose may prevent a significant burden of invasive 4T1 with a sufficient margin of safety.

5.4.6 *Reproducibility of GT DcNP's physicochemical and in vivo study data*

Due to inherent challenges in translating nanomedicine into clinical applications, it is important to validate the reproducibility of our GT DcNP regarding physicochemical properties and *in vivo* effectiveness. Due to high variance of the animal models, we carried out at least two independent effectiveness studies for each DcNP dose reported in Fig 5.2. A two-way ANOVA analysis indicates that the difference between mean bioluminescence of replications for the same doses are insignificant but significantly different between doses ($p=0.0854$ for replication factor and $p<0.0001$ for dose factor). Our results verified that the DcNPs produced in different batches exhibit similar characteristics—nearly identical mean particle size, drug loading and association efficiency, and more importantly, the ability to inhibit 4T1 metastasis in mice; thus these results were reproducible and consistent.

5.5 DISCUSSION

With early detection and targeted therapies, breast cancer survival rates have increased (Siegel et al., 2020), even as a cure remains elusive. When dealing with advanced metastatic disease, highly potent but toxic combination regimens such as GT are a limited option with dose-limiting toxicity as a significant barrier (Lim & Hortobagyi, 2016). Capitalizing on the drug combination nanoparticle (DcNP) platform's ability to stabilize water soluble gemcitabine and insoluble paclitaxel together into GT DcNP, we found that the DcNP enhanced the plasma drug exposure at higher and longer lasting levels in mice. In a 4T1-luc metastatic mouse model, a single dose of GT DcNP was able to completely suppress 4T1 metastasis in the lung tissues. Dose-response studies also revealed the enhanced efficacy of GT drug combination and extended safety margin when given in GT DcNP dosage form.

For metastatic breast cancer treatment, combination therapy has been proven more effective than monotherapy (Albain et al., 2008). However—due to the disparate physicochemical properties—co-formulation for the targeted delivery of hydrophilic and hydrophobic drugs such as GT has been challenging. The disparate physical properties of the two drug combinations prevent them from associating together in a stable form. While liposome encapsulation of doxorubicin—via a complex manufacturing process removing unbound drug and precise remote loading—is available as Doxil, it is a single agent that must be combined with other agents expressing different pharmacokinetics, tissue distribution, and time courses for combination therapy. The benefit of liposomal doxorubicin is derived from enhanced tumor tissue accumulation through the neovasculature, which is formed at a later stage of tumor nodule development. A product with two-drugs encapsulated in liposomes called Vyxeos was recently approved by the FDA. Vyxeos contains two water soluble drugs cytarabine and daunorubicin. However, both drugs were subjected to labor intensive purification mentioned above (followed by lyophilization as a finished product) and only intended for treating leukemia, which exhibits significantly different cancer biology from metastatic breast cancer. Unlike liposome encapsulation, the DcNP platform is based on water-soluble (i.e., gemcitabine) and insoluble (i.e. paclitaxel) drugs co-solubilized in a soft organic solvent (i.e., ethanol) together with lipid excipients serving as a bridge or glue. Removal of the solvent and rehydration allows the formation of a stable drug-combination complex that can be broken down into GT DcNP particles at a size that is amenable for use as an injectable dosage form. Thus, this simplified process requires no unbound drug separation, purification, or lyophilization, which could help with product scaling, reproducibility and cost-saving.

The current human GT combination is given in a sequence with IV infusions of paclitaxel followed by gemcitabine (after 2-3 h) at doses of ~1250/175 mg/m^2 GT, equivalent to ~35/3.5 mg/kg (Albain et al., 2008; Xu et al., 2010). Sequential dosing of conventional GT is necessary both to improve tolerability and reduce toxicity. In our study, we were able to combine both drugs while exhibiting sufficient safety in mouse models. The effective dose-range 10-50/1-5 mg/kg GT in mice is within the current range of human doses given in multiple cycles based on the plasma concentration under time curves of the free drug. While the exact mechanisms leading to this enhanced therapeutic index is not clear, it is likely through enhancement in differential drug distribution and pharmacokinetic profile. With two drugs in one intravenous injection, the DcNP formulation has prolonged the apparent elimination half-life of gemcitabine by more than 8x and enhanced its AUC by 61x, higher than known previous achievements (Paolino et al., 2010; J. Zhang et al., 2018). Such enhancement may be due to association to DcNP (together with paclitaxel), and potentially reduced metabolism of DcNP bound gemcitabine by cytidine deaminase (to 2',2'-difluorodeoxyuridine, or dFdU) in liver and cells (Frese et al., 2012). Regardless of the pharmacokinetic and physiologic mechanisms, the DcNP formulation has enhanced the GT pharmacokinetic and pharmacodynamic profile resulting in an ~10-fold lower GT dose needed to inhibit metastatic cancer with a safety margin (TI of 15.8).

The therapeutic effects mediated by DcNP on GT were evaluated in 4T1 inoculated systematically to produce the lung metastasis model. This model is immunocompetent and relevant to human disease, where immune contribution is important. A genomic profiling study revealed a high consistency between lung metastases from orthotopic (mammary fat pad) and IV inoculation models, demonstrating that this approach mimics the spread of metastatic breast cancer cells from the primary tumor site (Rashid et al., 2013). This model is also clinically relevant to human disease

due to reported spontaneous 4T1 metastasis to the lungs, brain, and bones in mice with functional immune systems (Pulaski & Ostrand-Rosenberg, 2001). Models generated with murine originated 4T1 cells have proven useful in metastasis disease and interventional studies (Brown et al., 2018; Pereira et al., 2018), and are used extensively in discovering immuno- and chemotherapeutics targeting metastatic breast cancer (Eckhardt, Francis, Parker, & Anderson, 2012; Rashid & Takabe, 2015).

Limited by safety concerns and the short half-lives of most current chemotherapeutic drugs, repeated dosing regimens are typically used in humans. Single agent drug resistance, and cumulative drug toxicity for some drugs could limit treatment options for metastatic diseases. In the mouse model of this study, cancer cells progress into the lungs from the blood to cause mortality in only ~14 days. In this time window, the highest achievable single dose of the CrEL drug combination (limited by paclitaxel solubility) inhibited the process marginally. For 80~90% inhibition of lung metastasis of 4T1 within a similar timeframe, multiple dosing was required in previous studies (Cao et al., 2016; Cao et al., 2015; Q. Chen & Ross, 2012; Dan et al., 2016). Even with more sophisticated nanoparticles with target-activated drug delivery (e.g., legumain), none of the reports were able to demonstrate clearing of the 4T1 lung metastasis in a single dose (X. He et al., 2017). In contrast, GT DcNP inhibited 100% of the lung metastasis with no detectable cancer *in vivo* and *ex vivo* with only one single IV injection (Fig 5.1 and 5.2). It should be noted that the intent of this 4T1 mouse model is to allow the evaluation of drug-combinations to inhibit and clear the metastatic spread of advancing breast cancer cells in blood and for lung nodules. Thus, it is not intended to evaluate effects on primary breast cancer which may be laden with neovasulature amenable for nanoparticle mediated drug delivery through commonly prescribed enhanced

permeability and retention or EPR effect. The enhanced 4T1 clearance of lung nodule formation is unlikely due to EPR.

The vast majority of breast cancer patients receive chemotherapy after surgical removal of the primary tumor. The timing of chemotherapy is often scheduled as soon as possible after surgery (and potentially radiation therapy) to eliminate residual cancer cells. The DcNP approach outlined in this report may translate to the intravenous administration of GT DcNPs after surgery to eliminate cancer cells that have escaped into the systemic circulation. Further assessment of safety is crucial for this translation, however, the enhancement of GT anticancer effect in the blood (by DcNP formulation) is clear. Whether a lower dose could be given in a multiple dosing scheme to produce a higher safety margin or TI is unclear but further study is warranted. GT ratio and excipient composition may also play a role in overall therapeutic and pharmacokinetic outcomes.

The ability of DcNP to enhance GT combination also opens other opportunities to enhance cancer chemotherapy. As lymphatic cancer invasion is believed to be an early site for metastasis, it is possible that DcNP loaded drugs may provide additional benefits. With at least 4 sets of HIV drug combinations formulated in DcNP, all drugs have been given subcutaneously in DcNP dosage for uptake of each composition into lymphatics in their first-pass (Koehn et al., 2018; Kraft et al., 2017; Kraft, Treuting, & Ho, 2018; McConnachie et al., 2018; Perazzolo et al., 2018). After subcutaneous administration and during the first passage, DcNP particles are shown to track preferentially into the lymph, but not blood capillaries, as observed with a near-infrared fluorophore (indocyanine green) tagged DcNP in mice (Kraft, Treuting, et al., 2018). In addition, DcNP has enabled the maintenance of cellular drug levels in lymph node mononuclear cells (above plasma drug levels) for over 2-4 weeks in non-human primates (NHP) (Kraft et al., 2017; McConnachie et al., 2018). In our current report, we were able to demonstrate less dramatic long-

acting effects due to DcNP for GT combinations when given in an IV dosage form. With an alternative subcutaneous route of GT DcNP administration, it is possible that drugs could be localized in the lymphatic system and stand ready to block the lymphatic metastasis pathway.

In summary, we have developed a simple, stable, and scalable GT DcNP dosage suitable for IV administration that transforms short-acting gemcitabine into a long-acting variation. We have also enhanced the pharmacokinetic profile of both drugs. The enhanced GT pharmacokinetic profile provided by DcNP dosage form parallels the GT effect against 4T1 metastatic breast cancer. A single GT DcNP injection completely inhibited lung metastasis in mice at levels that cannot be achieved with a CrEL dosage form at equal or higher doses. The enhanced dose-response was observed with a significant margin of safety. With the flexibility of the DcNP platform and impact on GT pharmacokinetics, pharmacodynamics, and safety windows, this approach could be generally applicable for use with other drug combinations intended to treat a number of cancer types, especially for the metastatic disease stage. The ability to transform current short-acting drugs into long-acting forms with preferential uptake could also accelerate clinical translation of the drug combinations in DcNP dosage form.

Table 5.1. The effect of gemcitabine and paclitaxel presented in a drug combination nanoparticle platform (DcNP) dosage form on the select pharmacokinetic parameters of the two drugs, compared to a CrEL drug dosage control form*

	Gemcitabine (G)		**Paclitaxel (T)**	
	CrEL	**DcNP[a]**	**CrEL**	**DcNP**
C_{max} (μg/mL)	165.12[b]	181.4	17.7	13.9
$AUC_{0\rightarrow\infty}$ (μg min/mL)	920.8	56218.6	156.5	588.8
$t_{1/2apparent}$ (h)	1.60	13.72	1.81	1.97

*GT (50/5 mg/kg in 100 μl) in DcNP or CrEL drug dosage form was given intravenously to mice. The plasma drug concentration time course was analyzed, and the listed pharmacokinetic parameters are generated based on non-compartmental analysis (n=3 composite sampling).

[a]CrEL drugs scaled to equivalent DcNP dosages.

bAll values are reported as the geometric mean

Abbreviations: C_{max}, maximum plasma drug concentration; $AUC_{0\rightarrow\infty}$, area under the plasma drug concentration-time extrapolated to infinity (Maximum % extrapolated <10%); $t_{1/2}$, apparent terminal plasma drug half-life.

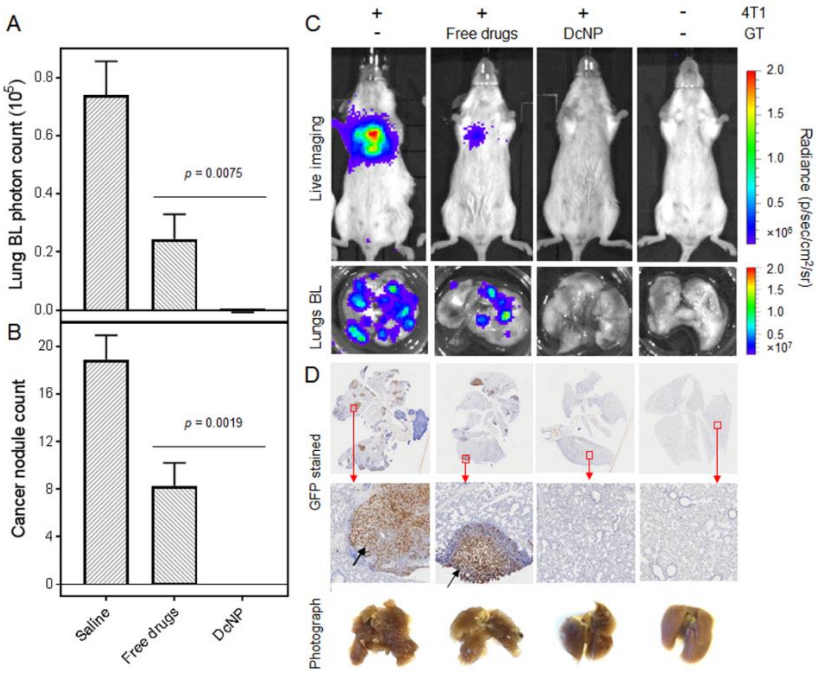

Figure 5.1. Effect of DcNP on gemcitabine and paclitaxel fixed-dose combination treatment on 4T1 metastatic tumor intensity and nodules in the lungs.

Mice inoculated with 4T1-luc via tail vein were administered with a 50/5 mg/kg GT fixed dose combination in DcNP (test) or CrEL (control) formulation as a single bolus IV dose. On day 14, the total tumor growth was estimated based on luciferase activity detected as total bioluminescence (BL) intensity (A), and the cancer nodule count (B). Equivalent single IV doses of conventional formulation of the GT fixed dose combination was given to mice as a control. The values in panels (A) and (B) are expressed as mean ± SEM. P values were obtained from two-tailed t-tests with unequal variations. Experimental animal numbers in each group were 8-15. (C) Representative 4T1-luc luciferase mediated bioluminescence intensities in saline control, CrEL drug combination, DcNP treated mice, and healthy mice, as well as the lung nodules harvested from these mice. (D) Images of GFP (expressed by 4T1-luc) stained lung cross-sections from mice in conditions of (C), and photographs of fixed lung tissues. Top row, whole lung cross-sections; Bottom row, enlarged images from red boxes in top row. Black arrows indicate cancer nodules.

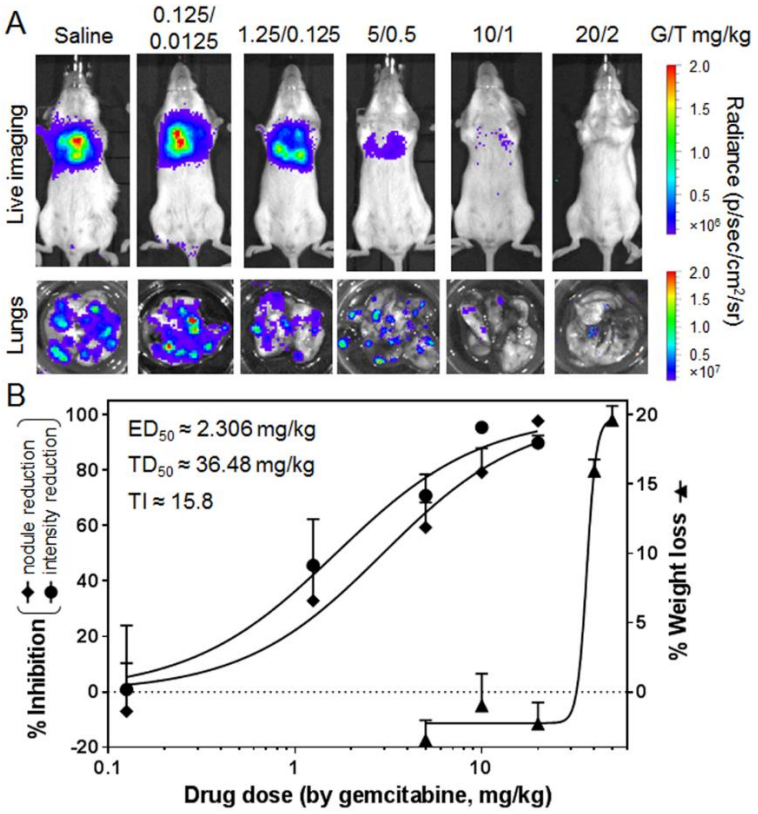

Figure 5.2. The dose-response of DcNP formulated gemcitabine-paclitaxel on inhibiting 4T1 lung metastasis; and bodyweight reduction.

The 4T1-luc breast cancer cells were inoculated via tail-vein and the indicated dose (anchored on gemcitabine containing 1/10 weight equivalent of paclitaxel in DcNP formulation) were administered as a single dose IV administration. The 4T1 tumor growth (based on 4T1-luc luciferase dependent bioluminescence) and tumor nodule counts were expressed as therapeutic effects. The bodyweight loss at day 4 was used as an indicator of gross toxicity. (A) Representative 4T1-luc luciferase mediated bioluminescence intensities in saline and DcNP (with different GT doses) treated mice, as well as the lung nodules harvested from these mice. (B) Dose-responsive curves of metastasis inhibition were determined by bioluminescence integration and nodule count, as well as body weight loss with DcNP treatment. The values expressed are mean ± SEM. Experimental animal numbers in each group were 8-15. The curves were fitted in GraphPad Prism software (dose response-inhibition) to estimate ED50s and TD50s based on gemcitabine doses. The ED50 was averaged from two measures. The average therapeutic index (TI) is estimated based on the ratio of TD50-to-ED50 which is 15.8.

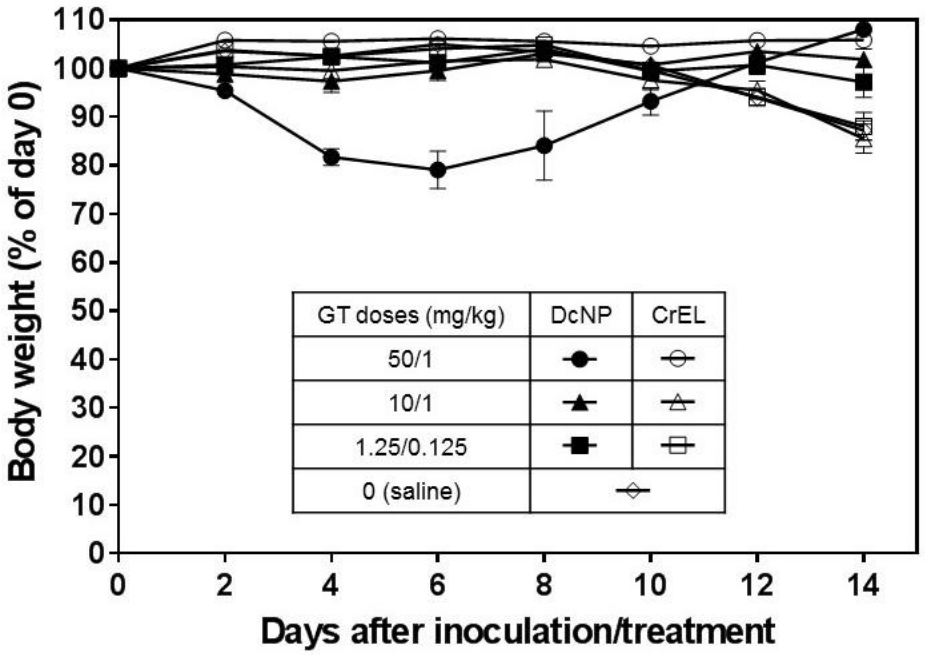

Figure 5.3. Time course body weight changes in 4T1-inoculated mice treated with placebo (saline), GT in Cremophor EL/EtOH/PBS (CrEL) suspension or DcNP (drug-combination nanoparticle) dosage form.

On day 0 GT in CrEL suspension or DcNP at 1.25/0.125, 10/1, or 50/5 mg/kg IV doses, and the 4T1 inoculated mice were monitored over 14 days. Each treatment group contains 8-15 mice and the data presented are mean ± SEM. In the group of 50/5 mg/kg of DcNP treated mice, 2 out of 5 animals were sacrificed ahead of schedule due to clinical necessity. The remaining animals in the high dose group recovered and by day 14 appeared to exhibit body weight higher than at entry. In comparison, the saline placebo treated animals exhibit significant (15%) weight loss by day 14 due to rapid growth of lung metastatic nodules. The same trend is seen in the group treated with GT in CrEL suspensions (at two lower doses—10/1 and 1.25/0.125 mg/kg).

Chapter 6. EFFECTS OF GEMCITABINE AND PACLITAXEL IN NOVEL DRUG COMBINATION NANOPARTICLES THAT ENHANCE DRUG LOCALIZATION AND REGRESSION OF ORTHOTOPIC 4T1 METASTATIC BREAST CANCER

This chapter is in preparation for submission.

6.1 ABSTRACT

The combination of surgery, radiation therapy, and drug therapy for the treatment of breast cancer is effective at extending 5-year survival. However, a cure for breast cancer remains elusive as even the best current therapies suffer from tumor recurrence. Cancer cells that migrate into poorly perfused lymphatic tissue may have low drug exposure from intravenous or oral chemotherapy, allowing proliferation of these residual cells that may lead to recurrence and disease progression. In order to address this gap in breast cancer treatment and enhance the limited drug exposure and retention in cancer cells migrating into lymphatic tissue, we have used a novel drug combination nanoparticle (DcNP) carrying gemcitabine and paclitaxel (GT) to target mammary tumors. To do so, we first developed and characterized an orthotopic model of aggressive breast cancer growth. These tumors composed of 4T1 cells rapidly developed blood and lymph vessels within 5 days of cell inoculation. Subcutaneous injection of GT DcNPs was shown to be taken up into local lymphatic vessels and transit to distant lymph nodes throughout the body including the axillary of the mouse. GT DcNPs enable long lasting drug concentrations in tumors and plasma. Compared to the same dose of freely solubilized drug, GT DcNPs produced a greater inhibition of tumor growth in the sub-iliac and axillary regions by 100- to 140-fold, respectively. Dose-ranging studies demonstrate that GT DcNP effect is dose-dependent and can cause tumor regression, which to our knowledge, could not be achieved with current free drug infusion strategies. The targeted delivery of GT to tumors implanted in mammary tissue, after transit through the lymph, may address the current gaps in cancer treatment and prevent tumor recurrence.

6.2 INTRODUCTION

Early stage breast cancer patients are treated through surgical resection of the primary tumor, radiation therapy and systemic therapy based on the molecular characteristics of the breast cancer (i.e. $HER2^+$, ER/PR^+, triple receptor negative etc) (Cardoso et al., 2019). This multi-modal approach is effective, and the 5-year survival rate of early stage breast cancer patients is high (>90%). Unfortunately, 30% of these patients progress to metastatic disease where disease prognosis is poor (Redig & McAllister, 2013). Disease progression is due to residual cancer cells that escape the initial interventions and proliferate in regional tissue or distant organs. As these cancer cells grow into tumors and spread, they invade into both the lymphatic and systemic circulation to produce metastasis. Hematogenous metastasis (or blood-based metastasis) is characterized by cancer cells transiting through the systemic circulation to form metastatic lesions in distant, highly perfused organs such as the lung or brain (Wong & Hynes, 2006). Lymphatic metastasis involves the spread of cancer cells into the regional draining lymph nodes of a tumor and is often observed as the first site of metastasis (Wong & Hynes, 2006). Recently, two studies have shown that cancer cells originating in the lymph nodes will migrate into blood vessels to produce distant metastasis; thus, transit through the lymph may be an important step in disease progression (Brown et al., 2018; Pereira et al., 2018). The circulatory dynamics of the lymphatic system is involved in the pathogenesis of breast cancer metastasis and numerous clinical associations have been established between the detection of cancer cells in the lymph and disease progression (Jones, Pereira, & Padera, 2018). Consequently, the treatment for breast cancer metastasis must consider the lymphatic system as a target site where cancer cells may proliferate.

In order to address the invasion of cancer cells into lymphatic or regional tissue, surgical, radiological and pharmacological interventions are used. Surgical oncologists, as a preventative

measure, can choose to remove a portion (sentinel lymph node biopsy) or all (axillary lymph node dissection) of the lymphatic architecture associated with the primary tumor. However, these procedures are highly invasive and can result in adverse events associated with the blockage of lymphatic flow such as lymphedema, seromas and reduced range of motion (Sakorafas, Peros, & Cataliotti, 2006). Radiation after surgery is an effective means of eliminating cancer cells remaining in the surgical margins but leads to significant inflammation and fibrosis in the irradiated tissue (Brownlee et al., 2018). The accumulated effects of surgery and radiation therapy can lead to disruptions in vasculature and growth of fibrotic tissue. As a result, systemic therapy typically given after surgery may not have direct access from the blood to cancer cells residing in lymphatic or regional breast tissue.

Chemotherapy used in the treatment of metastatic breast cancer is typically administered intravenously as combination regimens to prevent drug resistance and disease progression. Gemcitabine and paclitaxel (referred to as GT) is a taxane-based combination regimen used extensively in the treatment of metastatic breast cancer. GT can maximally inhibit cancer cells by targeting different points in cell cycle replication (Allouache et al., 2005). However, current GT infusions are administered in sequence to prevent infusion reactions due to intolerable effects in patients when given simultaneously. These infusions are administered after surgical intervention and radiation therapy, and may produce limited drug exposure to cancer cells in the regional tissue due to disruptions in local vasculature. In addition, gemcitabine and paclitaxel have widely diverging physicochemical and pharmacokinetic properties and are unlikely to distribute in a synchronized fashion to maximize therapeutic benefits. The diverging distribution of GT is demonstrated by the primary organs of toxicity for each drug. For example, gemcitabine is known to distribute extensively into off-target enterocytes and lead to gastro-intestinal or GI toxicity;

while paclitaxel distributes into off-target neuronal cells leading to peripheral neuropathy (Velasco & Bruna, 2015). The pairing of gemcitabine and paclitaxel for chemotherapy is partially due to these diverging toxicities, thus resulting in a safer chemotherapy combination. Unfortunately, this also limits the effect and coordination of both drugs in target cancer cells. If both gemcitabine and paclitaxel can be targeted and delivered to tissues where cancer cells reside (such as the lymph), then those residual cancer cells can be eliminated, and off target exposure (and toxicity) can be reduced.

Recently, our team has developed a method to co-formulate hydrophilic gemcitabine and hydrophobic paclitaxel as a stable drug combination nanoparticle (DcNP) (Jesse Yu et al., 2020). Gemcitabine and paclitaxel were stabilized with lipid excipients together in DcNP dosage form in a 10:1 G-to-T weight ratio. The resultant GT DcNPs had an average size of ~60 nm in diameter and suitable for use as an injectable dosage form. After intravenous administration, gemcitabine and paclitaxel were verified to be predominantly associated to DcNPs through pharmacokinetic studies and a mechanism based pharmacokinetic modeling (Jesse Yu et al., 2020). GT DcNPs were able to facilitate long-acting plasma circulation and higher accumulation of drugs in tumor burdened tissue compared to healthy tissue. In a model of hematogenous breast cancer metastasis, GT DcNPs were able to completely prevent lung cancer nodule formation, something that was not achievable at any dose of conventionally formulated GT (Mu et al., 2020). The elimination of remote metastatic cancer nodules in the lungs was an exciting observation and demonstrated the potential for GT DcNPs as a treatment for breast cancer metastasis. Although promising, the intravenous approach also had limitations such as systemic toxicity manifesting as weight loss at higher doses. Thus, an alternative approach may lead to further improved outcomes (Mu et al., 2020).

The goal of the current study is to determine whether GT DcNPs can selectively target and eliminate early-stage tumor growth when given subcutaneously to reduce systemic toxicity. Developing tumors are known to facilitate lymph-angiogenesis to produce new lymphatic vasculature through which metastasis can occur (Padera et al., 2002). Subcutaneous injection of nanoparticles ~60 nanometers in diameter have been shown to passively accumulate in the lymphatic tissue by draining into regional lymph nodes (Kraft, Treuting, et al., 2018). If GT DcNPs can preferentially accumulate in the lymphatic network and enhance GT exposure in advancing cancer cells in the lymph and lymph nodes, GT DcNP delivery via this novel route of transit may have a greater effect on advancing cancer cells. We hypothesize that targeting of GT DcNPs to tumors can be achieved through the lymph and exhibit greater inhibitory effects against growing orthotopic tumors than conventionally solubilized controls. By doing so, tumor targeted GT DcNPs may be used to prevent early stage post-surgical growth of cancer cells and mitigate systemic toxicity.

6.3 MATERIALS AND METHODS

6.3.1 *Materials*

Gemcitabine [4-amino-1-[(2R,4R,5R)-3,3-difluoro-4-hydroxy-5-(hydroxymethyl)oxolan-2-yl]pyrimidin-2-one] free base or G (>99%) and paclitaxel [[(1S,2S,3R,4S,7R,9S,10S,12R,15S)-4,12-diacetyloxy-15-[(2R,3S)-3-benzamido-2-hydroxy-3-phenylpropanoyl]oxy-1,9-dihydroxy-10,14,17,17-tetramethyl-11-oxo-6-oxatetracyclo[11.3.1.03,10.04,7]heptadec-13-en-2-yl] benzoate] referred to as T (>99.5%) were purchased from LC Laboratories (Woburn, Massachusetts). 1,2-distearoyl-sn-glycero-3-phosphocholine (DSPC) and 1,2-distearoyl-sn-glycero-3-phosphoethanolamine-N- [amino (polyethylene glycol)-2000] (ammonium salt) (DSPE-PEG_{2000}) (GMP grade) were purchased from Cordon Pharma (Liestal, Switzerland). D-

Luciferin was purchased from Perkin Elmer (Waltham, MA). Indocyanine green (ICG, $C_{43}H_{47}N_2NaO_6S_2$, sodium 2-[7-[3,3-dimethyl-1-(4-sulfonatobutyl)-benz[e]indolin- 2-ylidene]hepta-1,3,5-trien-1-yl]-3,3-dimethyl-1-(4-sulfonatobutyl)benz) was purchased from Sigma-Aldrich (St. Louis, MO). Anhydrous ethanol was purchased from Decon Pharmaceuticals (King of Prussia, PA). All other reagents used were of analytical grade or higher. The 4T1 cell line transfected with luciferase and green fluorescence protein (GFP) (referred to as 4T1-luc) was kindly provided by Stanley Riddell laboratory (Riddell et al., 2014), from the Fred Hutchinson Cancer Research Center. Luciferase and GFP expression were validated before performing experiments.

6.3.2 *Preparation and characterization of gemcitabine and paclitaxel (GT) drug combination nanoparticles*

GT DcNPs were prepared as described in previous work (Jesse Yu et al., 2020). Briefly, G and T were solubilized together in hot ethanol (60°C) with DSPC and DSPE-PEG_{2000} in a round bottom flask. The total concentration of solutes (drugs + excipients) in ethanol was 5% w/v. Solvent was removed by rotary evaporation followed by vacuum desiccation at room temperature. The dry film was removed from the round bottom flask and triturated to achieve a uniform dry powder. Dry powder was rehydrated in 0.45% NaCl with 20 mM $NaHCO_3$ buffer at 70°C and a pH of 7.4 to achieve a nominal concentration of 100 mM total lipids. Particle size reduction was achieved through bath sonication (Avanti Polar Lipids, Inc. Alabaster, AL) (5 min on, 5 min off, 3 cycles). Previous results have shown that the vast majority of GT is associated to DcNPs; thus, filtration of free drug was not performed (Chapter 4.4.4). Particle size and zeta potential was confirmed by photon correlation spectroscopy using a NICOMP 380 ZLS (Particle Sizing Systems, Santa Barbara, CA).

To prepare ICG labeled GT DcNPs, ICG was added into the GT DcNP composition with a molar content of 0.4% [ICG : (DSPC + DSPE-PEG_{2000}) = 0.4 : 100]. ICG was solubilized in methanol as a stock solution prior to mixing with drugs and lipids in hot ethanol. Solvent removal, rehydration and particle size reduction were performed as stated above in the absence of direct light exposure to prevent ICG degradation.

6.3.3 *Preparation of freely solubilized gemcitabine and paclitaxel (GT) combination*

To prepare an equivalent GT drug combination for use as a control formulation G and T were dissolved in DMSO (G: 50 mg/mL, T: 5 mg/mL). Serial dilution was performed to reach target dose concentrations. The control drug combination in DMSO was used in animal studies within the same day of preparation. Free drug was administered with 9 volumes of normal saline for a 10% (v/v) concentration of DMSO and saline. In previous studies (Chapters 4 and 5), the GT control was formulated in ethanol and Cremophor EL to represent the commercial formulation of paclitaxel (Taxol). However, Taxol is a micellar solution and paclitaxel is not present as freely soluble drug. In this study, we are interested in comparing the behavior of DcNP bound drug versus freely soluble drug (as opposed to a micelles) and DMSO was used instead of Cremophor EL.

6.3.4 *Development of 4T1 orthotopic tumor mouse model for breast cancer growth*

Animal studies were conducted in accordance with the University of Washington Institute of Animal Care and Use Committee (IACUC) approved protocol number 2372-06 and federal guidelines. In general, the life phases in mice are categorized into 4 sections: young age (0-3 months), mature adults (3-6 months), middle age (10-15 months) and old age (18-24 months). The following animal studies were performed in young, female, BALB/c mice (specifically 6-12 weeks old). 4T1-luc cells were confirmed to express luciferase and GFP to enable monitoring of cancer

cell growth by bioluminescence. 4T1-luc (0.2, 0.5 or 1 million cells) suspended in a 50 µL ice-cold HBSS suspension were subcutaneously inoculated in the left and right fat pads adjacent to the axillary and sub iliac lymph nodes (Fig 6.1 panel A). Injections were mirrored across the midline of the mouse. Multiple cell inoculations on singular mice were used to facilitate more robust data and reduce the total number of animals needed for the study. Mice were monitored for a 1 week period. Bioluminescence of 4T1-luc from living mice was examined by a XENOGEN IVIS 200 imaging system (PerkinElmer, Inc. Waltham, MA). Mice received 150 mg/kg D-luciferin through intraperitoneal injections 10~15 min before imaging. The *in vivo* imaging parameters for mice were set as follows: field of view, 12; excitation filter, closed; emission filter, open; exposure time, 120 sec; binning factor, 4; f/stop, 2. Total 4T1-luc bioluminescence emission from mice was integrated using Live Image software (PerkinElmer, Waltham, MA). Luminescence was used as the only measurement for cancer growth from Days 0-3. Once tumors were palpable, caliper measurements were taken to corroborate the luminescent signals. A total of 10 mice were used for the development of the tumor model.

6.3.5 *Immunohistochemistry (IHC) staining of CD31 and podoplanin to detect developing tumor blood and lymphatic vasculature*

Mouse tumor tissues were fixed in 10% formalin and stored in 70% EtOH before being embedded in paraffin blocks. CD31 and podoplanin were used to stain tumor tissues and visualize blood and lymphatic vasculatures, respectively (Mohammed, Ellis, Lee, & Martin, 2009). Staining was performed by UW histology and imaging core facility. Briefly, slides with thin sections (5 µm) were deparaffinized on the Leica Bond Automated Immunostainer followed by antigen retrieval with HIER 2 (EDTA). Slides were then incubated with normal goat serum (10% in TBS) for 20 min at room temperature before incubation with primary antibody against CD31 (rat

monoclonal, Clone SZ31. Dianova, Cat. No. DIA-310, 1:250) or podoplanin (syrian hamster polyclonal, Biolegend, Cat. No. 127402, 1:250) for 30 min at room temperature. Following primary and secondary antibody incubations, specific reactivity was detected with Leica Bond Mixed Refine (DAB) detection kit (Leica Microsystems). Counterstaining was performed using hematoxylin (Leica Microsystems). Slides were then cleared in Xylene and mounted with synthetic resin mounting medium and #1.5 coverslips.

ImageJ Fiji software was used to perform a semi-quantitative analysis of CD31 and podoplanin in axillary and sub-iliac tumors as described by Crowe and Yue (Crowe & Yue, 2019). Briefly, raw image files of IHC stained axillary and sub-iliac tumors were imported into ImageJ Fiji. Color deconvolution was used to isolate the positive CD31 or podoplanin stain. The extracted positive stain was then isolated in the image file and measured as pixel counts (arbitrary units).

6.3.6 *Time course of gemcitabine and paclitaxel (GT) in tumors and plasma in 4T1 tumor bearing mouse model*

Young, female BALB/c mice (5 to 6 weeks old) were purchased from The Jackson Laboratory (Bar Harbor, Maine) and housed in an animal research facility for at least one week before use. Mice were approximately 6 to 8 weeks old for the pharmacokinetic studies. Mice were first inoculated with 1 million 4T1-luc cells in the axillary and sub-iliac fat pads. To simplify the model, tumors were inoculated only on the left side of the mouse in the supine position (2 tumors per mouse). Sub-iliac and axillary tumors were allowed to grow until palpable or 5 to 6 days. Tumors were grown for a relatively longer period of time (5 to 6 days) to allow for the consistent excision of the tumors. Mice were then administered GT as DcNP or in free form subcutaneously in the center of the belly, adjacent to the sub-iliac fat pad. GT was dosed at 5/0.5 mg/kg (G/T) in a 20 µl bolus volume (G ~5 mg/mL, T ~0.5 mg/mL). Blood was collected through retro-orbital

bleeding at .083, 1, 3, 6, 24 and 48 hours for DcNP and at 1 and 3 hours for the freely soluble GT. Each mouse represented a single biological replicate and 3 mice were used to estimate the geometric mean plasma concentration time course of G and T at each time point. Necropsies were performed on each animal and tumors were harvested at the prescribed time points for tumor concentration time course studies.

6.3.7 *Drug extraction from tissues*

Protein precipitation was used to extract G and T from plasma or tumor homogenates. Briefly, 50 µL of sample was transferred into 1.5 mL tubes with or without dilution by blank matrix to an appropriate concentration range. Samples were spiked with internal standards followed by the addition of 9 volumes of acetonitrile (450 µL). Samples were then vortexed for 6 minutes and centrifuged at 4°C for 15 minutes at 20,817 RCF. The supernatant was removed and dried under nitrogen at 40°C. The dried samples were reconstituted to 50 µL containing 20% methanol and 80% water.

For tumor homogenization, the density of a tumor is assumed to be equivalent to water (1 g/mL). After 5 days of growth, tumors range from 10-50 mg in mass. Harvested tumors were diluted in 9 volumes of PBS. The suspended tumor was then homogenized using a Dounce homogenizer due to the limited mass/volume of the sample. Tumor tissue was ground until no visible tissue aggregates could be observed. The Dounce homogenizer consisted of a borosilicate mortar (2 mL working volume) with a piston-type Teflon pestle with stainless steel shaft.

6.3.8 *Quantification of gemcitabine and paclitaxel in plasma and tumors by LC-MS/MS*

Drugs extracted from biological matrices such as plasma or tumor homogenates were quantified by a Shimadzu HPLC system coupled to a 3200 QTRAP mass spectrometer (Applied

Biosystems, Grand Island, NY). The HPLC system consisted of two Shimadzu LC-20A pumps, a DGU-20A5 degasser, and a Shimadzu SIL-20AC HT autosampler. The mass spectrometer was equipped with an electrospray ionization (ESI) TurboIonSpray source. The system was operated with Analyst software, version 1.5.2 (ABSciex, Framingham, MA). Chromatographic separation of G and T was achieved using a Synergi column (100 × 2.0 mm; 4-µm particle size) (Phenomenex, Torrance, CA) with an inline C8 guard column (4.0 × 2.0 mm) also from Phenomenex. The flow rate was set to 0.5 mL/min with a 5 µl sample injection volume. The mobile phase for separation consisted of pump A (20 mM Ammonium Acetate in water) and B (Reagent Alcohol). The gradient program used was as follows: pump B was maintained at 20% for 1.0 minute, then increased to 97% at 2.0 minutes, held at 97% until 3.0 minutes, ramped to 3% by 4.0 minutes and held until 5.5 minutes. The needle was washed with isopropanol after each injection. Analytes were monitored using multiple-reaction monitoring (MRM) for positive ions. The following ion transitions were monitored: gemcitabine, m/z 264.066→112.000; paclitaxel, m/z 854.266→286.200; a stable labeled isotope of gemcitabine ($C_8C^{13}H_{12}ClF_2N^{15}N_2O_4$) (m/z 267.067→115.100) was used as an internal standard for gemcitabine docetaxel (m/z 830.312→549.3) was used as an internal standard for paclitaxel.

6.3.9 *Comparison of tumor inhibition effects of equivalent doses of gemcitabine and paclitaxel in DcNP or free form*

5- to 8-week-old, female BALB/c mice were inoculated with 1 million 4T1-luc cells SC in 50 µL HBSS on day 0. 4T1-luc cells were inoculated in both axillary fat pads and both sub-iliac fat pads for a total of 4 tumors per mouse. After 24 hours, mice were given a single administration of saline, a free drug combination (GT in DMSO/water), or GT DcNP through SC injections (n = 4-5) in the upper abdomen area equidistant from the 4 tumors. The GT doses were G:20 mg/kg

and T:2 mg/kg for free and DcNP formulations. Early stages of cancer cell growth were monitored by bioluminescence from Days 1 to 3. On Day 4, caliper measurements were performed in parallel to bioluminescence if possible. In general, untreated tumors were consistently palpable by Day 5. Cancer cell growth was monitored for a total of 7 days from cell inoculation. Bioluminescent images were acquired with the IVIS imaging system as described above. Bioluminescence intensity from living mice and lungs was integrated using Live Image software.

6.3.10 *Dose dependence of gemcitabine and paclitaxel DcNP on cancer cell growth inhibition or elimination and observation of toxicity*

5- to 8-week-old, female BALB/c mice were inoculated with 1 million 4T1-luc cells SC in 50 µL HBSS on day 0. 4T1-luc cells were inoculated in both axillary fat pads and both sub-iliac fat pads for a total of 4 tumors per mouse. After 24 hours, mice were given a single dose of GT DcNPs (5/0.5 mg/kg, 10/1 mg/kg or 20/2 mg/kg, G/T). Cancer cell growth monitoring was performed with caliper measurement and bioluminescent imaging as described above. Mouse behavior and overall health conditions were observed by 1 of 3 experimentalists daily. Dermal reactions in the subcutaneous injection site were rated by the experimentalist daily using the Draize scoring system (Draize, Woodard, & Calvery, 1944). Experimentalists were not blinded in this study. Briefly, erythema or eschar formation was scored from 0 to 4 with (0) representing no erythema, (1) very slight, barely perceptible erythema, (2) well-defined erythema, (3) moderate to severe erythema and (4) severe erythema (beet redness) to slight eschar formation. The Draize scoring system also includes the same scale for observations of edema (for a total score out of 8). No edema was observed in any treatment group, so the scoring system was abbreviated to only account for erythema (0 to 4).

6.3.11 *Statistical analysis*

Tumor signal, weight or volume were presented as mean ± standard deviation of the mean. The number of mice in all groups range from 4 to 5. Students' t-tests were performed to determine statistical significance between two groups, and two-way ANOVA was used to evaluate differences between treatment groups over time. A P-value of <0.05 was considered statistically significant. Statistical analyses were performed using GraphPad Prism (Version 7.0).

6.4 RESULTS

6.4.1 *Development and characterization of an orthotopic 4T1 breast cancer model*

To evaluate the treatment effects of targeted and synchronized GT combination therapy in nanoparticle form, an orthotopic model of breast cancer growth is necessary. While human xenograft models have been described, they do not provide the native immune response; which may be a critical component to evaluate treatment effects on breast cancer growth. Syngeneic tumor models do provide the native immune response but can exhibit inconsistent tumor development and significant biological variability from mouse to mouse, making evaluation of therapeutic effect challenging. Many preclinical cancer treatment studies are performed with tumor inoculation in the subcutaneous space of the flank which does not reflect the condition intended to treat (breast cancer). Thus, we have evaluated a syngeneic and aggressive, metastatic 4T1 breast cancer tumor model in Balb/C mice through fat pad inoculation which allows the cells to grow in native tissue. By growing in the native tissues, orthotopic cancer cells recapitulate the stroma and vasculature of naturally developing tumors. We also investigated whether inoculating in multiple mammary fat pads can provide multiple distinct tumors on a single mouse for assessment of therapeutic effect (although there may be regional differences in tumor growth). The 4T1 breast

cancer cells (also known as 4T1-luc) used in this study are transfected with stable expression of the luciferase (luc) enzyme to allow for bioluminescent imaging in early stages of tumor growth, before palpable nodule formation.

Based on these rationale, 4T1-luc cancer cells were injected in 4 mammary fat pads: 2 adjacent to the proper axillary lymph nodes and 2 adjacent to the sub-iliac lymph nodes. The axillary and sub-iliac fat pads were inoculated symmetrically across the midline of the mouse in the ventral medial view (Figure 6.1 panel A). At early time intervals (days 1-3), tumors were not palpable and could not be measured with calipers. Thus, the transfected luciferase marker was used to monitor early growth with bioluminescence. We first performed a pilot study to investigate 3 doses of 4T1 cells (0.2, 0.5 or 1 million cells per injection). In a single mouse bearing 4 tumors, we found that higher doses of 4T1 cells (0.5 and 1 million) could produce a bioluminescent signal as early as one hour after injection (Day 0). The bioluminescent signals were dose-proportional across 4 tumors in single mice with 1 million (2065 ± 877, mean ± S.D of 4 tumors) and 0.5 million cell inoculations (1025 ± 940, mean ± S.D). No signal above baseline (>500 counts) was detected in the mouse administered 0.2 million cells until 24 hours after injection (760± 894, mean ± S.D). Tumor growth was evaluated by calculating the change in luminescent signal over time. These results show that the cell inoculation number is proportional with tumor signal and the overall growth over time is consistent. During cancer inoculation, it was noted that the 100 µl injection volume exceeded the capacity of the mammary fat pad and resulted in excess fluid buildup. Based on these observations, 1 million 4T1-luc cells in 50 µl was selected for further evaluation and model development. Sequential studies were performed to assess the reproducibility of the model and more mice were tested to evaluate biological variability. In these sequential studies, mice were monitored for up to 7 days. Due to the longer growth period, tumors became palpable on Day 5

and tumor volume was measured on that day via calipers. The results from the pilot and sequential studies are presented in Table 6.1 for comparison. Across studies, there are differences observed in the average tumor intensity; however, the general growth pattern is very consistent when comparing the change in tumor signal over time. The overall tumor volume is consistent between studies despite the observed differences in luminescence on Day 1.

Interestingly, we found that tumors inoculated in different mammary fat pads had different growth patterns. Tumor growth was consistent across the midline of the mouse (left and right sides), but differences in tumor signal over time were observed between tumors injected in the axillary and sub-iliac fat pads (Figure 6.1 panel B, $p<0.05$ 2-way ANOVA). These differences were responsible for the inter-tumor variability observed in Table 6.1. To further understand the differences in tumor growth from axillary and sub-iliac inoculations, tumors were resected at a fixed time point (5 days) for physical measurement. After 5 days of growth, the weight of 20 tumors were compared using a student's T-test (mean ± S.D). For axillary tumors, no difference was observed in tumor mass across the midline (left axillary, 76.9 mg ± 25.8 mg; right axillary, 86 mg ± 41.1, $p=0.7$). For sub-iliac tumors, no difference was observed across the midline (left sub-iliac, 46.9 mg ± 10.8 mg; right sub-iliac, 36.4 mg ± 18.5, $p=0.3$). However, when we compare the axillary tumor mass with the sub-iliac tumor mass across the transverse plane, the axillary tumors are significantly larger (left axillary vs left sub-iliac, $p=0.04$; right axillary vs right sub-iliac, $p=0.04$) in agreement with the luminescent signals. Caliper, tumor weight and bioluminescence measurements were all consistent and in agreement with the overall trend of tumor growth. Based on these results, there are likely biological factors that affect the growth of 4T1 cells in the axillary versus sub-iliac fat pad. This observation is in line with previous reports that indicate the growth

of tumors is heavily reliant on the inoculation sites (R. Auerbach, L. W. Morrissey, & Y. A. Sidky, 1978).

Taken together, these results show that a 4T1 breast cancer model implanted in the mammary fat pad can reproducibility generate tumor growth for therapeutic evaluation. By implanting at 2 sites each in anterior and posterior fat pads of the mouse, we can evaluate the overall tumor growth over time in the placebo and treated groups. The stratification of tumors into rapid growing (axillary) and slow growing tumors (sub-iliac) may be useful for therapeutic evaluation of GT by providing measures of effect on two representative tumor types. Tumor replicates across the midline of the mouse can be combined to add robustness to the data. Based on these results, this orthotopic tumor model (with 1 million 4T1-luc cells per inoculation) will be used to evaluate the treatment effects in the following experiments. We next investigated the development of lymphatic and blood vasculature in the early growth phase of 4T1 tumors in mammary tissues.

6.4.2 *Characterization of lymph and blood vasculature development in orthotopic 4T1 tumors*

In human breast cancer, there is clear lymphatic drainage from the mammary tissue to the lymphatic endothelial vessels and subsequent sentinel lymph node. Due to this directional flow, the sentinel lymph node is the first and most likely node for cancer cells to appear in. In general, humans have 20 to 30 lymph nodes in the axillary with connecting lymphatic endothelial vessels (Kyriacou & Khan, 2020). In mice, the lymphatic system is much simpler, and each mammary fat pad contains lymphatic vasculature that drains into a primary lymph node. In our orthotopic model, tumors were inoculated in fat pads that were adjacent to the axillary and sub-iliac lymph nodes. Thus, we expect that tumor associated lymphatic vasculature will sprout from the lymphatic

vessels associated with these nodes. In parallel, the tumors will also likely develop blood vessels to obtain the nutrients required for growth. New blood and lymph vessels will likely become the routes of transit for drugs to reach the tumors and so we next characterized the formation of lymph and blood vessels in 4T1 tumors. Given the growth pattern of 4T1 mammary tumors, we administered 1 million 4T1 cells in the axillary and sub-iliac regions of the mouse and allowed them to grow for 5 days to produce palpable tumors. It would be of interest to investigate cancer vasculature at earlier time points (Day 1 to 3), but the lack of a palpable tumor limits the ability to harvest those tissues. Tumors were harvested and fixed in 10% formalin buffered saline. Podoplanin was used as a marker for lymphatic vasculature and CD31 was used as a marker for blood endothelial cells (Mohammed et al., 2009).

Histological analysis of axillary and sub-iliac tumors reveals that after 5 days of growth, both tumors are well-vascularized by lymphatic and blood endothelial cells (based on positive staining of podoplanin and CD31, respectively). Using the ImageJ software, histological slides were analyzed to determine the relative intensity of staining by CD31 or podoplanin for a semi-quantitative comparison of lymphatic and endothelial vasculature. Axillary tumors had a higher degree of staining for podoplanin compared to CD31 (54 ± 15 AU versus 16 ± 3 AU, $p<0.05$). Sub-iliac tumors also had a higher degree of staining for podoplanin versus CD31 (136 ± 27 versus 21 ± 3, $p<0.05$). These data are presented in Figure 6.2 panels B and C, respectively.

These data suggest that 4T1 tumors rapidly develop vasculature 5 days after of tumor inoculation. Lymphatic endothelial cells in axillary tumors cover a surface area approximately ~4 times greater than blood endothelial cells. In sub-iliac tumors, lymphatic endothelial cells cover a surface area ~6 times greater than blood endothelial cells. If cytotoxic drugs, assembled in DcNP formulation, can preferentially deliver to and accumulate in tumors through these lymph vessels

instead of blood vessels, a greater fraction of the total dose of GT may be exposed to the cancer cells.

6.4.3 *Effects of drug combination nanoparticles on gemcitabine and paclitaxel transit and accumulation in lymphatic vessels and tumors*

To investigate if GT DcNPs can preferentially distribute into lymph vessels (as opposed to blood vessels) after SC administration for delivery to nearby nodules, we next performed a live imaging study with GT DcNPs tagged with indocyanine green (ICG). In previous work, hydrophobic ICG embedded within lipid nanoparticles were used to track the transit of nanoparticles from subcutaneous injection sites into regional lymph nodes (Kraft, Treuting, et al., 2018). In this study, we have taken a similar approach and tagged GT DcNPs with ICG to monitor the movement of particles from a central injection site (the belly), in tumor bearing mice. Mice were inoculated with 1 axillary and 1 sub-iliac tumor in their respective fat pads and the tumors were allowed to develop for 5 days (when both blood and lymph vessels have developed). The belly was chosen as the DcNP subcutaneous injection site to capture the upward flow of lymphatic fluid from the sub-iliac lymph node (SiLN) to the proper axillary lymph node (PaLN) as described by others (Kodama, Hatakeyama, Kato, & Mori, 2015; Yamaji et al., 2018). One hour after subcutaneous injection of ICG labeled GT DcNPs (G: 5 mg/kg, T: 0.5 mg/kg, ICG: 0.075 mg/kg), a fluorescent signal can be clearly observed transiting from the injection site (adjacent to the SiLN) to the axillary region of the mouse. The fluorescent signal runs parallel to the thoracoepigastric vein (Figure 6.3, Panel A, black arrows) and shows the transit of ICG-tagged GT DcNPs through lymph vessels (Figure 6.3, Panel A, white arrows). Importantly, ICG can also be detected on the surface of the axillary tumor (Figure 6.3, Panel A, T) suggesting that GT DcNPs have a direct route to tumors through the lymph.

6.4.4 *Ability of DcNP to enhance gemcitabine and paclitaxel retention in tumors and extend persistence of plasma drug concentrations*

We next performed a quantitative analysis of GT concentrations in tumor and plasma after administering the same dose of GT in DcNP or freely solubilized form (G: 5 mg/kg, T: 0.5 mg/kg). The ICG tracking study provided us with a qualitative indication that DcNPs are taken up into the lymphatic vessels 1 hour after injection, but ICG signal is a surrogate measure for drug concentration. Thus, for a quantitative analysis, we next measured GT concentrations in tumors and plasma, 1 and 3 hours after injection. The 1 hour time point was selected to match the same time point from the ICG study and 3 hours was chosen based on the known clearance of free GT. In this study, we assume that SC administered free GT can passively distribute into either the blood or lymph. However, blood flow is significantly greater than lymph flow and these conditions will favor drug uptake into the blood. If GT DcNPs are readily taken up into the lymphatics versus the blood, then we expect to observe different trends in GT concentration time profiles in plasma and tumors when comparing against the free drug control.

Figure 6.3 panel B shows the concentration of GT in the plasma, sub-iliac tumor and axillary tumor of mice administered a single SC dose of either GT DcNPs or free drug, 1 and 3 hours after injection. The observed concentrations of gemcitabine in these three compartments support our initial prediction. In mice administered free gemcitabine, a decrease in plasma and sub-iliac tumor concentrations is observed over time, while no change is seen with the axillary tumor. In mice administered GT DcNPs, we see a clear difference in the trend of gemcitabine concentrations over time. In plasma and both tumors, gemcitabine concentration after DcNP administration increase from the 1 to 3 hour time points. The quantitative concentration time profiles of GT given in free versus DcNP form corroborate our qualitative observations in Figure 6.3, Panel A. As DcNPs follow the upward flow of lymphatic fluid towards the thoracic duct,

gemcitabine may come into contact with the sub-iliac and axillary tumors. Due to the lack of clearance mechanisms for gemcitabine in the lymph, this slow transit is reflected by the steadily increasing concentrations of gemcitabine in the sub-iliac and axillary tumors from 1 to 3 hours. Gemcitabine bound to particles are then slowly released into the blood (as reflected by the increasing plasma concentrations) through the thoracic duct. In the free gemcitabine treatment, drug can be taken into the systemic circulation or tumor tissues but is instantly available for metabolism in the blood (as reflected by decreasing plasma concentrations). Although there is a slower decline of free gemcitabine in tumor compared to plasma, this slower decline could reflect tissue retention. Nevertheless, the tumor concentrations of gemcitabine at 1 and 3 hours are consistently higher when given in DcNP form compared to free. Interestingly, the behavior of paclitaxel administered as DcNPs did not differ significantly from the free drug. Paclitaxel given in either form results in an increase in axillary and no changes in sub-iliac tumor concentrations from 1 to 3 hours and a decrease in plasma concentrations. This observation could be due to the poor solubility and high tissue binding of paclitaxel. If paclitaxel in DMSO were to precipitate after injection, a depot of drug could form in the subcutaneous space. Consequently, the delayed absorption of paclitaxel from the DMSO injection could cause the observed trends in drug concentration over time.

Over 1 and 3 hours, formulating GT in DcNPs had a significant effect on the time course of gemcitabine when compared to the free drug. To further understand the extent of this DcNP effect, we next extended our monitoring interval up to 48 hours. When gemcitabine is administered in DcNP form, persistent levels of drug is detected in plasma, sub-iliac and axillary tumors for up to 48 hours. In contrast, the free drug levels in plasma approached the lower limit of quantification (LLOQ) of our bioanalytical assay by 3 hours. Remarkably, the tumor to plasma ratios of

gemcitabine are maintained at or above 1 throughout the entire time course (with the exception of axillary tumors at 24 hours) following DcNP injection. Our analysis of paclitaxel in DcNP form was limited by the lower dose administered compared to gemcitabine (1/10 by mass) and plasma/axillary tumor concentrations fell below the LLOQ of our bioanalytical assay after 6 hours. Persistent concentration of paclitaxel was detected in the sub-iliac tumors for up to 48 hours (data not shown).

Taken together, these data show that GT DcNPs can transit through the lymphatic vessels to produce higher concentrations of gemcitabine in axillary and sub-iliac tumors compared to free drug. In addition to yielding higher concentrations of drug, the first-passage of SC administered GT DcNPs through the lymph produces consistently higher levels of gemcitabine in tumors compared to the plasma (Figure 6.4). This suggests that the lymphatic transit of DcNP particles enables tumor targeting of gemcitabine and may reduce off-target toxicity associated with free gemcitabine. This long acting, targeted effect, facilitated by the DcNPs, may have a significant impact on tumor growth. Thus, for our next study we will compare the cancer inhibitory effects of GT in DcNP versus free form.

6.4.5 *Comparison of combination gemcitabine and paclitaxel efficacy against orthotopic tumor growth between DcNP and conventionally solubilized formulation*

An equivalent dose study of GT given in free and DcNP form was then performed to compare their abilities to inhibit cancer cell growth. In the preceding studies, tumors were resected after ~5 days of growth to yield palpable masses that could be used for fluorescent imaging or drug quantification. After 5 days of growth, the tumors can be precisely removed; however, the size and maturity of these tumors do not reflect the presentation of post-surgical breast cancer in the clinic. After excision of the primary tumor, residual cancer cells are likely in early stages of tumor growth

and would not have clearly defined or palpable tumor borders. Additionally, residual cancer cells are treated with chemotherapy as soon as possible for maximum effect. To recapitulate this early stage of cancer cell growth and the corresponding clinical treatment, cancer cells were inoculated in the axillary and sub-iliac fat pads on Day 0 and treated after 24 hours. Cancer cell inoculations were replicated across the midline (left and right side of the mouse) for robustness. Treatment was administered on Day 1 after a baseline measurement of cancer cells via bioluminescence. Mice were administered GT (G: 20 mg/kg, T: 2 mg/kg) in DcNP or free form on Day 1 and compared to a saline control. Cancer growth was monitored daily by bioluminescence and caliper measurements (once palpable) until termination of the study (Day 7).

Figure 6.5 presents the results of the study. Compared to the saline control, GT given in free form had modest effects on tumor growth with a 60% reduction in tumor signal (saline: 309,154 ± 184740 counts versus free: 123,994 ± 63419 counts, $p<0.05$) in the axillary tumor and 52% reduction in the sub-iliac tumor (saline: 132,450 ± 79,333 versus free: 64,743 ± 36,131 counts, $p<0.05$). Surprisingly, GT DcNPs produced an even greater inhibitory effect on tumor growth with a 99.7% reduction of the tumor signal (878.8 ± 450.8, $p<0.001$ compared to free) in the axillary tumor and 99.5% inhibition of the sub-iliac tumor (608.3 ± 436.8, $p<0.0001$ compared to free). These data taken together show that the lymphatic mediated transit of GT DcNPs not only produced higher concentrations of gemcitabine in tumors, but also had a significantly greater inhibitory effect on tumor growth compared to the same dose of free drug.

6.4.6 *Dose response study of gemcitabine and paclitaxel in DcNP form against orthotopic tumor growth*

To determine the optimal safe and effective dose of GT DcNPs, we next performed a dose ranging study for GT DcNPs. Mice were inoculated with cancer cells on Day 0 in the axillary and

sub-iliac fat pads and replicated across the midline as described above. On Day 1, mice were administered gemcitabine and paclitaxel in DcNPs at a dose (G/T) of 20/2 mg/kg, 10/1 mg/kg and 5/0.5 mg/kg and tumor growth was monitored by luminescence and caliper measurements (when palpable) until Day 7. 20/2 mg/kg was chosen as the highest dose due to the nearly complete suppression of tumor growth achieved in the previous experiment. Figure 6.6 shows the axillary and sub-iliac tumor growth patterns at varying doses of GT DcNPs normalized to the baseline luminescence on Day 1. The response to treatment is consistent in both axillary and sub-iliac tumors. At the lowest dose of GT DcNPs (5/0.5 mg/kg), tumor growth is inhibited from Day 1 to Day 3. On Day 4, mice administered 5/0.5 mg/kg GT DcNPs have a tumor signal ~3.5x the baseline value (Day 1) reflecting cancer growth and rebound. At 10 mg/kg, the same trend is observed but the cancer inhibition effect is extended until Day 5, demonstrating that the higher dose can prolong the suppressive effect of GT DcNPs. To our surprise, the highest dose of GT DcNPs (20/2 mg/kg) produced a new trend distinct from the previous doses. Treatment of 20 mg/kg GT DcNPs elicited a regressive effect on the cancer cells with the normalized luminescence falling below 1 for the entire course of the study. The normalized luminescence decreases from Day 1 to Day 5, and gradually trends upward on Day 7. Despite this upward trend, the average tumor luminescence on Day 7 is ~54% to ~106% of the baseline measurement (axillary and sub-iliac, respectively). This observation suggests that at higher doses GT DcNPs can eliminate a fraction of the baseline cells. This effect is observed only with GT DcNPs, and 20 mg/kg of free drug never achieves a normalized tumor signal below 1. With 20 mg/kg of free drug treatment, tumor rebound is observed within 48 hours of treatment (9x baseline). As described in the materials and methods, caliper measurements were taken when tumors became palpable. The physical measurements of

tumor volumes are proportional to the bioluminescent signals and support the use of luciferase as a marker for tumor growth.

Throughout the course of this dose-response study, mice were also observed daily for signs and symptoms of toxicity and those observations are summarized in Table 6.2. Local toxicity was dose-proportional and manifested as injection site erythema, which did not affect mouse ambulation, behavior or activity. Using the Draize scoring system for dermal reactions, no edema was observed but injection site erythema is present and increased in severity with dose (Draize et al., 1944). A single mouse given 20 mg/kg GT DcNP, exhibited other signs of toxicity manifesting as lethargy and diminished body weight on Day 7. At necropsy, the GI of the mouse was bloated and inflamed which may suggest damage to the epithelium commonly observed with antimetabolite therapy (Shaw, Spector, & Ladman, 1979). In the other 4 mice that received 20 mg/kg GT DcNP, no weight loss or change in behavior was observed despite the dermal reactions. Taken together, these data show that the extended concentrations of GT by DcNP lymphatic trafficking translate into an improved dose-proportional tumor inhibitory effect compared to free drug. Mild injection site erythema is observed as the primary adverse reaction, but further study is required to appreciate the full extent of toxicities.

6.5 DISCUSSION

The major barrier in the treatment of breast cancer is tumor recurrence or distant metastasis after initial treatment. Disease progression is due to cancer cells that escape initial interventions such as surgery, radiation therapy or drug therapy. When tumors recur, there are limited options for treatment (typically due to disseminated disease and drug resistance). In previous work, we co-formulated water soluble gemcitabine with water insoluble paclitaxel as a stable, drug combination nanoparticle. These particles were effective at eliminating cancer cells in the systemic circulation

to prevent metastasis (compared to free drug). In the current work, we demonstrated the tumor targeted effects of GT DcNPs during transition through the lymphatic system following SC administration. The antitumor effects of GT treatment were investigated using a model of breast cancer that captures both fast growing and slow growing tumors inoculated in the axillary and sub-iliac fat pads, respectively. Tumors inoculated in these regions were shown to be rapidly vascularized with both blood and lymph vessels, with total perfused area favoring the lymph (Fig 6.2). Subcutaneous administration of fluorescently labeled GT DcNPs showed a lymphatic vessel specific uptake of particles transiting from the injection site to the proper axillary lymph node and tumor. GT tumor and plasma concentrations over time show that DcNPs likely facilitate the trafficking of GT to tumors through the lymph vessels. In an equivalent dose comparison to freely solubilized GT, GT DcNPs were able to elicit a 99.5 to 99.7% tumor growth inhibition over 7 days. Tumor-targeted GT DcNPs through the lymph were shown to elicit tumor regression at higher doses and prolonged suppression at lower doses. By using the lymphatic system as the route of first-pass transit, GT DcNPs can avoid systemic, off-target toxicities and directly eliminate growing cancer cells in the mammary fat pad. These promising results translate into a therapeutic scenario whereby a single SC dose of GT DcNPs is given to breast cancer patients after ablation surgery to eliminate residual cancer cells and prevent disease recurrence.

Gemcitabine and paclitaxel are a potent chemotherapy regimen used in metastatic breast cancer treatment (Albain et al., 2008). Although effective, this regimen is associated with significant toxicity from off-target exposure and must be given sequentially to minimize infusions reactions. Separate intravenous infusions are safer for patients, but this approach limits the time course where both drugs are circulating at pharmacologically relevant concentrations in plasma. When infused into the systemic circulation, gemcitabine undergoes rapid metabolism by

ubiquitously expressed cytidine deaminase enzymes (Ciccolini, Serdjebi, Peters, & Giovannetti, 2016). Infusion of paclitaxel results in extensive tissue distribution and metabolism by liver CYP450 enzymes (Spratlin & Sawyer, 2007). These distinct characteristics limit the coordinated accumulation and retention of GT in target cancer cells. Primary tumors are vascularized with blood vessels that can carry GT to cancer cells from IV dosing, but in most patients primary tumors are surgically removed. Furthermore, cancer cells are known to migrate into the lymph which may have reduced exposure to intravenously administered medication (M. Rahman & Mohammed, 2015; Shao et al., 2016). Under these conditions, healthy organs that are heavily perfused (such as the liver or lungs) are exposed to high doses of GT; while cancer cells in poorly perfused tissue (such as the lymph) may never achieve pharmacologically relevant concentrations of GT.

Preclinical studies typically use a number of representative mouse models to evaluate the effects of drug treatment on tumor growth. These different models reflect the heterogeneity of breast cancer in the clinic, but also contribute to significant variability from study to study. Experimental considerations such as the site of cancer cell inoculation have been reported to impact tumor growth curves and may confound the interpretation of therapeutic effect (Robert Auerbach, Lawrence W. Morrissey, & Younan A. Sidky, 1978). In this report, the therapeutic effect of GT DcNPs was evaluated in aggressive, metastatic 4T1 breast cancer cells that were inoculated orthotopically in immunocompetent mice. An intact immune system plays a significant role in the regional and distant spread of cancer cells and is more representative of clinical disease. Treatment of GT DcNPs prior to the formation of palpable tumors also reflect the adjuvant chemotherapy regimen that breast cancer patients would receive. In order to determine the effect of GT DcNPs on breast cancer tumors with different growth rates, we have specifically designed an aggressive and metastatic breast cancer model that contains multiple tumors grown in the native

tissues of mice. Anterior tumors were shown to develop rapidly while posterior tumors exhibited a slower growth curve, in agreement with previous reports (Robert Auerbach et al., 1978; Dipersio, 1981; Kyriazis & Kyriazis, 1980). Duplicates across the midline of the mouse also act as an indicator of experimental variability and further reduce the total number of mice required per experiment (1 mouse instead of 4). If a single dose of GT DcNPs can eliminate 4 tumors on a mouse, there is greater confidence in the observed treatment effect. Based on these features, the results from this novel tumor model of breast cancer growth are expected to be more translational and impactful.

To overcome the toxicological limitations of systemic chemotherapy, targeted lymphatic drug delivery systems have been previously reported. In the work of Cai et al., hyaluronan-cisplatin conjugated nanoparticles were shown to enhance lymph node drug concentrations and co-localize within mammary tumors in a mouse model (Cai, Xie, Bagby, Cohen, & Forrest, 2008). Hyaluronan-doxorubicin conjugated nanoparticles were also shown to inhibit tumor growth and extend overall survival in xenografts of human breast cancer (Cai et al., 2010). In a clinical study, lymphatic chemotherapy was administered to patients via carboplatin carbon particles and high concentrations of carboplatin in axillary lymph nodes were achieved (J. Chen et al., 2004). These examples highlight the potential for lymphatic drug delivery as a promising approach to eliminating tumor recurrence. In our work, we present the targeted lymphatic delivery of a combination chemotherapy regimen composed of hydrophilic gemcitabine and hydrophobic paclitaxel. In contrast to previous studies, GT DcNPs enable the lymphatic targeting of multiple drugs stabilized within a single particle. The extensive lymphatic uptake of GT DcNPs also enables high concentrations and cytotoxic effect of drug in both sub-iliac (posterior) and axillary (anterior) tumors, reflecting the distribution of particles within the entire lymphatic network. It is possible

that this extensive lymphatic distribution of GT DcNPs could be used in the clinic to target combination chemotherapy to the entire axillary lymphatic network as opposed to just the primary draining sentinel lymph node.

Although GT DcNPs are fairly distinct in regard to lymphatic targeting, other GT combination nanoparticles have been reported to improve tumor inhibition and reduce toxicity when given intravenously. In the work of Zhang et al, GT was co-formulated in asymmetric lipid layers with cyclic RGD to enable tumor targeting. After three IV doses, nanoparticles produced tumors ~50% smaller than the free drug control and did not exhibit any systemic toxicity by Day 8 (J. Zhang et al., 2018). Self-assembling multi-functional nanoparticles carrying GT were also shown to result in 4T1 tumors 91% smaller than the free drug control from every other day IV dosing (Lei et al., 2019). In both these examples, active targeting ligands are used to reduce systemic toxicity and improve GT efficacy. In this report, GT DcNPs do not require active targeting ligands. Instead, tumor targeting is achieved through passive accumulation in the lymph based on the physical properties of the DcNP particles. With this approach, a single dose of GT DcNPs can produce an enhancement in GT tumor inhibition (99.5% to 99.7%, Fig 6.5) and may enable tumor regression with further dose and formulation optimization. Clearly, these outcomes provide greater results than the multiple IV dosing of targeted combination particles reported to-date by the studies referenced above. Since GT DcNPs accumulate in the lymph instead of the systemic circulation, systemic toxicity is also mitigated. By not requiring active targeting ligands but demonstrating a passive targeted effect, GT DcNPs may also be more amenable towards clinical scale up as the manufacturing process does not require chemical synthesis or purification associated with targeted drug delivery systems (Rosenblum, Joshi, Tao, Karp, & Peer, 2018).

The ability for the GT DcNPs to eliminate cancer cell growth through a lymphatic trafficking mechanism is an exciting discovery, but it also highlights the potential for future studies. The GT DcNPs used in this report were previously characterized and demonstrated robust *in vivo* stability after IV administration (Jesse Yu et al., 2020). Given the long acting tumor drug concentrations after SC dosing (Fig 6.4), it is likely that GT DcNPs are also stable in the SC space and lymphatic vasculature. However, further optimization of GT DcNPs can improve lymphatic uptake. For example, the surface properties of subcutaneously injected nanoparticles are known to affect lymphatic uptake. In the work of Kaur et al, the localization of liposomes in lymph nodes was enhanced for negatively charged liposomes (-34.8 mV) compared to positively charged liposomes(+54.2 mV) (Kaur, Nahar, & Jain, 2008). GT DcNPs carry a slightly negative surface charge of -16.4 mV, which may partially explain the observed distribution into the lymph, but increasing the negative charge may further enhance the movement of DcNPs from the injection site and lymphatic uptake. Since GT DcNPs are not liposomes and have a non-spherical morphology, future studies can also investigate the effect of morphology on lymphatic uptake (Jesse Yu et al., 2020). This study also showed that GT DcNPs do result in dose-dependent and reversible injection site erythema under the current experimental conditions. This toxicity may be alleviated by optimizing the dose administration, such as increasing the injection volume to allow the DcNPs to spread through a wider area of the subcutaneous space.

To verify that GT DcNP effects can extend to human breast cancer, we have evaluated the effects of GT DcNPs on metastatic human breast cancer cells, MDA-MB-231-HM, orthotopically implanted in 4 mammary fat pads of athymic nude mice (NU/J also known as Foxn1^{nu}). Athymic nude mice were chosen to minimize cell-mediated immunogenic reactions to the implanted MDA-MB-231-HM human breast cancer cells. Mouse immune response against human cancer cells

could lead to unpredictable tumor formation and progression. While athymic nude mice do not have functional T-cells, some residual B-cell function has been reported (Kariya et al., 2014). Similar to the murine 4T1 breast cancer cells, human MDA-MB-231-HM cells stably express the luciferase enzyme which can convert luciferin to luminescence and can be used to monitor tumor growth. In a preliminary experiment, a total of 10 nude mice were inoculated with 2 million human MDA-MB231-HM cells in the 4 mammary fat pads near the axillary and sub-iliac lymph nodes (as presented in Figure 6.1, A). These 10 mice bearing cancer nodules were treated with either saline (negative control, n=4, 16 total tumors), free GT (positive control, n=3, 12 total tumors) or GT DcNPs (treatment, n=3, 12 total tumors). Free drug and DcNP treated mice were given a single dose of 20/2 mg/kg (G/T) subcutaneously on day 1 and 10/1 mg/kg (G/T) on days 7, 14 and 21. Preliminary results reveal that the human MDA-MB231-HM orthotopic xenograft model is slower growing and more variable than the syngeneic 4T1 mouse model. The baseline variability of tumor luminescence on day 1 (pre-treatment) is presented in Table 6.3 and these data indicate that the human MDA-MB-231-HM tumors (with identical inoculation dose) are quite variable. Although the differences in pretreatment tumor signals is not statistically significant, it is important to note that the average pretreatment intensity for the DcNP group is 2.1 times higher than the two comparator groups, the saline and free drug controls. In general, larger tumors are harder to treat and this difference may affect the interpretation of the results.

To account for this variability, the data were normalized to the individual tumor signals on day 1 and the effects of GT given in free or DcNP form were compared (normalized mean ± standard deviation, Table 6.4). On day 14, GT DcNPs elicited a greater inhibition of tumor signal in the sub-iliac fat pad compared to free drug (unpaired student's t-test, $p<0.05$). Tumor signal variability increases over time and statistical significance fades; however, the trend continues over

28 days. At the termination of the study, GT DcNPs inhibit axillary tumor growth by 24-fold compared to saline while free drug inhibited axillary tumor growth by 20-fold compared to saline. Free drug was very effective on sub-iliac tumor growth compared to saline with a 430-fold reduction in tumor signal. In comparison, GT DcNP treated mice had no detectable tumor signal in the sub-iliac fat pad after 28 days. In order to improve the statistical power of our comparative design, future studies should focus on reducing variability. Other immunodeficient mouse strains such as NOD/SCID mice do not have functional B- and T-cells which may produce more consistent tumors to reduce baseline variability. Cell dose and GT treatment schedule can also be optimized to accommodate for the slower growth pattern of human MDA-MB-231-HM cells. With further optimization of drug composition and the use of an appropriate mouse host (such as the NOD/SCID model), GT DcNPs could be shown effective against human breast cancer. Our preliminary study paves the way for further investigation in the near future.

DcNP technology was originally developed to stabilize hydrophobic and hydrophilic HIV drugs within lipid excipients. A simple, scalable manufacturing process was used to combine 4 different sets of HIV combination therapy (Yu, Yu, Lane, McConnachie, & Ho, 2020). This process has been successful in scaling up to and supporting large, non-human primate (NHP) studies. By combining chemically diverse drugs together in a stable particle, DcNPs are able to enhance target cell drug exposure and maintain long acting plasma circulation (Koehn et al., 2018; Kraft et al., 2017; McConnachie et al., 2018; Perazzolo et al., 2018). GT DcNPs are an extension of that much larger body of work and represent an application of this technology towards a new therapeutic area, specifically breast cancer. With the successful formulation of GT DcNPs presented here, it is possible that DcNP technology can stabilize other breast cancer combination regimens that are more potent or have a safer toxicity profile. In future studies, we hope to directly

investigate that possibility and test their effects in other hard to treat cancers such as pancreatic ductal adenocarcinoma. The ability to target cancer cells through the lymphatics with chemically diverse chemotherapy stabilized as a single particle highlights the potential for DcNPs to eliminate cancer cells in regional or lymphatic tissue. In doing so, the DcNP approach may represent a promising tool to prevent tumor recurrence and distant metastasis, something that has not been achieved with current chemotherapy approaches.

In summary, we have shown that the subcutaneous administration of GT in DcNP form significantly improves the inhibitory effect of GT combination therapy on metastatic breast cancer in an orthotopic tumor model. A single SC dose of GT DcNP resulted in a decrease in cancer signal from orthotopic tumors, compared to soluble GT which can only slow the growth of tumors (without achieving tumor regression) over a 7 day study. It is likely that DcNP mediated preferential lymphatic distribution and accumulation of GT facilitates this enhanced antitumor effect. GT DcNPs can gain access to tumors through tumor associated lymphatic vasculature and the retention of GT in lymph nodes (and the associated cancer nodules) result in tumor regression. Overall, asynchronous and short-acting combination regimens such as GT used in metastatic breast cancer treatment can be transformed into targeted, long acting nanoparticles with DcNP enabling technology. In doing so, the DcNP platform may have the potential to design a curative treatment for breast and other cancers by eliminating residual or advancing metastatic cells and prevent tumor recurrence.

Table 6.1. Effect of cell number and injection volume on orthotopic tumor growth over time

Cell # ($x10^6$ cells)	Volume (µl)	# of tumors	Tumor Luminescence (counts)			Tumor Volume (mm^3)[a]
			Day 1	Day 3	Tumor growth (fold-change)	
0[b]	0	0	-	-	-	-
0.2	20	4	760 ± 894	7769 ± 6975	10.2	-
0.5	50	4	2617 ± 3294	14759 ± 17201	5.6	-
1	100[c]	4	4350 ± 995	23435 ± 11180	5.4	-
1[e]	50	12	3244 ± 1942	16021 ± 13247	4.9	40 ± 17
1	50	16	1386 ± 1950	8389 ± 9889	6	53 ± 44

[a]Tumor volume measured on Day 5
[b]Baseline luminescence of 58 ± 39 in mice with no tumors (+luciferin)
[c]100 µl injection volume was too large for the mammary fat pads and resulted in excessive fluid buildup

Table 6.2. Effect of GT DcNP dose on toxicological observations in tumor bearing mice after subcutaneous injection

DcNP Dose (mg/kg)	Injection Volume (µl)	Injection GT Concentration (mg/mL)	Days After Injection	Injection Site Reaction[a]	# of mice	>15% original weight loss[b] (Y/N)	# of mice
0	0	0	4	0	0/4	-	0/4
			7	0	0/4	-	0/4
5	100	G/T: 1/0.1	4	0	0/5	N	0/5
			7	0	0/5	N	0/5
10	100	G/T: 2/0.2	4	-	0/5	N	0/5
			7	2	5/5	N	0/5
20	100	G/T: 4/0.4	4	2	5/5	N	0/5
			7	4	5/5	Y[c]	1/5

[a]Injection site reactions were scored using the Draize Scoring system with (0) representing no erythema, (1) barely perceptible erythema, (2) well-defined erythema, (3) moderate to severe erythema and (4) severe erythema to slight eschar formation.
[b]Variation in body weight is expected but significant loss (>15%) with other clinical symptoms (lethargy, loss of mobility) is indicative of gross toxicity.
[c]The single mouse that exhibited weight loss also showed signs of GI toxicity at necropsy (potentially due to gemcitabine exposure) but was active and mobile prior to euthanasia

Table 6.3. Baseline luminescence of MDA-MB231-HM tumors orthotopically inoculated in the axillary and sub-iliac fat pads of athymic nude mice.

Tumor Site	Tumor Treatment Group[a]	Baseline tumor luminescence[b] (mean ± SD)	ANOVA (p-value)[c]
Axillary	GT DcNP (n=6)	55,471 ± 26,024	
	Free GT (n=6)	27,101 ± 18,371	
	Saline (n=8)	26,684 ± 27,269	
			0.31
Sub-iliac	GT DcNP (n=6)	190,663 ± 304,341	
	Free GT (n=6)	96,627 ± 110,746	
	Saline (n=8)	109,606 ± 197,689	
			0.85

[a]Each treatment group consisted of 3 nude mice bearing 2 axillary and 2 sub-iliac tumors. The saline group consists of 4 nude mice with 2 axillary and 2 sub-iliac tumors.
[b]Luminescence was used as a marker for tumor growth and is presented in total counts mean ± standard deviation
[c]ANOVA analysis was used to assess whether there was a statistically significant difference between baseline tumor luminescence across treatment groups

Table 6.4. Effect of gemcitabine and paclitaxel combination therapy in freely soluble or DcNP form on orthotopically inoculated MDA-MB231-HM cells in athymic nude mice

Tumor Treatment Group [a]	Days after inoculation	% of original axillary tumor signal (mean ± SD)	% of original sub-iliac tumor signal (mean ± SD)
DcNP (n=6)	1	100	100
	7	27 ± 23	11 ± 14
	14	23 ± 13	5 ± 5[c]
	21	65 ± 56	1 ± 1
	28	120 ± 102	-[b]
Free (n=6)	1	100	100
	7	7 ± 10	22 ± 28
	14	32 ± 32	37 ± 28[c]
	21	91 ± 97	12 ± 15
	28	142 ± 169	3 ± 5
Saline (n=8)	1	100	100
	7	113 ± 145	81 ± 165
	14	272 ± 625	811 ± 2054
	21	2453 ± 4473	589 ± 1409
	28	2846 ± 5450	1291 ± 3074

[a]*Data are presented as the mean and standard deviation of 6 tumors per injection site (axillary or sub-iliac) normalized to the day 1 luminescence of each individual tumor (DcNP and Free). The saline control consists of 4 mice with 8 tumors per injection site normalized to day 1 luminescence.*

[b]*In DcNP treated mice on Day 28, no tumor signal was detected during imaging and no cancer cells could be observed during necropsy.*

[c]*Unpaired student's T-test for free versus DcNP on day 14, $p<0.05$, no other time points or treatment comparisons to saline were statistically significant due to large variance within the group*

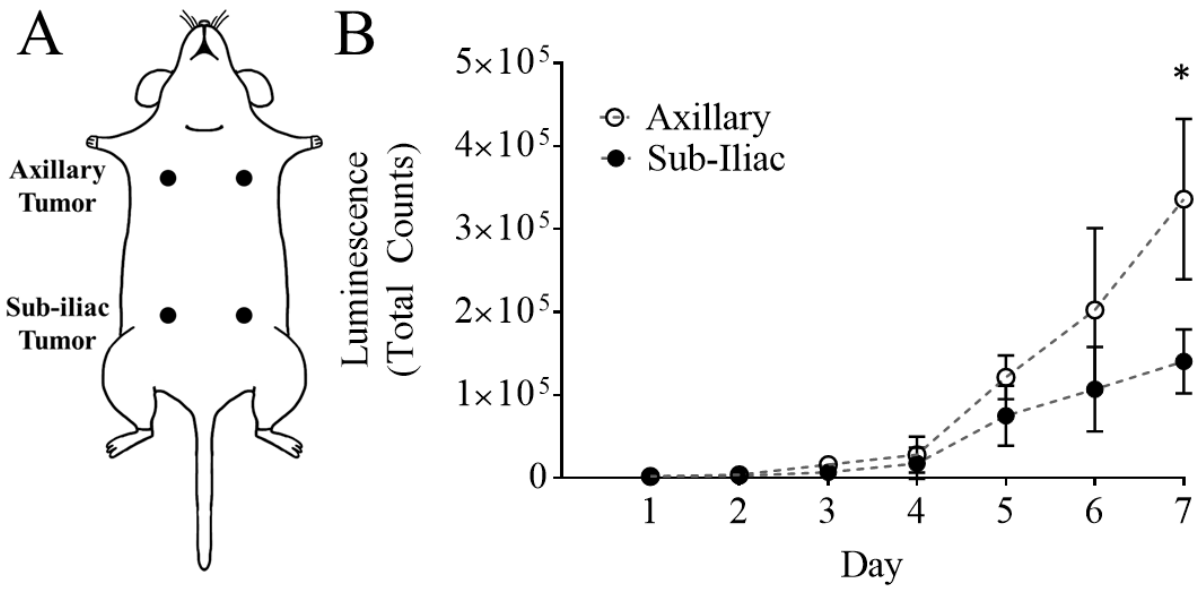

Figure 6.1. Development and characterization of an orthotopic 4T1-based model of breast cancer growth

Mice were orthotopically inoculated with 1 million 4T1-luc cells at 4 different sites (Panel A). Tumors located near the axillary fat pads exhibited statistically distinct growth patterns compared to tumors located near the sub-iliac fat pads (Panel B) as determined by luminescent measurements over time ($p<0.05$, 2-way ANOVA). Error bars are presented as the 95% confidence intervals.

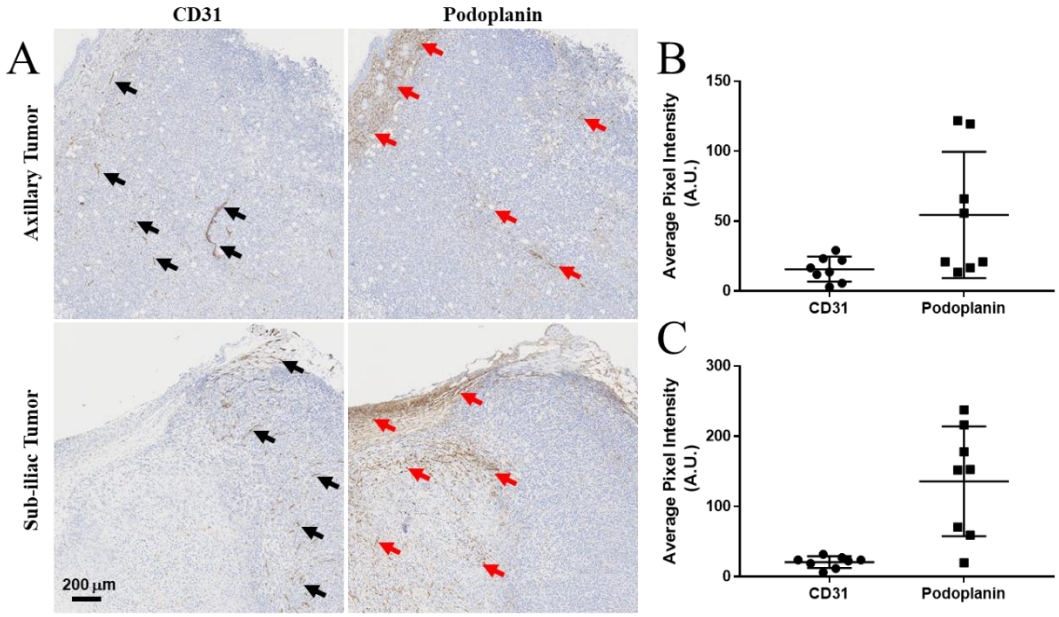

Figure 6.2. Characterization of blood and lymphatic vasculature development in growing orthotopic tumors

After 5 days of growth, 4T1 tumors harvested from the axillary and sub-iliac fat pads display vascularization with both blood and lymphatic vessels. CD31 was used as a marker for blood endothelial cells and blood vessels are highlighted by black arrows. Podoplanin was used as a marker for lymphatic vascular system and highlighted by red arrows. Representative IHC slides are presented in (Panel A). ImageJ analysis was performed to as a semi-quantitative measure of positive staining for CD31 and Podoplanin in the axillary (Panel B) and sub-iliac tumor (Panel C).

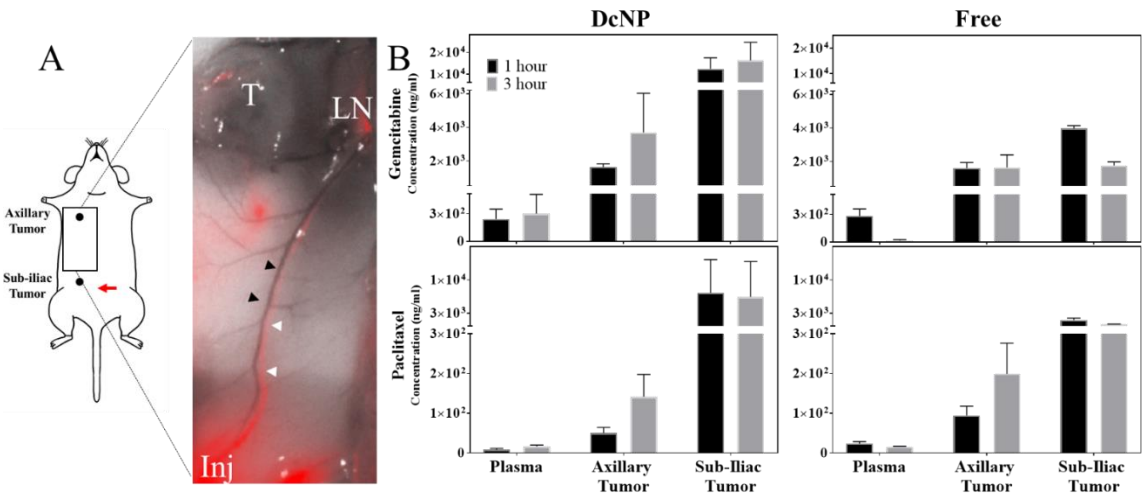

Figure 6.3. Effect of DcNPs on the transit and accumulation of gemcitabine and paclitaxel into lymphatic vessels and tumors from a subcutaneous injection site

ICG labeled GT DcNPs were subcutaneously inject in the belly of tumor bearing mice (red arrow). After 1 hour, a fluorescent signal can be observed transiting from the injection site (Inj, red arrow) through lymphatic vessels (white arrows) running adjacent to the thoracoepigastic vein (black arrows). Fluorescent signal can also be observed in the axillary node (LN) with small traces on the surface of the tumor (T). The concentration of GT in tumors correspond with the observed transit of ICG labeled DcNPs (Panel B). From 1 to 3 hours after subcutaneous injection, we observe a decrease in gemcitabine concentrations from the blood and sub-iliac tumors of mice administered free drug. In that time span, no change is observed in the axillary tumor. When administered as a DcNP, gemcitabine concentrations increase from 1 to 3 hours in all 3 compartments. Interestingly, the trend for paclitaxel over time given in either DcNP or free form are similar. Paclitaxel in DcNP form may result in slightly higher concentrations in the sub-iliac tumor compared to free drug. The bar graph shows the mean ± standard deviation of 3 biological replicates.

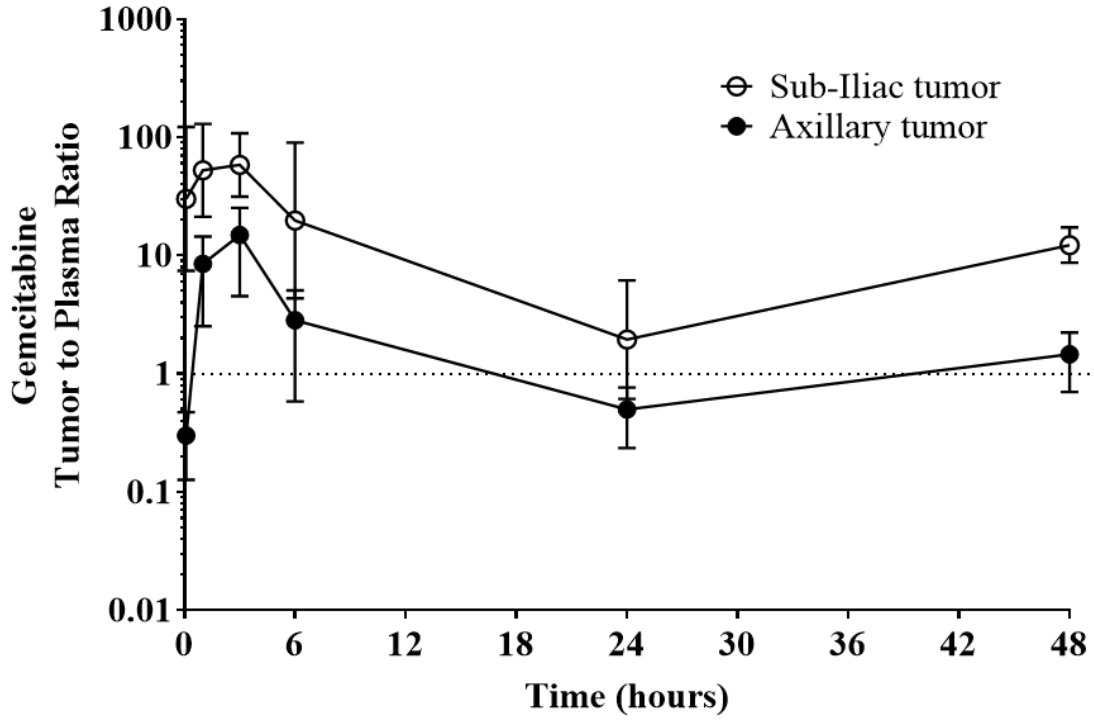

Figure 6.4. Effect of DcNPs to enhance and prolong plasma and tumor concentrations of gemcitabine and paclitaxel over time

GT DcNP administered subcutaneously in the belly enable consist tumor to plasma concentration ratios of gemcitabine above or near 1 throughout the 48 hour time course reflecting lymphatic transit prior to entering the systemic circulation.

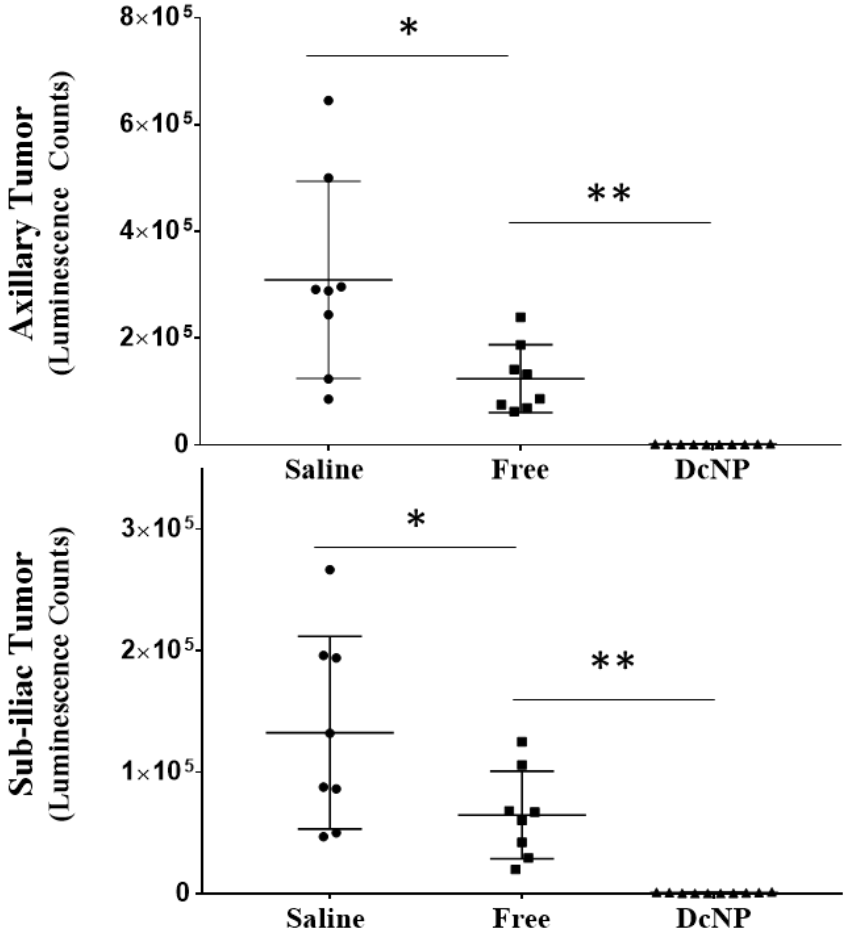

Figure 6.5. Effect of DcNPs on tumor inhibition of gemcitabine and paclitaxel when compared to the same dose of free drug

Mice were treated with either saline, GT in DMSO (20 mg/kg) or GT in DcNP (20 mg/kg) 24 hours after cancer cell inoculation. Mice were monitored for 7 days and tumor growth was evaluated by luminescence. The mean and standard deviation of luminescence are presented (n=4-5) are presented above. *Denotes $p<0.05$, **$p<0.001$, Student's T-test.

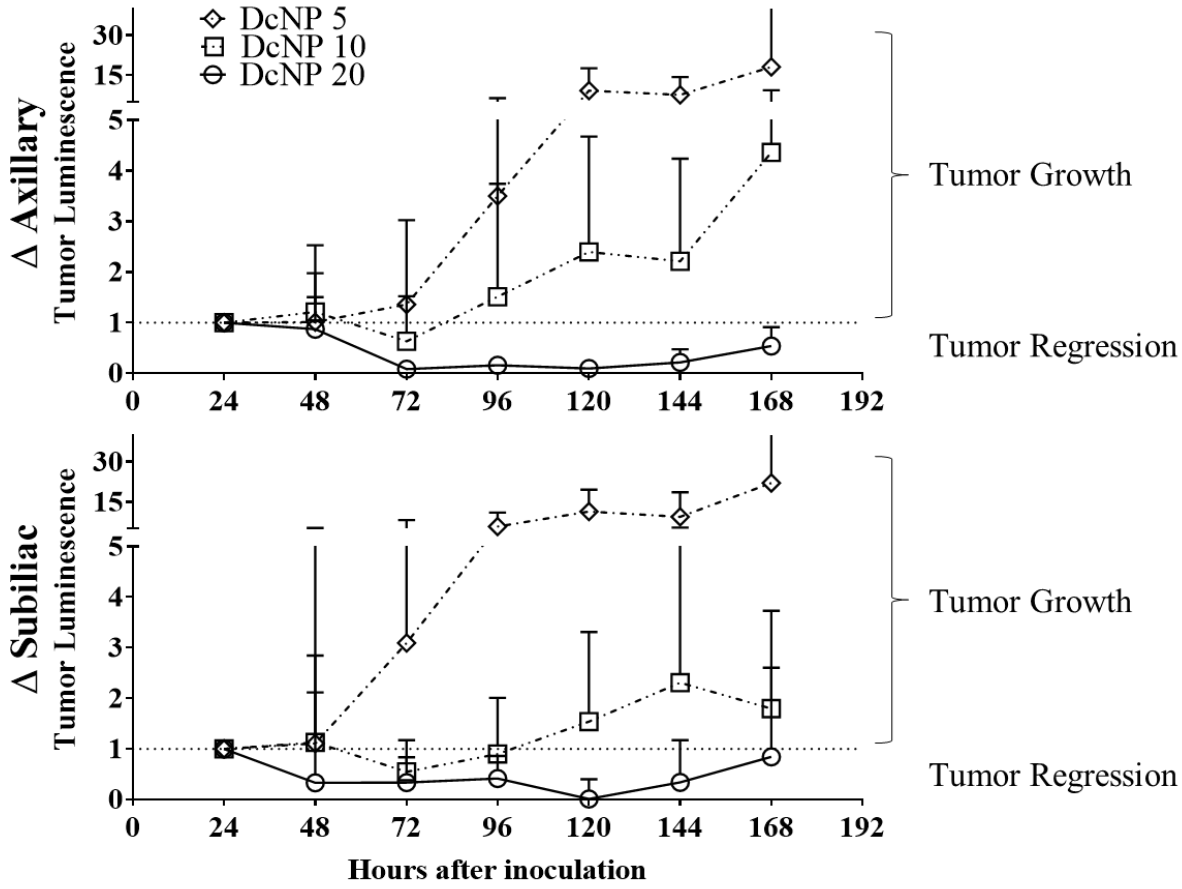

Figure 6.6. Dose proportional effects of gemcitabine and paclitaxel DcNP tumor inhibition

Mice were treated with GT in DcNP at 5 mg/kg (◊), 10 mg/kg (□) or 20 mg/kg (○) 24 hours after cancer cell inoculation. Mice were monitored for 7 days and tumor growth was evaluated by luminescence. The mean and standard deviation of luminescence are presented (n=4-5) are presented above. A dashed line is included at y=1 to show the relative growth from baseline.

Chapter 7. SUMMARY AND FUTURE DIRECTIONS

7.1 SUMMARY AND FUTURE DIRECTIONS

The current limitation in breast cancer treatment is the inability to eliminate residual cancer cells after surgical resection of the primary tumor by either lumpectomy (removal of a portion of the mammary fat pad) or mastectomy (complete removal of the breast). Although there are many drugs available to inhibit disease progression (such as the estrogen receptor targeted or HER2 targeted drugs that exploit protein overexpression in tumor cells); these treatments lose effect over time and tumor recurrence is a lifelong concern for patients diagnosed with breast cancer. When disease progression occurs after treatment with oral hormone or molecular targeted drugs, chemotherapy is used to treat breast cancer progression and the combination of gemcitabine (G) and paclitaxel (T) represents one such regimen with potent anticancer effects and generally manageable patient toxicities. However, the anticancer effect is limited by an inability to synchronize the exposure of both drugs in plasma and cancer cells and by short-acting pharmacokinetics. This dissertation has investigated a drug combination nanoparticle (DcNP) approach to simultaneously and preferentially deliver GT to cancer cells for enhanced cancer cell retention and exposure. In doing so, this approach can overcome the current clinical limitations in finding a cure for breast cancer metastasis. We found that the DcNP platform with controlled solvent removal was able to combine the unlikely partners of water soluble gemcitabine and water insoluble paclitaxel together in a novel MDM structure and enable the development of a stable, long acting injectable dosage form of GT in DcNP form. Prior to this discovery, there was no readily available process (including polymeric, protein or liposomal formulations) to stabilize hydrophilic gemcitabine with hydrophobic paclitaxel together in an injectable formulation. The prolonged plasma circulation of GT in DcNPs was demonstrated through experimental and modeling approaches, with both drugs remaining associated to the DcNPs together after IV

administration. GT DcNPs administered to mice bearing cancer nodules in the lung produced a 10:1 gemcitabine to paclitaxel lung concentration ratio 24 hours after injection. This concentration ratio is consistent with the initial dose ratio of gemcitabine and paclitaxel in the formulation, and may reflect the targeting and retention of GT in DcNPs taken up by tumor burdened tissue. The successful transit of GT in DcNP through the biological milieu and retention in cancer tissues and cells support the stability of DcNPs as a combination drug delivery platform. In mouse models of breast cancer, a single IV dose completely eliminated advancing cancer cells to the lungs while a single SC dose caused breast tumor regression and recovery of the mammary gland. If these results can be translated to the clinic, GT DcNPs may be able to eliminate metastatic or residual breast cancer cells in both the blood and lymph after surgery; thus, overcoming the current gap in breast cancer treatment.

The results presented in this dissertation highlight the potential for GT DcNPs to improve breast cancer treatment but there are also limitations that need to be addressed in future studies. Laboratory scale methods (such as rotary evaporation and sonication) were used to generate GT DcNPs. These methods can be adequately controlled for small scale mouse studies but are limited in scale (~50 mL of GT DcNP maximum). Therefore, a future direction could include the transition from rotary evaporation to spray drying to facilitate a larger batch capacity and greater process control for GT DcNPs. Further development of the GT DcNP manufacturing process can increase the potential to translate into a clinical product where liters of drug product are required. Although scale up is a challenging process, the DcNP platform has successfully transitioned from rotary evaporation to spray drying with antiviral drug combinations to support large, non-human primate studies. Furthermore, the previously scaled antiviral drug combinations are more complex with combinations of 3 to 4 drugs (instead of the two for GT DcNPs). Given the similarities between

the antiviral and GT DcNPs, it is likely that GT DcNPs are also capable of transitioning to spray drying to enable further development as a clinical product.

The pharmacokinetic model developed in this dissertation to estimate the associated and dissociated fractions of drugs *in vivo* can also be expanded in future studies. From the pharmacokinetic data, there are distinct differences observed in the retention of gemcitabine and paclitaxel in DcNPs after IV administration. These differences may be due to protein binding of paclitaxel which may require further investigation. It is possible that paclitaxel is partially exposed in DcNPs which allows for binding with plasma proteins such as albumin (either forming a DcNP-protein complex or exchanging a fraction of paclitaxel from DcNPs to albumin). Additional studies are needed to define the degree and time-course of paclitaxel exchange and dissociation from DcNPs. Further understanding of the dynamic interactions between DcNPs and plasma proteins would allow us to refine our pharmacokinetic model and improve our projections of drug release from DcNPs. The pharmacokinetic (PK) model can also be expanded to include the pharmacodynamic (PD) data presented in the subsequent chapters. The expanded PK-PD model could be used to predict the tumor inhibitory effects of GT DcNPs across various dosing regimens (such as multiple dosing or extended infusions).

Finally, the anticancer effect of GT DcNPs was evaluated against syngeneic models of breast cancer metastasis using the 4T1 cell line. Although the models are designed to reflect human breast cancer treatment, the cells themselves are murine in origin and homogeneous. Thus, they may not capture the heterogeneous nature of human breast cancers. Patient derived xenografts (PDX) models would be of interest to evaluate the effect of GT DcNPs on heterogeneous tumors of human origin to support the translation of GT DcNPs into a clinical product. Despite these

limitations, the data from this dissertation clearly show an enhanced anticancer effect of GT when given in DcNP form and these promising results warrant further study.

This dissertation has shown that the targeted delivery of gemcitabine and paclitaxel together to cancer cells can improve antitumor effect. In pursuit of testing the overarching hypothesis, this dissertation has advanced the field of pharmaceutical science by developing a novel combination nanoparticle that stabilizes both hydrophilic gemcitabine and hydrophobic paclitaxel together. Through this development, this dissertation not only validates the concept of targeted combination particles, but also presents a potential combination drug product that may lead to more effective and safer therapy. GT DcNPs have the potential to not only control tumor growth but also reverse the course of metastatic breast cancer disease progress; thus, GT DcNPs can be considered a product candidate worthy of clinical development. If GT DcNPs can be translated to clinical treatment, a single subcutaneous dose after surgical resection of a primary tumor could be sufficient to eliminate residual cancer cells. A multi-dosing regimen could also be considered to keep patients in remission as the search for a breast cancer cure continues. GT DcNP accumulation in the sentinel lymph nodes of breast cancer patients could overcome the need for systemic chemotherapy, which is associated with significant off-target, systemic toxicities. The tools and approaches used in this dissertation can act as the foundation for the future development of GT or other novel drug combinations for treating metastatic disease progression in a wide range of cancer types. The development of stable, combination injectables can also be applied to other chronic medical conditions where long-acting and targeted therapies provide significant benefit to patients.

BIBLIOGRAPHY

Abbasi, E., Aval, S. F., Akbarzadeh, A., Milani, M., Nasrabadi, H. T., Joo, S. W., . . . Pashaei-Asl, R. (2014). Dendrimers: synthesis, applications, and properties. *Nanoscale Res Lett, 9*(1), 247. doi:10.1186/1556-276X-9-247

Agus, D. B., Akita, R. W., Fox, W. D., Lewis, G. D., Higgins, B., Pisacane, P. I., . . . Sliwkowski, M. X. (2002). Targeting ligand-activated ErbB2 signaling inhibits breast and prostate tumor growth. *Cancer Cell, 2*(2), 127-137. doi:https://doi.org/10.1016/S1535-6108(02)00097-1

Ait-Oudhia, S., Mager, D. E., & Straubinger, R. M. (2014). Application of pharmacokinetic and pharmacodynamic analysis to the development of liposomal formulations for oncology. *Pharmaceutics, 6*(1), 137-174. doi:10.3390/pharmaceutics6010137

Albain, K. S., Nag, S. M., Calderillo-Ruiz, G., Jordaan, J. P., Llombart, A. C., Pluzanska, A., . . . O'Shaughnessy, J. (2008). Gemcitabine plus Paclitaxel versus Paclitaxel monotherapy in patients with metastatic breast cancer and prior anthracycline treatment. *J Clin Oncol, 26*(24), 3950-3957. doi:10.1200/JCO.2007.11.9362

Allen, T. M., & Everest, J. M. (1983). Effect of liposome size and drug release properties on pharmacokinetics of encapsulated drug in rats. *J Pharmacol Exp Ther, 226*(2), 539-544. Retrieved from https://www.ncbi.nlm.nih.gov/pubmed/6875864

Allouache, D., Gawande, S. R., Tubiana-Hulin, M., Tubiana-Mathieu, N., Piperno-Neumann, S., Mefti, F., . . . Genot, J. Y. (2005). First-line therapy with gemcitabine and paclitaxel in locally, recurrent or metastatic breast cancer: a phase II study. *BMC Cancer, 5*, 151. doi:10.1186/1471-2407-5-151

Arca, H. C., Mosquera-Giraldo, L. I., Dahal, D., Taylor, L. S., & Edgar, K. J. (2017). Multidrug, Anti-HIV Amorphous Solid Dispersions: Nature and Mechanisms of Impacts of Drugs on Each Other's Solution Concentrations. *Mol Pharm, 14*(11), 3617-3627. doi:10.1021/acs.molpharmaceut.7b00203

Arpino, G., Bardou, V. J., Clark, G. M., & Elledge, R. M. (2004). Infiltrating lobular carcinoma of the breast: tumor characteristics and clinical outcome. *Breast Cancer Res, 6*(3), R149-156. doi:10.1186/bcr767

Aryal, S., Hu, C.-M. J., & Zhang, L. (2010). Combinatorial Drug Conjugation Enables Nanoparticle Dual-Drug Delivery. *Small, 6*(13), 1442-1448. doi:10.1002/smll.201000631

Auerbach, R., Morrissey, L. W., & Sidky, Y. A. (1978). Regional Differences in the Incidence and Growth of Mouse Tumors following Intradermal or Subcutaneous Inoculation. *Cancer Research, 38*(6), 1739. Retrieved from http://cancerres.aacrjournals.org/content/38/6/1739.abstract

Auerbach, R., Morrissey, L. W., & Sidky, Y. A. (1978). Regional differences in the incidence and growth of mouse tumors following intradermal or subcutaneous inoculation. *Cancer Research, 38*(6), 1739-1744. Retrieved from https://www.ncbi.nlm.nih.gov/pubmed/647684

Austin Doyle, L., & Ross, D. D. (2003). Multidrug resistance mediated by the breast cancer resistance protein BCRP (ABCG2). *Oncogene, 22*(47), 7340-7358. doi:10.1038/sj.onc.1206938

Autran, B., Carcelain, G., Li, T. S., Blanc, C., Mathez, D., Tubiana, R., . . . Leibowitch, J. (1997). Positive effects of combined antiretroviral therapy on CD4+ T cell homeostasis and

function in advanced HIV disease. *Science, 277*(5322), 112-116. doi:10.1126/science.277.5322.112

Bargh, J. D., Isidro-Llobet, A., Parker, J. S., & Spring, D. R. (2019). Cleavable linkers in antibody–drug conjugates. *Chemical Society Reviews, 48*(16), 4361-4374. doi:10.1039/C8CS00676H

Barok, M., Joensuu, H., & Isola, J. (2014). Trastuzumab emtansine: mechanisms of action and drug resistance. *Breast Cancer Res, 16*(2), 209. doi:10.1186/bcr3621

Baselga, J., Cortes, J., Kim, S. B., Im, S. A., Hegg, R., Im, Y. H., . . . Group, C. S. (2012). Pertuzumab plus trastuzumab plus docetaxel for metastatic breast cancer. *N Engl J Med, 366*(2), 109-119. doi:10.1056/NEJMoa1113216

Baselga, J., Lewis Phillips, G. D., Verma, S., Ro, J., Huober, J., Guardino, A. E., . . . Pegram, M. D. (2016). Relationship between Tumor Biomarkers and Efficacy in EMILIA, a Phase III Study of Trastuzumab Emtansine in HER2-Positive Metastatic Breast Cancer. *Clinical Cancer Research, 22*(15), 3755-3763. doi:10.1158/1078-0432.Ccr-15-2499

Beane, J. D., Griffin, K. F., Levy, E. B., Pandalai, P., Wood, B., Abi-Jaoudeh, N., . . . Rudloff, U. (2015). Duodenal ischemia and upper GI bleeding are dose-limiting toxicities of 24-h continuous intra-arterial pancreatic perfusion of gemcitabine following vascular isolation of the pancreatic head: early results from the Regional Chemotherapy in Locally Advanced Pancreatic Cancer (RECLAP) study. *Invest New Drugs, 33*(1), 109-118. doi:10.1007/s10637-014-0157-7

Bhujbal, S. V., Zemlyanov, D. Y., Cavallaro, A., Mangal, S., Taylor, L. S., & Zhou, Q. T. (2018). Qualitative and Quantitative Characterization of Composition Heterogeneity on the Surface of Spray Dried Amorphous Solid Dispersion Particles by an Advanced Surface Analysis Platform with High Surface Sensitivity and Superior Spatial Resolution. *Mol Pharm, 15*(5), 2045-2053. doi:10.1021/acs.molpharmaceut.8b00122

Blackstein, M., Vogel, C. L., Ambinder, R., Cowan, J., Iglesias, J., & Melemed, A. (2002). Gemcitabine as first-line therapy in patients with metastatic breast cancer: a phase II trial. *Oncology, 62*(1), 2-8. doi:10.1159/000048240

Blackwell, K. L., Burstein, H. J., Storniolo, A. M., Rugo, H. S., Sledge, G., Aktan, G., . . . O'Shaughnessy, J. (2012). Overall survival benefit with lapatinib in combination with trastuzumab for patients with human epidermal growth factor receptor 2-positive metastatic breast cancer: final results from the EGF104900 Study. *J Clin Oncol, 30*(21), 2585-2592. doi:10.1200/JCO.2011.35.6725

Bombonati, A., & Sgroi, D. C. (2011). The molecular pathology of breast cancer progression. *J Pathol, 223*(2), 307-317. doi:10.1002/path.2808

Breslin, S., Lowry, M. C., & O'Driscoll, L. (2017). Neratinib resistance and cross-resistance to other HER2-targeted drugs due to increased activity of metabolism enzyme cytochrome P4503A4. *Br J Cancer, 116*(5), 620-625. doi:10.1038/bjc.2016.445

Brown, M., Assen, F. P., Leithner, A., Abe, J., Schachner, H., Asfour, G., . . . Kerjaschki, D. (2018). Lymph node blood vessels provide exit routes for metastatic tumor cell dissemination in mice. *Science, 359*(6382), 1408-1411. doi:10.1126/science.aal3662

Brownlee, Z., Garg, R., Listo, M., Zavitsanos, P., Wazer, D. E., & Huber, K. E. (2018). Late complications of radiation therapy for breast cancer: evolution in techniques and risk over time. *Gland Surg, 7*(4), 371-378. doi:10.21037/gs.2018.01.05

Bulbake, U., Doppalapudi, S., Kommineni, N., & Khan, W. (2017). Liposomal Formulations in Clinical Use: An Updated Review. *Pharmaceutics, 9*(2). doi:10.3390/pharmaceutics9020012

Bunone, G., Briand, P. A., Miksicek, R. J., & Picard, D. (1996). Activation of the unliganded estrogen receptor by EGF involves the MAP kinase pathway and direct phosphorylation. *EMBO J, 15*(9), 2174-2183. Retrieved from https://www.ncbi.nlm.nih.gov/pubmed/8641283

Cai, S., Thati, S., Bagby, T. R., Diab, H. M., Davies, N. M., Cohen, M. S., & Forrest, M. L. (2010). Localized doxorubicin chemotherapy with a biopolymeric nanocarrier improves survival and reduces toxicity in xenografts of human breast cancer. *J Control Release, 146*(2), 212-218. doi:10.1016/j.jconrel.2010.04.006

Cai, S., Xie, Y., Bagby, T. R., Cohen, M. S., & Forrest, M. L. (2008). Intralymphatic chemotherapy using a hyaluronan-cisplatin conjugate. *J Surg Res, 147*(2), 247-252. doi:10.1016/j.jss.2008.02.048

Canonici, A., Gijsen, M., Mullooly, M., Bennett, R., Bouguern, N., Pedersen, K., . . . Kong, A. (2013). Neratinib overcomes trastuzumab resistance in HER2 amplified breast cancer. *Oncotarget, 4*(10), 1592-1605. doi:10.18632/oncotarget.1148

Cao, H., Dan, Z., He, X., Zhang, Z., Yu, H., Yin, Q., & Li, Y. (2016). Liposomes Coated with Isolated Macrophage Membrane Can Target Lung Metastasis of Breast Cancer. *ACS Nano, 10*(8), 7738-7748. doi:10.1021/acsnano.6b03148

Cao, H., Zhang, Z., Zhao, S., He, X., Yu, H., Yin, Q., . . . Li, Y. (2015). Hydrophobic interaction mediating self-assembled nanoparticles of succinobucol suppress lung metastasis of breast cancer by inhibition of VCAM-1 expression. *J Control Release, 205*, 162-171. doi:10.1016/j.jconrel.2015.01.015

Cardoso, F., Kyriakides, S., Ohno, S., Penault-Llorca, F., Poortmans, P., Rubio, I. T., . . . clinicalguidelines@esmo.org, E. G. C. E. a. (2019). Early breast cancer: ESMO Clinical Practice Guidelines for diagnosis, treatment and follow-updagger. *Annals of Oncology, 30*(8), 1194-1220. doi:10.1093/annonc/mdz173

Chen, J., Wang, L., Yao, Q., Ling, R., Li, K., & Wang, H. (2004). Drug concentrations in axillary lymph nodes after lymphatic chemotherapy on patients with breast cancer. *Breast Cancer Research, 6*(4), R474. doi:10.1186/bcr819

Chen, L., Wang, L., Shion, H., Yu, C., Yu, Y. Q., Zhu, L., . . . Gao, K. (2016). In-depth structural characterization of Kadcyla(R) (ado-trastuzumab emtansine) and its biosimilar candidate. *MAbs, 8*(7), 1210-1223. doi:10.1080/19420862.2016.1204502

Chen, M. L. (2008). Lipid excipients and delivery systems for pharmaceutical development: a regulatory perspective. *Adv Drug Deliv Rev, 60*(6), 768-777. doi:10.1016/j.addr.2007.09.010

Chen, Q., & Ross, A. C. (2012). All-trans-retinoic acid and the glycolipid alpha-galactosylceramide combined reduce breast tumor growth and lung metastasis in a 4T1 murine breast tumor model. *Nutr Cancer, 64*(8), 1219-1227. doi:10.1080/01635581.2012.718404

Ciccolini, J., Serdjebi, C., Peters, G. J., & Giovannetti, E. (2016). Pharmacokinetics and pharmacogenetics of Gemcitabine as a mainstay in adult and pediatric oncology: an EORTC-PAMM perspective. *Cancer Chemother Pharmacol, 78*(1), 1-12. doi:10.1007/s00280-016-3003-0

Clemons, M., Leahy, M., Valle, J., Jayson, G., Ranson, M., & Howell, A. (1997). Review of recent trials of chemotherapy for advanced breast cancer: the taxanes. *European Journal of Cancer, 33*(13), 2183-2193. doi:https://doi.org/10.1016/S0959-8049(97)00260-8

Collins, D. M., Gately, K., Hughes, C., Edwards, C., Davies, A., Madden, S. F., . . . Crown, J. (2017). Tyrosine kinase inhibitors as modulators of trastuzumab-mediated antibody-dependent cell-mediated cytotoxicity in breast cancer cell lines. *Cell Immunol, 319*, 35-42. doi:10.1016/j.cellimm.2017.07.005

Constantinides, P. P., Chaubal, M. V., & Shorr, R. (2008). Advances in lipid nanodispersions for parenteral drug delivery and targeting. *Adv Drug Deliv Rev, 60*(6), 757-767. doi:10.1016/j.addr.2007.10.013

Crowe, A. R., & Yue, W. (2019). Semi-quantitative Determination of Protein Expression using Immunohistochemistry Staining and Analysis: An Integrated Protocol. *Bio Protoc, 9*(24). doi:10.21769/BioProtoc.3465

Dan, Z., Cao, H., He, X., Zhang, Z., Zou, L., Zeng, L., . . . Li, Y. (2016). A pH-Responsive Host-guest Nanosystem Loading Succinobucol Suppresses Lung Metastasis of Breast Cancer. *Theranostics, 6*(3), 435-445. doi:10.7150/thno.13896

Daniel, A. R., Hagan, C. R., & Lange, C. A. (2011). Progesterone receptor action: defining a role in breast cancer. *Expert Rev Endocrinol Metab, 6*(3), 359-369. doi:10.1586/eem.11.25

de Jonge, M. E., Huitema, A. D., Schellens, J. H., Rodenhuis, S., & Beijnen, J. H. (2005). Population pharmacokinetics of orally administered paclitaxel formulated in Cremophor EL. *Br J Clin Pharmacol, 59*(3), 325-334. doi:10.1111/j.1365-2125.2004.02325.x

Dent, R., Trudeau, M., Pritchard, K. I., Hanna, W. M., Kahn, H. K., Sawka, C. A., . . . Narod, S. A. (2007). Triple-Negative Breast Cancer: Clinical Features and Patterns of Recurrence. *Clinical Cancer Research, 13*(15), 4429. doi:10.1158/1078-0432.CCR-06-3045

Desai, D., Wang, J., Wen, H., Li, X., & Timmins, P. (2013). Formulation design, challenges, and development considerations for fixed dose combination (FDC) of oral solid dosage forms. *Pharm Dev Technol, 18*(6), 1265-1276. doi:10.3109/10837450.2012.660699

Dhillon, S. (2014). Trastuzumab Emtansine: A Review of Its Use in Patients with HER2-Positive Advanced Breast Cancer Previously Treated with Trastuzumab-Based Therapy. *Drugs, 74*(6), 675-686. doi:10.1007/s40265-014-0201-0

Dipersio, L. P. (1981). Regional growth differences of human tumour xenografts in nude mice. *Lab Anim, 15*(2), 179-180. doi:10.1258/002367781780959044

Dong, S., Guo, Y., Duan, Y., Li, Z., Wang, C., Niu, L., . . . Zhang, M. (2018). Co-delivery of paclitaxel and gemcitabine by methoxy poly(ethylene glycol)-poly(lactide-coglycolide)-polypeptide nanoparticles for effective breast cancer therapy. *Anticancer Drugs, 29*(7), 637-645. doi:10.1097/CAD.0000000000000631

Doronina, S. O., Toki, B. E., Torgov, M. Y., Mendelsohn, B. A., Cerveny, C. G., Chace, D. F., . . . Senter, P. D. (2003). Development of potent monoclonal antibody auristatin conjugates for cancer therapy. *Nature Biotechnology, 21*(7), 778-784. doi:10.1038/nbt832

Draize, J. H., Woodard, G., & Calvery, H. O. (1944). METHODS FOR THE STUDY OF IRRITATION AND TOXICITY OF SUBSTANCES APPLIED TOPICALLY TO THE SKIN AND MUCOUS MEMBRANES. *Journal of Pharmacology and Experimental Therapeutics, 82*(3), 377. Retrieved from http://jpet.aspetjournals.org/content/82/3/377.abstract

Duan, J., Freeling, J. P., Koehn, J., Shu, C., & Ho, R. J. (2014). Evaluation of atazanavir and darunavir interactions with lipids for developing pH-responsive anti-HIV drug combination nanoparticles. *J Pharm Sci, 103*(8), 2520-2529. doi:10.1002/jps.24046

Duncan, R., & Izzo, L. (2005). Dendrimer biocompatibility and toxicity. *Adv Drug Deliv Rev, 57*(15), 2215-2237. doi:10.1016/j.addr.2005.09.019

Eckel, F., Schmelz, R., Erdmann, J., Mayr, M., & Lersch, C. (2003). Phase II trial of a 24-hour infusion of gemcitabine in previously untreated patients with advanced pancreatic adenocarcinoma. *Cancer Invest, 21*(5), 690-694. doi:10.1081/cnv-120023767

Eckhardt, B. L., Francis, P. A., Parker, B. S., & Anderson, R. L. (2012). Strategies for the discovery and development of therapies for metastatic breast cancer. *Nat Rev Drug Discov, 11*(6), 479-497. doi:10.1038/nrd2372

Feher, O., Vodvarka, P., Jassem, J., Morack, G., Advani, S. H., Khoo, K. S., . . . von Minckwitz, G. (2005). First-line gemcitabine versus epirubicin in postmenopausal women aged 60 or older with metastatic breast cancer: a multicenter, randomized, phase III study. *Annals of Oncology, 16*(6), 899-908. doi:10.1093/annonc/mdi181

Franklin, M. C., Carey, K. D., Vajdos, F. F., Leahy, D. J., de Vos, A. M., & Sliwkowski, M. X. (2004). Insights into ErbB signaling from the structure of the ErbB2-pertuzumab complex. *Cancer Cell, 5*(4), 317-328. doi:https://doi.org/10.1016/S1535-6108(04)00083-2

Frasor, J., Stossi, F., Danes, J. M., Komm, B., Lyttle, C. R., & Katzenellenbogen, B. S. (2004). Selective estrogen receptor modulators: discrimination of agonistic versus antagonistic activities by gene expression profiling in breast cancer cells. *Cancer Research, 64*(4), 1522-1533. doi:10.1158/0008-5472.can-03-3326

Freeling, J. P., Koehn, J., Shu, C., Sun, J., & Ho, R. J. (2014). Long-acting three-drug combination anti-HIV nanoparticles enhance drug exposure in primate plasma and cells within lymph nodes and blood. *AIDS, 28*(17), 2625-2627. doi:10.1097/QAD.0000000000000421

Freeling, J. P., Koehn, J., Shu, C., Sun, J., & Ho, R. J. (2015). Anti-HIV drug-combination nanoparticles enhance plasma drug exposure duration as well as triple-drug combination levels in cells within lymph nodes and blood in primates. *AIDS Res Hum Retroviruses, 31*(1), 107-114. doi:10.1089/aid.2014.0210

Frese, K. K., Neesse, A., Cook, N., Bapiro, T. E., Lolkema, M. P., Jodrell, D. I., & Tuveson, D. A. (2012). nab-Paclitaxel potentiates gemcitabine activity by reducing cytidine deaminase levels in a mouse model of pancreatic cancer. *Cancer Discovery, 2*(3), 260-269. doi:10.1158/2159-8290.CD-11-0242

Fuentes, G., Scaltriti, M., Baselga, J., & Verma, C. S. (2011). Synergy between trastuzumab and pertuzumab for human epidermal growth factor 2 (Her2) from colocalization: an in silico based mechanism. *Breast Cancer Res, 13*(3), R54. doi:10.1186/bcr2888

Gao, L., Liu, G., Ma, J., Wang, X., Zhou, L., & Li, X. (2012). Drug nanocrystals: In vivo performances. *J Control Release, 160*(3), 418-430. doi:10.1016/j.jconrel.2012.03.013

Gelderblom, H., Verweij, J., Nooter, K., & Sparreboom, A. (2001). Cremophor EL: the drawbacks and advantages of vehicle selection for drug formulation. *European Journal of Cancer, 37*(13), 1590-1598. doi:10.1016/s0959-8049(01)00171-x

Gianni, L., Kearns, C. M., Giani, A., Capri, G., Vigano, L., Lacatelli, A., . . . Egorin, M. J. (1995). Nonlinear pharmacokinetics and metabolism of paclitaxel and its pharmacokinetic/pharmacodynamic relationships in humans. *J Clin Oncol, 13*(1), 180-190. doi:10.1200/JCO.1995.13.1.180

Giles, F. J. (2002). Gemtuzumab ozogamicin: promise and challenge in patients with acute myeloid leukemia. *Expert Review of Anticancer Therapy, 2*(6), 630-640. doi:10.1586/14737140.2.6.630

Golombek, S. K., May, J. N., Theek, B., Appold, L., Drude, N., Kiessling, F., & Lammers, T. (2018). Tumor targeting via EPR: Strategies to enhance patient responses. *Adv Drug Deliv Rev, 130*, 17-38. doi:10.1016/j.addr.2018.07.007

Gould, S. E., Junttila, M. R., & de Sauvage, F. J. (2015). Translational value of mouse models in oncology drug development. *Nature Medicine, 21*(5), 431-439. doi:10.1038/nm.3853

Gradishar, W. J. (2006). Albumin-bound paclitaxel: a next-generation taxane. *Expert Opin Pharmacother, 7*(8), 1041-1053. doi:10.1517/14656566.7.8.1041

Grunewald, R., Abbruzzese, J. L., Tarassoff, P., & Plunkett, W. (1991). Saturation of 2',2'-difluorodeoxycytidine 5'-triphosphate accumulation by mononuclear cells during a phase I trial of gemcitabine. *Cancer Chemother Pharmacol, 27*(4), 258-262. doi:10.1007/bf00685109

Grunewald, R., Kantarjian, H., Keating, M. J., Abbruzzese, J., Tarassoff, P., & Plunkett, W. (1990). Pharmacologically Directed Design of the Dose Rate and Schedule of 2′,2′-Difluorodeoxycytidine (Gemcitabine) Administration in Leukemia. *Cancer Research, 50*(21), 6823-6826. Retrieved from https://cancerres.aacrjournals.org/content/canres/50/21/6823.full.pdf

Gudena, V., Montero, A. J., & Gluck, S. (2008). Gemcitabine and taxanes in metastatic breast cancer: a systematic review. *Ther Clin Risk Manag, 4*(6), 1157-1164. Retrieved from https://www.ncbi.nlm.nih.gov/pubmed/19337423

Hall, J. M., & McDonnell, D. P. (2005). Coregulators in nuclear estrogen receptor action: from concept to therapeutic targeting. *Mol Interv, 5*(6), 343-357. doi:10.1124/mi.5.6.7

Harari, D., & Yarden, Y. (2000). Molecular mechanisms underlying ErbB2/HER2 action in breast cancer. *Oncogene, 19*(53), 6102-6114. doi:10.1038/sj.onc.1203973

Harris, M., Howell, A., Chrissohou, M., Swindell, R. I., Hudson, M., & Sellwood, R. A. (1984). A comparison of the metastatic pattern of infiltrating lobular carcinoma and infiltrating duct carcinoma of the breast. *Br J Cancer, 50*(1), 23-30. doi:10.1038/bjc.1984.135

Hashizume, H., Baluk, P., Morikawa, S., McLean, J. W., Thurston, G., Roberge, S., . . . McDonald, D. M. (2000). Openings between defective endothelial cells explain tumor vessel leakiness. *Am J Pathol, 156*(4), 1363-1380. doi:10.1016/S0002-9440(10)65006-7

He, X., Cao, H., Wang, H., Tan, T., Yu, H., Zhang, P., . . . Li, Y. (2017). Inflammatory Monocytes Loading Protease-Sensitive Nanoparticles Enable Lung Metastasis Targeting and Intelligent Drug Release for Anti-Metastasis Therapy. *Nano Lett, 17*(9), 5546-5554. doi:10.1021/acs.nanolett.7b02330

He, Y., Rajantie, I., Pajusola, K., Jeltsch, M., Holopainen, T., Yla-Herttuala, S., . . . Alitalo, K. (2005). Vascular Endothelial Cell Growth Factor Receptor 3–Mediated Activation of Lymphatic Endothelium Is Crucial for Tumor Cell Entry and Spread via Lymphatic Vessels. *Cancer Research, 65*(11), 4739. doi:10.1158/0008-5472.CAN-04-4576

Ho, R. J., & Chien, J. (2014). Trends in translational medicine and drug targeting and delivery: new insights on an old concept-targeted drug delivery with antibody-drug conjugates for cancers. *J Pharm Sci, 103*(1), 71-77. doi:10.1002/jps.23761

Ho, R. J., Yu, J., Li, B., Kraft, J. C., Freeling, J. P., Koehn, J., & Shao, J. (2015). Systems Approach to targeted and long-acting HIV/AIDS therapy. *Drug Deliv Transl Res, 5*(6), 531-539. doi:10.1007/s13346-015-0254-y

Hou, H. H., Rajesh, A., Pandya, K. M., Lubach, J. W., Muliadi, A., Yost, E., . . . Nagapudi, K. (2019). Impact of Method of Preparation of Amorphous Solid Dispersions on Mechanical Properties: Comparison of Coprecipitation and Spray Drying. *J Pharm Sci, 108*(2), 870-879. doi:10.1016/j.xphs.2018.09.008

Hu, Q., van Rooijen, N., & Liu, D. (1996). Effect of Macrophage Elimination Using Liposome-Encapsulated Dichloromethylene Diphosphonate on Tissue Distribution of Liposomes. *Journal of Liposome Research, 6*(4), 681-698. doi:10.3109/08982109609039921

Ishida, T., Harada, M., Wang, X. Y., Ichihara, M., Irimura, K., & Kiwada, H. (2005). Accelerated blood clearance of PEGylated liposomes following preceding liposome injection: effects of lipid dose and PEG surface-density and chain length of the first-dose liposomes. *J Control Release, 105*(3), 305-317. doi:10.1016/j.jconrel.2005.04.003

Jain, R. K. (2001). Delivery of molecular and cellular medicine to solid tumors. *Adv Drug Deliv Rev, 46*(1-3), 149-168. doi:10.1016/s0169-409x(00)00131-9

Johnston, S. R., Martin, L. A., Head, J., Smith, I., & Dowsett, M. (2005). Aromatase inhibitors: combinations with fulvestrant or signal transduction inhibitors as a strategy to overcome endocrine resistance. *J Steroid Biochem Mol Biol, 95*(1-5), 173-181. doi:10.1016/j.jsbmb.2005.04.004

Jones, D., Pereira, E. R., & Padera, T. P. (2018). Growth and Immune Evasion of Lymph Node Metastasis. *Front Oncol, 8*, 36. doi:10.3389/fonc.2018.00036

Jordan, M. A., & Wilson, L. (2004). Microtubules as a target for anticancer drugs. *Nat Rev Cancer, 4*(4), 253-265. doi:10.1038/nrc1317

Kariagina, A., Aupperlee, M. D., & Haslam, S. Z. (2008). Progesterone receptor isoform functions in normal breast development and breast cancer. *Crit Rev Eukaryot Gene Expr, 18*(1), 11-33. doi:10.1615/critreveukargeneexpr.v18.i1.20

Kariya, R., Matsuda, K., Gotoh, K., Vaeteewoottacharn, K., Hattori, S., & Okada, S. (2014). Establishment of nude mice with complete loss of lymphocytes and NK cells and application for in vivo bio-imaging. *In Vivo, 28*(5), 779-784. Retrieved from https://www.ncbi.nlm.nih.gov/pubmed/25189889

Kaur, C. D., Nahar, M., & Jain, N. K. (2008). Lymphatic targeting of zidovudine using surface-engineered liposomes. *Journal of Drug Targeting, 16*(10), 798-805. doi:10.1080/10611860802475688

Kearney, B. P., Flaherty, J. F., & Shah, J. (2004). Tenofovir disoproxil fumarate: clinical pharmacology and pharmacokinetics. *Clin Pharmacokinet, 43*(9), 595-612. doi:10.2165/00003088-200443090-00003

Kelleher, J. F., Gilvary, G. C., Madi, A. M., Jones, D. S., Li, S., Tian, Y., . . . Healy, A. M. (2018). A comparative study between hot-melt extrusion and spray-drying for the manufacture of anti-hypertension compatible monolithic fixed-dose combination products. *Int J Pharm, 545*(1-2), 183-196. doi:10.1016/j.ijpharm.2018.05.008

Kiani, A., Kohne, C. H., Franz, T., Passauer, J., Haufe, T., Gross, P., . . . Schleyer, E. (2003). Pharmacokinetics of gemcitabine in a patient with end-stage renal disease: effective clearance of its main metabolite by standard hemodialysis treatment. *Cancer Chemother Pharmacol, 51*(3), 266-270. doi:10.1007/s00280-003-0574-3

King, P. D., & Perry, M. C. (2001). Hepatotoxicity of chemotherapy. *Oncologist, 6*(2), 162-176. doi:10.1634/theoncologist.6-2-162

Kinman, L., Brodie, S. J., Tsai, C. C., Bui, T., Larsen, K., Schmidt, A., . . . Ho, R. J. (2003). Lipid-drug association enhanced HIV-1 protease inhibitor indinavir localization in lymphoid

tissues and viral load reduction: a proof of concept study in HIV-2287-infected macaques. *J Acquir Immune Defic Syndr, 34*(4), 387-397. doi:10.1097/00126334-200312010-00005

Kodama, T., Hatakeyama, Y., Kato, S., & Mori, S. (2015). Visualization of fluid drainage pathways in lymphatic vessels and lymph nodes using a mouse model to test a lymphatic drug delivery system. *Biomed Opt Express, 6*(1), 124-134. doi:10.1364/BOE.6.000124

Koehn, J., Iwamoto, J. F., Kraft, J. C., McConnachie, L. A., Collier, A. C., & Ho, R. J. Y. (2018). Extended cell and plasma drug levels after one dose of a three-in-one nanosuspension containing lopinavir, efavirenz, and tenofovir in nonhuman primates. *AIDS, 32*(17), 2463-2467. doi:10.1097/QAD.0000000000001969

Kojima, C. (2015). Preclinical studies of dendrimer prodrugs. *Expert Opin Drug Metab Toxicol, 11*(8), 1303-1315. doi:10.1517/17425255.2015.1052404

Kraft, J. C., McConnachie, L. A., Koehn, J., Kinman, L., Collins, C., Shen, D. D., . . . Ho, R. J. (2017). Long-acting combination anti-HIV drug suspension enhances and sustains higher drug levels in lymph node cells than in blood cells and plasma. *AIDS, 31*(6), 765-770. doi:10.1097/QAD.0000000000001405

Kraft, J. C., McConnachie, L. A., Koehn, J., Kinman, L., Sun, J., Collier, A. C., . . . Ho, R. J. Y. (2018). Mechanism-based pharmacokinetic (MBPK) models describe the complex plasma kinetics of three antiretrovirals delivered by a long-acting anti-HIV drug combination nanoparticle formulation. *J Control Release, 275*, 229-241. doi:10.1016/j.jconrel.2018.02.003

Kraft, J. C., Treuting, P. M., & Ho, R. J. Y. (2018). Indocyanine green nanoparticles undergo selective lymphatic uptake, distribution and retention and enable detailed mapping of lymph vessels, nodes and abnormalities. *J Drug Target, 26*(5-6), 494-504. doi:10.1080/1061186X.2018.1433681

Kyriacou, H., & Khan, Y. S. (2020). Anatomy, Shoulder and Upper Limb, Axillary Lymph Nodes. In *StatPearls*. Treasure Island (FL).

Kyriazis, A. A., & Kyriazis, A. P. (1980). Preferential sites of growth of human tumors in nude mice following subcutaneous transplantation. *Cancer Research, 40*(12), 4509-4511. Retrieved from https://www.ncbi.nlm.nih.gov/pubmed/7438084

Lee, H., & Pastor, R. W. (2011). Coarse-grained model for PEGylated lipids: effect of PEGylation on the size and shape of self-assembled structures. *J Phys Chem B, 115*(24), 7830-7837. doi:10.1021/jp2020148

Lei, M., Sha, S., Wang, X., Wang, J., Du, X., Miao, H., . . . Zhu, Y. (2019). Co-delivery of paclitaxel and gemcitabine via a self-assembling nanoparticle for targeted treatment of breast cancer. *RSC Advances, 9*(10), 5512-5520. doi:10.1039/C9RA00276F

Li, C., Newman, R. A., Wu, Q.-P., Ke, S., Chen, W., Hutto, T., . . . Wallace, S. (2000). Biodistribution of paclitaxel and poly(l-glutamic acid)-paclitaxel conjugate in mice with ovarian OCa-1 tumor. *Cancer Chemotherapy and Pharmacology, 46*(5), 416-422. doi:10.1007/s002800000168

Li, C., Newman, R. A., Wu, Q. P., Ke, S., Chen, W., Hutto, T., . . . Wallace, S. (2000). Biodistribution of paclitaxel and poly(L-glutamic acid)-paclitaxel conjugate in mice with ovarian OCa-1 tumor. *Cancer Chemother Pharmacol, 46*(5), 416-422. doi:10.1007/s002800000168

Liedtke, C., Mazouni, C., Hess, K. R., André, F., Tordai, A., Mejia, J. A., . . . Pusztai, L. (2008). Response to Neoadjuvant Therapy and Long-Term Survival in Patients With Triple-

Negative Breast Cancer. *Journal of Clinical Oncology, 26*(8), 1275-1281. doi:10.1200/JCO.2007.14.4147

Lim, B., & Hortobagyi, G. N. (2016). Current challenges of metastatic breast cancer. *Cancer Metastasis Rev, 35*(4), 495-514. doi:10.1007/s10555-016-9636-y

Loehrer, P. J., Sr., Feng, Y., Cardenes, H., Wagner, L., Brell, J. M., Cella, D., . . . Benson, A. B., 3rd. (2011). Gemcitabine alone versus gemcitabine plus radiotherapy in patients with locally advanced pancreatic cancer: an Eastern Cooperative Oncology Group trial. *J Clin Oncol, 29*(31), 4105-4112. doi:10.1200/JCO.2011.34.8904

Longmire, M. R., Ogawa, M., Choyke, P. L., & Kobayashi, H. (2011). Biologically optimized nanosized molecules and particles: more than just size. *Bioconjug Chem, 22*(6), 993-1000. doi:10.1021/bc200111p

Lu, Y., Zi, X., Zhao, Y., Mascarenhas, D., & Pollak, M. (2001). Insulin-like growth factor-I receptor signaling and resistance to trastuzumab (Herceptin). *J Natl Cancer Inst, 93*(24), 1852-1857. doi:10.1093/jnci/93.24.1852

Luo, K., Li, C., Li, L., She, W., Wang, G., & Gu, Z. (2012). Arginine functionalized peptide dendrimers as potential gene delivery vehicles. *Biomaterials, 33*(19), 4917-4927. doi:10.1016/j.biomaterials.2012.03.030

Luu, T., Chow, W., Lim, D., Koczywas, M., Frankel, P., Cristea, M., . . . Morgan, R. J. (2010). Phase I trial of fixed-dose rate gemcitabine in combination with bortezomib in advanced solid tumors. *Anticancer Res, 30*(1), 167-174. Retrieved from https://www.ncbi.nlm.nih.gov/pubmed/20150632

Maartens, G., Celum, C., & Lewin, S. R. (2014). HIV infection: epidemiology, pathogenesis, treatment, and prevention. *Lancet, 384*(9939), 258-271. doi:10.1016/S0140-6736(14)60164-1

Mager, D. E., Mody, V., Xu, C., Forrest, A., Lesniak, W. G., Nigavekar, S. S., . . . Balogh, L. P. (2012). Physiologically based pharmacokinetic model for composite nanodevices: effect of charge and size on in vivo disposition. *Pharm Res, 29*(9), 2534-2542. doi:10.1007/s11095-012-0784-7

Maitland, D., Jackson, A., Osorio, J., Mandalia, S., Gazzard, B. G., Moyle, G. J., & Epivir-Ziagen Switch Study, T. (2008). Switching from twice-daily abacavir and lamivudine to the once-daily fixed-dose combination tablet of abacavir and lamivudine improves patient adherence and satisfaction with therapy. *HIV Med, 9*(8), 667-672. doi:10.1111/j.1468-1293.2008.00618.x

Marcinkowska, M., Sobierajska, E., Stanczyk, M., Janaszewska, A., Chworos, A., & Klajnert-Maculewicz, B. (2018). Conjugate of PAMAM Dendrimer, Doxorubicin and Monoclonal Antibody-Trastuzumab: The New Approach of a Well-Known Strategy. *Polymers (Basel), 10*(2). doi:10.3390/polym10020187

Mayer, L. D., Fulton, J., Kim-Kang, H., Yi, Y., Wang, P., Tardi, P., . . . Heller, D. (2014). CPX-351 Markedly Reduces Renal and Hepatic Clearance Rates for Cytarabine (Cyt) and Daunorubicin (Daun) in Rats with an Associated Decrease in Excretory and Metabolic Burden Despite Providing Dramatic Increases in Systemic Drug Exposure Compared to Conventional Cyt+Daun. *Blood, 124*(21), 2305-2305. doi:10.1182/blood.V124.21.2305.2305

McConnachie, L. A., Kinman, L. M., Koehn, J., Kraft, J. C., Lane, S., Lee, W., . . . Ho, R. J. Y. (2018). Long-Acting Profile of 4 Drugs in 1 Anti-HIV Nanosuspension in Nonhuman

Primates for 5 Weeks After a Single Subcutaneous Injection. *J Pharm Sci, 107*(7), 1787-1790. doi:10.1016/j.xphs.2018.03.005

McDonnell, D. P., & Wardell, S. E. (2010). The molecular mechanisms underlying the pharmacological actions of ER modulators: implications for new drug discovery in breast cancer. *Curr Opin Pharmacol, 10*(6), 620-628. doi:10.1016/j.coph.2010.09.007

Meng, H., Wang, M., Liu, H., Liu, X., Situ, A., Wu, B., . . . Nel, A. E. (2015). Use of a lipid-coated mesoporous silica nanoparticle platform for synergistic gemcitabine and paclitaxel delivery to human pancreatic cancer in mice. *ACS Nano, 9*(4), 3540-3557. doi:10.1021/acsnano.5b00510

Mercier, C., Raynal, C., Dahan, L., Ortiz, A., Evrard, A., Dupuis, C., . . . Ciccolini, J. (2007). Toxic death case in a patient undergoing gemcitabine-based chemotherapy in relation with cytidine deaminase downregulation. *Pharmacogenet Genomics, 17*(10), 841-844. doi:10.1097/FPC.0b013e32825ea6e3

Mini, E., Nobili, S., Caciagli, B., Landini, I., & Mazzei, T. (2006). Cellular pharmacology of gemcitabine. *Annals of Oncology, 17 Suppl 5*, v7-12. doi:10.1093/annonc/mdj941

Mohammed, R. A., Ellis, I. O., Lee, A. H., & Martin, S. G. (2009). Vascular invasion in breast cancer; an overview of recent prognostic developments and molecular pathophysiological mechanisms. *Histopathology, 55*(1), 1-9. doi:10.1111/j.1365-2559.2008.03169.x

Mu, Q., Yu, J., Griffin, J. I., Wu, Y., Zhu, L., McConnachie, L. A., & Ho, R. J. Y. (2020). Novel drug combination nanoparticles exhibit enhanced plasma exposure and dose-responsive effects on eliminating breast cancer lung metastasis. *PLOS ONE, 15*(3), e0228557. doi:10.1371/journal.pone.0228557

Muller, R. H., Radtke, M., & Wissing, S. A. (2002a). Nanostructured lipid matrices for improved microencapsulation of drugs. *Int J Pharm, 242*(1-2), 121-128. doi:10.1016/s0378-5173(02)00180-1

Muller, R. H., Radtke, M., & Wissing, S. A. (2002b). Solid lipid nanoparticles (SLN) and nanostructured lipid carriers (NLC) in cosmetic and dermatological preparations. *Adv Drug Deliv Rev, 54 Suppl 1*, S131-155. doi:10.1016/s0169-409x(02)00118-7

Murphy, R. L., Brun, S., Hicks, C., Eron, J. J., Gulick, R., King, M., . . . Sun, E. (2001). ABT-378/ritonavir plus stavudine and lamivudine for the treatment of antiretroviral-naive adults with HIV-1 infection: 48-week results. *AIDS, 15*(1), F1-9. doi:10.1097/00002030-200101050-00002

Nachega, J. B., Parienti, J. J., Uthman, O. A., Gross, R., Dowdy, D. W., Sax, P. E., . . . Giordano, T. P. (2014). Lower pill burden and once-daily antiretroviral treatment regimens for HIV infection: A meta-analysis of randomized controlled trials. *Clin Infect Dis, 58*(9), 1297-1307. doi:10.1093/cid/ciu046

Nagy, J. A., Chang, S. H., Dvorak, A. M., & Dvorak, H. F. (2009). Why are tumour blood vessels abnormal and why is it important to know? *Br J Cancer, 100*(6), 865-869. doi:10.1038/sj.bjc.6604929

Nakada, T., Sugihara, K., Jikoh, T., Abe, Y., & Agatsuma, T. (2019). The Latest Research and Development into the Antibody–Drug Conjugate, [fam-] Trastuzumab Deruxtecan (DS-8201a), for HER2 Cancer Therapy. *Chemical and Pharmaceutical Bulletin, 67*(3), 173-185. doi:10.1248/cpb.c18-00744

Nandi, S., Kaur, A., & Bansal, A. K. (2020). Dual drug nanocrystals loaded microparticles for fixed dose combination of simvastatin and ezetimibe. *Pharm Dev Technol, 25*(1), 40-53. doi:10.1080/10837450.2019.1669181

Nathanson, S. D., Krag, D., Kuerer, H. M., Newman, L. A., Brown, M., Kerjaschki, D., . . . Padera, T. P. (2018). Breast cancer metastasis through the lympho-vascular system. *Clin Exp Metastasis, 35*(5-6), 443-454. doi:10.1007/s10585-018-9902-1

Ng, I. O., Lam, K. Y., Ng, M., Kwong, D. L., & Sham, J. S. (1998). Expression of P-glycoprotein, a multidrug-resistance gene product, is induced by radiotherapy in patients with oral squamous cell carcinoma. *Cancer, 83*(5), 851-857. doi:10.1002/(sici)1097-0142(19980901)83:5<851::aid-cncr8>3.0.co;2-l

Nguyen, D. N., & Van den Mooter, G. (2014). The fate of ritonavir in the presence of darunavir. *Int J Pharm, 475*(1-2), 214-226. doi:10.1016/j.ijpharm.2014.08.062

Nicholson, R. I., Gee, J. M. W., Manning, D. L., Wakeling, A. E., Montano, M. M., & Katzenellenbogen, B. S. (1995). Responses to Pure Antiestrogens (Ici-164384, Ici-182780) in Estrogen-Sensitive and Estrogen-Resistant Experimental and Clinical Breast-Cancer. *Steroid Receptors and Antihormones, 761*, 148-163. doi:DOI 10.1111/j.1749-6632.1995.tb31376.x

Noh, I., Kim, H. O., Choi, J., Choi, Y., Lee, D. K., Huh, Y. M., & Haam, S. (2015). Co-delivery of paclitaxel and gemcitabine via CD44-targeting nanocarriers as a prodrug with synergistic antitumor activity against human biliary cancer. *Biomaterials, 53*, 763-774. doi:10.1016/j.biomaterials.2015.03.006

Northfelt, D. W., Martin, F. J., Working, P., Volberding, P. A., Russell, J., Newman, M., . . . Kaplan, L. D. (1996). Doxorubicin encapsulated in liposomes containing surface-bound polyethylene glycol: pharmacokinetics, tumor localization, and safety in patients with AIDS-related Kaposi's sarcoma. *J Clin Pharmacol, 36*(1), 55-63. doi:10.1002/j.1552-4604.1996.tb04152.x

O'Brien, M. E., Wigler, N., Inbar, M., Rosso, R., Grischke, E., Santoro, A., . . . Group, C. B. C. S. (2004). Reduced cardiotoxicity and comparable efficacy in a phase III trial of pegylated liposomal doxorubicin HCl (CAELYX/Doxil) versus conventional doxorubicin for first-line treatment of metastatic breast cancer. *Annals of Oncology, 15*(3), 440-449. doi:10.1093/annonc/mdh097

Okuda, T., Kawakami, S., Akimoto, N., Niidome, T., Yamashita, F., & Hashida, M. (2006). PEGylated lysine dendrimers for tumor-selective targeting after intravenous injection in tumor-bearing mice. *Journal of Controlled Release, 116*(3), 330-336. doi:https://doi.org/10.1016/j.jconrel.2006.09.012

Okuda, T., Kawakami, S., Maeie, T., Niidome, T., Yamashita, F., & Hashida, M. (2006). Biodistribution characteristics of amino acid dendrimers and their PEGylated derivatives after intravenous administration. *Journal of Controlled Release, 114*(1), 69-77. doi:https://doi.org/10.1016/j.jconrel.2006.05.009

Osborne, C. K., Bardou, V., Hopp, T. A., Chamness, G. C., Hilsenbeck, S. G., Fuqua, S. A., . . . Schiff, R. (2003). Role of the estrogen receptor coactivator AIB1 (SRC-3) and HER-2/neu in tamoxifen resistance in breast cancer. *J Natl Cancer Inst, 95*(5), 353-361. doi:10.1093/jnci/95.5.353

Osborne, C. K., Wakeling, A., & Nicholson, R. I. (2004). Fulvestrant: an oestrogen receptor antagonist with a novel mechanism of action. *Br J Cancer, 90 Suppl 1*, S2-6. doi:10.1038/sj.bjc.6601629

Paal, K., Muller, J., & Hegedus, L. (2001). High affinity binding of paclitaxel to human serum albumin. *Eur J Biochem, 268*(7), 2187-2191. doi:10.1046/j.1432-1327.2001.02107.x

Padera, T. P., Kadambi, A., di Tomaso, E., Carreira, C. M., Brown, E. B., Boucher, Y., . . . Jain, R. K. (2002). Lymphatic Metastasis in the Absence of Functional Intratumor Lymphatics. *Science, 296*(5574), 1883. doi:10.1126/science.1071420

Pan, H., Gray, R., Braybrooke, J., Davies, C., Taylor, C., McGale, P., . . . Ebctcg. (2017). 20-Year Risks of Breast-Cancer Recurrence after Stopping Endocrine Therapy at 5 Years. *N Engl J Med, 377*(19), 1836-1846. doi:10.1056/NEJMoa1701830

Paolino, D., Cosco, D., Racanicchi, L., Trapasso, E., Celia, C., Iannone, M., . . . Fresta, M. (2010). Gemcitabine-loaded PEGylated unilamellar liposomes vs GEMZAR: biodistribution, pharmacokinetic features and in vivo antitumor activity. *J Control Release, 144*(2), 144-150. doi:10.1016/j.jconrel.2010.02.021

Park, J., Park, J. E., Hedrick, V. E., Wood, K. V., Bonham, C., Lee, W., & Yeo, Y. (2018). A Comparative In Vivo Study of Albumin-Coated Paclitaxel Nanocrystals and Abraxane. *Small, 14*(16), e1703670. doi:10.1002/smll.201703670

Perazzolo, S., Shireman, L. M., Koehn, J., McConnachie, L. A., Kraft, J. C., Shen, D. D., & Ho, R. J. Y. (2018). Three HIV Drugs, Atazanavir, Ritonavir, and Tenofovir, Coformulated in Drug-Combination Nanoparticles Exhibit Long-Acting and Lymphocyte-Targeting Properties in Nonhuman Primates. *J Pharm Sci, 107*(12), 3153-3162. doi:10.1016/j.xphs.2018.07.032

Perazzolo, S., Shireman, L. M., McConnachie, L. A., Koehn, J., Kinman, L., Lee, W., . . . Ho, R. J. Y. (2020). Integration of Computational and Experimental Approaches to Elucidate Mechanisms of First-Pass Lymphatic Drug Sequestration and Long-Acting Pharmacokinetics of the Injectable Triple-HIV Drug Combination TLC-ART 101. *J Pharm Sci, 109*(5), 1789-1801. doi:10.1016/j.xphs.2020.01.016

Pereira, E. R., Kedrin, D., Seano, G., Gautier, O., Meijer, E. F. J., Jones, D., . . . Padera, T. P. (2018). Lymph node metastases can invade local blood vessels, exit the node, and colonize distant organs in mice. *Science, 359*(6382), 1403-1407. doi:10.1126/science.aal3622

Pernas, S., & Tolaney, S. M. (2019). HER2-positive breast cancer: new therapeutic frontiers and overcoming resistance. *Therapeutic Advances in Medical Oncology, 11*. doi:Unsp 1758835919833519

10.1177/1758835919833519

Peters, G. J., Clavel, M., Noordhuis, P., Geyssen, G. J., Laan, A. C., Guastalla, J., . . . Vermorken, J. B. (2007). Clinical Phase I and Pharmacology Study of Gemcitabine (2', 2'-Difluorodeoxycytidine) Administered in a Two-Weekly Schedule. *Journal of Chemotherapy, 19*(2), 212-221. doi:10.1179/joc.2007.19.2.212

Pistelli, M., Mora, A. D., Ballatore, Z., & Berardi, R. (2018). Aromatase inhibitors in premenopausal women with breast cancer: the state of the art and future prospects. *Curr Oncol, 25*(2), e168-e175. doi:10.3747/co.25.3735

Preusser, M., De Mattos-Arruda, L., Thill, M., Criscitiello, C., Bartsch, R., Ruhstaller, T., . . . Zielinski, C. C. (2018). CDK4/6 inhibitors in the treatment of patients with breast cancer: summary of a multidisciplinary round-table discussion. *ESMO Open, 3*(5), e000368. doi:10.1136/esmoopen-2018-000368

Pulaski, B. A., & Ostrand-Rosenberg, S. (2001). Mouse 4T1 breast tumor model. *Curr Protoc Immunol, Chapter 20*, Unit 20 22. doi:10.1002/0471142735.im2002s39

Rahman, A. M., Yusuf, S. W., & Ewer, M. S. (2007). Anthracycline-induced cardiotoxicity and the cardiac-sparing effect of liposomal formulation. *Int J Nanomedicine, 2*(4), 567-583. Retrieved from https://www.ncbi.nlm.nih.gov/pubmed/18203425

Rahman, M., & Mohammed, S. (2015). Breast cancer metastasis and the lymphatic system. *Oncol Lett, 10*(3), 1233-1239. doi:10.3892/ol.2015.3486

Rashid, O. M., Nagahashi, M., Ramachandran, S., Dumur, C. I., Schaum, J. C., Yamada, A., . . . Takabe, K. (2013). Is tail vein injection a relevant breast cancer lung metastasis model? *J Thorac Dis, 5*(4), 385-392. doi:10.3978/j.issn.2072-1439.2013.06.17

Rashid, O. M., & Takabe, K. (2015). Animal models for exploring the pharmacokinetics of breast cancer therapies. *Expert Opin Drug Metab Toxicol, 11*(2), 221-230. doi:10.1517/17425255.2015.983073

Redig, A. J., & McAllister, S. S. (2013). Breast cancer as a systemic disease: a view of metastasis. *J Intern Med, 274*(2), 113-126. doi:10.1111/joim.12084

Reid, J. M., Qu, W., Safgren, S. L., Ames, M. M., Krailo, M. D., Seibel, N. L., . . . Holcenberg, J. (2004). Phase I trial and pharmacokinetics of gemcitabine in children with advanced solid tumors. *J Clin Oncol, 22*(12), 2445-2451. doi:10.1200/JCO.2004.10.142

Riddell, S. R., Sommermeyer, D., Berger, C., Liu, L. S., Balakrishnan, A., Salter, A., . . . Turtle, C. J. (2014). Adoptive therapy with chimeric antigen receptor-modified T cells of defined subset composition. *Cancer J, 20*(2), 141-144. doi:10.1097/PPO.0000000000000036

Roberts, J. C., Bhalgat, M. K., & Zera, R. T. (1996). Preliminary biological evaluation of polyamidoamine (PAMAM) StarburstTM dendrimers. *Journal of Biomedical Materials Research, 30*(1), 53-65. doi:10.1002/(SICI)1097-4636(199601)30:1<53::AID-JBM8>3.0.CO;2-Q

Rosenblum, D., Joshi, N., Tao, W., Karp, J. M., & Peer, D. (2018). Progress and challenges towards targeted delivery of cancer therapeutics. *Nature Communications, 9*(1), 1410. doi:10.1038/s41467-018-03705-y

Rowinsky, E. K., Jiroutek, M., Bonomi, P., Johnson, D., & Baker, S. D. (1999). Paclitaxel steady-state plasma concentration as a determinant of disease outcome and toxicity in lung cancer patients treated with paclitaxel and cisplatin. *Clin Cancer Res, 5*(4), 767-774. Retrieved from https://www.ncbi.nlm.nih.gov/pubmed/10213211

Sakorafas, G. H., Peros, G., & Cataliotti, L. (2006). Sequelae following axillary lymph node dissection for breast cancer. *Expert Rev Anticancer Ther, 6*(11), 1629-1638. doi:10.1586/14737140.6.11.1629

Scaltriti, M., Verma, C., Guzman, M., Jimenez, J., Parra, J. L., Pedersen, K., . . . Baselga, J. (2009). Lapatinib, a HER2 tyrosine kinase inhibitor, induces stabilization and accumulation of HER2 and potentiates trastuzumab-dependent cell cytotoxicity. *Oncogene, 28*(6), 803-814. doi:10.1038/onc.2008.432

Shao, J., Kraft, J. C., Li, B., Yu, J., Freeling, J., Koehn, J., & Ho, R. J. (2016). Nanodrug formulations to enhance HIV drug exposure in lymphoid tissues and cells: clinical significance and potential impact on treatment and eradication of HIV/AIDS. *Nanomedicine (Lond), 11*(5), 545-564. doi:10.2217/nnm.16.1

Sharma, A., & Straubinger, R. M. (1994). Novel taxol formulations: preparation and characterization of taxol-containing liposomes. *Pharm Res, 11*(6), 889-896. doi:10.1023/a:1018994111594

Sharma, P., & Garg, S. (2010). Pure drug and polymer based nanotechnologies for the improved solubility, stability, bioavailability and targeting of anti-HIV drugs. *Adv Drug Deliv Rev, 62*(4-5), 491-502. doi:10.1016/j.addr.2009.11.019

Shaw, M. T., Spector, M. H., & Ladman, A. J. (1979). Effects of cancer, radiotherapy and cytotoxic drugs on intestinal structure and function. *Cancer Treat Rev, 6*(3), 141-151. doi:10.1016/s0305-7372(79)80066-3

Shibuya, M. (2011). Vascular Endothelial Growth Factor (VEGF) and Its Receptor (VEGFR) Signaling in Angiogenesis: A Crucial Target for Anti- and Pro-Angiogenic Therapies. *Genes Cancer, 2*(12), 1097-1105. doi:10.1177/1947601911423031

Shipley, L. A., Brown, T. J., Cornpropst, J. D., Hamilton, M., Daniels, W. D., & Culp, H. W. (1992). Metabolism and disposition of gemcitabine, and oncolytic deoxycytidine analog, in mice, rats, and dogs. *Drug Metab Dispos, 20*(6), 849-855. Retrieved from https://www.ncbi.nlm.nih.gov/pubmed/1362937

Siegel, R. L., Miller, K. D., & Jemal, A. (2020). Cancer statistics, 2020. *CA Cancer J Clin, 70*(1), 7-30. doi:10.3322/caac.21590

Simoni, J. M., Tapia, K., Lee, S. J., Graham, S. M., Beima-Sofie, K., Mohamed, Z. H., . . . Collier, A. C. (2020). A Conjoint Analysis of the Acceptability of Targeted Long-Acting Injectable Antiretroviral Therapy Among Persons Living with HIV in the U.S. *AIDS Behav, 24*(4), 1226-1236. doi:10.1007/s10461-019-02701-7

Simpson, E. R., & Davis, S. R. (2001). Minireview: aromatase and the regulation of estrogen biosynthesis--some new perspectives. *Endocrinology, 142*(11), 4589-4594. doi:10.1210/endo.142.11.8547

Singer, J. W., Shaffer, S., Baker, B., Bernareggi, A., Stromatt, S., Nienstedt, D., & Besman, M. (2005). Paclitaxel poliglumex (XYOTAX; CT-2103): an intracellularly targeted taxane. *Anticancer Drugs, 16*(3), 243-254. doi:10.1097/00001813-200503000-00003

Skoczen, S., McNeil, S. E., & Stern, S. T. (2015). Stable isotope method to measure drug release from nanomedicines. *J Control Release, 220*(Pt A), 169-174. doi:10.1016/j.jconrel.2015.10.042

Sliwkowski, M. X., Lofgren, J. A., Lewis, G. D., Hotaling, T. E., Fendly, B. M., & Fox, J. A. (1999). Nonclinical studies addressing the mechanism of action of trastuzumab (Herceptin). *Semin Oncol, 26*(4 Suppl 12), 60-70. Retrieved from https://www.ncbi.nlm.nih.gov/pubmed/10482195

Smith, C. L., Nawaz, Z., & O'Malley, B. W. (1997). Coactivator and corepressor regulation of the agonist/antagonist activity of the mixed antiestrogen, 4-hydroxytamoxifen. *Mol Endocrinol, 11*(6), 657-666. doi:10.1210/mend.11.6.0009

Smith, R. E., Brown, A. M., Mamounas, E. P., Anderson, S. J., Lembersky, B. C., Atkins, J. H., . . . Thirlwell, M. P. (1999). Randomized trial of 3-hour versus 24-hour infusion of high-dose paclitaxel in patients with metastatic or locally advanced breast cancer: National Surgical Adjuvant Breast and Bowel Project Protocol B-26. *J Clin Oncol, 17*(11), 3403-3411. doi:10.1200/JCO.1999.17.11.3403

Sowinska, M., & Urbanczyk-Lipkowska, Z. (2014). Advances in the chemistry of dendrimers. *New Journal of Chemistry, 38*(6), 2168-2203. doi:10.1039/C3NJ01239E

Spratlin, J., & Sawyer, M. B. (2007). Pharmacogenetics of paclitaxel metabolism. *Crit Rev Oncol Hematol, 61*(3), 222-229. doi:10.1016/j.critrevonc.2006.09.006

Steeg, P. S. (2006). Tumor metastasis: mechanistic insights and clinical challenges. *Nat Med, 12*(8), 895-904. doi:10.1038/nm1469

Sverdlov Arzi, R., & Sosnik, A. (2018). Electrohydrodynamic atomization and spray-drying for the production of pure drug nanocrystals and co-crystals. *Adv Drug Deliv Rev, 131*, 79-100. doi:10.1016/j.addr.2018.07.012

Tan, B., Piwnica-Worms, D., & Ratner, L. (2000). Multidrug resistance transporters and modulation. *Curr Opin Oncol, 12*(5), 450-458. doi:10.1097/00001622-200009000-00011

Tan, M., & Yu, D. (2007). Molecular mechanisms of ErbB2-Mediated breast cancer chemoresistance. *Breast Cancer Chemosensitivity, 608*, 119-129. Retrieved from <Go to ISI>://WOS:000249799800009

Tao, K., Fang, M., Alroy, J., & Sahagian, G. G. (2008). Imagable 4T1 model for the study of late stage breast cancer. *BMC Cancer, 8*, 228. doi:10.1186/1471-2407-8-228

Tardi, P., Johnstone, S., Harasym, N., Xie, S., Harasym, T., Zisman, N., . . . Mayer, L. (2009). In vivo maintenance of synergistic cytarabine:daunorubicin ratios greatly enhances therapeutic efficacy. *Leukemia Research, 33*(1), 129-139. doi:https://doi.org/10.1016/j.leukres.2008.06.028

Tempero, M., Plunkett, W., Ruiz Van Haperen, V., Hainsworth, J., Hochster, H., Lenzi, R., & Abbruzzese, J. (2003). Randomized phase II comparison of dose-intense gemcitabine: thirty-minute infusion and fixed dose rate infusion in patients with pancreatic adenocarcinoma. *J Clin Oncol, 21*(18), 3402-3408. doi:10.1200/JCO.2003.09.140

Thakkar, J. P., & Mehta, D. G. (2011). A review of an unfavorable subset of breast cancer: estrogen receptor positive progesterone receptor negative. *Oncologist, 16*(3), 276-285. doi:10.1634/theoncologist.2010-0302

Tolaney, S. (2014). New HER2-Positive Targeting Agents in Clinical Practice. *Current Oncology Reports, 16*(1). doi:ARTN 359

10.1007/s11912-013-0359-8

Trasi, N. S., Bhujbal, S., Zhou, Q. T., & Taylor, L. S. (2019). Amorphous solid dispersion formation via solvent granulation - A case study with ritonavir and lopinavir. *Int J Pharm X, 1*, 100035. doi:10.1016/j.ijpx.2019.100035

Trasi, N. S., & Taylor, L. S. (2015). Thermodynamics of Highly Supersaturated Aqueous Solutions of Poorly Water-Soluble Drugs-Impact of a Second Drug on the Solution Phase Behavior and Implications for Combination Products. *J Pharm Sci, 104*(8), 2583-2593. doi:10.1002/jps.24528

Trezza, C., Ford, S. L., Spreen, W., Pan, R., & Piscitelli, S. (2015). Formulation and pharmacology of long-acting cabotegravir. *Curr Opin HIV AIDS, 10*(4), 239-245. doi:10.1097/COH.0000000000000168

van der Wall, E., Beijnen, J. H., & Rodenhuis, S. (1995). High-dose chemotherapy regimens for solid tumors. *Cancer Treatment Reviews, 21*(2), 105-132. doi:https://doi.org/10.1016/0305-7372(95)90023-3

Vasconcelos, T., Sarmento, B., & Costa, P. (2007). Solid dispersions as strategy to improve oral bioavailability of poor water soluble drugs. *Drug Discov Today, 12*(23-24), 1068-1075. doi:10.1016/j.drudis.2007.09.005

Velasco, R., & Bruna, J. (2015). Taxane-Induced Peripheral Neurotoxicity. *Toxics, 3*(2), 152-169. doi:10.3390/toxics3020152

Veltkamp, S. A., Beijnen, J. H., & Schellens, J. H. (2008). Prolonged versus standard gemcitabine infusion: translation of molecular pharmacology to new treatment strategy. *Oncologist, 13*(3), 261-276. doi:10.1634/theoncologist.2007-0215

Veltkamp, S. A., Pluim, D., van Tellingen, O., Beijnen, J. H., & Schellens, J. H. (2008). Extensive metabolism and hepatic accumulation of gemcitabine after multiple oral and intravenous administration in mice. *Drug Metab Dispos, 36*(8), 1606-1615. doi:10.1124/dmd.108.021048

Waks, A. G., & Winer, E. P. (2019). Breast Cancer Treatment: A Review. *JAMA, 321*(3), 288-300. doi:10.1001/jama.2018.19323

Wang, L. R., Liu, J., Huang, M. Z., & Xu, N. (2007). Comparison of pharmacokinetics, efficacy and toxicity profile of gemcitabine using two different administration regimens in Chinese patients with non-small-cell lung cancer. *J Zhejiang Univ Sci B, 8*(5), 307-313. doi:10.1631/jzus.2007.B0307

Wang, R., Zhu, Y., Liu, X., Liao, X., He, J., & Niu, L. (2019). The Clinicopathological features and survival outcomes of patients with different metastatic sites in stage IV breast cancer. *BMC Cancer, 19*(1), 1091. doi:10.1186/s12885-019-6311-z

Weiss, R. B., Donehower, R. C., Wiernik, P. H., Ohnuma, T., Gralla, R. J., Trump, D. L., . . . Leyland-Jones, B. (1990). Hypersensitivity reactions from taxol. *J Clin Oncol, 8*(7), 1263-1268. doi:10.1200/JCO.1990.8.7.1263

Widdison, W. C., Wilhelm, S. D., Cavanagh, E. E., Whiteman, K. R., Leece, B. A., Kovtun, Y., . . . Chari, R. V. (2006). Semisynthetic maytansine analogues for the targeted treatment of cancer. *J Med Chem, 49*(14), 4392-4408. doi:10.1021/jm060319f

Williams, P. E., Crauwels, H. M., & Basstanie, E. D. (2015). Formulation and pharmacology of long-acting rilpivirine. *Curr Opin HIV AIDS, 10*(4), 233-238. doi:10.1097/COH.0000000000000164

Williams, R. M., Shah, J., Ng, B. D., Minton, D. R., Gudas, L. J., Park, C. Y., & Heller, D. A. (2015). Mesoscale nanoparticles selectively target the renal proximal tubule epithelium. *Nano Lett, 15*(4), 2358-2364. doi:10.1021/nl504610d

Wong, S. Y., & Hynes, R. O. (2006). Lymphatic or hematogenous dissemination: how does a metastatic tumor cell decide? *Cell Cycle, 5*(8), 812-817. doi:10.4161/cc.5.8.2646

Xu, B., Shen, Z., Jiang, Z., Guan, Z., & Zhang, X. (2010). A phase II study of gemcitabine plus paclitaxel in patients with metastatic breast cancer and prior anthracycline treatment. *Asia Pac J Clin Oncol, 6*(4), 320-329. doi:10.1111/j.1743-7563.2010.01323.x

Yamaji, Y., Akita, S., Akita, H., Miura, N., Gomi, M., Manabe, I., . . . Mitsukawa, N. (2018). Development of a mouse model for the visual and quantitative assessment of lymphatic trafficking and function by in vivo imaging. *Sci Rep, 8*(1), 5921. doi:10.1038/s41598-018-23693-9

Yu, J., Mu, Q., Perazzolo, S., Griffin, J., Zhu, L., McConnachie, L., . . . Ho, R. (2020). Novel Long-Acting Drug Combination Nanoparticles Composed of Gemcitabine and Paclitaxel Enhance Localization of Both Drugs in Metastatic Breast Cancer Nodules. *Pharmaceutical Research, 37*, 197. doi:10.1007/s11095-020-02888-8

Yu, J., Yu, D., Lane, S., McConnachie, L., & Ho, R. J. Y. (2020). Controlled Solvent Removal from Antiviral Drugs and Excipients in Solution Enables the Formation of Novel Combination Multi-Drug-Motifs in Pharmaceutical Powders Composed of Lopinavir, Ritonavir and Tenofovir. *J Pharm Sci*. doi:10.1016/j.xphs.2020.08.003

Zhang, J., Zhang, P., Zou, Q., Li, X., Fu, J., Luo, Y., . . . Jin, Y. (2018). Co-Delivery of Gemcitabine and Paclitaxel in cRGD-Modified Long Circulating Nanoparticles with Asymmetric Lipid Layers for Breast Cancer Treatment. *Molecules, 23*(11). doi:10.3390/molecules23112906

Zhang, Y. N., Poon, W., Tavares, A. J., McGilvray, I. D., & Chan, W. C. W. (2016). Nanoparticle-liver interactions: Cellular uptake and hepatobiliary elimination. *J Control Release, 240*, 332-348. doi:10.1016/j.jconrel.2016.01.020

VITA

Jesse Yu was born in Canada. He earned his Bachelor of Science degree in Pharmaceutical Sciences and Doctor of Pharmacy degree from Duquesne University in Pittsburgh, PA.